Analytical characterization of electrohydrodynamic liquid bridging

Master thesis

Mathias Eisenhut

Supervisor:

Ao. Univ.-Prof. Dipl.-Ing. Dr. techn. Tit. Univ.-Prof. Ernst Lankmayr

Institute for analytical and food chemistry

Technical university of Graz

2012

Acknowledgement

STATUTORY DECLARATION

I declare that I have authored this thesis independently, that I have not used other than the declared sources / resources, and that I have explicitly marked all material which has been quoted either literally or by content from the used sources.

…… ……..

date (signature)

Abstract:

The formation of aqueous bridges containing phenol and ethylene glycol as well as bisphenol- A, hydrochinone, p- cresol and some anorganic salts under the application of high voltage DC ("liquid bridges") is reported. Detailed studies were made for phenol and glycol with concentrations from 0.005 to 0.531 mol L^{-1}. Studies of the mass transport of ethylene glycol were carried out by measuring the final concentrations using gas chromatogtraphy-mass spectrometry and that for phenol by photometric measurement. Conductivity as well as substance and mass transfers through these aqueous bridges are discussed and compared with pure water bridges. Previously suggested bidirectional mass transport is confirmed for the substances tested. Anodic oxidation happens more efficiently when phenol or glycol are transported from the cathode to the anode since in this case the formation of a passivation layer or electrode poisoning are retarded by the electrohydrodynamic (EHD) flow. The conductivity in the cathode beaker decreases in all experiments except experiment 13 due to electrophoretic transport of naturally dissolved carbonate and bicarbonate to the anode. The observed electrochemical behavior is discussed and compared to known mechanisms.

Kurzfassung:

Inhalt dieser Arbeit ist es Wasserbrücken mit wässrigen Phenol- und Ethylenglykol-Lösungen, als auch mit Bisphenol-A, Hydrochinon, p-Kresol und einigen anorganischen Salzen mittels Einsatz einer Gleichstrom-Hochspannungsquelle zu analysieren. Genaue Untersuchungen wurden für Phenol (photometrisch) und Glykol (GC-MS) in einem Konzentrationsbereich von 0.005 bis 0.531 mol L^{-1} angestellt. Die Leitfähigkeit als auch der Analyt- und Massentransfer durch die Wasserbrücken werden mit reinen Wasserbrücken verglichen und diskutiert. Ein bidirektionaler Massentransport ist für alle Substanzen nachweisbar. Die anodische Oxidation ist stärker ausgeprägt, wenn Phenol oder Glykol von der Kathode zur Anode transportiert werden, weil die Bildung einer Passivierungsschicht und/oder eine Elektrodenvergiftung durch den elektrohydrodynamischen Fluss unterdrückt wird. Die Leitfähigkeit im Kathodenbecher nimmt in allen Experimenten durch elektrophoretischen Transport von gelösten Karbonat und Bikarbonat Ionen hin zur Anode ab. Das beobachtete elektrochemische Verhalten wird kurz diskutiert und mit bekannten Mechanismen verglichen.

Table of contents

1 Introduction

In the year 1893 Sir Armstrong put a cotton thread between two wine glasses filled with chemically pure water and applied a high voltage to the system. The emerging watery connection was stable for a short while, even when the cotton thread was pulled in one of the glasses leaving a suspended rope of water between the lips of the glasses.

Pellat performed a similar experiment in 1896; he showed that an insulating, dielectric liquid with two immersed electrodes and an applied high potential, resulted in an upward fluid motion between the electrodes. In a modern version of this experiment Woisetschläger et al. (Woisetschläger, J. 2012) show that if the electrodes are pulled out of a cuvette containing glycerol the horizontal liquid connection remains stable, thereby reproducing Sir Armstrong's experiment using another liquid.

Since rediscovered by W. Uhlig (ETH Zürich) in 2005 (Uhlig, W, 2005) Armstrong's experiment had an enormous impact in the scientific community. The advances in Electrohydrodynamics from the early 20th century on were huge, the physical principles of the interaction of polar molecules with an electric field were investigated thoroughly and possible applications were considered (Sumoto, I. 1955; Pohl, H.A. 1958; Pohl, H.A. 1951), but no technological breakthrough was achieved. G.I Taylor wrote a remarkable review of his predecessors in 1964, founding the area of Electrospraying with a detailed description of the emerging cone ('Taylor cone') when applying a high potential to a polar liquid (Taylor, G. 1964; de la Mora, J. F. 2007). In 1968, Raco tested the stabilizing effect on a dielectric liquid when a high potential was applied. He concluded that 'a liquid column of uniform diameter will be formed parallel to the electric field (Raco, R.J. 1968), with its diameter proportional to the potential'. Melcher and Warren (Melcher, J.R. 1971) were interested in the dynamics between the air- liquid interface of a semi-insulating liquid, when gravity and the longitudinal electrical field counteracted on each other.

A liquid bridge is defined as a vertical column of liquid, pinned at each end between planar electrodes and surrounded by a non-conducting, dielectric gas' (Woisetschlaeger, J. 2012). Gonzales et al. showed that a liquid bridge in zero gravity is dependent on the ratio of dielectric constants of the used liquid, the ratio between applied voltages, surface tension and the slenderness (ratio of length/diameter) of the bridge (Gonzalez, H. 1989). Saville (Saville, D.A. 1997) gave a well established review of the leaky dielectric model first mentioned by Taylor, developing a more sophisticated approach to EHD considerations than anyone before him. Castellanos wrote a good review about the parameters influencing

electrophoresis in his book: Electrohydrodynamics (Castellanos, A. 1998). Burcham and Saville (Burcham, C.L. 2000) made detailed experiments of leaky dielectrics under microgravity conditions surrounded by a dielectric gas.

In 2002, J. B. Fenn received the Nobel Prize for chemistry for his work concerning Electrospraying as a soft ionization method for organic molecules and consequent mass spectrometry analysis.

A large number of theories regarding basic properties, stability and electrochemical processes taking place in aqueous high- energy systems had been proposed, but are still controversially discussed in the scientific community.

This work intends to highlight some of the most important recent developments in the fundamental research of electrohydrodynamic liquid bridging (Fuchs, E. C. 2010; Fuchs, E. C. 2008). The attention is turned to the effect of non-ionic, organic, aqueous solutions in the phenomenon of the floating water bridge (Fuchs, E. C. 2011; Fuchs, E. C. 2009), or also referred to as liquid bridge, (Raco, R.J. 1968; Gonzalez, H. 1989; Saville, D.A. 1997; Burcham, C.L. 2000; Burcham, C.L. 2002) and it's deviances compared to the pure water phase. Recently, lots of physical-analytical data were presented concerning the fluid mechanics (Marin, A. G. 2010), the applicability of different solvents with a high dielectric permittivity and a low conductivity (Burcham, C.L. 2000; Burcham, C.L. 2002), the energy relaxation using infrared pumping probe spectroscopy (Gonzalez, H. 1989), the neutron scattering (Fuchs, E. C. 2009; Fuchs, E. C. 2010) and the inelastic UV scattering of the bridge (Fuchs, E.C. 2011) next to some more visualization techniques and modelling (Saija, F. 2010; Aerov, A. A. 2011). Also some Raman scattering studies in vertical bridges (Ponterio, R.C. 2010) and some experiments under reduced gravity (Fuchs, E. C. 2011) have been carried out. Therefore, organic molecules with a low conductivity are the next step to compare the properties and features from a liquid bridge to its inorganic pendant. The possibility to use living organisms in electrohydrodynamic structures has also been of special interest and was carried out by Paulitsch-Fuchs et al. (Paulitsch–Fuchs, A.H. 2012).

2 Theory

2.1 Water - a protic solvent

Water covers nearly 70% of the earths' surface and is a prerequisite for all known life forms. The research in this area is extremely controversial, since the possibility to look from a microscopic or macroscopic point yields different properties of the aqueous system. By now, 67 anomalies are known for water, which are discussed either on a micro- or macroscopic scale and most of them are nowadays scientifically investigated and at least partially explained in one of these categories.

There is still a gap at the mesoscopic scale. Especially, the dynamics of water molecules around heteromolecules or the structure of hydrogen bonded water has been scientifically discussed for over two centuries with no final conclusions.

Water is a symmetric molecule with two mirror planes of symmetry and a twofold rotation axis (point group C_{2v}). Its' high intrinsic dielectric constant originates from the differences in electronegativity from the oxygen and the hydrogen atom, which leads to a polar covalent bond with most of the electron density located around the oxygen (Fig. 1).

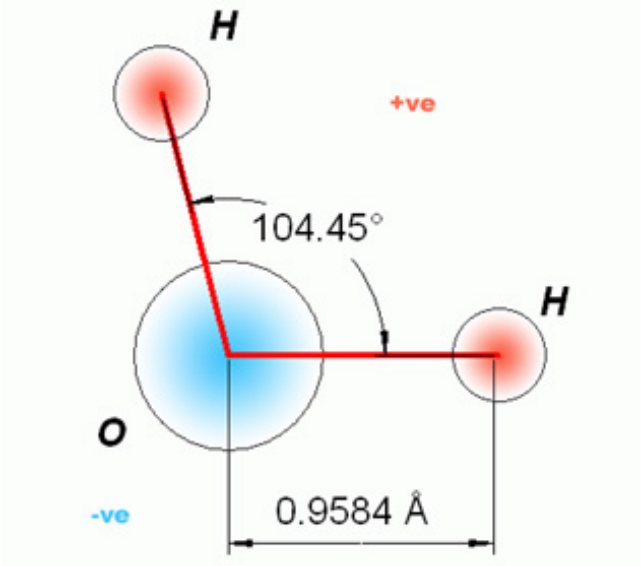

Fig. 1: Water molecule geometry

2.2 Hydrogen bonding

First mentioned by Latimer and Rodebush (Latimer, W.M. 1920), the picture of protons hopping between different water molecules became more and more prominent, since basic properties of water could be explained by this additional, unusually high, energy contribution. In the early fifties Pauling explained protein structures as a consequence of the H-bonding

network in water (Pauling, L. 1951). Since the strength of a hydrogen bond (5-40 $kJmol^{-1}$) in water lies between Van der Waals attraction forces and covalent bonding, it affects all chemical reactions in aqueous media. Markovitch and Agmon recently 'determined the Gibbs energy and the enthalpy for hydrogen bonds donated or accepted by the first two solvation shells, in comparison to bulk water by means of 'multistate-empirical valence-bond methodology' (Markovitch, O. 2007), stating free Gibbs energy values between 13.8 $kJmol^{-1}$ for the strongest donating bond of a H_3O^+ cation and 2.7 $kJmol^{-1}$ for bulk water.

2.3 Water networks

The first famous theory was the Grotthuss (1806) mechanism, which suggested a cluster size of two to four water molecules per unit with water molecules of the chemical formula OH (!). This theory is not in agreement with molecular modeling calculations (Agmon, N. 1995), but it already suggests a proton-hopping mechanism, which became refined in the early 1960s by Eigen und Zundel. The main aspect of this theory was that the transition from the $H_9O_4^+$ cation (Eigen) to the $H_5O_2^+$ cation (Zundel) and the linked hydrogen bond-cleavage could explain the high mobility of protons in aqueous solutions. Lots of more theories followed with the rise of computational power at the end of the 20th century, concluding that pentameric and tetrameric cyclic water structures, which were readily available by means of molecular dynamic simulations with the TIP4P basis set $(H_2O)_n$, $2 \leq n \leq 20$, (Wales, D.J. 1998), ab-initio simulations with HF calculations with the 6- 31G(d,p), 6-311++G(2d, 2p) basis set, or DFT calculations using B3LYP basis sets (Maheshwary, S. 2001). Svanberg et al. (Svanberg, M. 1998) investigated the 'magic' number [$(H_2O)_n$; n=21] with Monte Carlo algorithm, and Lenz et al. developed an IR-method to approximate the average H- bond number of a single water molecule as a function of temperature (Lenz, A. 2006). Some refined structures can be seen in Fig. 2.

Another theory argued that quantum entanglement mechanisms take place in the mixture of H_2O/D_2O with electronic charges mediating quantum variations of the nuclei. Therefore, tunnelling of protons seemed to be confirmed in water intermediate structures (Chatzidimitriou Dreismann, C.A. 1997). All of these theories are still being discussed nowadays, with the proton-hopping mechanism named after Grotthuss being the most accepted one.

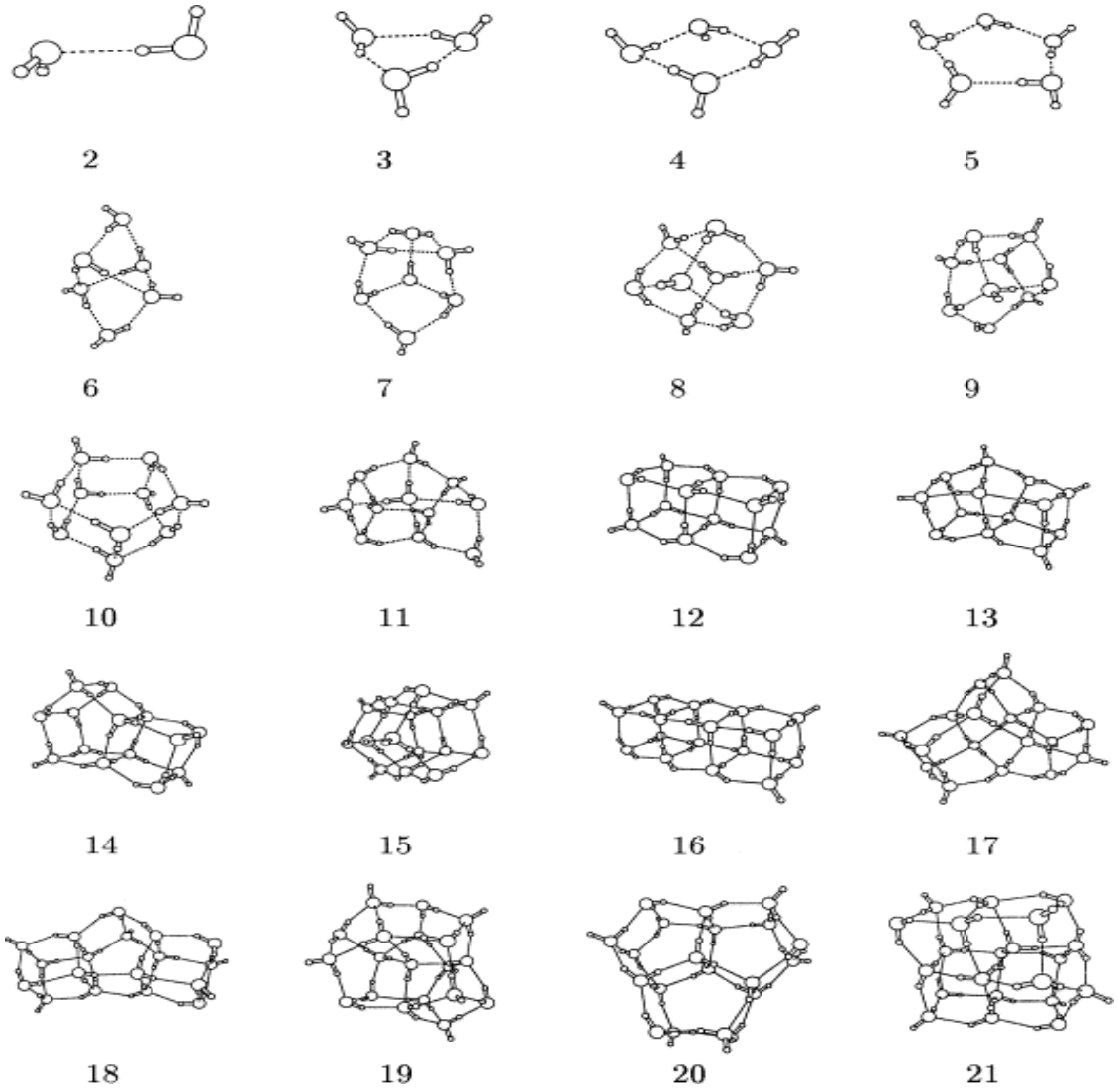

Fig. 2: Water clusters at their potential minima (Wales, D.J. 1998)

In the course of a better understanding of the involved physical phenomena, the next section will deal with important interaction possibilities described in the literature of a dipole molecule in an electric field: See Appendix Part IV for a chronologically detailed description in literature.

2.4 Definitions

2.4.1 Dielectrophoresis

Sumoto (Sumoto, I. 1955) and Pohl (Pohl, H.A. 1958) investigated the influence of electric fields on dielectric liquids and thereby founded the field of dielectrophoretic research. A non-uniform field force acting on all permanent or induced dipoles causes them to be constrained to move towards the region of highest field density (Pohl, H.A. 1951). The difference in electrophoretic mobility (a function of the electric field strength E and the viscosity of the solvent η) between particles and solvent decides whether coagulation will occur or not.

2.4.2 Electric double layer

When putting a solid body into a liquid, an electrical region in the vicinity to the surface of the body is formed due to the interactions of different chemical, physical, coulomb forces and thermal movement. Next to the charged surface a layer of hydrated counter ions builds the so-called Stern layer. The Stern layer can be categorized into an inner Helmholtz layer (IHL) and an outer Helmholtz layer (OHL). Ions beyond the IHL form the Gouy- Chapman or diffuse layer. This layer is governed by electrostatic forces only, whereas within the IHL adsorption and other chemical mechanisms, except Coulomb forces, dominate. Behind the diffuse layer potential which is marked by the end of the outer Helmholtz plane the potential drops to a value 1/e. This is called the zeta-potential often used for contact angle measurements (see 2.4.7).

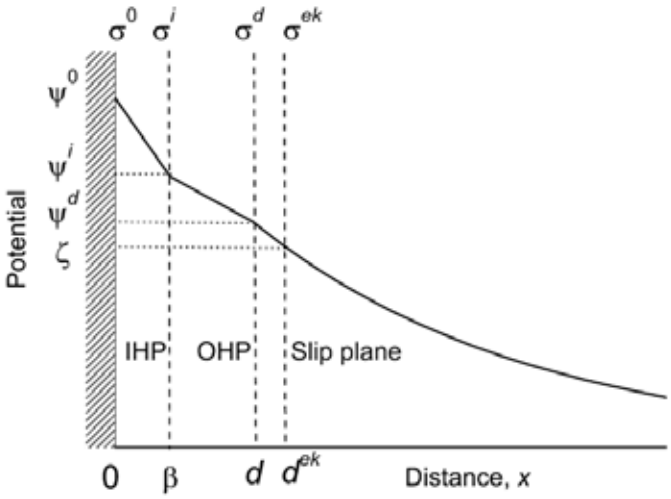

Schematic representation of the charges and potentials at a positively charged interface. The region between the surface (electric potential ψ^0; charge density σ^0) and the IHP (distance β from the surface) is free of charge. The IHP (electric potential ψ^i; charge density σ^i) is the locus of specifically adsorbed ions. The diffuse layer starts at $x = d$ (OHP), with potential ψ^d and charge density σ^d. The *slip plane* or *shear plane* is located at $x = d^{ek}$. The potential at the slip plane is the *electrokinetic* or *zeta*-potential, ζ; the *electrokinetic charge density* is σ^{ek}.

Fig. 3: Graphic representation of the different zones close to a charged surface, see text above for detailed explanations (Delgado, A. V. 2005)

2.4.3 Electrohydrodynamics (EHD)

Based on Maxwells' theories and conservation' of momentum and mass equations, EHD is based upon a set of differential equations for the description of the conversion of electrical energy in kinetic energy and vice versa in solutions. Two main aspects of electric fields in a fluid media are the change of hydrostatic pressure and an induced potential difference at the electrodes EHD considerations play a key role in: electrophoresis, electrokinesis, dielectrophoresis, electro-osmosis and electrorotation. Quantum-mechanical refinements of EHD considerations are called QEHD.

2.4.4 Electrooptic (Kerr-) effect

Birefringence is induced in dielectric liquids when an external electric field is applied, but in contrast to the Pockels effect, electro-optic Kerr effect is proportional to the square of the field strength, but needs much higher electric fields This nonlinear optical effect is often witnessed with intense beams (e.g. lasers) or used in a Kerr cell to modulate light.

2.4.5 Electroosmosis

In general, the motion of a liquid through an immobilized set of particles, a porous plug, a capillary, or a membrane, in response to an applied electric field is called electroosmosis. It is the result of the force exerted by the field on the counter-charge in the liquid inside the charged capillaries, pores, etc. The moving ions drag along the liquid, in which they are embedded. The electroosmotic velocity, v_{eo} (m s^{-1}), is the uniform velocity of the liquid far from the charged interface. Usually, the measured quantity is the volume flow rate of liquid (m^3 s^{-1}) through the capillary, plug, or membrane, divided by the electric field strength, Q_{eo},E (m^4 V^{-1} s^{-1}), or divided by the electric current, Q_{eo},I (m^3 C^{-1}). A related concept is the electro-osmotic counter-pressure, Δp_{eo} (Pa), the pressure difference that must be applied across the system to stop the electro-osmotic volume flow. The value Δp_{eo} is considered to be positive if the high pressure is on the higher electric potential side.

2.4.6 Electrophoresis

Electrophoresis is the movement of charged colloidal particles or polyelectrolytes immersed in a liquid under the influence of an external electric field. The electrophoretic velocity, v_e (m s^{-1}) is the velocity during electrophoresis. The electrophoretic mobility, μ_e (m^2 V^{-1} s^{-1}), is the magnitude of the velocity divided by the magnitude of the electric field strength. The mobility is considered positive if the particles move toward lower potential (negative electrode) and negative in the opposite case.

2.4.7 Electrowetting

Gabriel Lippmann investigated effects of electrocapillarity in 1875, which laid the basis of modern electrowetting. The electric charges in water on a surface are free to move, and so with the operation of the voltage the positive and negative charges are concentrated in different locations of a droplet. The forces operating on the charges within the liquid cause the contact region between the droplet and the metal to widen. They also cause a certain flattening of the droplet. Thus, by means of electric voltage the amount of wetting of a droplet

can be controlled precisely. Electrowetting has a number of interesting applications which have recently been developed. They are all based on the possibility of using an external electric field without mechanical parts to control movement or a quick change (hundredth of a second) between numerous states of the system. It is important to point out that with this technique systems can be miniaturized to scales of less than a millimeter and still be controlled with great precision using a miniscule amount of energy for a long period of time. Applications from recent years include transport of liquids for purposes of changing the characteristics of optical conductors and creating optical switches, cooling of electronic circuits by transport of cold drops across them, transport of micro-drops for purposes of printing, suction of liquids in microtubes, and lab-on-a-chip applications for analysis of the chemical composition of liquids, particularly physiological liquids (blood, urine…) by means of transport of drops of the fluid to examination cells on the chip. There they are mixed with other chemicals and undergo various optical measurements, all at miniscule length scales of less than one millimeter.

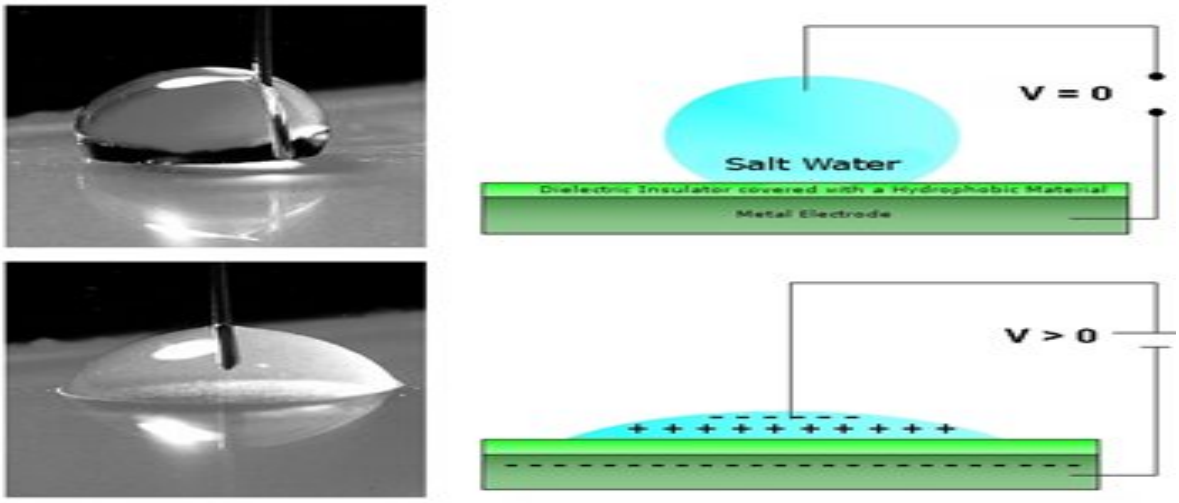

Fig. 4: Contact angle change of water in dependence of applied voltage on a metal surface covered with a hydrophilic material (left: picture; right: scheme)
(http://physicaplus.org.il/zope/home/en/1185176174/water_elect_en)

2.4.8 Faraday effect

This phenomenon concerns the interaction of a magnetic field with light in a medium, causing a rotation of the plane of polarization. The polarization plane of a transparent dielectric is linearly proportional to the magnetic field in the direction of propagation. This effect is used in e.g. optical isolators and optical circulators as well as a remote sensor for magnetic fields.

2.4.9 Leyden jar

First found by Muschenbroek and von Kleist (1745); a glass beaker filled with water and an outer and inner electrode can store charge and therefore act as a capacitor when an electrostatic machine is connected to the inner electrode. When short-circuiting the round inner electrode with the outer electrode a discharge is produced. It is named after the Dutch city in which Muschenbroek taught at this time.

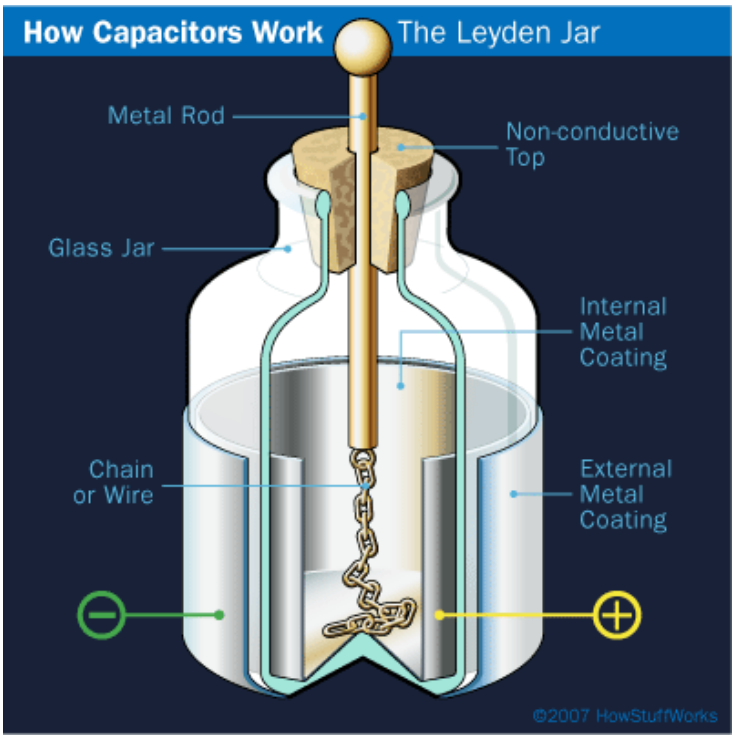

Fig. 5: Working principle of a leyden jar (from: http://electronics.howstuffworks.com/capacitor3.htm)

2.4.10 Liquid bridging

A vertical or horizontal column of dielectric liquid, pinned at each end between planar electrodes, and surrounded by a non-conducting dielectric gas which is formed due to AC or DC fields, can be called a liquid bridge. The theoretical basics were set by Melcher and Taylor in the late sixties, by introducing the leaky dielectric model for polar solvents (Saville, D.A. 1997). This model proposes that 'whenever interfacial regions do exist in a fluid system, and electrical parameters suffer discontinuity, the electromechanics of these interfaces dominate the electrohydrodynamics of the system. If, e.g. a liquid surface supports a surface charge, tangential electric fields and interfacial electrical shear forces are induced leading to cellular convection in the liquid.'(from Woisetschläger, J. 2012)

2.4.11 Pockels effect

Applying an electric field to an optic medium evokes birefringence linearly proportional to the field strength. The effect can only occur to non-centrosymmetric crystals with no inversion symmetry. This effect is used when crystals like lithium niobate or gallium arsenide are combined with a polarizer to create shutters which can modulate laser pulses.

2.4.12 Pellat effect

Pellat demonstrated in 1896 (Pellat, H. 1896) that an insulating dielectric liquid rises upwards against the pull of gravity when a voltage is applied between parallel electrodes. The height–of-rise can be approximated with equation (1) if the plate spacing is small enough and an uniform electric field is given.(Jones, T.B. 2002)

$$h \approx \frac{(\kappa_1 - 1)\epsilon_0 E^2}{2\rho_1 g}$$

equation (1): h…rise of height, ρ_1….density of liquid, ε_0…dielectric constant of vacuum, g…gravitational constant ,κ dielectric constant, E…electric field (Jones,T.B. 2002)

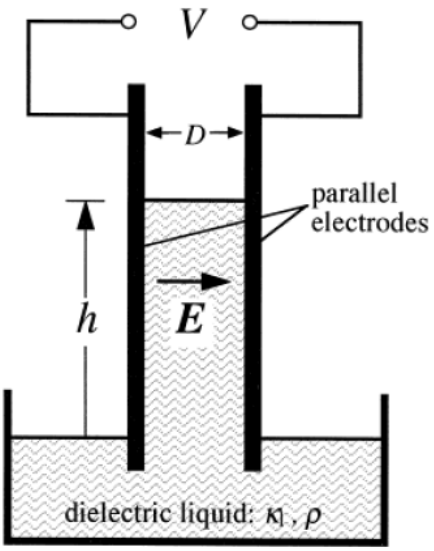

Fig. 6: Scheme of Pellat's experiment (Jones, T.B. 2002)

2.4.13 Quantum hall effect

When current is sent through a conductor at low temperatures and a magnetic field is applied perpendicular to the current, the resistance of the material is quantized in units of h/e^2 divided by an integer.

2.4.14 Taylor cone

When the interface between an electrically conducting liquid and an insulator (often air or a vacuum), but sometimes a dielectric liquid (Barrero, A. 2004) is charged electrically beyond a certain critical level, it becomes unstable and evolves from a rounded shape to another, including several remarkably stable conical features called Taylor cones. The angle of this cone structure has been shown to be exactly 98.58°(de la Mora, J. F. 2007). The biggest application nowadays is in Electrospray ionization- Mass spectrometry, in which an analyte solution is ionized very softly, forming positively or negatively charged analyte-pseudomolecules.

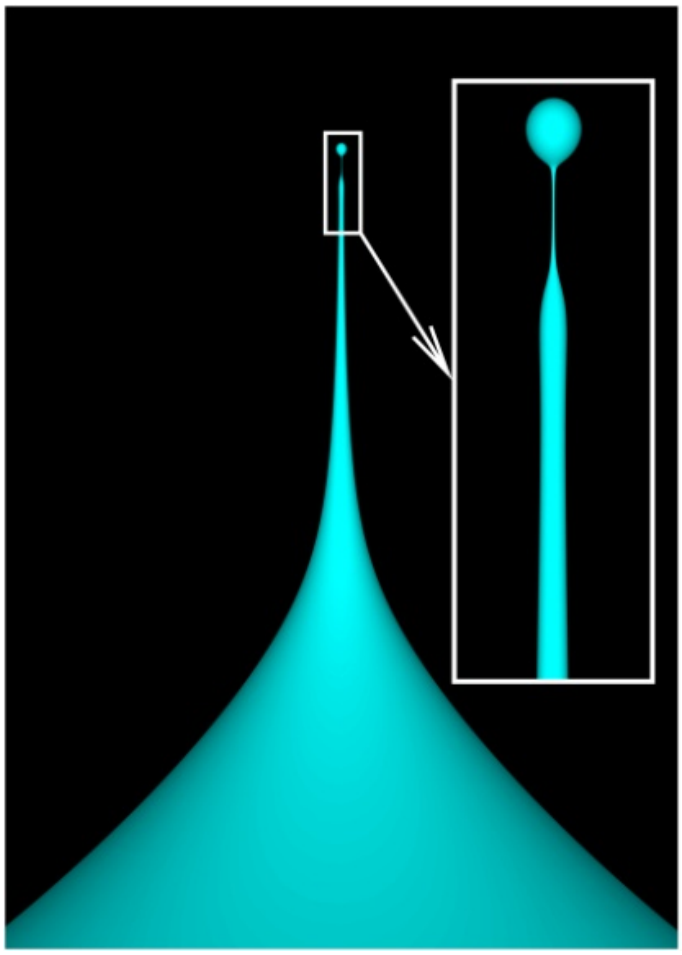

Fig. 7: Taylor cone angle and droplet formation (schematic) (http://news.uns.purdue.edu/images/+2007/basaran-droplet.jpg)

2.5 Organic compounds

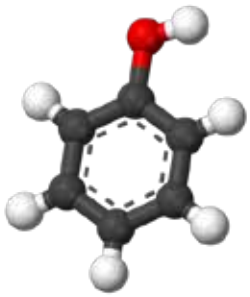

Phenol, , is the simplest aromatic alcohol with oxygen donating p electrons into the aromatic system. The pK_a is around 10, which makes it one million times more acidic than any aliphatic alcohol, but not as acidic as carbonic or carboxylic acids. The enol form is dominant with an equilibrium constant of 10^{13} in the enol:keto tautomerism. Main applications of this substance include the condensation with acetone to produce Bisphenol-A (polycarbonates, epoxies), the hydrogenation to cyclohexanone (nylon precursor), or the alkylation and subsequent ethoxylation to form non-ionic detergents. Furthermore, it is the starting point for the synthesis of aspirine and similar pharmaceuticals. (http://en.wikipedia.org/wiki/Phenol)

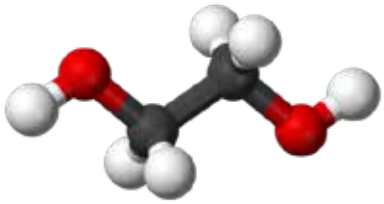

Ethylene glycol, , is an aliphatic alcohol compound with a hydroxyl group each at C 1 and C 2. Main uses include the production of PET melt, its application as antifreeze compound and as a desiccant. It is also used in pipelines to prevent gas clathrate formation; it is a good corrosion inhibitor and if frequently used in the manufacture of capacitors. (http://en.wikipedia.org/wiki/Ethylene_glycol). Next to these, some other substances were tested in a liquid bridging set- up. Table 1 gives an overview of important physical parameters of both phenol and ethylene glycol; table 2 provides similar information for Hydrochinone, Pyrogallol, Bisphenol A and p-Cresol, and table 3 contains data about the Rhodamine B and Calceine.

Table 1: Physical properties of phenol and ethylene glycol

CAS no.:	108-95-2	107-21-1
Molecular formula	C_6H_6O	$C_2H_6O_2$
Molar mass	94.11 g mol^{-1}	62.07 g mol^{-1}
Appearance	Transparent, crystalline solid	transparent fluid
Density	1.07 g cm^{-3}	1.113 g cm^{-3}
Melting point	314 K	260 K

Boiling point	455 K	470 K
Solubility in water	83 g l^{-1} (20°C)	Miscible in all proportions
Dipole moment	1.7 D	2.28 D

Table 2: Physical properties of Hydrochinone, Pyrogallol, Bisphenol-A, p-Cresol

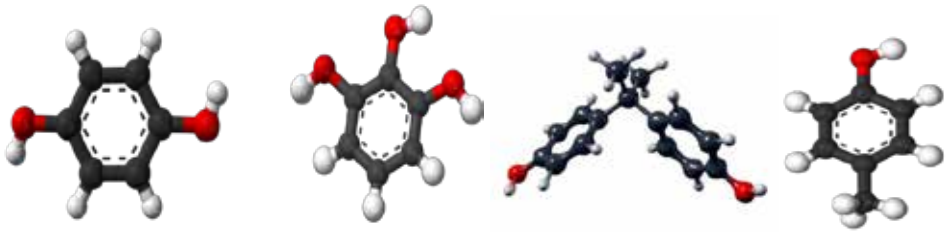

Substance	Hydrochinone	Pyrogallol	Bisphenol A	p-Cresol
CAS no.:	123-31-9	87-66-1	80-05-7	106-44-5
Molecular formula	$C_6H_6O_2$	$C_6H_6O_3$	$C_{15}H_{16}O_2$	C_7H_8O
Molar mass	110.11 g mol^{-1}	126.11 g mol^{-1}	228.29 g mol^{-1}l	108.14 g mol^{-1}
Appearance, color	Crystalline, colorless	Crystalline, beige	Crystalline, beige	Crystalline, colorless
Density	1.332 g cm^{-3}	1.450 g cm^{-3}	1.2 g cm^{-3}	1.034 g cm^{-3}
Melting point	172 - 175 °C	131.0 – 135.0 °C	155-156	34.8 °C
Boiling point	285 °C	309 °C	360 °C	202 °C
Solubility in water	50 g l^{-1} (20°C)	soluble	300mg l^{-1} (20°C)	20g l^{-1} (20°C)

Table 3: Physical properties of Rhodamine B and Calceine

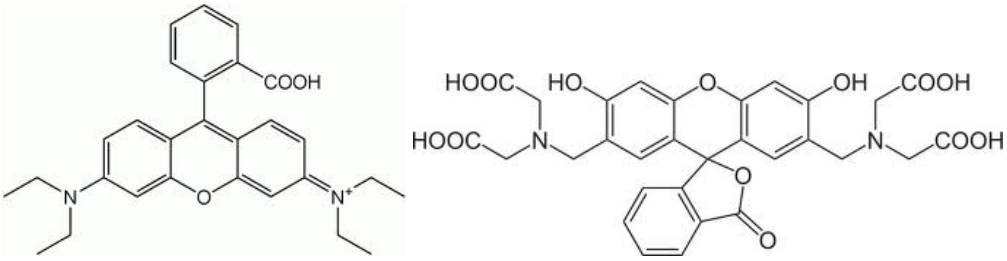

Substance	Rhodamine B	Calceine
CAS no.:	81-88-9	1461-15-0
Molecular formula	$C_{28}H_{31}ClN_2O_3$	$C_{30}H_{26}N_2O_{13}$
Molar mass	479.02 g mol^{-1}	622.53 g mol^{-1}
Appearance, color	Crystalline, green	Crystalline, orange
Density	0.79 g cm^{-3}	-
Melting point	210 - 211°C	200 °C
Solubility in water	soluble	4 g l^{-1} (20°C)

2.6 Inorganic compounds:

Table 4 contains a summary of the inorganic substances tested in a liquid bridging set-up including some important physical and chemical properties.

Table 4: Physical properties of sodium triphosphate, sodium carbonate, ammonium hydroxide, sodium thiocyanide and calcium carbonate

Molecular formula	Na_3PO_4	Na_2CO_3	NH_4OH	NaSCN	$CaCO_3$
Molar mass	163.94 g mol^{-1}	105.97 g mol^{-1}	35.04 g mol^{-1}	81.07 g mol^{-1}	100.09 g mol^{-1}
Appearance, color	White, crystalline	White, crystalline	White, crystalline	White, crystalline	White, crystalline
Density	2.52 g cm^{-3}	2.54 g cm^{-3}	0.91 g cm^{-3}	1.73 g cm^{-3}	2.71 g cm^{-3}
Melting point	622 °C	851 °C	-57.5 (25%)	287 °C	1339 °C
Boiling point	-	1633 °C	37.7 (25%)	-	-
Solubility in water	14.5 g l^{-1} (20°C)	-	miscible	1,39 kg l^{-1} (21 °C)	1.5 g l^{-1} (25°C)

3 Analytical techniques

3.1 SEM-EDX

Scanning electron microscopy- energy dispersive x- ray analysis (SEM- EDX) is a method to quantify the elemental composition of a metal surface on a micrometer scale. Since precipitation occurs at the electrodes when a phenol solution is used in a liquid bridge set-up, it was the method of choice for investigation of the deposited layer on the anode.

The principle of SEM- EDX is that a high energy electron beam is focused on a small surface area of the specimen. The electrons are scattered on and beneath the surface molecules (wavelength- dependent: penetration depth: ~1000nm; see Fig.8) and the energy of the released electrons is characteristic for the specimens' elements. This x- ray response is detected, converted into voltage signals and processed via an analyzer which arranges the collected data into an interpretable spectrum. This process is repeated for the selected area rendering an elemental topography of the surface.

The interaction of the electron beam with the outer shells of the atoms of the surface results either in an excitation of the shell electrons, in an electron- hopping mechanism (see Jablonski diagram), or their ejection (x- ray). This process is statistically dependent on the energy of the incident beam and the mass of the atoms. In general, heavier atoms produce a weaker x-ray signal and a higher energy content of the beam produces excitations of even deeper shells.

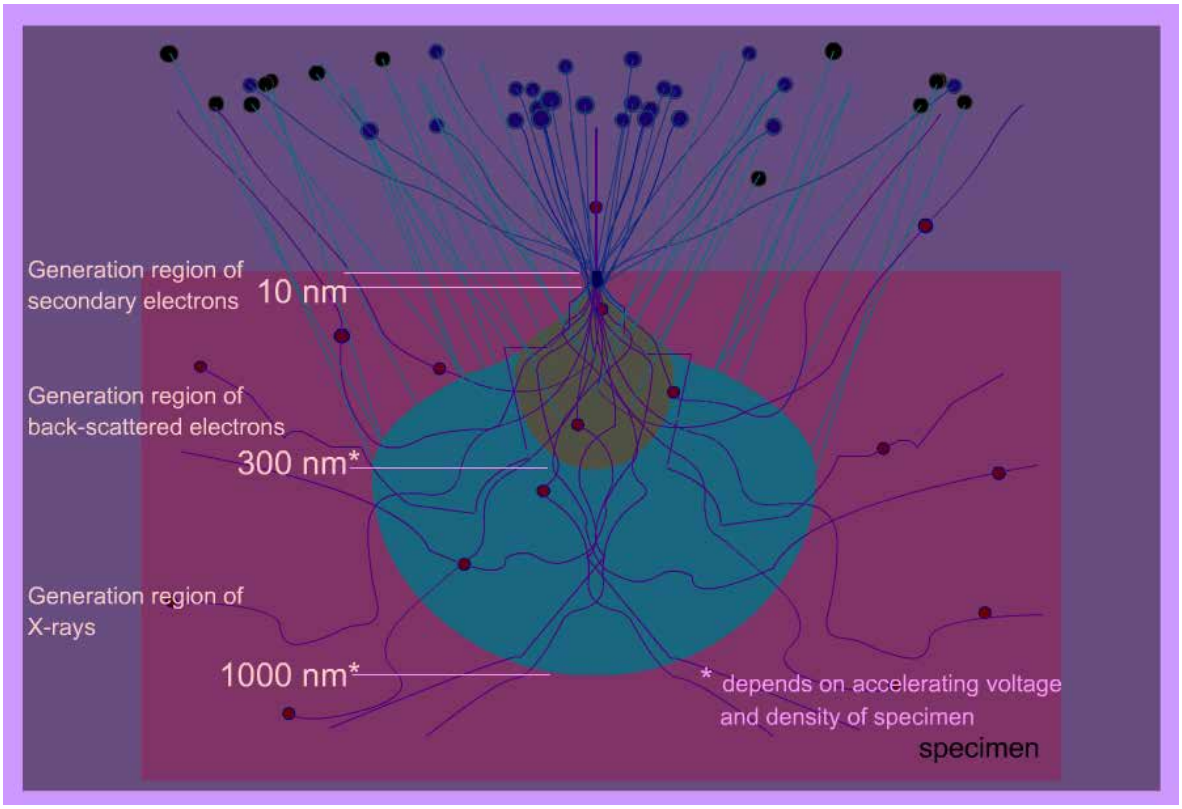

Fig. 8: Interaction possibilities of an electron beam with a solid surface (Saf, R. 2010)

Fig. 9: Hitachi S-640 SEM-EDX of Tohuku University, Japan
(http://www.tech.eng.tohoku.ac.jp/sosiki/goudou/jpg/SEM-EDX.jpg)

3.2 GC-MS

In this work an adequately altered GC-MS procedure was used to quantify the ethylene glycol content in the aqueous samples. In a GC-MS system the gaschromatograph performs the separation of the sample, the mass spectrometer acts as analyzer. In principle, gas chromatography is dependent on the volatility and the solubility of the component under examination. If these basic requirements are fulfilled by the compounds, evaporated analytes in the sample are transported through a metal column (made of metal or glass) with an inner layer (stationary phase for capillary gas chromotagrophy) by the means of a mobile phase (carrier gas). The interactions of the more or less polar analytes in this two-phase system are responsible for their separation. The column is subject to a specific temperature gradient in order to increase fractionation and sensitivity. Different column matrices are available for an optimal interaction of the stationary phase with the analyte, resulting in sharp, clearly separated peaks. Many different materials are used for the stationary phase in order to guarantee efficient working conditions over a broad polarity spectrum. Moreover, parameters like column diameter, film thickness, particle size and length of a column have to be optimized to get reasonable results. Possible carrier gases are hydrogen, helium, nitrogen, argon or air, depending on the detector and compounds to be analyzed.

The gas flow is then connected to a mass spectrometer inlet, in which the gaseous analytes get ionized. For detection, the ionized pseudomolecules are transported through an, e.g., electromagnetic field (quadrupole), which is tuned in a way to only let through certain mass/charge ratios. These ions are in the final step counted with a photomultiplier. The intensities of the ions are proportional to their concentration in the sample.

3.3 Photometric quantification

Phenol has a conjugated p-electron system and is therefore sensible to radiation in the range between 250-400nm, which is absorbed by the aromatic system. A standard procedure for the determination of its concentration is to measure the transmission or absorption in the range of near UV (200-400 nm) up to near IR (800-2500 nm). According to Lambert-Beers' rule every substance has a discrete extinction coefficient, which multiplied with the cell length and the concentration gives a certain absorption (see equation 2). If the absorption can be measured and the length of the cuvette and the extinction coefficient of the substance are known, the concentration of the analyte can be calculated. Limitations of this method are,

e.g.: the media does not scatter the incident light; the sample is inhomogenous; there is no turbidity in the cuvette; the incident radiation is monochromatic and parallel; and there is no photoactivity of the analytes with the incident radiation.

$$A = \frac{\log I}{I_0} = \varepsilon \; c \; d$$

equation (2): A…absorption, I…light intensity, I_0…incident light intensity, ε…absorption coefficient, c… concentration, d… cell length

For a quick test of Phenol we used the test kit LCK 345 with a Dr. Lange spectrometer, using an indirect measuring principle by conversion of the colorless phenol into the oxidized form of indophenolhydrogensulfate (yellow to red) via nitrification and condensation. This process is described below.

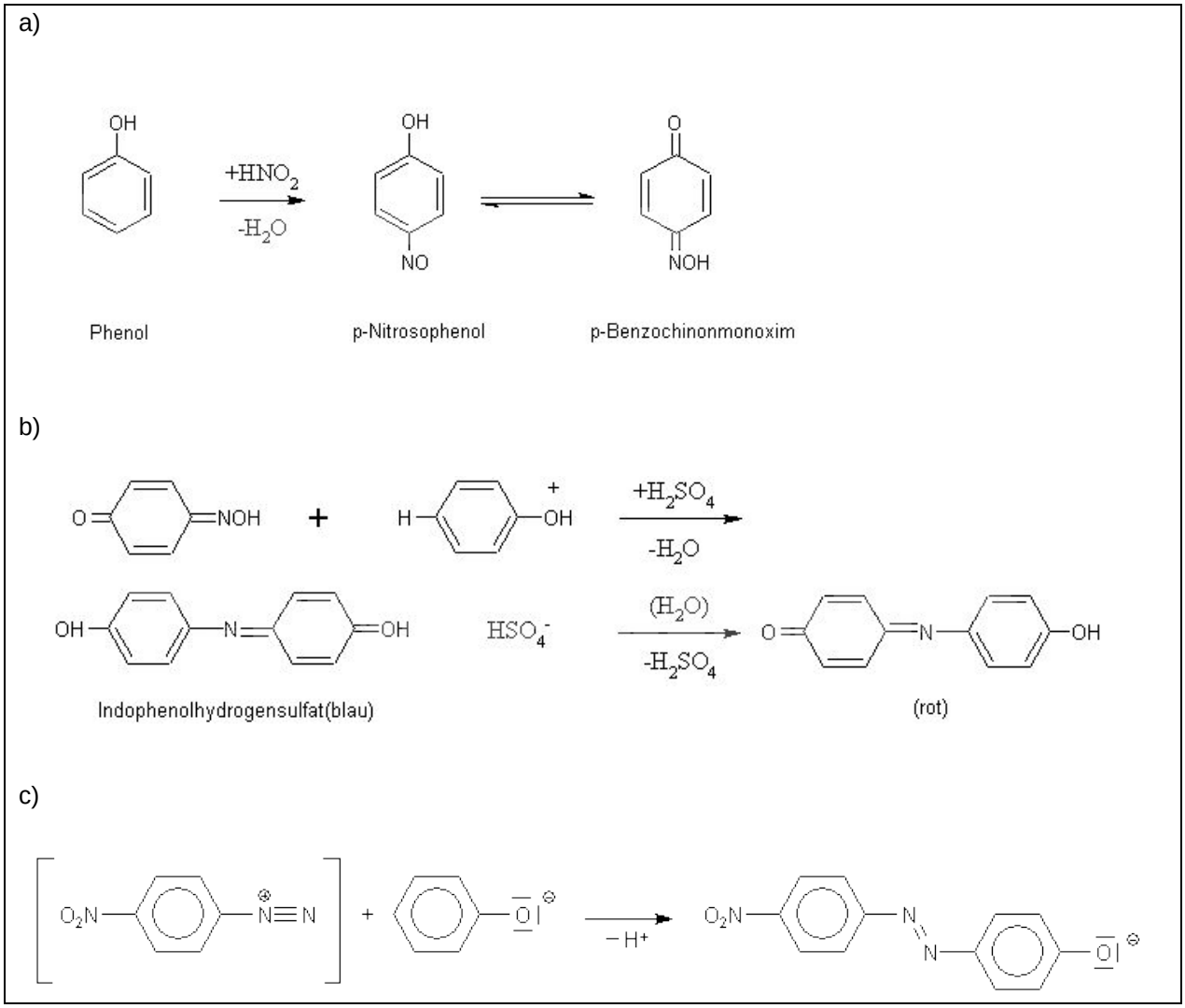

Fig. 10: Reaction pathway of phenol with sodiumnitrite to form a photometric quantifiable product (http://www.chemieunterricht.de/dc2/phenol/nachw.htm)

In the test sodium nitrite reacts with phenol to p-Nitrosophenol, which is mesomeric to p-Benzochinonmonoxim (see Fig. 10a). Under acidic conditions, this product condensates forming a red dye (Fig. 10b). Better results are attainable if p-nitroaniline is freshly diazotidated and the solution of the salt is mixed with the basic phenol solution. If traces of phenol are existent, an orange- red dye will be produced after (Fig. 10c).

4 Experimental details

4.1 Preliminary tests

Feasibility tests were carried out to make sure that the planned concentration ranges of the different compounds support a stable water bridge and that the equipment worked properly and repeatable.

The bridge surface area was tested for linear function of the resistance and the current density was also determined as a function of the voltage (see Fig. 11). These tests were made for pure water and a 106 µmol phenol solution.

Fig. 11: Bridge diameter as function of applied potential and current in water (a: 7 kV, 5mA; b: 11 kV, 5 mA; c: 22 kV, 5 mA)

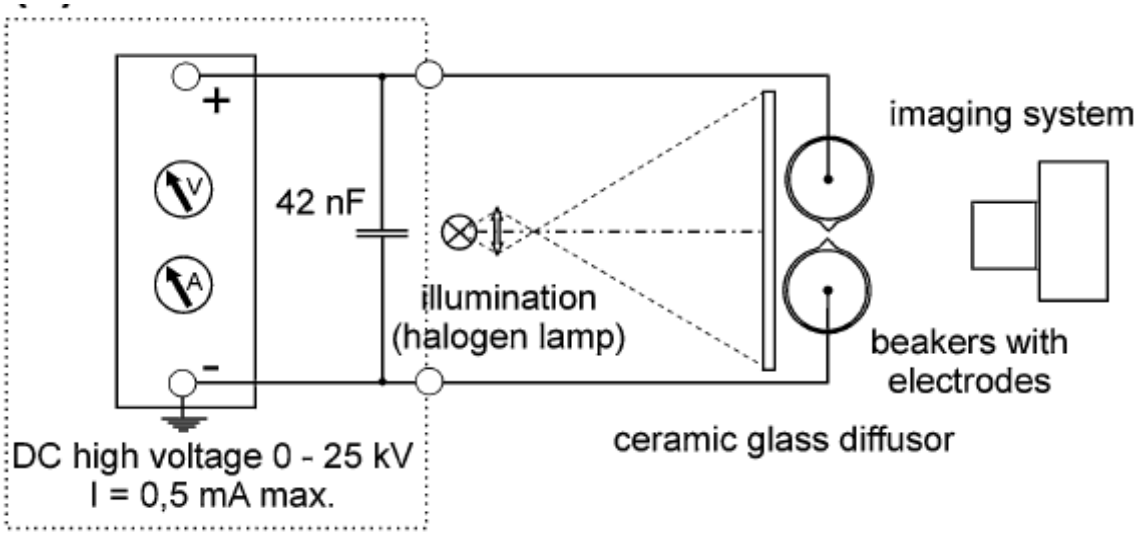

Fig. 12: Scheme of experimental setup used for measurements **(Woisetschläger, J. 2012)**

Table 5: List of conducted bridge experiments (Eisenhut, M. 2011).

Nr.	Cathodic beaker		Anodic beaker		Analyses
	substance	conc.	substance	conc.	transport,
1a	**phenol**	1 mM	water		transport,
1b	water		**phenol**	1 mM	transport,
2a	**phenol**	10 mM	water		transport,
2b	water		**phenol**	10 mM	transport,
3a	**phenol**	0.53 mM	**phenol**	0.53 mM	concentration
3b	**phenol**	5 mM	**phenol**	5 mM	concentration
3c	**phenol**	10 mM	**phenol**	10 mM	concentration
3d	**phenol**	50 mM	**phenol**	50 mM	concentration
3e	**phenol**	100 mM	**phenol**	100 mM	concentration
3f	**phenol**	531 mM	**phenol**	531 mM	SEM, EDX, optical
4a	**glycol**	10 mM	water		transport,
4b	water		**glycol**	10 mM	transport,
5a	**glycol**	3.6 mM	**glycol**	3.6 mM	concentration
5b	**glycol**	11.3 mM	**glycol**	11.3 mM	concentration
5c	**glycol**	46 mM	**glycol**	46 mM	concentration
5d	**glycol**	450 mM	**glycol**	450 mM	concentration
6a	**bisphenol-A**	100 µg l^{-1}	water		feasibility
6b	water		**bisphenol-A**	100 µg l^{-1}	feasibility
7a	**hydrochinone**	50 g l^{-1}	water		feasibility
7b	water		**hydrochinone**	50g l^{-1}	feasibility
7c	**hydrochinone**	500 mg l^{-}	water		feasibility
7d	water		**hydrochinone**	500 mg l^{-1}	feasibility
8a	**p-cresol**	100 µg l^{-1}	water		feasibility
8b	water		**p-cresol**	100 µg l^{-1}	feasibility
8c	**p-cresol**	100 mg l^{-}	water		feasibility
8d	water		**p-cresol**	100 mg l^{-1}	feasibility
9a	Water (ambient)		Water (warm)		
9b	Water (warm)		Water (ambient)		
10	**Na_3PO_4 (44C°)**	55mg l^{-1}	Water		feasibility
11a	**Na_2CO_3**	17mg l^{-1}	**NH_4OH**(54C°)	150mg l^{-1}	feasibility
11b	**NH_4OH**(57C°)	150mg l^{-1}	water		feasibility
11c	**Na_2CO_3(55C°)**		**NH_4OH**	150mg l^{-1}	feasibility
11d	**Water (40C°)**		**NH_4OH**	150mg l^{-1}	
12	Water(50C°)		**NaSCN**	57mg l^{-1}	feasibility
13	**$CaCO_3$**	195mg l^{-1}	Water(48C°)		feasibility
14	**Rhodamin B**	1mg l^{-1}	**Calcein**	1.5mg l^{-1}	feasibility

4.2 Phenol solutions

Phenol solutions were prepared with phenol for synthesis, Sigma Aldrich, purity: ≥99.9 and triply deionized water (Milli-Q system, Ω internal > 18 MΩ·cm) and stored in dark glass bottles until right before the experiment. The complete mixing was visually controlled and stirring was stopped after no crystals could be seen any more. Accuracy of the balance used was ±0.001g. For detection a Dr. Lange spectrometer with the appropriate quicktest was utilized, LCK 345, applicable in a concentration range between 0.05- 5 mgl^{-1}. The concentrations of the beakers were estimated after the experiment and, if necessary, diluted to the appropriate concentration.

4.3 Ethylene glycol solutions

The ethylene glycol solutions of ethylene glycole, VWR, purity: ≥99% and triply deionized water from the same Milli- Q- system mentioned above were prepared on an analytical scale with an accuracy of ±0,001g. The ethylene glycol was quantified using GC- MS (Agilent 6890 GC coupled with a 5973 MSD, Agilent, Waldbronn, Germany) with a polar capillary column consisting of cross-linked polyethylene glycol (Innowax, 30 m×2.5 mm×25 µm). The temperature gradient of 80°C to 260 °C with a heating rate of 10°C min^{-1} was used. The temperature of the injector was 250°C. The ionization energy was 70 eV (EI). The selected ion monitoring (SIM) mode was applied. An external calibration in the range of 0.05 to 6 mM was used for the quantification of ethylene glycol. The samples were diluted 10-100 times with water before measurements.

5 Results and Discussion

A 95 % confidence interval should be considered for all experiments. The self- saturation with carbon dioxide of the triply deionized water led to a conductivity increase over time from 0.18 to 2 µS cm^{-1}(Kendall, J. 1916). The separation of the beakers, after the experiment started, was done manually. The temperature of the solution was dependent on daytime and on the resistive heating of the more or less conducting liquid, caused by the applied high voltage and their tendency to produce sparks prior to the bridge build- up.

5.1 Typical bridge instabilities

Of all the experiments conducted about 20% resulted in unstable bridges and did thus not allow evaluation. In these ‘breakdown’, ‘sparking’ or ‘dripping’ cases, some reasons for the instability could be identified. Often polluted solutions/beakers or not prethermostatted solutions as well as manual mistakes e.g.: no contact of the beaker’s spouts at the start or fast separation of the beakers resulted in unstable bridging. Also, in some cases the applied current/voltage was too high too early and led to several of the before mentioned events after short operation time (see Fig. 11). One special feature was visually detectable in the case of phenol: a thin layer of phenol degradation products was adsorbed on the platinum anode, leaving a brown- golden layer on the electrode, favorably on the front side. This layer could not be simply washed off, but had to be cleaned off with a concentrated solution of hydrogen peroxide (20%) after each experiment.

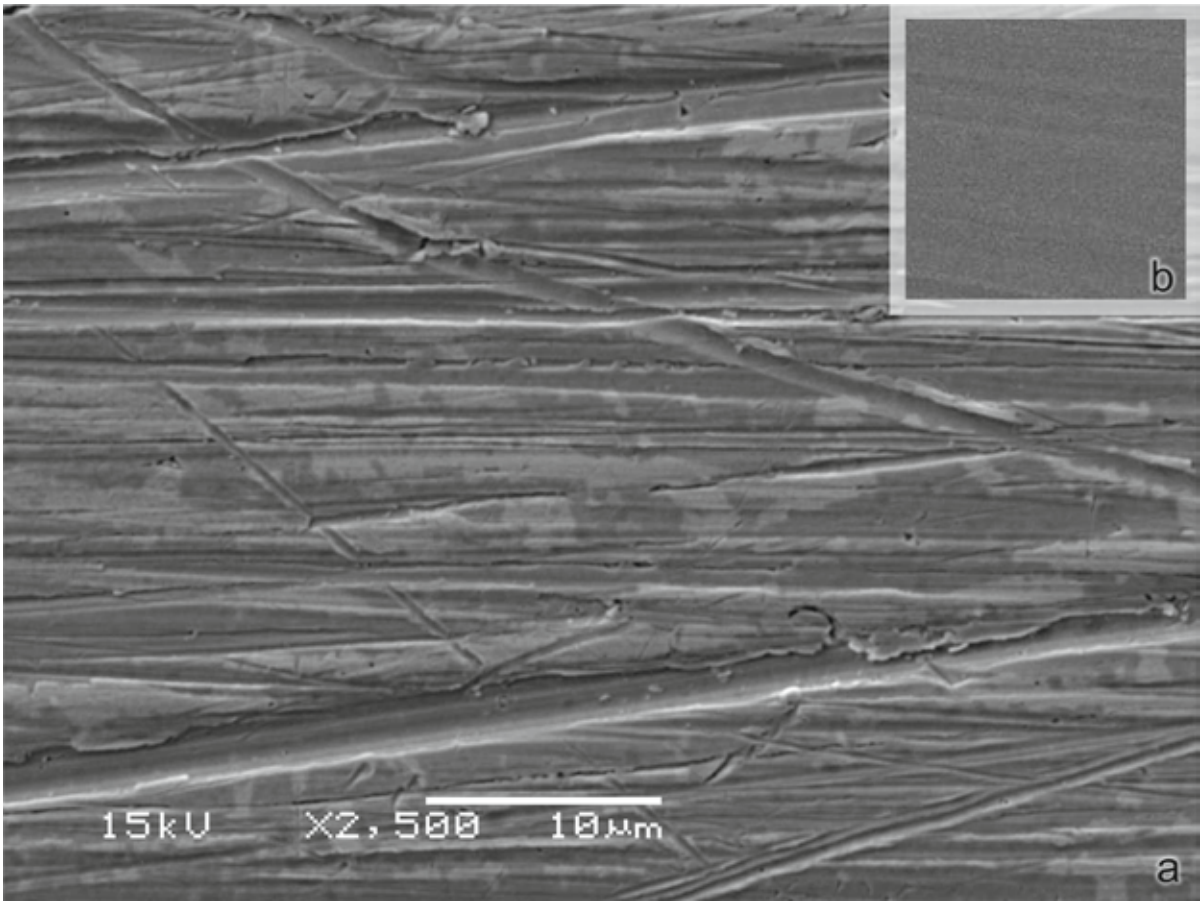

Fig. 13: (a) SEM-picture of the anode electrode surface after 600s in a 0.5M phenol solution at 9 kV and 0.75 mA, (b) picture of the cathode electrode surface under same conditions (same magnification) (Eisenhut, M. 2011)

Sometimes the reason could not be clearly identified, but left some interesting facts behind: For example, a highly concentrated hydroquinone solution (50 g l^{-1}) in the anodic beaker led to the formation of giant bubbles, occasionally running through the bridge region, from cathode to anode, thereby destabilizing the mass transport (see Fig. 14).

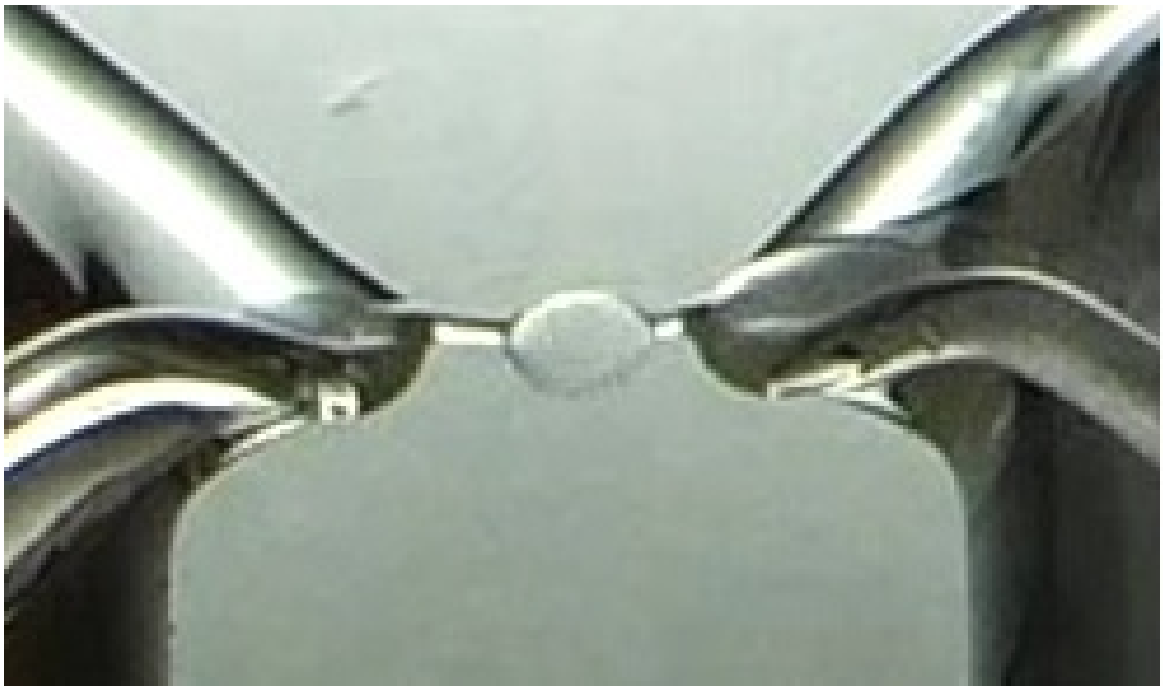

Fig. 14: Bubble running through the bridge (from right to left); 50 gl^{-1} hydrochinone in anodic beaker (left)

5.2 Temperature/ conductivity dependencies

In each experiment temperature and conductivity were recorded manually right before the start of each experiment and directly after the high-voltage supply was switched off. The individual deviance from experiment to experiment made it difficult to always measure at the same time intervals. Nevertheless, the charts (Fig 18, 19, 22, 23, 30, 31) help to better understand the electrochemical (dissociation, recombination, adsorption) and physical (resistive heating, conductivity changes) processes which took place during the experiments.

The conductivity in particular played a limiting role, since the bridges always broke down above ~50 µS cm^{-1}. As one can see in the charts, the initial concentration of the organic compounds did not make a big difference to the final conductivity of the solution. Moreover, it became clear that the flow direction (anode→ cathode; cathode→ anode) of the organic compound also changed the amount of polymers precipitated on the anode (in the phenol case) and the conductivity increase for both substances. Detailed discussion can be found in the phenol solution / ethylene glycol solution section.

The temperature was did not prove to be a limiting factor since the stability of the bridge was not noticeably influenced in the range between 15- 60 C°. In general, the temperature rise was linear over time and in the area of 5 C° over 600 s, staying the same even with lower heat capacities in the more concentrated (0.531 mM) solutions.

5.3 Phenol solutions

With phenol as a lead substance, it was investigated whether aromatic compounds in general can be transported through the bridge region and if so, if a preferred stream direction or other effects induced by the compound would exist. Possible concentration effects were the reason to measure at two different concentrations, 1 mM and 10 mM.

To be able to study the transport rates and to calculate a theoretical linear equilibrium (TLE), different operation times (between 30 and 3060 s) of the bridge showed that the mass transport is rather hyperbolical than linear. The reason for this was that only in the first moment of bridging a mono-directional flow of pure water into organic solution and vice versa occurs. Nevertheless, a linear extrapolation as a first approximation proved to be a good opportunity to compare the transport phenomena at different concentrations of phenol.

For the 1 mM series (1a, 1b, see table) the flow direction was the same as for pure water. So, while the water got transported from anode to cathode until a labile equilibrium was reached, the effects of heating of the solution, decomposition of phenol, absorption on the electrode and conductivity changes were under investigation. The results for these series can be seen in Fig. 16 and Fig.17. The interesting fact that no abnormalities in comparison to pure water occurred favor the assumption that the electrophoretic transport phenomena were not prominent at a phenol concentration that low. The heating of the solutions and the small conductivity increase in the anode beaker were comparable to pure water. The TLE, which is defined as the linearly extrapolated time to achieve the exact same concentration of organic compound in both beakers support the hypothesis that the system was not influenced by phenol addition. The TLE times for series 1a and 1b were 4623 s and 4667 s, respectively.

Experiments series 2a and 2b (Figs. 20, 21), with a concentration of 10 mM of phenol either in the anode or cathode beaker changed the analytical situation completely: The decrease of phenol in the cathode beaker was much faster than the increase in the anode beaker, which supports the theory that oxidation processes are involved at the anode. This oxidation seems to be favored by a low concentration of phenol, so that in the case, when phenol was in the anode beaker, oxidation processes were hindered more than when the phenol was in the cathode beaker. The flow direction also changed which can be seen in Figs. 20 and 21, with TLE times of 3124 s (anode to cathode) and 3974 s (cathode to anode), thereby not influencing the net mass transport direction from anode to cathode. A conductivity increase for series 2a and 2b (Figs. 22, 23) was found in the anode beaker only, leaving the cathode beaker seemingly uninvolved to the intermediate structures formed by the oxidation at the anode. The decomposition was accompanied by an adsorption of phenol degradation

products on the anode, for high concentrations visible as a golden-brownish layer remaining on the electrode.

The anode reactions of aqueous phenol solutions in low voltage electrolysis are very well understood and discussed in the literature (Gattrell, M. 1993; Fino, D. 2005; Andreescu, S. 2003; Li, X. Y. 2005). In low-voltage electrolysis an inhibited electrochemical process takes place on the anode platinum surface; Gattrell and Kirk showed that the oxidation of phenol to a phenoxy- radical- and subsequent quinone- and ether structures at the outer Helmholtz layer is followed by an oxidation of these structures at the inner Helmholtz layer leading to a polymeric film on the anode, carboxylic acids in solution and finally CO_2 (see Figs. 24, 25). The formation of such a layer is common for low-voltage electrolysis of phenolic solutions (see also Fino, D. 2005; Andreescu, S. 2003; Li, X. Y. 2005) and was also found in the current experiments. Gas formation at the anode could be observed as well, albeit only at very high (Exp. 5f, c = 50 g L^{-1}) concentrations (see Figs. 13 and 23). The chemical composition determined with EDX revealed a surface composition of 51% Pt, 46% C and 3% O (atom %, see table 6), which is consistent with partial covering of the electrode with the polymeric film mentioned above (see Fig. 15).

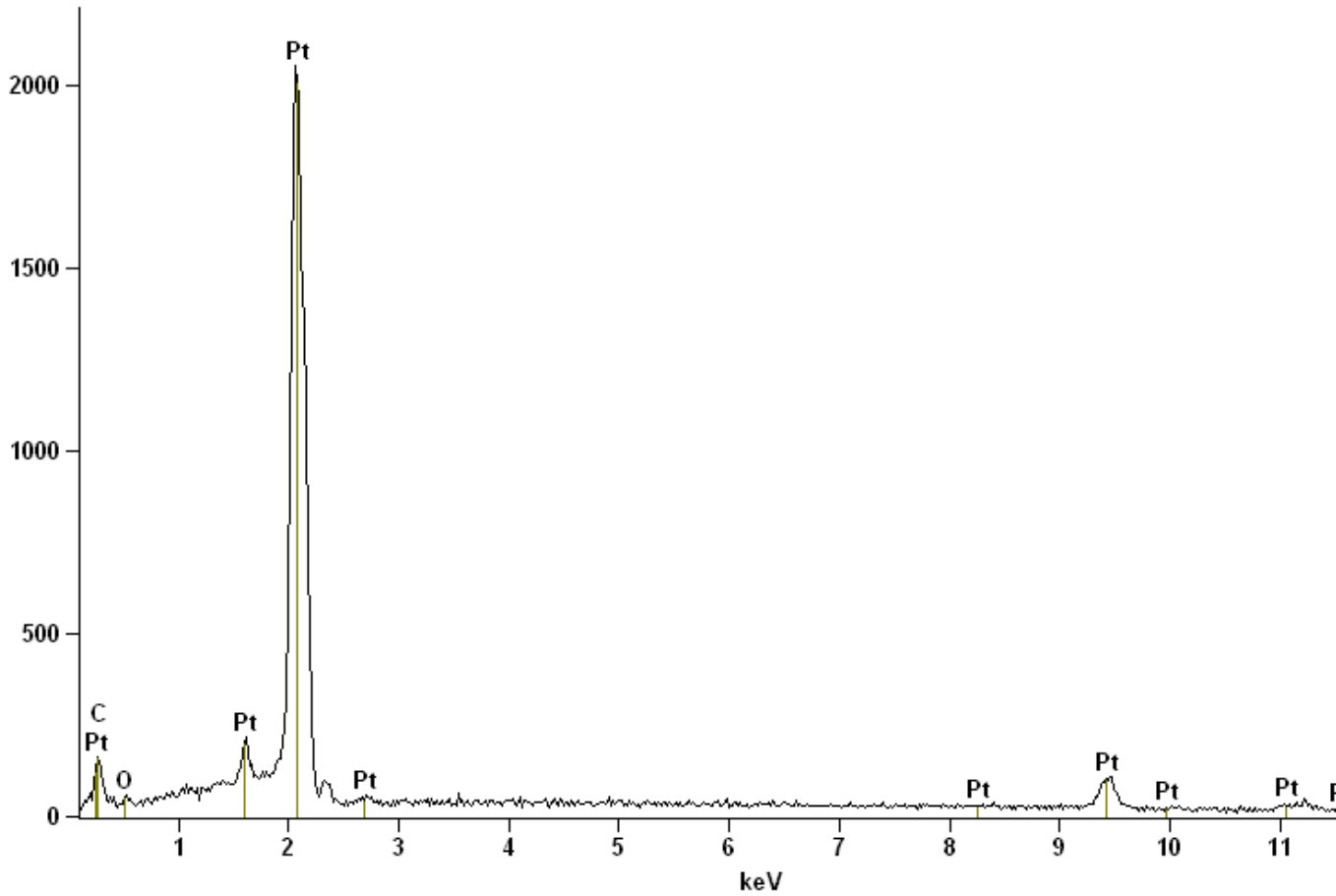

Fig. 15: EDX analysis results for anode after 420 s run at 0.75 mA with a concentration of 50 gl^{-1} phenol

Table 6: Elemental composition of anode surface found by SEM-EDX investigation

Element Line	*Net Counts*	*Weight %*	*Atom %*
C K	917	5.16	45.59
O K	69	0.46	3.07
Pt L	2517	94.38	51.34
Pt M	34635	---	---
Total		100.00	100.00

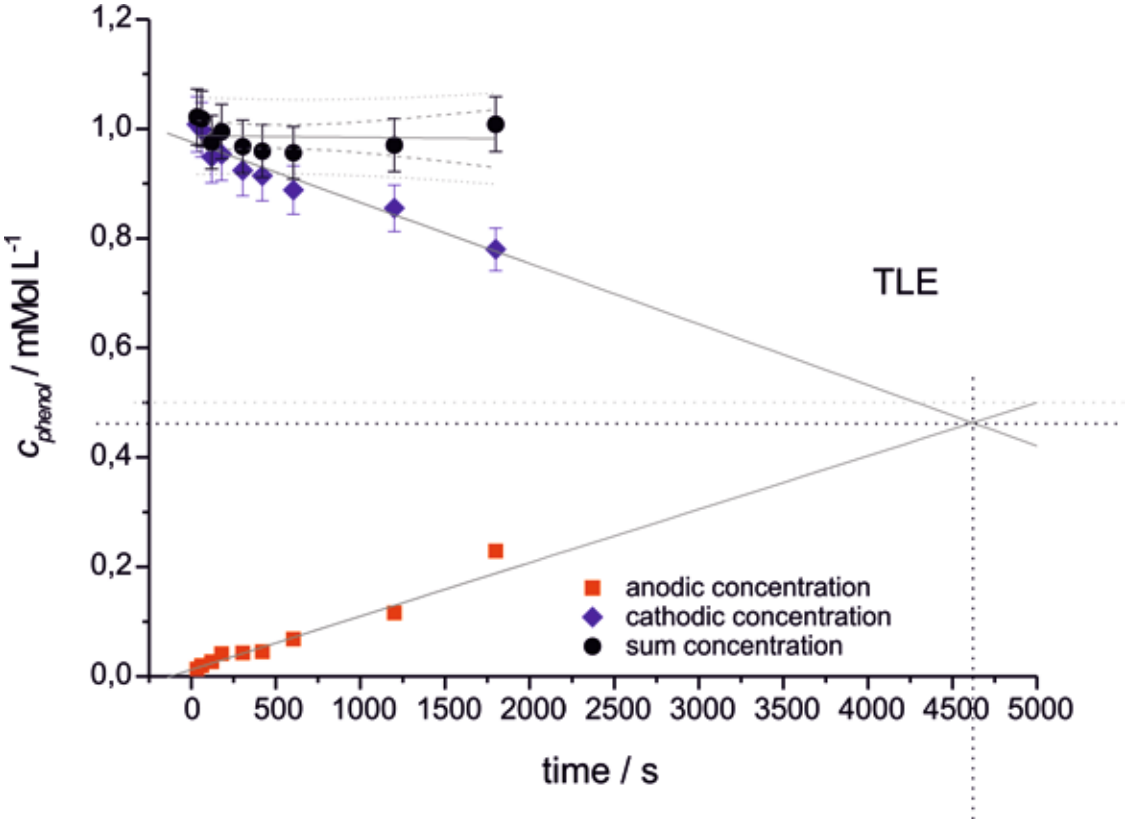

Fig. 16: : Exp. 1a: Transport of phenol from cathode to anodic beaker. The grey dashed line marks the theoretical mixture concentration (0.5 mmol L^{-1}); the black dashed lines show concentration and time at the theoretical linear equilibrium (TLE). The concentration sum is evaluated with a linear fit including 95% confidence (dashed) and 95% prediction (dotted) intervals (Eisenhut, M. 2011).

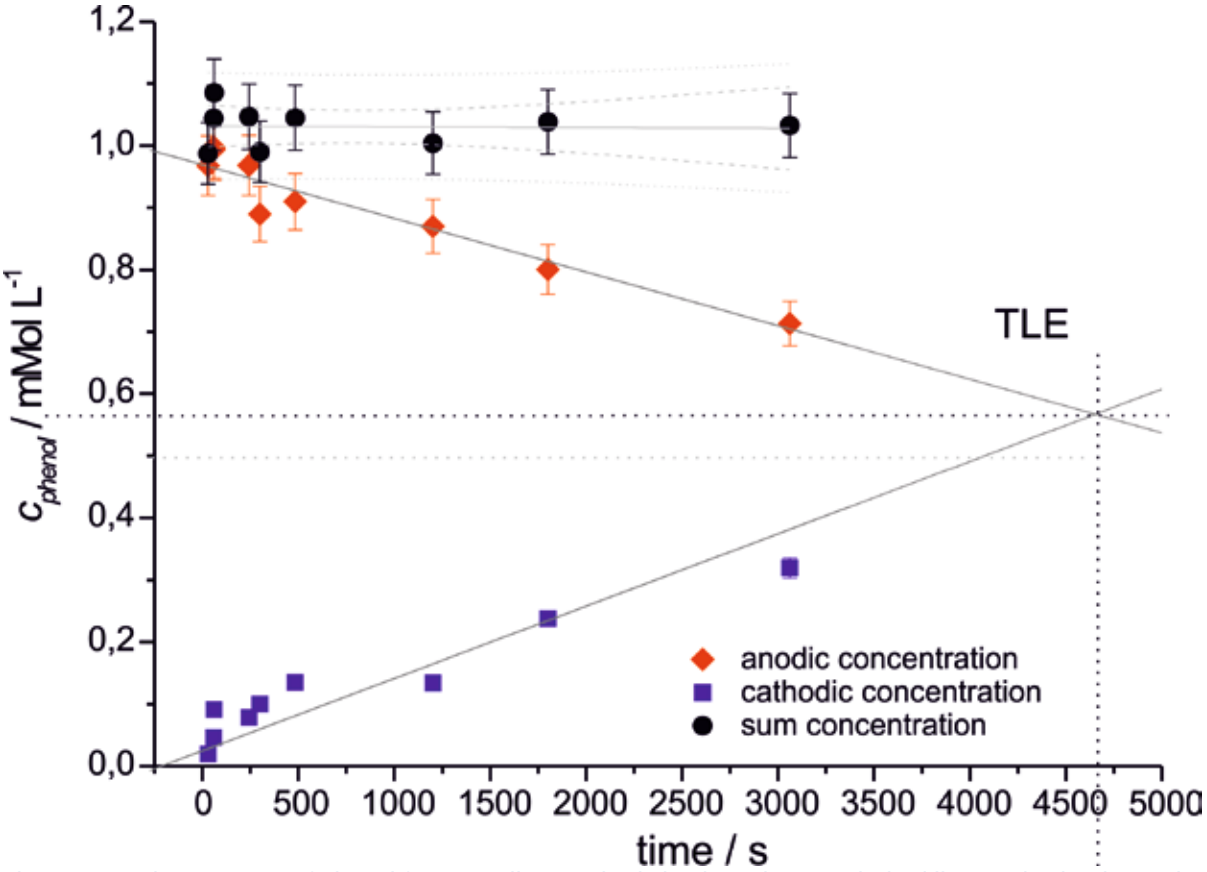

Fig. 17: Exp. 1b: Transport of phenol from anodic to cathode beaker. The grey dashed line marks the theoretical mixture concentration (0.5 mmol L^{-1}); the black dashed lines show concentration and time at the theoretical linear equilibrium (TLE). The concentration sum is evaluated with a linear fit including 95% confidence (dashed) and 95% prediction (dotted) intervals. . (Eisenhut, M. 2011)

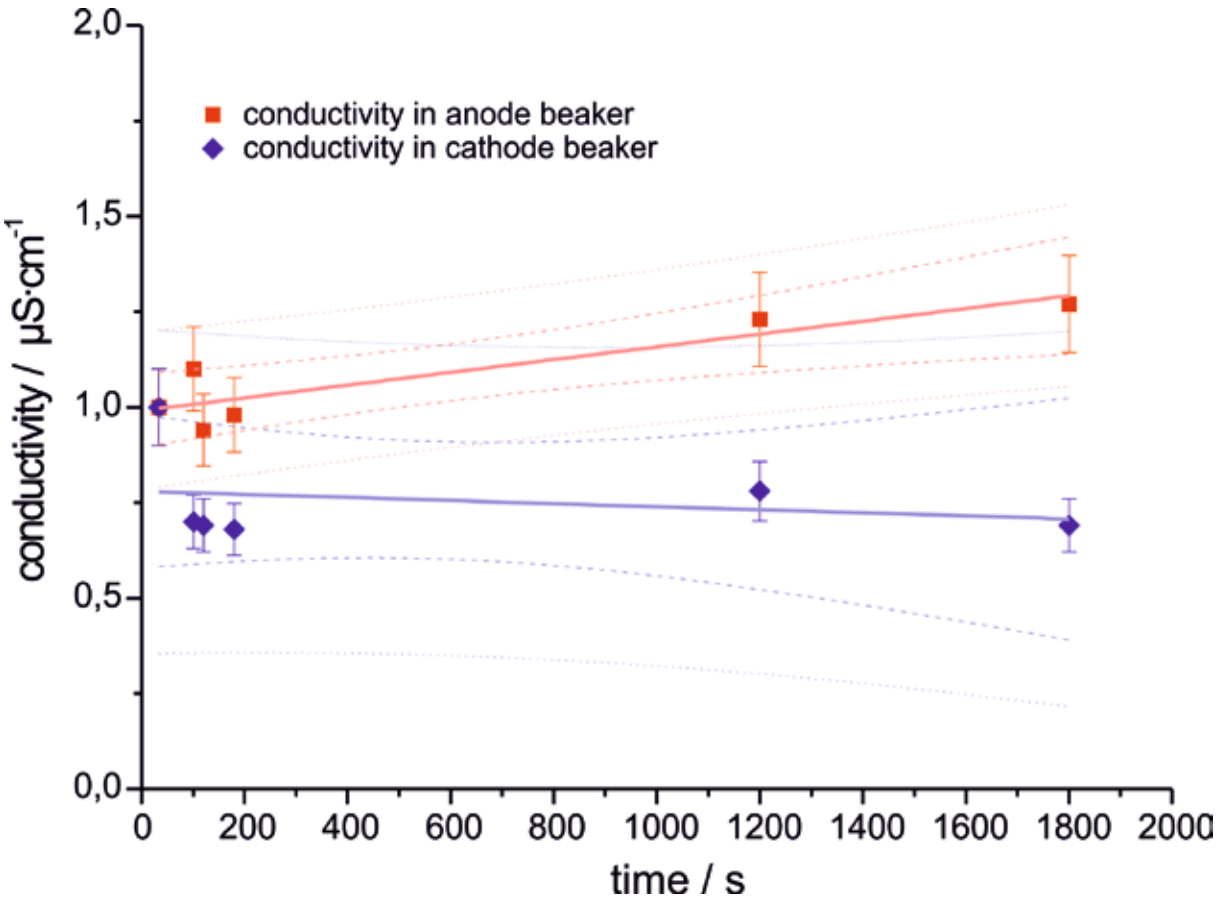

Fig. 18: Exp. 1a: Transport of phenol from cathode to anodic beaker, conductivity measurement evaluated with a linear fit including 95% confidence (dashed) and 95% prediction (dotted) intervals. (Eisenhut, M. 2011)

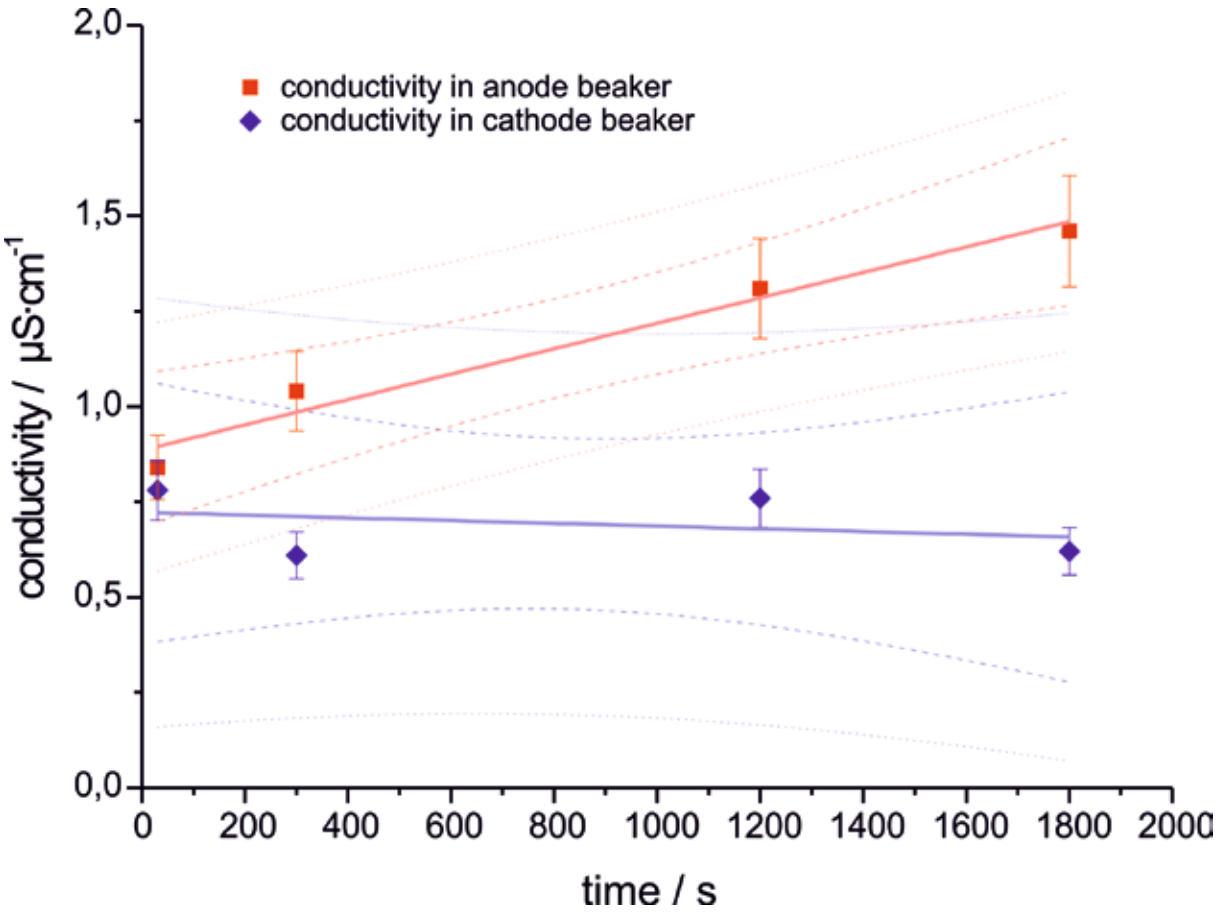

Fig. 19: Exp. 1b: Transport of phenol from anodic to cathodic beaker, conductivity measurement evaluated with a linear fit including 95% confidence (dashed) and 95% prediction (dotted) intervals. (Eisenhut, M. 2011)

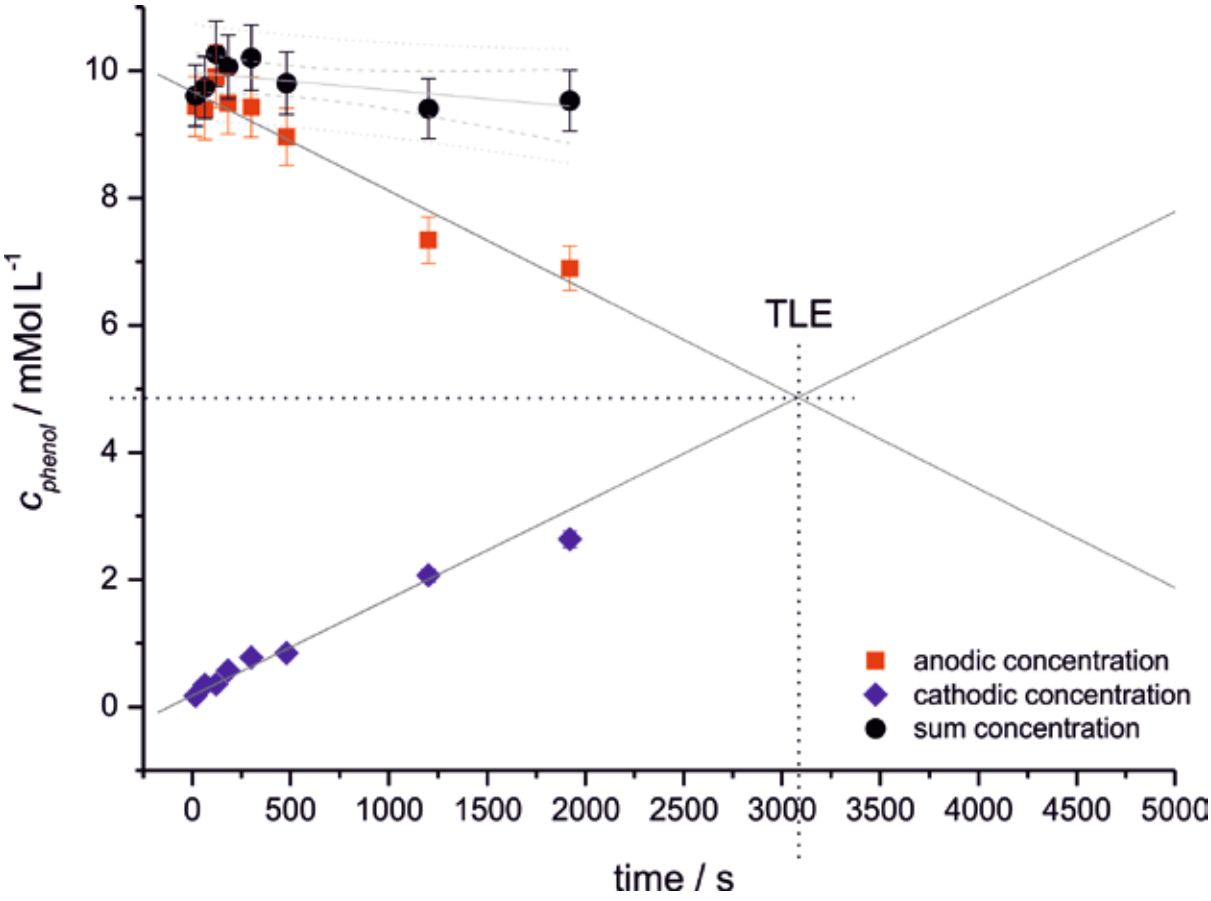

Fig. 20: Exp. 2a: Transport of phenol from anode to cathode beaker. The grey dashed line marks the theoretical mixture concentration (5 mMol/L); the black dashed lines show concentration and time at the theoretical linear equilibrium (TLE). The concentration sum is evaluated with a linear fit including 95% confidence (dashed) and 95% prediction (dotted) intervals. (Eisenhut, M. 2011)

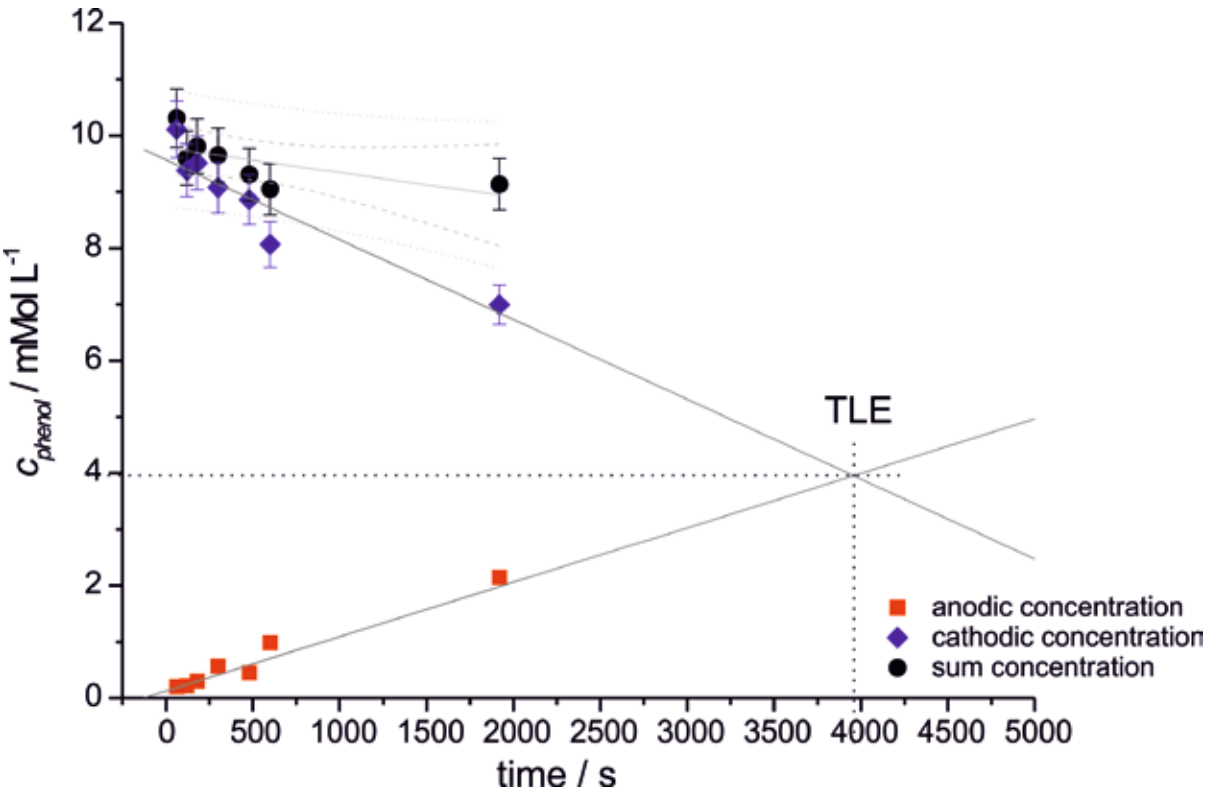

Fig. 21: Exp. 2b: Transport of phenol from cathode to anode beaker. The grey dashed line marks the theoretical mixture concentration (5 mMol/L); the black dashed lines show concentration and time at the theoretical linear equilibrium (TLE). The concentration su sum is evaluated with a linear fit including 95% confidence (dashed) and 95% prediction (dotted) intervals. (Eisenhut, M. 2011)

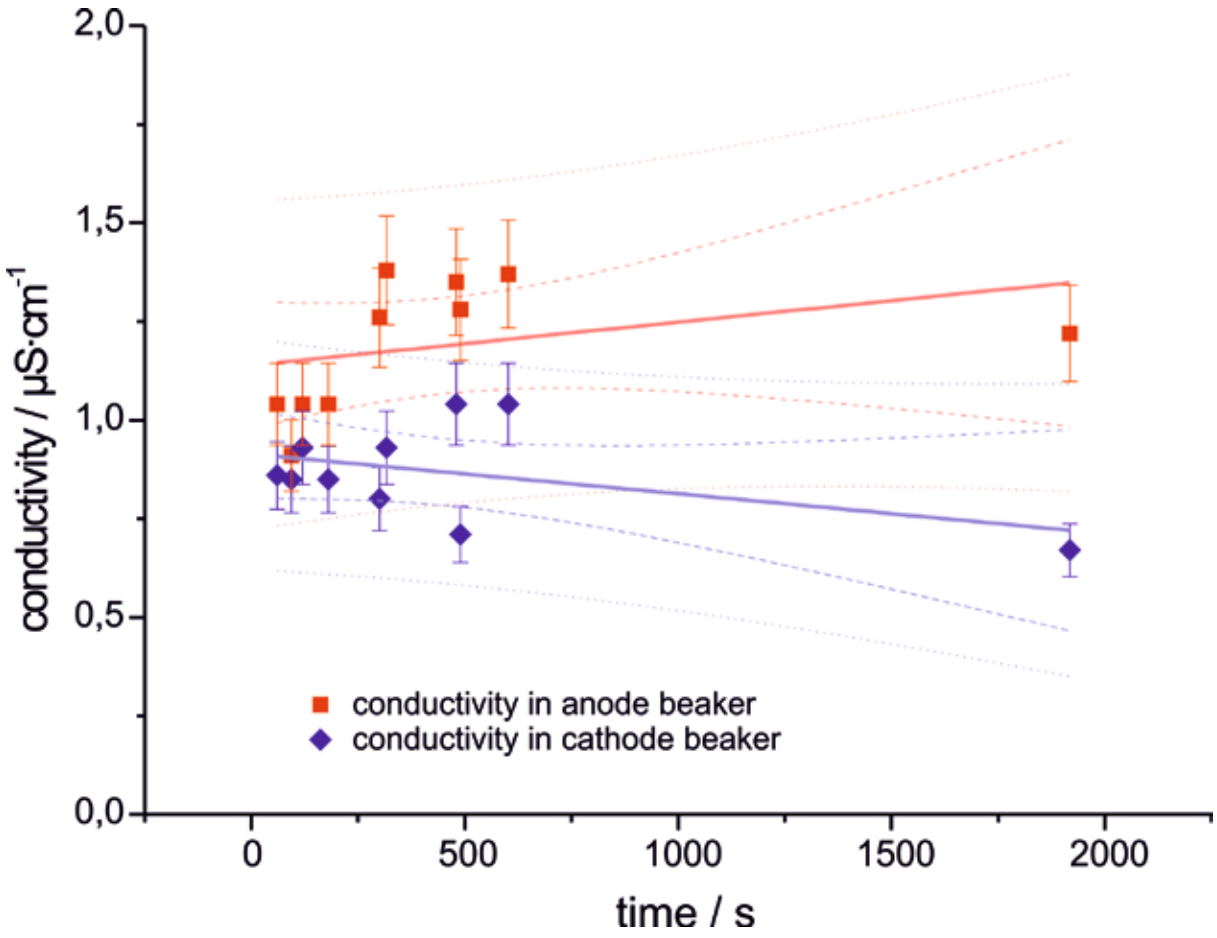

Fig. 22: Exp. 2a: Transport of phenol from cathode to anodic beaker, conductivity measurement. The values are evaluated with a linear fit including 95% confidence (dashed) and 95% prediction (dotted) intervals. (Eisenhut, M. 2011)

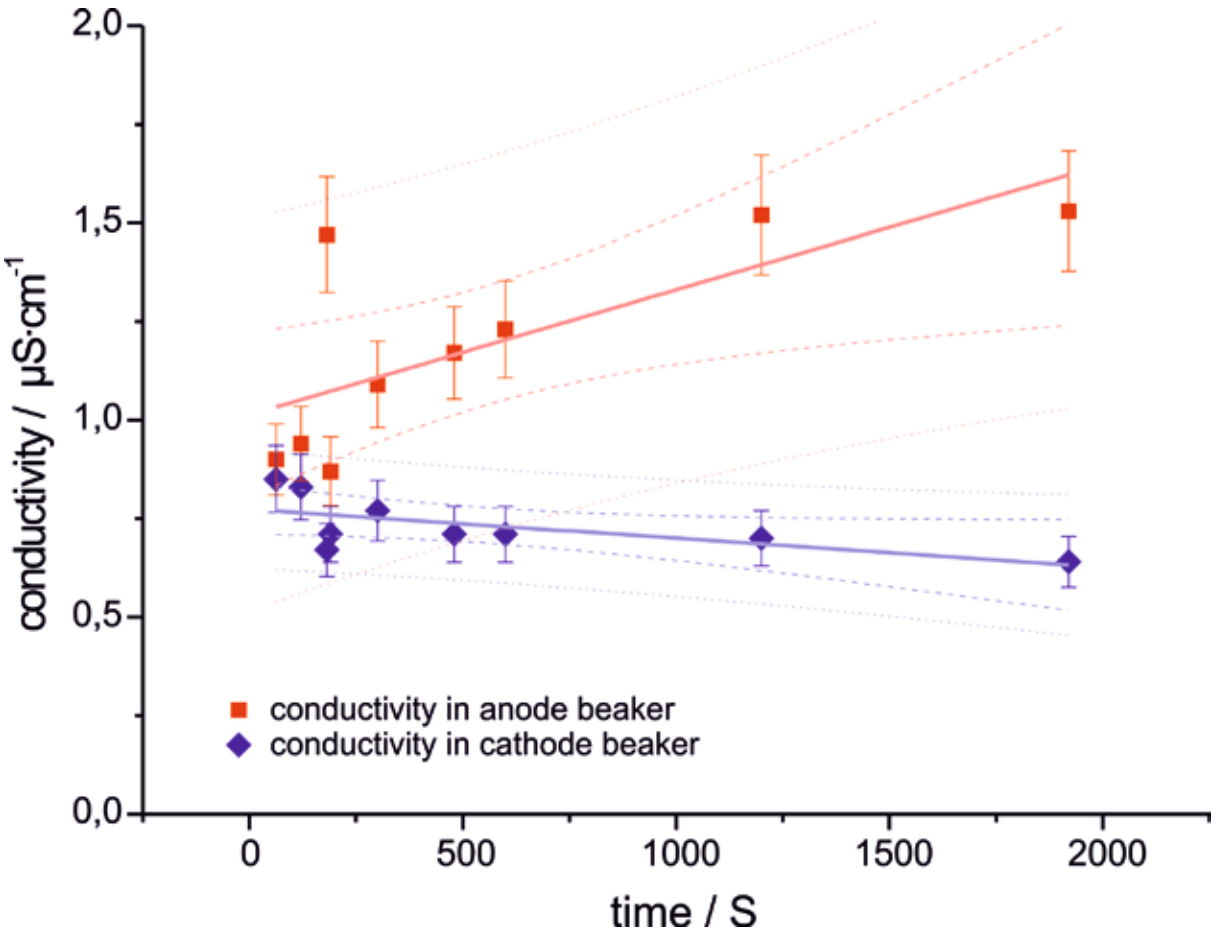

Fig. 23: Exp. 2b: Transport of phenol from anodic to cathode beaker, conductivity measurement. The values are evaluated with a linear fit including 95% confidence (dashed) and 95% prediction (dotted) intervals. (Eisenhut, M. 2011)

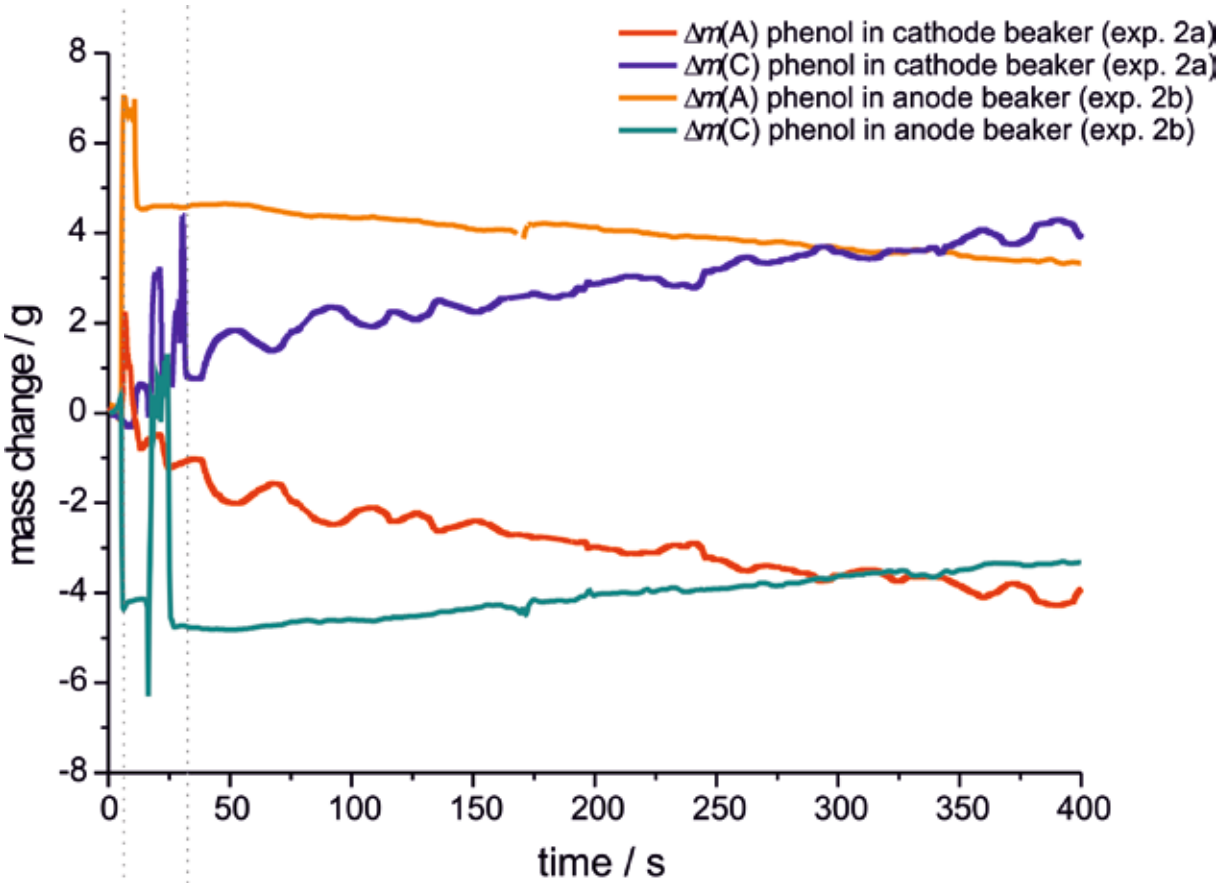

Fig. 24: Comparison of the measured mass flow of one exemplary experiment of the series 2a with an extraordinary one of series 2b. The dotted grey lines mark the beaker separation time during which the read out of the balances is partly erroneous. (Eisenhut, M. 2011)

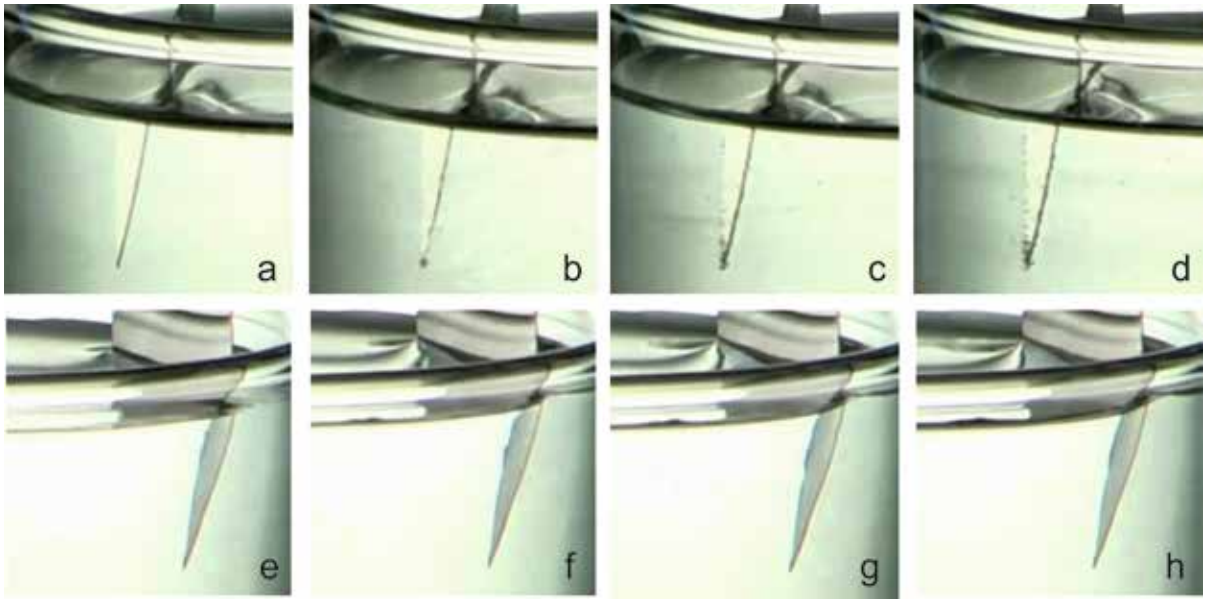

Fig. 25: Gas formations over time at the anode (a-d) during experiment 5f (531mM phenol in both beakers) in comparison to the cathode where no gas formation could be observed (e-h). The pictures were taken after 34 (a, e), 94 (b, f), 214 (c, g), 294 s (d, h), respectively. (Eisenhut, M. 2011)

5.3.1 Anodic phenol oxidation

Three pathways for phenol oxidation are described by Canizarez et al. (Canizares, P. 1999):

(a) Electrochemical cold combustion: $Pt(OH\bullet) + R \Rightarrow m\,CO_2 + n\,H_2O + Pt$

Physisorbed hydroxyl radicals on a metal surface catalyze the formation of water and carbon dioxide in a complete oxidation cycle.

(b) Chemical oxidation: $MO + R \Rightarrow RO + M$

A heterogenous electro-oxidation at the active sites of the electrode via chemisorbed hydroxyls selectively form phenol intermediates.

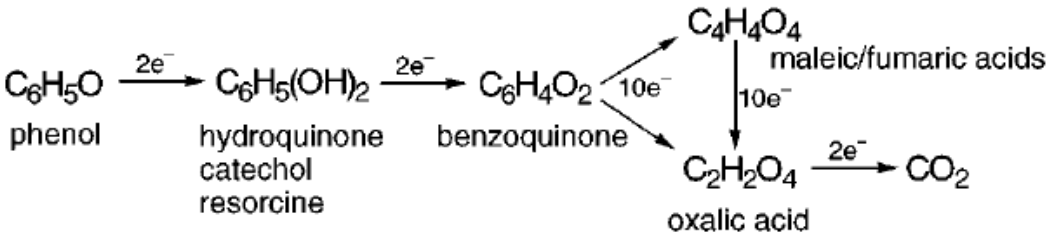

Fig. 26: Oxidation intermediates suggested by Canizares et al. in the chemical oxidation pathway of phenol . (Canizares, P. 1999)

(c) polymerization: $C_6H_5OH + OH\bullet \Rightarrow C_6H_5O\bullet + H_2O \Rightarrow polymers$

In the phenol oxidation process an electrophilic attack of hydroxyl on phenol starts a radical polymerization. As the polymers formed have a lower oxidation potential than phenol, they are more easily oxidized to radicals, which can interact to form polymers of higher molecular weights, leading to a passivation layer on the surface of the electrode.

According to Gatrell and Kirk (Gattrell M. 1993), the preferred oxidation pathway in platinum/phenol/water systems is the chemical oxidation (b). The oxidation rate is dependent on available active sites (PtOH•) in the inner Helmholtz layer, 'IHL', catalyzing this process. In the outer Helmholtz layer, 'OHL', the number of desorbing hydroxyls is indirect proportional to the amount of oxidized products, e.g.: benzoquinone, hydroquinone and other aromatic phenoxy radical polymer precursors. Those species block OHL reactions, letting IHL reactions predominate. Polymerization (c) is always active, depending on experimental parameters, constantly reducing active electrode surface as a function of time. If phenol is directly adsorbed on the electrode surface, oxidation is suppressed, but polymerization can still occur.

A scheme of the possible pathways is shown in Fig. 27. In our experiments phenol was always deposited as a polymeric film on the anode surface. Additionally, at the highest used concentration (0.531M) gas formation could be observed at the anode.

We draw following conclusions from the experimental data: Generally, polymerization seems to be the predominant pathway for low–concentration, high-voltage applications. In higher concentrations chemical (b) or electrochemical oxidation (a) could become more relevant.

Since this work presents, to the author, the first known high voltage (four to five orders of magnitude higher than usually) set-up for phenol oxidation, it is plausible to assume that the IHL and OHL expand themselves to a higher degree into the bulk, while at the surface EHD flows are dominant. Thus, if the IHL is partially inhibited by EHD flows and the OHL expands, the number of polymerization educts, formed in the OHL, would be increased. These educts could precipitate on the anode before pathway (a) or (b) can become relevant. Another hypothesis is, that the competition between EHD flow and IHL reaction leads to a continuously depletion of the IHL, flushing away all intermediates into the diffusion layer before full oxidation can take place. If this is true, the observed concentration effect could be explained by a higher rate of already pre-oxidized intermediates in the stream, which circle around the electrodes. (Fuchs, E. C. 2010)

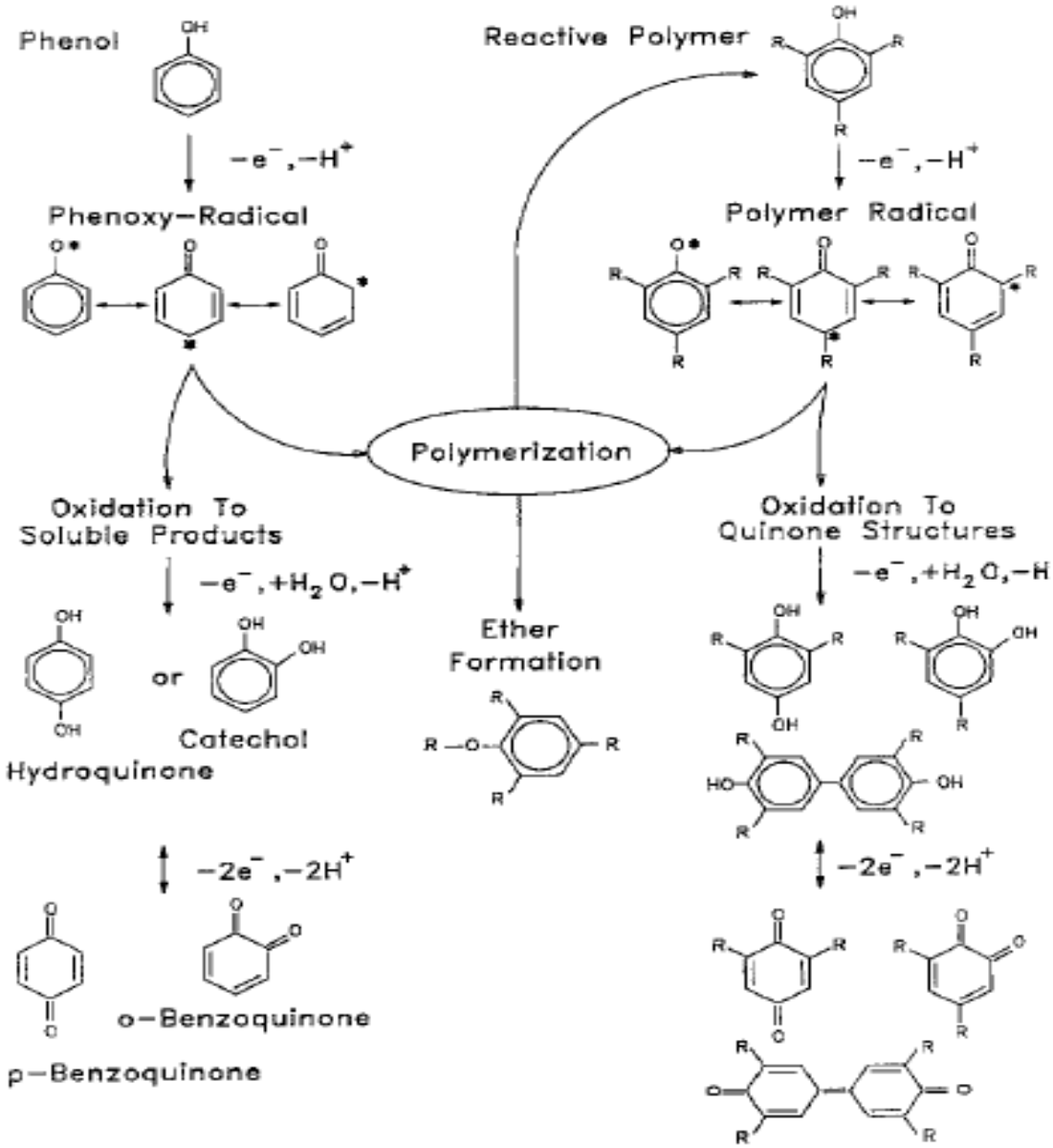

Fig. 27: Phenol oxidation and polymerization pathways, (Gattrell, M. 1993)

5.4 Ethylene glycol solutions

The 10 mM solution of ethylene glycol was more resistant against electro- oxidation processes, no precipitates or polymers could be detected on either of the electrodes. The behavior concerning conductivity and mass transport were similar to phenol (Figs. 16-19). The concentration sum in Fig. 28 seems to be increasing, which is naturally impossible since the start concentration was not changed from 10 mM. Results are still in a 5% confidence interval, which is the reason why the concentrations are assumed constant. TLE times were significantly different (Figs. 28, 29) and both TLE concentrations were below the optimum

mixture concentration. The glycol concentration seems to decrease faster in the cathode beaker (Fig. 29), whereas this is not the case when glycol is transported from the anode to the cathode beaker (Fig. 28). The explanation for this behavior could be electrode poisoning, similar to and as discussed with phenol solutions earlier.

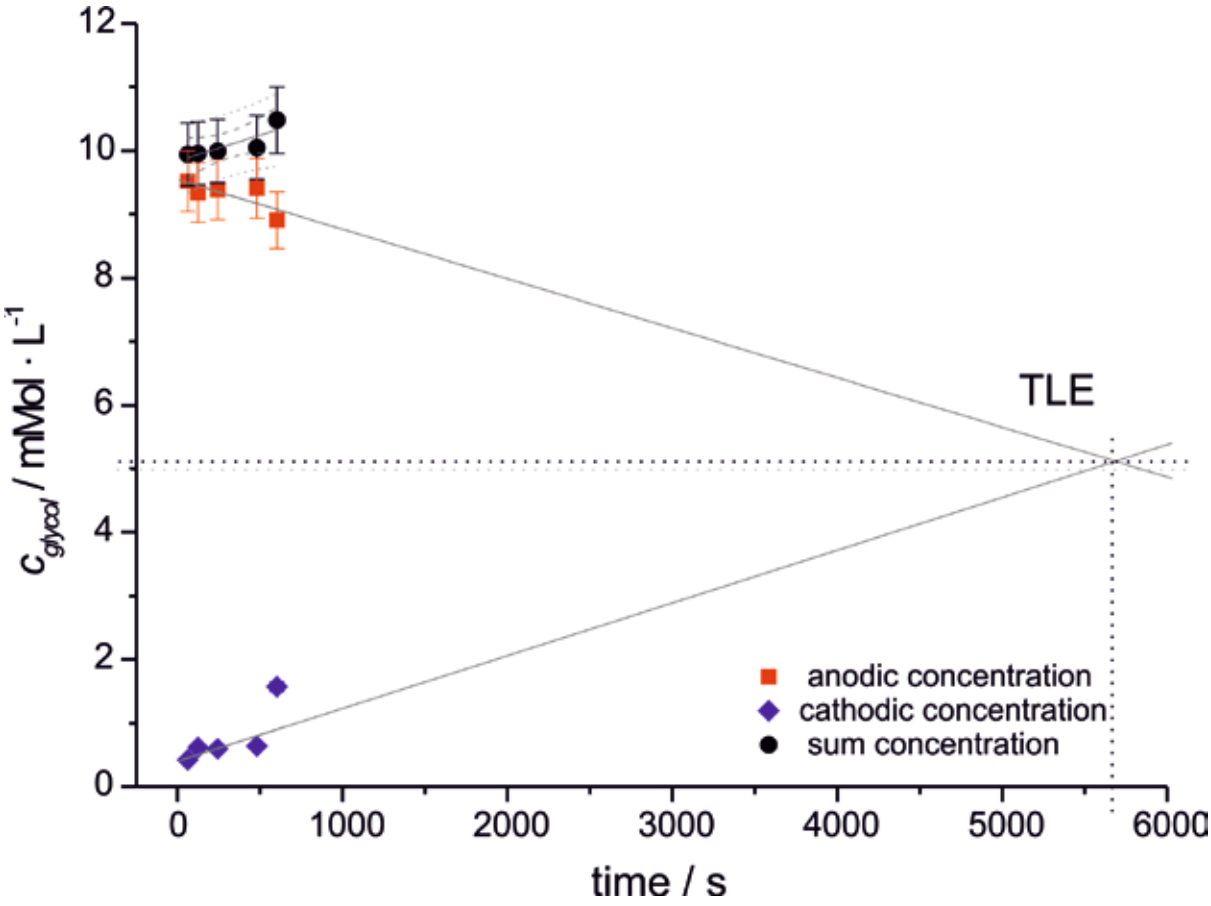

Fig. 28: Exp. 4a: Transport of glycol from anode to cathode beaker. The grey dashed line marks the theoretical mixture concentration (5 mM); the black dashed lines show concentration and time at the theoretical linear equilibrium (TLE). The concentration sum is evaluated with a linear fit including 95% confidence (dashed) and 95% prediction (dotted) intervals. (Eisenhut, M. 2011)

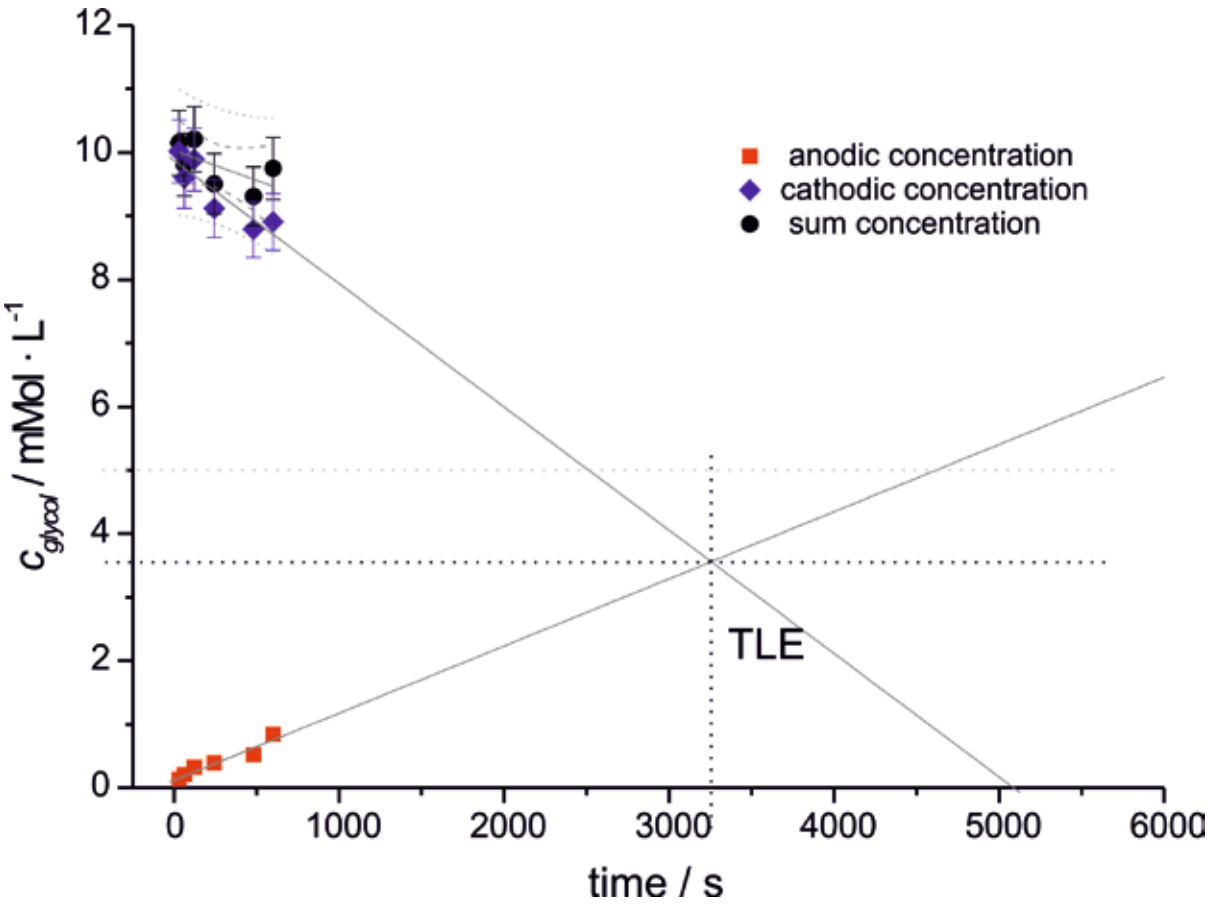

Fig. 29: Exp. 4b: Transport of glycol from cathode to anode beaker. The grey dashed line marks the theoretical mixture concentration (5 mM); the black dashed lines show concentration and time at the theoretical linear equilibrium (TLE). The concentration sum is evaluated with a linear fit including 95% confidence (dashed) and 95% prediction (dotted) intervals. (Eisenhut, M. 2011)

5.4.1 Anodic ethylene glycol oxidation

The oxidation of ethylene glycol in low voltage electrolysis in acidic conditions is governed by active sites on the electrode, according to Christensen et al.(Christensen, P.A. 1989), yielding mainly carbon dioxide and glycolic acid. The active sites can be reduced if carbon monoxide adsorption occurs on the electrode, terminally bonding to the platinum. The products are different in alkaline media, producing glycolate, oxalate and carbonate. De Lima et al. (de Lima, R. B. 2003) also describe the formation of oxalic and formic acid as side products. The conversion to glycolate and carbonate seems to be mediated via the same intermediate, but oxalate is produced by further oxidation of desorbed glycolate. Matsuoka et al. (Matsuoka, K. 2005) found poisoning (formate formation) and a non-poisoning (oxalate formation) pathway for the electro-oxidation of ethylene glycol. They suggest that the process consists of a cascade of steps, involving glycol aldehyde-, glyoxal-, glycolate-, glyoxylate- and oxalate as intermediary products before the formation of carbon dioxide and carbonate.

The oxygen-transfer agent on platinum appears to be adsorbed water or hydroxyl species. Platinum surfaces have been long known for their ability to dissociatively chemisorb organic reactants in aqueous and gas- phase environments.

As far as the presented experiments are concerned, no detectable electro- oxidative processes were found. No gas formation on the electrode took place, and the conductivity increase at the anode and decrease at the cathode, respectively, was comparable to pure water. Presumably, pH values, due to different carbon dioxide saturation, were shifted in both beakers, but in no correlation to the ethylene glycol. Finally, it can be assumed that decomposition of ethylene glycol took place in line with phenol decomposition discussed earlier, but no intermediate products which could be adsorbed or escape as gases were involved. If the reaction rate was not too high, carbon dioxide formation could also have happened at a rate in which it immediately got dissolved in water, thereby avoiding bubbling. Another hindrance could come from a poisoning effect of hydroxyl ions, adsorbing preferably on the electrode surface, preventing all other intermediates (glycolate, oxalate) to adsorb. This would be plausible, according to Kelaidopoulou et al. (Kelaidopoulou, A. 1998), who state that with an increase in potential the oxidation of ethylene glycol is shifted to a hydroxyl chemisorptions. Another possible explanation, as mentioned earlier, could be that the EHD mass flow disrupts and thus slows down chemical surface reactions significantly - or even prevents them completely.

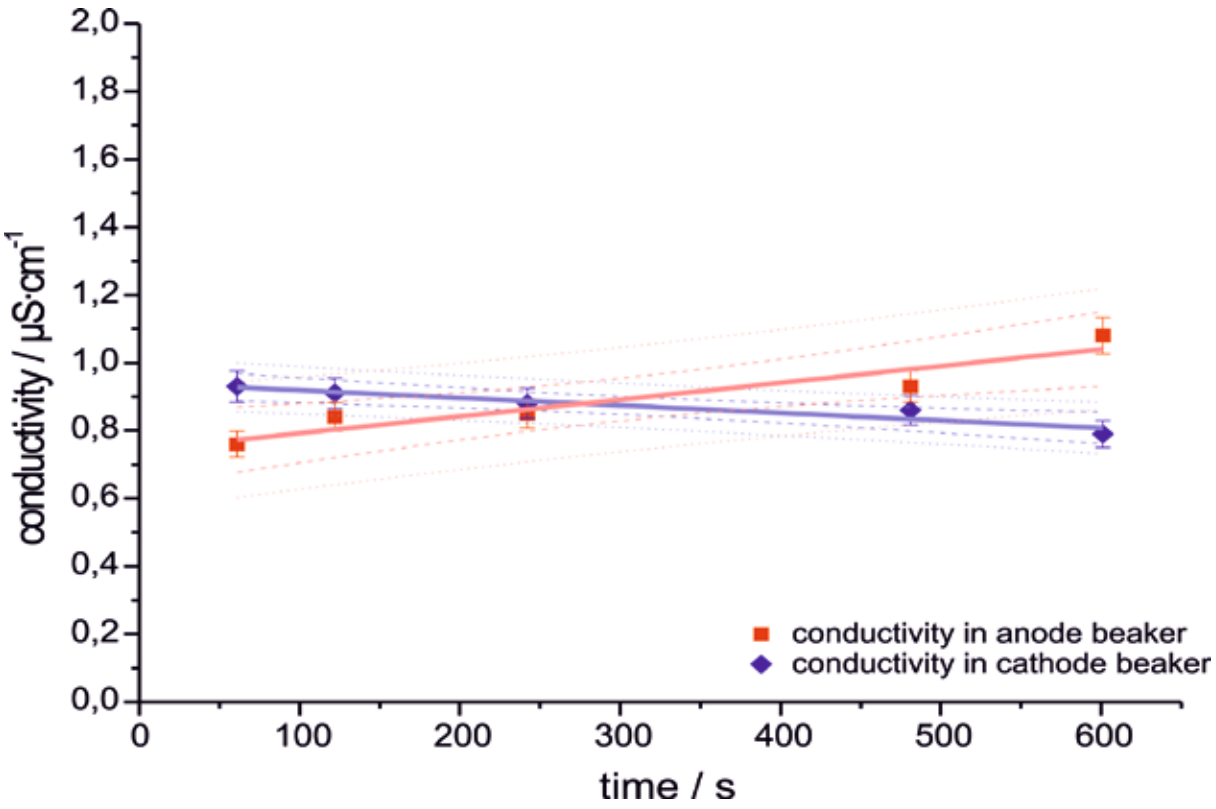

Fig. 30: Exp. 4a: Transport of glycol from anode to cathode beaker, conductivity measurement evaluated with a linear fit including 95% confidence (dashed) and 95% prediction (dotted) intervals. (Eisenhut, M. 2011)

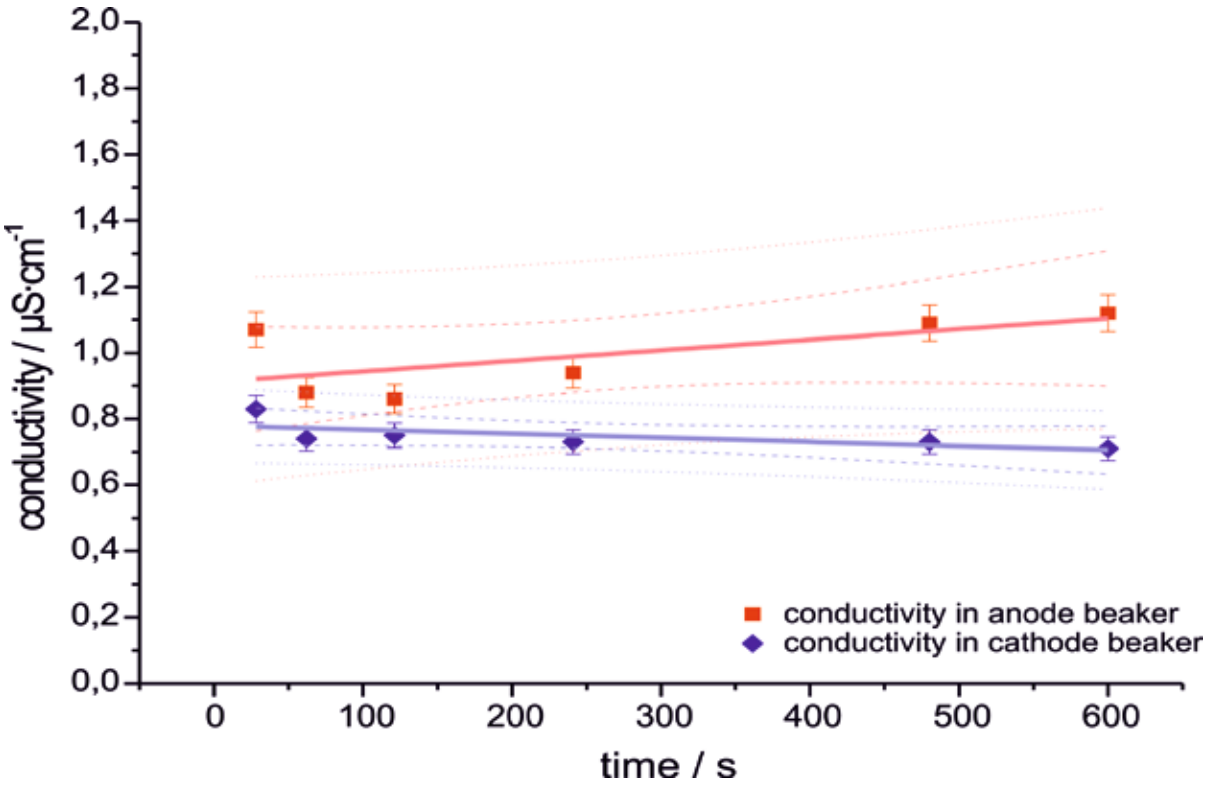

Fig. 31: Exp. 4b: Transport of phenol from cathode to anode beaker, conductivity measurement. The values are evaluated with a linear fit including 95% confidence (dashed) and 95% prediction (dotted) intervals. (Eisenhut, M. 2011)

5.5 Equilibrium experiments

One objective target of this thesis was to determine whether the water bridge be utilized to quickly separate phenol or its oxidation products from water due to selective electrophortic transport of the (ionic) intermediates or products. Such a process would constitute a great separation technique in which marginal amounts of organics could be extracted by means of high voltage in aqueous systems. The so-called equilibrium experiments aimed exactly at this question. A solution with a certain concentration of analytes was divided in two beakers and after a certain operation time of the bridge, generally ten minutes, the concentration difference was measured. This was carried out for six concentrations (0.53 mM, 5 mM, 10 mM, 50 mM, 100 mM and 531 mM), the results are shown in Figs. 32 and 33. It becomes obvious that within the chosen time window no selective transport is mediated through the bridge but the small differences of concentration can be attributed to oxidation processes at the anode or are within the standard deviation.

.

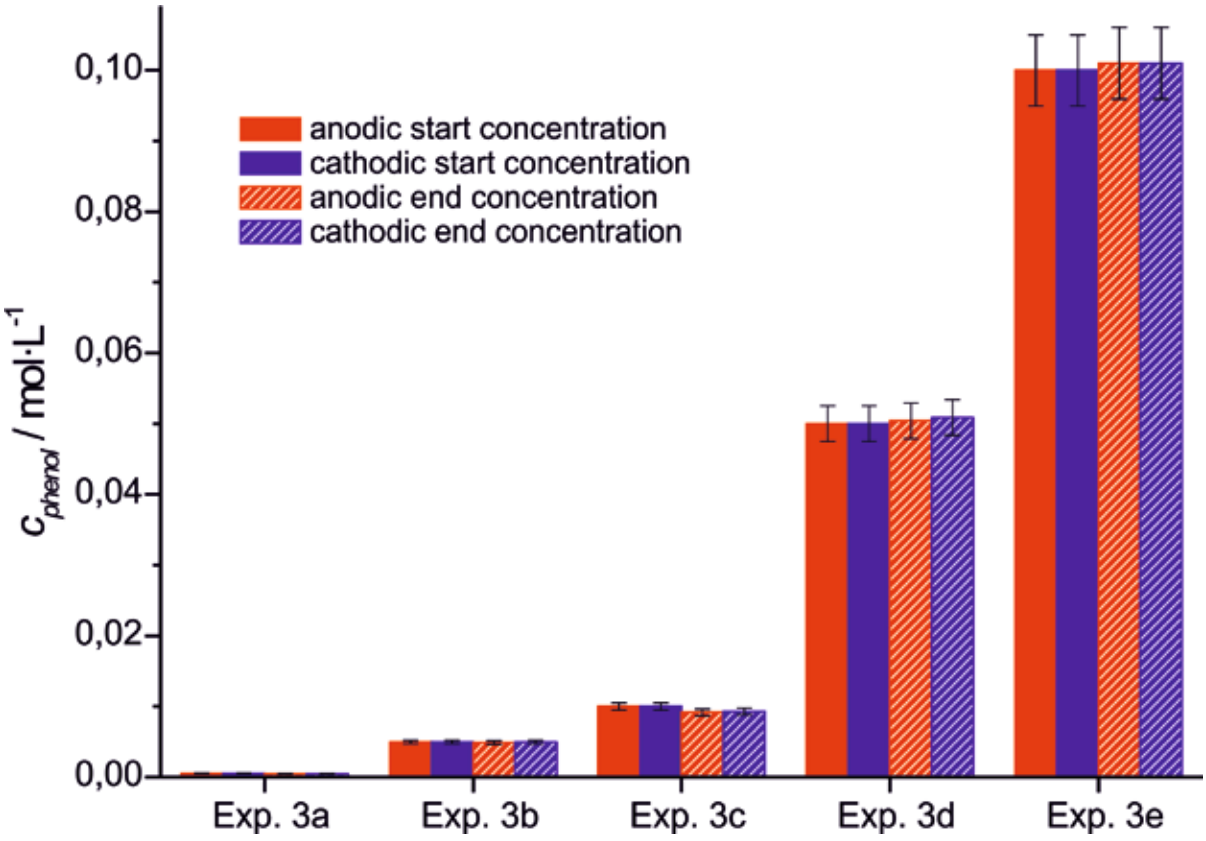

Fig. 32: Concentration comparison after the phenol equilibrium experiments (3a-3e). The bridges were run for 600 s except Exp. 3c which was run for 250 s. (Eisenhut, M. 2011)

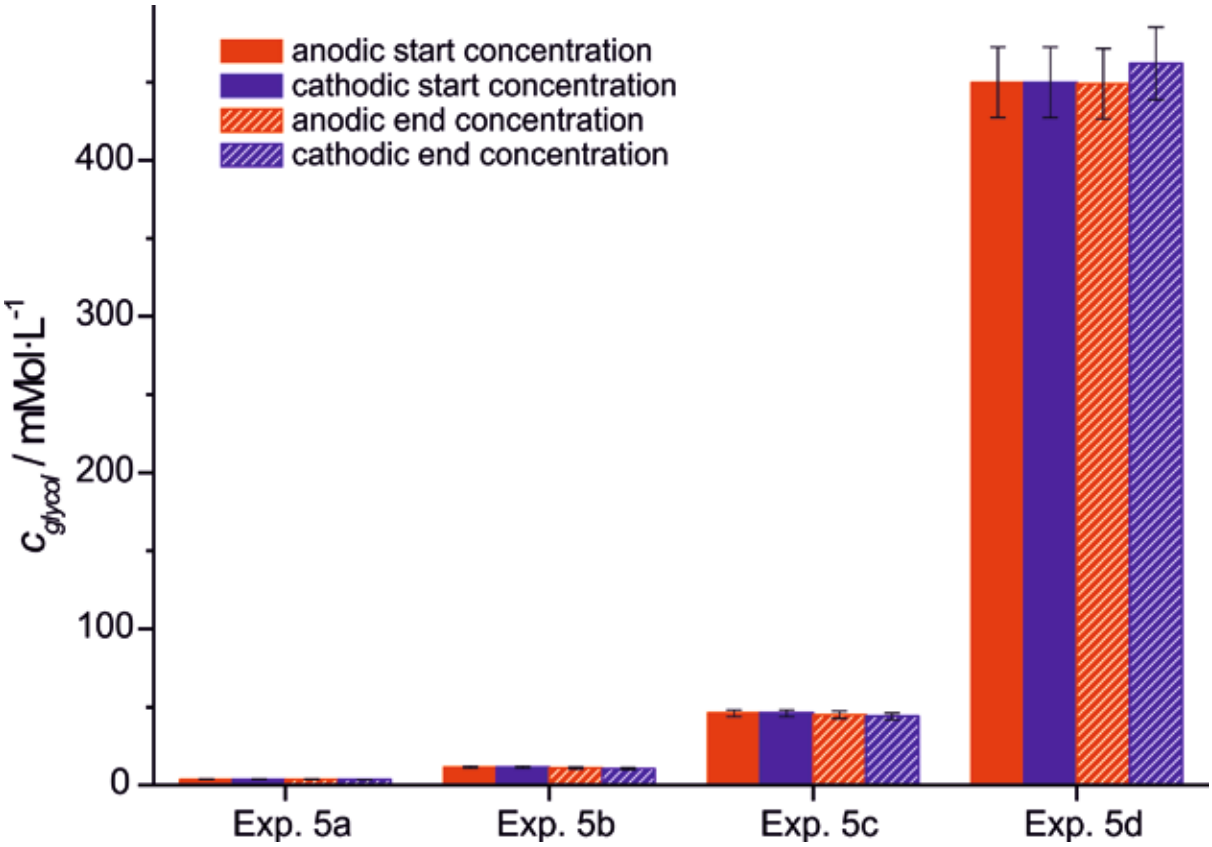

Fig. 33: Concentration comparison after the glycol equilibrium experiments (5a-5e). The bridges were run for 600 s except Exp. 5c which was run for 250 s. (Eisenhut, M. 2011)

5.6 Feasibility studies

Next to the organic compounds, feasibility studies of temperature differences between the beakers as well as the addition of anorganic salts and of fluorescent dyes were carried out.

In experiment 9a the simple test of putting warm water in one of the beakers had an impressive consequence on the flow direction of the bridge. When warm (around 50°C) water was put in the anodic beaker and water at ambient temperature (around 20°C) was in the cathodic beaker, not only did the voltage necessary to build up a stable bridge rose to nearly twice the normal value, but net flow direction of the bridge was reversed approximately every 120 s in a period of 600 s operation time. So the mass difference between the two beakers was marginal at the end, the transport rate was high but the temperature difference was still very high between the two beakers after the end of the experiment.

In experiment 9b warm water (~50°C) was filled into the cathodic beaker, and cold into the anodic one. Here a clear net mass transport into the cathodic beaker was noticeable. Furthermore, the same high voltage was needed to get a stable bridge and some

electrospraying between the beakers occurred. The current had big deviances during the runtime of 380s before it finally broke down. (see Fig. 34)

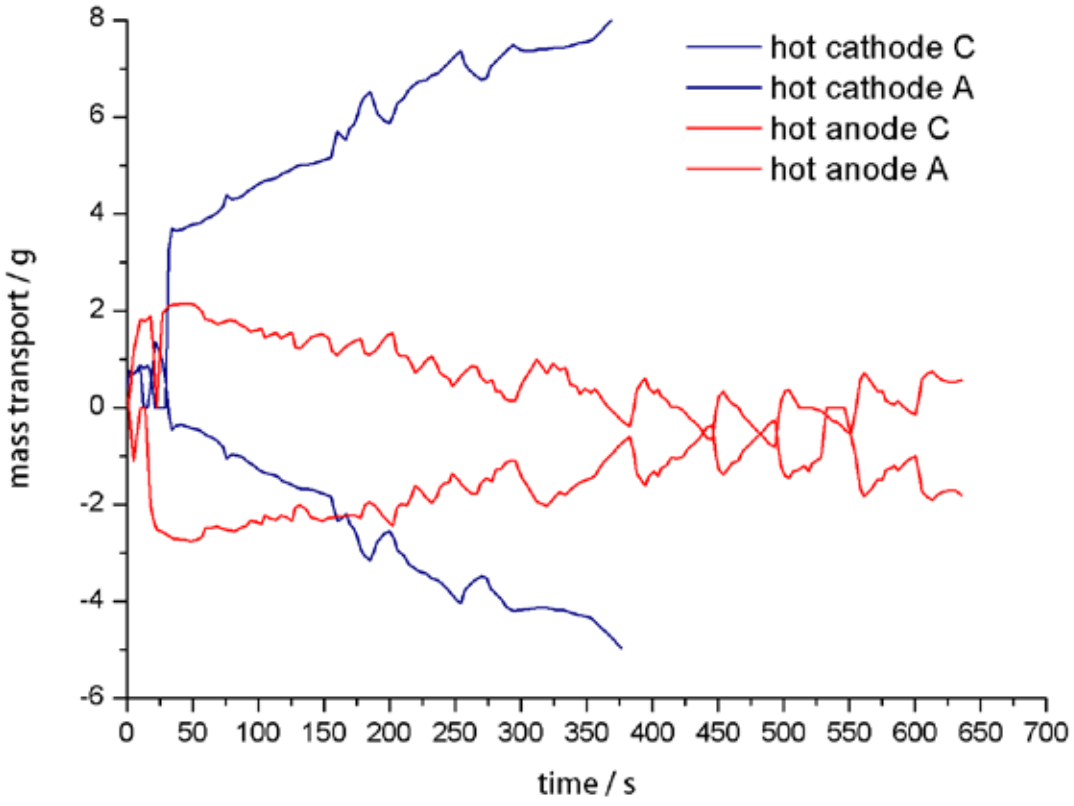

Fig. 34: Mass transport of combination of hot anode and ambient cathode water and vice versa (red lines: hot anode; blue lines: hot cathode)

The inorganic salts had interesting effects on the (net) flow direction, the conductivities, operating currents, necessary voltage to start the bridge and the stability of the bridge in general. To address the electrochemical pathways involved was not the aim of this work, but is planned for future work.

In experiment 10 ambient-temperature anode water and warm cathode water mixed with Na_3PO_4 led to sparking and electrospraying at around 7 kV, also some bubbles appeared near the beakers' spouts at the start and during the experiment on the surface of the electrodes. The net flow direction was from cathode to anode, adding 1.8 mL into the anode

beaker and loosing 5 mL in the cathode beaker, with the other flow direction suppressed, probably due to the ions in the cathode beaker. The conductivity in the anodic beaker increased from 0.83 to 8.42 μScm^{-1}, whereas the conductivity around the cathode decreased from 58.3 to 57.5 μScm^{-1}.

In experiment 11a warm water at the anode with a small amount of NH_4OH and water at ambient temperature mixed with Na_2CO_3 at the cathode was prepared. The net mass transport was quite high here (+8 mL anode; -11.7 mL cathode, 3.7mL spilled and evaporated), but the current was jumping all the time, making it difficult to maintain a stable bridge. Interestingly, an air bubble was located between the beakers' spouts right at one end of the bridge, not moving but apparently stuck there. The conductivity increased from 6.15 μScm^{-1} to 10.7 μScm^{-1} in the cathode beaker and decreased from 3.62 μScm^{-1} to 1.56 μScm^{-1} in the anode beaker. Also, a lot of evaporation occurred.

In experiment 11b ambient-temperature anode water with a marginal amount of NH_4OH and warm cathode water were used, and the net mass transport was the highest for all experiments carried out. Exceptional 22 mL were transported from the cathode but only 8 mL arrived at the anode, leaving 14 mL to evaporation and dripping. The conductivity rose from 11.84 μScm^{-1} to 15 μScm^{-1} at the anode and from 0.61 μScm^{-1} to 6.55 μScm^{-1} at the cathode. Bubbles could be seen after the experiment at both anode and cathode.

In experiment 11c water at ambient temperature with a very small amount of NH_4OH at the anode and a warm cathode containing Na_2CO_3 showed a net mass transport in the direction of the anode (+3.5mL) and a loss of six milliliters at the cathode while bubbles wandered through the bridge from cathode to anode. At the start both beakers had a vibrating surface. The cathode was the more interesting one in this case, because of the bubbles which formed at the electrode. Moreover, the bridge was very small, but a high current was flowing (4 mA) and the operating voltage was comparable to water (6 kV). In terms of conductivities a decrease in the anode beaker (3.62 μScm^{-1} à 1.56 μScm^{-1}) and an increase in the cathode beaker (6.5 μScm^{-1} à 10.7 μScm^{-1}) were measured.

In experiment 11d NH_4OH was added to the warm cathode beaker, and a mass transport was visually detectable (anode: -2.8 mL; cathode: -0.3 mL) but evaporation was most prominent (3.1 mL). The conductivity increased from 0.64 μScm^{-1} to 1.28 μScm^{-1} in the anode beaker and increased from 14.67 μScm^{-1} to 13.72 μScm^{-1} in the cathode beaker.

A general trend here seems to be that NH_4OH at the anode gets transported either to the cathode or is evaporated, since the conductivity decrease at the anode is difficult to be explained otherwise.

In experiment 12 the addition of NaSCN into the anode beaker and warm water in the cathode beaker led to a high initial conductivity at the anode (65.7 μScm^{-1}). After five minutes of the applied voltage at a current of 5 mA, the conductivity rose in both beakers (anode: 78.8 μScm^{-1}; cathode from 0.66 μScm^{-1} to 4.4 μScm^{-1}), indicating the disproportion of ions due to the strong electric field, since no stable connection could be formed. The water surface was rigorously vibrating on both sides, bubbles were formed prior to a stable connection. A bridge was established only for a very short time (approximately 30 s) and the sparking between the beakers was clearly detectable. There was smoke-like vapor visible above the bridge. The net mass transport was rather low with two milliliters lost at the anode and 0.6 mL gained at the cathode beaker.

In experiment 13 for the combination of warm anode water with cathode water at ambient temperature mixed with $CaCO_3$, the starting voltage was 12 kV and increased up to 21 kV, the bridge became unstable (dripping) and sparks between the beakers along with dense vapor above the bridge were detectable during the experiment. The mass transport was negative for both beakers, which indicates that a lot of solution was evaporated and/or dripped out of the beakers over the duration of 300s. The formation of bubbles on the electrodes was stronger on the cathode than the anode. The conductivity rose from 0.57 to 0.94 μScm^{-1} in the anode beaker and from 5.45 to 13.16 μScm^{-1} in the cathode beaker.

In experiment 14 the fluorescent dyes seemingly did not influence the bridge during its operation time of 600 s, since the concentrations were measured not to exceed a conductivity of 2 μScm^{-1}. The electrochemical processes which probably took place (as discussed in Woisetschlaeger, J. 2010; Fuchs, E. C. 2010), were probably not prominent. A mixing of the dyes was visually detectable over the bridge region.

Selected images of the feasibility experiments are given in Fig. 35.

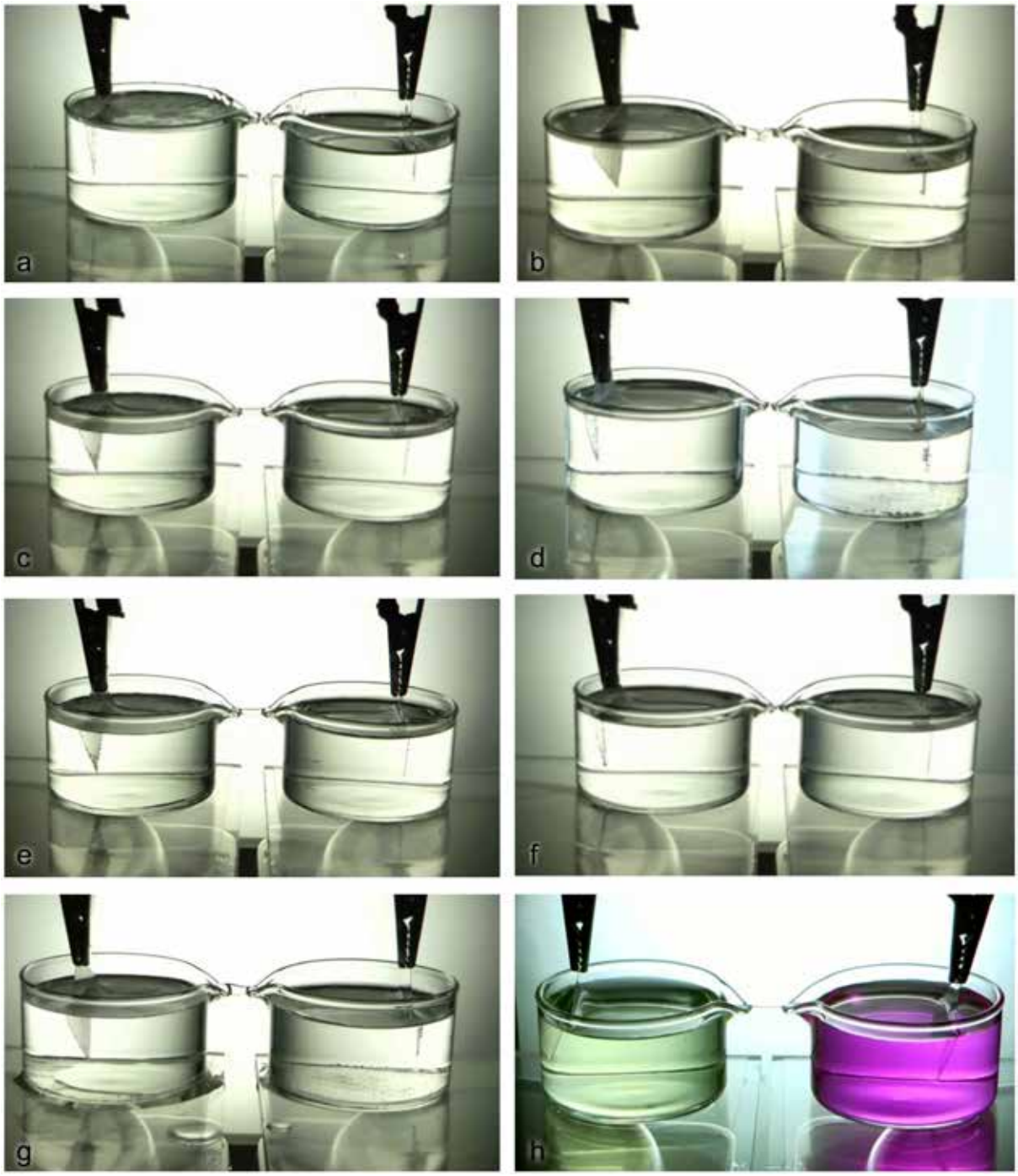

Fig. 35: pictures of anorganic salt experiments: (a) exp. 10 after 180 s ; (b) exp. 11a after 300 s; (c) exp. 11b after 360 s; (d) exp. 11c after 300 s; (e) exp. 11d after 360 s; (f) exp. 12 after 240 s; (g) exp. 13 after 240 s; (h) exp. 14 after 240 s.

6 Conclusions

The phenomenon of 'liquid bridging' or 'the floating water bridge' can be understood as a special behavior of dielectric liquids with a certain range of relative permittivity (best between 20 and 100) in AC or DC non-uniform electric fields. When the field is strong enough, a force is created, counteracting gravity, which is called the Kelvin polarization force density. This force is directly proportional to the (negative) pressure, pushing the dielectric liquid in the area of greatest field strength and thereby replenishing the zone of the bridge constantly with liquid (equation 3).

$$\vec{f}_{kelvin} = -p_{Maxwell} = \frac{1}{2}[\![(\varepsilon]\!]_r - 1)\varepsilon_0 \overrightarrow{\nabla(E.E)} \qquad \textbf{equation (3)}$$

Since the Maxwell pressure from the Maxwell tensor is also proportional to the square of the electric field (equation 4),

$$W_{el} = \frac{1}{2}\varepsilon_0\varepsilon_r \overrightarrow{E.E} \qquad \textbf{equation (4)}$$

equalize Bernoulli's equation (equation 5) with it to find a theoretical fluid velocity of about 0.2-0.4 ms^{-1}, which is in agreement with laser velocity measurements carried out by Woisetschläger et al.(Woisetschläger, J. 2010).

It was found that phenol is transported over the bridge region in both direction leading to different electrochemistry when phenol is present in one beaker only but revealing no separation over a short time if present in both. Furthermore, temperature differences drastically changed the flow direction. This effect could be used in future experiments to change the space charge injection into the media and to change the solubility of certain substances with a very low solubility product.

One very striking aspect of the bridge is the ambivalence of its constituting powers: surface tension and the electric field gradient have to be held in a very narrow window of operation to maintain a stable liquid bridge.

Water has an enormously high surface tension (equation 6), as discussed earlier.

$$W_{tension} = \frac{\gamma \Delta A}{\Delta V} = \frac{2\gamma}{r} \qquad \textbf{equation (6)}$$

This energy is in a fragile equilibrium with the energy density of the electric field and can be correlated to the electrocapillary number (equation 7).

$$C = \frac{\varepsilon_0 \varepsilon_r E^2 d}{\gamma}$$ **equation (7)**

So, when the electric field density is about the factor 1.25 to 1.6 higher than the energy density of the surface tension, a stable bridge is produced. This simple relation can be used to determine many different diameters and necessary field strengths of bridges in other dielectric liquids. A depiction of the forces involved including a numerical simulation of the electric displacement is given below (Fig. 36).

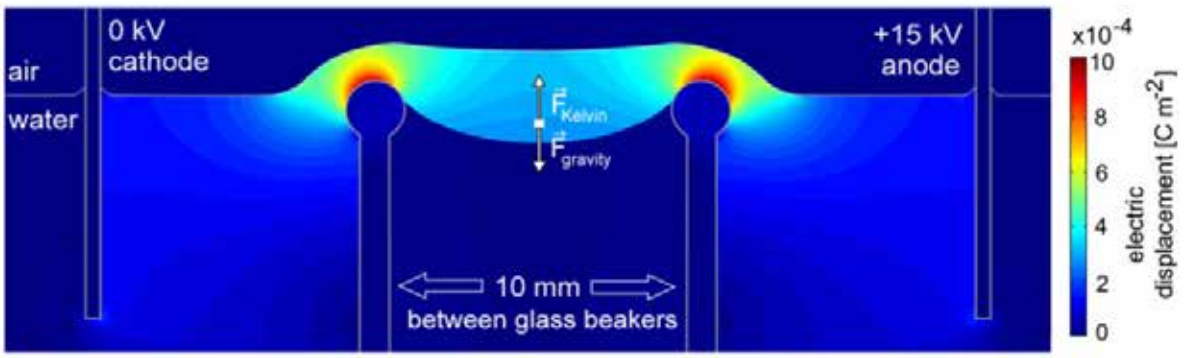

Fig. 36: Numerical simulation of the electric field within the water bridge using Comsol 4.1 software. Displayed are the absolute values of the electric displacement field. Ground potential is at infinity, cathode is at 0 kV (left), anode at 15 kV (right). The glass beakers have a slightly rounded brim. The Kelvin force density counteracts gravitational force (Woisetschläger, J. 2010).

As a final remark I would like to emphasize that this fundamental research should serve as a little step towards a more detailed understanding of natural processes which are influencing our environment nowadays more than ever. The acidification of our oceans which threatens over 1 million species (“a sea change”, http://www.aseachange.net/), the one billion people who have no access to clean drinking water and not at least the extremely high developed, industrial processes involving water, could benefit from this work.

7 References

Aerov, A.A. 2011, "Why the water bridge does not collapse", *Physical Review E,* vol. 84, no. 3, pp. 036314.

Agmon, N. 1995, "The Grotthuss Mechanism", *Chemical Physics Letters,* vol. 244, no. 5-6, pp. 456-462.

Andreescu, S., Andreescu, D. & Sadik, O.A. 2003, "A new electrocatalytic mechanism for the oxidation of phenols at platinum electrodes", *Electrochemistry Communications,* vol. 5, no. 8, pp. 681-688.

Anglada, A., Urtiaga, A., Inmaculada Ortiz 2009, "Contributions of electrochemical oxidation to waste-water treatment: fundamentals and review of applications", *Wiley Interscience,* .

Arani, R., Bono, I., Delgiudice, E. & Preparata, G. 1995, "Qed Coherence and the Thermodynamics of Water", *International Journal of Modern Physics B,* vol. 9, no. 15, pp. 1813-1841.

Barrero, A., Lopez-Herrera, J.M., Boucard, A., Loscertales, I.G. & Marquez, M. 2004, "Steady cone-jet electrosprays in liquid insulator baths", *Journal of colloid and interface science,* vol. 272, no. 1, pp. 104-108.

Boudenne, J.L., Cerclier, O., Galea, J., van der Vliest, E., 1996, "Electrochemical oxidation of aqueous phenol at a carbon black slurry electrode", *Applied Catalysis A,* vol. 143, pp. 185-202.

Burcham, C.L. & Saville, D.A. 2002, "Electrohydrodynamic stability: Taylor-Melcher theory for a liquid bridge suspended in a dielectric gas", *Journal of Fluid Mechanics,* vol. 452, pp. 163-187.

Burcham, C.L. & Saville, D.A. 2000, "The electrohydrodynamic stability of a liquid bridge: microgravity experiments on a bridge suspended in a dielectric gas", *Journal of Fluid Mechanics,* vol. 405, pp. 37-56.

Canizares, P., Dominguez, J.A., Rodrigo, M.A., Villasenor, J. & Rodriguez, J. 1999, "Effect of the current intensity in the electrochemical oxidation of aqueous phenol wastes at an activated carbon and steel anode", *Industrial & Engineering Chemistry Research,* vol. 38, no. 10, pp. 3779-3785.

Canizares, P., Dıaz, M., Domınguez, J. A., Garcıa-Gomez, J., Rodrigo, M. A., 2002, "Electrochemical Oxidation of Aqueous Phenol Wastes on Synthetic Diamond Thin-Film Electrodes", *Ind. Eng. Chem. Res.,* vol. 41, pp. 4187-4194.

Canizares, P., Martınez, F., Dıaz, M., Garcıa-Gomez, J. & Rodrigo, M. A. 2002, "Electrochemical Oxidation of Aqueous Phenol Wastes Using active and Nonactive Electrodes", *Journal of The Electrochemical Society,* vol. 8, no. 149, pp. D118-D124.

Castellanos, A. 1998, "Electrohydrodynamics", *No. 380 (Courses and Lectures); Springer, Springer Vienna, Austria,* .

Chatzidimitriou Dreismann, C.A., Redah, T.A., Streffer, R.M.F. & Mayers, J. 1997, "Anomalous deep inelastic neutron scattering from liquid H2O-D2O: Evidence of nuclear quantum entanglement", *Physical Review Letters,* vol. 79, no. 15, pp. 2839-2842.

Christensen, P.A. & Hamnett, A. 1989, "The Oxidation of Ethylene-Glycol at a Platinum-Electrode in Acid and Base - an Insitu Ftir Study", *Journal of Electroanalytical Chemistry,* vol. 260, no. 2, pp. 347-359.

Comninellis Ch., N.A. 1995, "Anodic oxidation of phenol in the presence of NaCl for wastewater treatment", *JOURNAL OF APPLIED ELECTROCHEMISTRY,* vol. 25, pp. 23-28.

Comninellis Ch., P.C. 1993, "Electrochemical oxidation of phenol for wastewater treatment using SnO2 anodes", *JOURNAL OF APPLIED ELECTROCHEMISTRY,* , no. 23, pp. 108-112.

Comninellis Ch., P.C. 1991, "Anodic oxidation of phenol for wastewater treatment", *JOURNAL OF APPLIED ELECTROCHEMISTRY,* vol. 21, pp. 703-708.

Corti, H.R. & Colussi, A.J. 2009, "Response to Reply to Comment on Can Water Store Charge?", *Langmuir,* vol. 25, no. 18, pp. 11203-11203.

Cramer, T., Zerbetto, F. & Garcia, R. 2008, "Molecular mechanism of water bridge buildup: Field-induced formation of nanoscale menisci", *Langmuir,* vol. 24, no. 12, pp. 6116-6120.

de la Mora, J.F. 2007, "The fluid dynamics of Taylor cones", *Annual Review of Fluid Mechanics,* vol. 39, pp. 217-243.

de Lima, R.B., Paganin, V., Iwasita, T. & Vielstich, W. 2003, "On the electrocatalysis of ethylene glycol oxidation", *Electrochimica Acta,* vol. 49, no. 1, pp. 85-91.

Delgado A.V., Gonzalez-Caballero F., Hunter R.J. , Koopal L. K., Lyklema J. 2005, "Measurement and interpretation of elektrokinetic phenomena", *Pure Appl. Chem.,* vol. 77, no. 10, pp. 1753-1805.

Del Giudice, E. 2007, "Old and new views on the structure of matter and the special case of living matter", Journal of Physics: Conference Series, vol. 67, no. 1, pp. 7pp.

Eisenhut. M, Guo. X, Paulitsch-Fuchs. AH, Fuchs EC, 2011, Aqueous phenol and ethylene glycol solutions in electrohydrodynamicliquid bridging. Cent Eur J Chem 9(3):391–403

Fino D., Carlesi-Jara C., Saracco G., Specchia V. and Spinelli V. 2005, "Deactivation and regeneration of Pt anodes for the electro-oxidation of phenol", *Journal of Applied Electrochemistry,* vol. 35, pp. 405-411.

Fino, D., Jara, C., Saracco, G., Specchia, V. & Spinelli, P. 2005, "Deactivation and regeneration of Pt anodes for the electro-oxidation of phenol", *Journal of Applied Electrochemistry,* vol. 35, no. 4, pp. 405-411.

Fleszar, B., J.P. 1985, "An attempt to defince benzene and phenol electrochemical oxidation mechansim", *Electrochemica Acta,* vol. Vol. 30, no. 1, pp. 31-42.

Fockedey , A., Van Lierde, F., 2002, "Coupling of anodic and cathodic reactions for phenol electro-oxidation using three-dimensional electrodes", *Water Research,* vol. 36, pp. 4169-4175.

Fuchs, E.C., Agostinho, L.L.F., Eisenhut, M. & Woisetschlaeger, J. 2010, "Mass and charge transfer within a floating water bridge", *Laser Applications in Life Sciences,* vol. 7376, pp. 73761E.

Fuchs, E.C., Agostinho, L.L.F., Wexler, A., Wagterveld, R.M., Tuinstra, J. & Woisetschlaeger, J. 2011, "The behaviour of a floating water bridge under reduced gravity conditions", *Journal of Physics D-Applied Physics,* vol. 44, no. 2, pp. 025501.

Fuchs, E.C, Brigitte Bitschnau, Silvia Di Fonzo, Alessandro Gessini, Jakob Woisetschläger and Filippo Bencivenga 2011, "Inelastic UV Scattering in a Floating Water Bridge", *Journal of Physical Science and Application,* , no. 1, pp. 147.

Fuchs, E.C., Baroni, P., Bitschnau, B. & Noirez, L. 2010, "Two-dimensional neutron scattering in a floating heavy water bridge", *Journal of Physics D-Applied Physics,* vol. 43, no. 10, pp. 105502.

Fuchs, E.C., Bitschnau, B., Woisetschlaeger, J., Maier, E., Beuneu, B. & Teixeira, J. 2009, "Neutron scattering of a floating heavy water bridge", *Journal of Physics D-Applied Physics,* vol. 42, no. 6, pp. 065502.

Fuchs, E.C., Gatterer, K., Holler, G. & Woisetschlaeger, J. 2008, "Dynamics of the floating water bridge", *Journal of Physics D-Applied Physics,* vol. 41, no. 18, pp. 185502.

Fuchs, E.C., Woisetschlaeger, J., Gatterer, K., Maier, E., Pecnik, R., Holler, G. & Eisenkoelbl, H. 2007, "The floating water bridge", *Journal of Physics D-Applied Physics,* vol. 40, no. 19, pp. 6112-6114.

Gattrell, M. & Kirk, D.W. 1993, "A Study of Electrode Passivation during Aqueous Phenol Electrolysis", *Journal of the Electrochemical Society,* vol. 140, no. 4, pp. 903-911.

Gattrell, M. & Kirk, D.W. 1993, "A Study of the Oxidation of Phenol at Platinum and Preoxidized Platinum Surfaces", *Journal of the Electrochemical Society,* vol. 140, no. 6, pp. 1534-1540.

Gonzalez, H., Mccluskey, F.M.J., Castellanos, A. & Barrero, A. 1989, "Stabilization of Dielectric Liquid Bridges by Electric-Fields in the Absence of Gravity", *Journal of Fluid Mechanics,* vol. 206, pp. 545-561.

Head-Gordon, T. & Johnson, M.E. 2006, "Tetrahedral structure or chains for liquid water (vol 103, pg 7973, 2006)", *Proceedings of the National Academy of Sciences of the United States of America,* vol. 103, no. 44, pp. 16614-16614.

Jones, T.B. 2002, "On the relationship of dielectrophoresis and electrowetting", *Langmuir,* vol. 18, no. 11, pp. 4437-4443.

Jorgensen, W.L. & Tirado-Rives, J. 2005, "Potential energy functions for atomic-level simulations of water and organic and biomolecular systems", *Proceedings of the National Academy of Sciences of the United States of America,* vol. 102, no. 19, pp. 6665-6670.

Kelaidopoulou, A., Abelidou, E., Papoutsis, A., Polychroniadis, E.K. & Kokkinidis, G. 1998, "Electrooxidation of ethylene glycol on Pt-based catalysts dispersed in polyaniline", *Journal of Applied Electrochemistry,* vol. 28, no. 10, pp. 1101-1106.

Kendall, J. 1916, "The specific conductivity of pure water in equilibrium with atmospheric carbon dioxide", *Journal of the American Chemical Society,* vol. 38, pp. 1480-1497.

Latimer, W.M. & Rodebush, W.H. 1920, "Polarity and ionization from the standpoint of the Lewis theory of valence", *Journal of the American Chemical Society,* vol. 42, pp. 1419-1433.

Lenz, A. & Ojamae, L. 2006, "Theoretical IR spectra for water clusters (H2O)(n) (n=6-22, 28, 30) and identification of spectral contributions from different H-bond conformations in gaseous and liquid water", *Journal of Physical Chemistry a,* vol. 110, no. 50, pp. 13388-13393.

Li, X., Cui, Y., Feng, Y., Xie, Z. & Gu, J. 2005, "Reaction pathways and mechanisms of the electrochemical degradation of phenol on different electrodes", *Water research,* vol. 39, no. 10, pp. 1972-1981.

M. Gattrell , D. W. Kirk 1993, "A Study of the Oxidation of Phenol at Platinum and Preoxidized Platinum Surfaces", *J. Electrochem. Soc., Vol. 140, No. 6,* vol. Vol. 140, no. No. 6.

Maheshwary, S., Patel, N., Sathyamurthy, N., Kulkarni, A.D. & Gadre, S.R. 2001, "Structure and stability of water clusters (H2O)(n), n=8-20: An ab initio investigation", *Journal of Physical Chemistry a,* vol. 105, no. 46, pp. 10525-10537.

Marchettini, N., Del Giudice, E., Voeikov, V. & Tiezzi, E. 2010, "Water: A medium where dissipative structures are produced by a coherent dynamics", *Journal of theoretical biology,* vol. 265, no. 4, pp. 511-516.

Marin, A.G. & Lohse, D. 2010, "Building water bridges in air: Electrohydrodynamics of the floating water bridge", *Physics of Fluids,* vol. 22, no. 12, pp. 122104.

Markovitch, O. & Agmon, N. 2007, "Structure and energetics of the hydronium hydration shells", *Journal of Physical Chemistry a,* vol. 111, no. 12, pp. 2253-2256.

Matsuoka, K., Iriyama, Y., Abe, T., Matsuoka, M. & Ogumi, Z. 2005, "Electro-oxidation of methanol and ethylene glycol on platinum in alkaline solution: Poisoning effects and product analysis", *Electrochimica Acta,* vol. 51, no. 6, pp. 1085-1090.

Melcher, J.R. & Warren, E.P. 1971, "Electrohydrodynamics of a Current-Carrying Semi-Insulating Jet", *Journal of Fluid Mechanics,* vol. 47, no. MAY14, pp. 127-&.

Mrazek, J. & Burda, J.V. 2006, "Can the pH value of water solutions be estimated by quantum chemical calculations of small water clusters?", *Journal of Chemical Physics,* vol. 125, no. 19, pp. 194518.

Mugele, F. & Baret, J.C. 2005, "Electrowetting: From basics to applications", *Journal of Physics-Condensed Matter,* vol. 17, no. 28, pp. R705-R774.

Nasr Bensalah , Gadri Abdellatif, Pablo Canizarez, Cristina Sa`ez , Justo Lobato, Manuel A . Rodrigo 2005, "Electrochemical Oxidation ofHydroquinone, Resorcinol, andCatechol on Boron-Doped Diamond Anodes", *Environ. Sci. Technol,* , no. 39, pp. 7234-7239.

Nishiumi, H. & Honda, F. 2009, "Effects of electrolyte on floating water bridge", *Research Letters in Physical Chemistry,* .

Ovchinnikova, K. & Pollack, G.H. 2009, "Can Water Store Charge?", *Langmuir,* vol. 25, no. 1, pp. 542-547.

Ovchinnikova, K. & Pollack, G.H. 2009, "Reply to Comment on Can Water Store Charge?", *Langmuir,* vol. 25, no. 18, pp. 11202-11202.

Parsons, R. & Vandernoot, T. 1988, "The Oxidation of Small Organic-Molecules - a Survey of Recent Fuel-Cell Related Research", *Journal of Electroanalytical Chemistry,* vol. 257, no. 1-2, pp. 9-45.

Pauling, L. & Corey, R.B. 1951, "Configurations of Polypeptide Chains with Favored Orientations Around Single Bonds - 2 New Pleated Sheets", *Proceedings of the National Academy of Sciences of the United States of America,* vol. 37, no. 11, pp. 729-740.

Pauling, L. & Corey, R.B. 1951, "The Pleated Sheet, a New Layer Configuration of Polypeptide Chains", *Proceedings of the National Academy of Sciences of the United States of America,* vol. 37, no. 5, pp. 251-256.

Paulitsch-Fuchs A.H., E.C. Fuchs, A.D. Wexler, F.T. Freund, L. J. Rothschild, A. Cherukupally, G. J. W Euverink 2012, "Prokaryotic transport in electrohydrodynamic structures", vol. 9Phys Biol.

Pellat, H. 1896, "Mesure de la force agissant sur les die´lectriques liquides non e´lectrise´s place´s dans un champ e´litrique.", *C R Acad Sci Paris,* vol. 123, pp. 691-696.

Pohl, H.A. 1958, "Some Effects of Nonuniform Fields on Dielectrics", *Journal of Applied Physics,* vol. 29, no. 8, pp. 1182-1188.

Pohl, H.A. 1951, "The Motion and Precipitation of Suspensoids in Divergent Electric Fields", *Journal of Applied Physics,* vol. 22, no. 7, pp. 869-871.

Ponterio, R.C., Pochylski, M., Aliotta, F., Vasi, C., Fontanella, M.E. & Saija, F. 2010, "Raman scattering measurements on a floating water bridge", *Journal of Physics D-Applied Physics,* vol. 43, no. 17, pp. 175405.

Raco, R.J. 1968, "Electrically Supported Column of Liquid", *Science,* vol. 160, no. 3825, pp. 311-&.

Ramos, A. & Castellanos, A. 1993, "Bifurcation Diagrams of Axisymmetrical Liquid Bridges of Arbitrary Volume in Electric and Gravitational Axial Fields", *Journal of Fluid Mechanics,* vol. 249, pp. 207-225.

Saf, R. Material science and characterization II, lecture at TU Graz, 2010

Saija, F., Aliotta, F., Fontanella, M.E., Pochylski, M., Salvato, G., Vasi, C. & Ponterio, R.C. 2010, "Communication: An extended model of liquid bridging", *Journal of Chemical Physics,* vol. 133, no. 8, pp. 081104.

Saville, D.A. 1997, Electrohydrodynamics: the Taylor-Melcher leaky dielectric model*, A. Rev. Fluid Mechanics, Vol 29: 27-64*

Silvana Andreescu, Daniel Andreescu & Omowunmi A. Sadik (2003), "A new electrocatalytic mechanism for the oxidation of phenols at platinum electrodes", *Electrochemistry Communications 5 , 681–688,* .

Stanley, H.E., Buldyrev, S.V., Franzese, G., Giovambattista, N. & Starr, F.W. 2005, "Static and dynamic heterogeneities in water", *Philosophical Transactions of the Royal Society of London Series A-Mathematical Physical and Engineering Sciences,* vol. 363, no. 1827, pp. 509-523.

Sumoto, I. 1955, "An Interesting Phenomenon Observed on some Dielectrics", *Journal of the Physical Society of Japan,* vol. 10, no. 6, pp. 494-494.

Svanberg, M. & Pettersson, J.B.C. 1998, "Structure and thermodynamics of H+(H2O)(n) (n = 9, 21, 40) clusters between 0 and 300 K. A Monte Carlo study", *Journal of Physical Chemistry a,* vol. 102, no. 10, pp. 1865-1872.

Taylor, G. 1969, "Electrically Driven Jets", *Proceedings of the Royal Society of London Series A-Mathematical and Physical Sciences,* vol. 313, no. 1515, pp. 453-&.

Taylor, G. 1964, "Disintegration of Water Drops in Electric Field", *Proceedings of the Royal Society of London Series A-Mathematical and Physical Sciences,* vol. 280, no. 1380, pp. 383-+.

Uhlig, W. "Personal communication, laboratory of inorganic chemistry. ETH Hönggerberg, HCI, Zürich"

Wales, D.J. & Hodges, M.P. 1998, "Global minima of water clusters (H2O)(n), n <= 21, described by an empirical potential", *Chemical Physics Letters,* vol. 286, no. 1-2, pp. 65-72.

Widom, A., Swain, J., Silverberg, J., Sivasubramanian, S. & Srivastava, Y.N. 2009, "Theory of the Maxwell pressure tensor and the tension in a water bridge", *Physical Review E,* vol. 80, no. 1, pp. 016301.

Woisetschlaeger, J., Gatterer, K. & Fuchs, E.C. 2010, "Experiments in a floating water bridge", *Experiments in Fluids,* vol. 48, no. 1, pp. 121-131.

Woisetschlaeger, J., Wexler, A.D., Holler, G., Eisenhut, M., Gatterer, K. & Fuchs, E.C. 2012, "Horizontal bridges in polar dielectric liquids", *Experiments in Fluids,* vol. 52, no. 1, pp. 193-205.

Yoon, J.H. & Lee, H. 1997, "Clathrate phase equilibria for the water phenol carbon dioxide system", *AIChE Journal,* vol. 43, no. 7, pp. 1884-1893.

Yousef Marei Awad & Nabil S. Abuzaid 1999, "Electrochemical Oxidation of Phenol Using Graphite Anodes", *Separation Science and Technology,* vol. 4, no. 34, pp. 699-708.

Yuen, M.C. 1968, "Non-Linear Capillary Instability of a Liquid Jet", *Journal of Fluid Mechanics,* vol. 33, pp. 151-&.

8 List of the figure captions

9 Appendix

Part I

9.1 **Aqueous phenol and ethylene glycol solutions in electrohydrodynamic liquid bridging**

Mathias Eisenhut, Xinghua Guo, Astrid H. Paulitsch-Fuchs, Elmar C. Fuchs
Central European Journal of Chemistry, 9(3), pp.391-403, 2011

Part II

9.2 **Methanol, Ethanol and Propanol in EHD liquid bridging**

Elmar C. Fuchs, Adam D. Wexler, Luewton L. F. Agostinho, Michael Ramek, Jakob Woisetschläger
Journal of Physics: Conference Series 329, 2011

Part III

9.3 **Horizontal bridges in polar dielectric Liquids**

Jakob Woisetschläger, Adam D. Wexler, Gert Holler, Mathias Eisenhut, Karl Gatterer & Elmar C. Fuchs
Experiments in Fluids, Volume 52 Number 1, 2012

Part IV

9.4 **Literature search of water related science**

Mathias Eisenhut, Karl Gatterer, Elmar C. Fuchst

TU Graz, physical chemistry project, 2008

Cent. Eur. J. Chem. • 9(3) • 2011 • 391-403
DOI: 10.2478/s11532-011-0029-3

VERSITA

Central European Journal of **Chemistry**

Aqueous phenol and ethylene glycol solutions in electrohydrodynamic liquid bridging

Invited Paper

Mathias Eisenhut[1,2], Xinghua Guo[2],
Astrid H. Paulitsch-Fuchs[1], Elmar C. Fuchs[1,*]

[1]*Wetsus – Centre of Excellence for Sustainable Water Technology, 8900 CC Leeuwarden, The Netherlands*

[2]*Institute of Analytical Chemistry and Food Chemistry, Graz University of Technology, 8010 Graz, Austria*

Received 30 November 2010; Accepted 10 February 2011

Abstract: The formation of aqueous bridges containing phenol and ethylene glycol as well as bisphenol-A, hydrochinone and p-cresol under the application of high voltage DC ("liquid bridges") is reported. Detailed studies were made for phenol and glycol with concentrations from 0.005 to 0.531 mol L^{-1}. Conductivity as well as substance and mass transfers through these aqueous bridges are discussed and compared with pure water bridges. Previously suggested bidirectional mass transport is confirmed for the substances tested. Anodic oxidation happens more efficiently when phenol or glycol are transported from the cathode to the anode since in this case the formation of a passivation layer or electrode poisoning are retarded by the electrohydrodynamic (EHD) flow. The conductivity in the cathode beaker decreases in all experiments due to electrophoretic transport of naturally dissolved carbonate and bicarbonate to the anode. The observed electrochemical behavior is shortly discussed and compared to known mechanisms.

Keywords: *Floating water bridge • Electrohydrodynamics • Phenol oxidation • Glycol oxidation*

1. Introduction

In 1893, Sir William Armstrong placed a cotton thread between two wine glasses filled with chemically pure water. After applying a high voltage, a watery connection formed between the two glasses, and after some time, the cotton thread was pulled into one of the glasses, leaving, for a few seconds, a rope of water suspended between the lips of the two glasses [1]. Although easy to reproduce, this watery connection with more or less cylindrical shape between the two beakers, henceforth referred to as 'water bridge', holds a number of interesting static and dynamic phenomena [2-7].

Molecular and nanoscale field-induced formations of liquid bridges of ethanol have been investigated in the framework of silicon carbide nanowire fabrication [8]; a molecular mechanism of the formation of a nanoscale water pillar has been presented [9]. On a macroscopic level, several of these phenomena can be explained by modern electrohydrodynamics, analyzing the motion of fluids in electric fields (see, *e.g.* the Maxwell pressure tensor considerations by Widom *et al.* [10], or the book of Castellanos [11]), while on the molecular scale water can be described by quantum mechanics (*e.g.* [12,13]). The gap at the mesoscopic scale is bridged by a number of theories including quantum mechanical entanglement and coherent structures in water, theories which are currently discussed (*e.g.* [14-18] for water in general, and [19] specifically for the water bridge). Previous experiments [2] suggested a possible change of the water microstructure inside the water bridge; first neutron scattering experiments [4] showed no difference in the microdensity of a D_2O bridge compared to the bulk; recent 2D neutron scattering experiments [5] indicated a preferred molecular orientation within a floating heavy water bridge; detailed optical investigations [6] suggested the existence of a mesoscopic bubble network within the water bridge; and a Raman scattering study on vertical water bridges reported on a polarized water structure induced by the electric field [20]. There is a comprehensive review about water bridge research [21] comprising its most important features, and the behavior of the phenomenon under low gravity conditions has been investigated recently [22].

* *E-mail: elmar.fuchs@wetsus.nl*

The properties of water at mesoscopic scales have drawn special attention due to their suggested relevance to human physiology [23].

Recently, the mechanism of charge storage and transfer in water in general has been reevaluated [24] and intensely discussed [25-27]. From the previous water bridge investigations [2-6] charge transport and possible nano-bubble formation in this experiment remains to be satisfactorily explained. Another recent study [28] indicates the existence of a mesoscopic charge and mass and transport mechanism in pure water.

As far as the basic mechanism of the water-bridge formation is concerned, the phenomenon is well-established [21] and was explained in some recent papers using simple schemes [29-31]. According to those schemes, the most important properties necessary for a liquid bridge formation are high dielectric permittivity, low electric conductivity and a permanent molecular dipole moment. Thus the phenomenon is not water-specific but can be reproduced with any liquid of similar properties like methanol [21] or glycerol [30].

One feature which is not very well understood is the electrochemical behavior. Although there is a significant current flow, electrolysis is not observed [2-6], and the addition of substances which increase the conductivity like salts [7] or pH dyes [28] destabilizes the bridge and promotes electrochemical reactions. So far, the electrochemistry of non-ionic solvents has not been investigated in the set-up described. This work intends to start filling this gap. Therefore, the high voltage electrochemistry of phenol and ethylene glycol was investigated. Since the anodic oxidation of phenol is very well-studied due to its importance in waste water treatment [32-40], its electrochemical behavior is very well known. Therefore it was chosen as sample substance. For comparative reasons, the behavior of the simple aliphatic alcohol ethylene glycol, whose anodic decomposition has also been thoroughly investigated [41-46], was examined as well.

2. Experimental Procedure

Experiments were carried out using glass beakers (Pyrex) with 60 mm diameter and 35 mm height filled with de-ionized water. Each beaker had a wall strength of 1.5 mm, a 2.2 – 2.5 mm (diameter) lip around the upper edge and a single spout. The beakers were filled with de-ionized water such that the water surface was about 3 mm below the beaker's edge which resembled, for pure water at room temperature, a mass of 66.0±0.5 g. The initial conductivity of the de-ionized water was 0.055 µS cm^{-1} measured with the integrated conductivity/TOC meter of the Millipore A10 TOC type water supply system (Millipore Corp., Billerica, MA, USA). This value rose quickly to 0.4 - 1.0 µS cm^{-1} depending on the atmospheric conditions and storage time in a dark glass bottle. The pH value of the water was around 5 due to CO_2 saturation and a TOC amount of three ppb. For pH estimations a Merck pH-Box paper (pH 1-10, Art. Nr. 109526) was used. For conductivity measurements, a conductivity meter 3210 from WTW (Wissenschaftlich-Technische Werkstätten GmbH, Weilheim, Germany) was used, which was calibrated by the manufacturer and had a measurement range from 0.01 – 200 µS cm^{-1}. For all experiments thin platinum plates (2.5×2.5 cm^2, 0.5 mm thickness) were used as electrodes. These plates were placed in the rear part of the beakers so that the distance between the electrodes was ~12 cm. The aqueous bridges were created by positioning the beakers' spouts pointing at each other in line with the electrodes.

The power was provided by a FUG HCP 350-65000 (serial no.: 161119-01-01, FUG Elektronik GmbH, Rosenheim, Germany) with the dc output stable up to 5 mA and the voltage continuously adaptable up to 70 kV with a waviness smaller than 0.05% and a 0.1 kV accuracy. The operating voltage of the floating water bridge varied between 5 kV and 20 kV at a current of 0.5 mA. In all experiments, the anode (+ pole, high voltage) was on the left, the cathode (- pole, ground) on the right. For imaging, a Panasonic HDC-SD100 camera with a 2.95 - 35.4 mm lens was used. All images were scaled. With this scaling and the above macro lenses, the bridge diameter and length were measured within ± 0.2 mm accuracy (± 0.1 mm at each side). To record the mass flow through the water bridge both beakers rested on electronic scales (EW 1500-2M, Kern, Balingen, Germany), each equipped with a serial interface with a measurement range of 0 – 1500 g and ±0.01 g accuracy.

The phenol or ethylene glycol stock solution (1 mM, 10 mM) were prepared (phenol for synthesis, Sigma Aldrich, purity: ≥99.9; ethylene glycol, VWR, purity: ≥99%) with de-ionized water (Milli-Q system, $\Omega_{internal}$ > 18 MΩ cm) for all experiments and then filled in a clean glass beaker right before the experiment. The beakers were always filled with the same weight of the solutions (measured with a B3001-S balance produced by Mettler Toledo, accuracy: ± 0.1g) before the voltage was applied. Temperature and conductivity of the solutions were measured in both beakers before and directly after the experiment. As soon as the bridge was formed, the beakers were pulled apart to a distance of 1.0 (± 0.1) cm between the spout tips. The average time between the formation and final beaker position was ~35 s. In this time the balances showed high

Table 1. List of conducted bridge experiments.

Nr.	Cathodic beaker		Anodic beaker		Analyses
	substance	conc.	substance	conc.	transport, concentration
1a	**phenol**	1 mM	water		transport, concentration
1b	water		**phenol**	1 mM	transport, concentration
2a	**phenol**	10 mM	water		transport, concentration
2b	water		**phenol**	10 mM	transport, concentration
3a	**phenol**	0.53 mM	**phenol**	0.53 mM	concentration
3b	**phenol**	5 mM	**phenol**	5 mM	concentration
3c	**phenol**	10 mM	**phenol**	10 mM	concentration
3d	**phenol**	50 mM	**phenol**	50 mM	concentration
3e	**phenol**	100 mM	**phenol**	100 mM	concentration
3f	**phenol**	531 mM	**phenol**	531 mM	SEM, EDX, optical
4a	water		**glycol**	10 mM	transport, concentration
4b	**glycol**	10 mM	**water**		transport, concentration
5a	**glycol**	3.6 mM	**glycol**	3.6 mM	concentration
5b	**glycol**	11.3 mM	**glycol**	11.3 mM	concentration
5c	**glycol**	46 mM	**glycol**	46 mM	concentration
5d	**glycol**	450 mM	**glycol**	450 mM	concentration
6a	**bisphenol-A**	100 μg L^{-1}	water		feasibility
6b	water		**bisphenol-A**	100 μg L^{-1}	feasibility
7a	**hydrochinone**	50 g L^{-1}	water		feasibility
7b	water		**hydrochinone**	50 g L^{-1}	feasibility
8a	**hydrochinone**	500 mg L^{-1}	water		feasibility
8b	water		**hydrochinone**	500 mg L^{-1}	feasibility
9a	**p-cresol**	100 μg L^{-1}	water		feasibility
9b	water		**p-cresol**	100 μg L^{-1}	feasibility
10a	**p-cresol**	100 mg L^{-1}	water		feasibility
10b	water		**p-cresol**	100 mg L^{-1}	feasibility

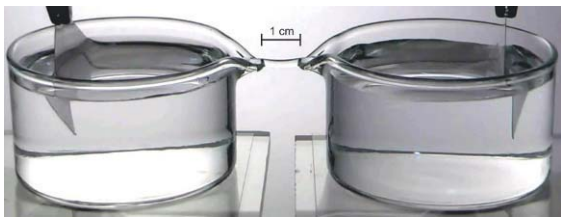

Figure 1. Stable liquid bridging with deionized water, 10 kV DC, 0.3 mA, Pt electrodes.

fluctuations due to the beaker movement, which are thus not taken into consideration in the consequent graphs and calculations. The experiments carried out are summarized in Table 1. In all experiments, the operating voltage was 10 (±1) kV; the current was ~0.3 mA for concentrated solutions of 1 mM or less, and ~0.75 mA for concentrations of 10 mM or more.

It should be noted that "experiment" does not equal a single measurement but a number of measurements. Six measurement series were carried out with the concentrations of 1 mM (phenol) and 10 mM (phenol, ethylene glycol), in either anodic or cathode beaker with the other beaker filled with pure water (Exp. 1, 2 and 4). The experiments lasted between 60 and 3000 seconds enabling the determination of the solute's concentration and the mass transport as a function of time. The equilibrium experiments (Exp. 3 and 5) were run as long as possible, where bridges using solutions with higher concentrations tended to be less stable than those with lower concentrations. Finally, the feasibility of bridge formation using solutions of bisphenol-A, hydrochinone and p-cresol was investigated (Exp. 6-10). If an unexpected breakdown of the bridge

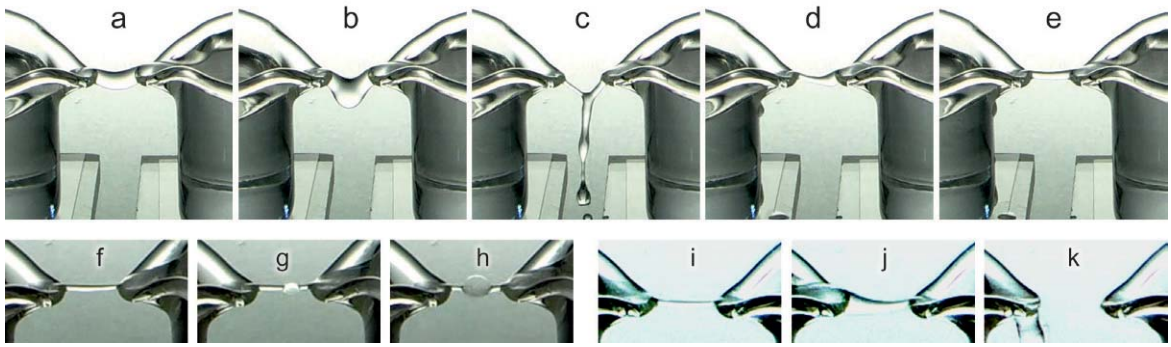

Figure 2. Typical bridge instabilities: leaking bridge (a-e) (0.531 mol L^{-1} phenol in anode beaker); bubble in bridge (f-h) (50 g L^{-1} hydrochinone in anode beaker); asymmetric shape and breakdown (i-k) (50 g hydrochinone in cathode beaker)

or visible discharges between the beakers occurred, the experiment was excluded from the evaluation. The detection of the phenol concentration was done using a 'Dr.Lange' quick test with an approximate error of 5 %. Due to the formation of polymeric phenol derivatives on the anode, the electrodes had to be cleaned chemically (conc. H_2O_2 and conc. HNO_3) after each experiment [37].

The ethylene glycol was quantified using GC-MS (Agilent 6890 GC coupled with a 5973 MSD, Agilent, Waldbronn, Germany) with a polar capillary column consisting of cross-linked polyethylene glycol (Innowax, 30 m×2.5 mm×25 µm). The temperature gradient of 80°C to 260C° with a heating rate of 10°C min^{-1} was used. The temperature of the injector was 250°C. The ionization energy was 70 eV (EI). The selected ion monitoring (SIM) mode was applied. An external calibration in the range of 0.05 to 6 mM was used for the quantification of ethylene glycol. The samples were diluted 10-100 times with water before measurements.

3. Results and Discussion

Stable liquid bridging (see Fig. 1) could be accomplished with solutions of all substances listed in Table 1. If not mentioned otherwise, the temperature change of the beakers was similar to that of pure water [6] starting from 19°C and slowly rising up to ~24°C after the longest measurement time (30 min).

Some of the stable bridges became unstable and/or broke down during the experiments. The most common instability observed was leaking (see Fig. 2a). This also happened to a water bridge if the amount of water in the beakers was too large and/or the current was too high so that bridges with diameter thicker than ~4 mm were formed. Moreover, this kind of instability was also caused by very high concentrations of phenol. Interestingly, high concentrations of hydrochinone caused different instabilities depending on where the substance was located: When a 50 g L^{-1} hydrochinone solution was bridged to water in the cathode beaker, sometimes bubbles would form within the bridge (Figs. 2f-h). It should be mentioned here that the bubbles shown in Figs. 2g-h show two separate events and not a time evolution. With the position of the beakers interchanged the shape of the bridge became more cone-like (see Figs. 2i-k) before breaking down.

3.1. Phenol solutions

Previous studies with pure water have shown that there is a general trend of more water flowing into the cathode beaker than vice versa, resulting in an increase of the water level in the cathode beaker until a labile equilibrium is reached [3].

Low concentrations (1 mM L^{-1}) of phenol did not change this behavior.

The concentrations obtained after a series of measurements run for times between 30 and 3060 seconds of a 1 mM phenol solution are shown in Figs. 3 and 4 for transport from anode to cathode and *vice versa*, respectively (exp. 1a and 1b).

The concentration sum (here fitted with a linear slope including 95% confidence and prediction bands) shows that in these experiments the electrochemical decomposition of phenol seems negligible, however, the conductivity measurements clearly indicate a partial decomposition in the anodic beaker (Figs. 5 and 6).

This happened at a faster rate when the phenolic solution was already present at the anode (Fig. 6) than when it had to be transported there (Fig. 5). Interestingly, the conductivity in the cathode beaker seems to decrease – not only when the phenolic solution is present in that beaker (Fig. 5), but also in the case of pure water (Fig. 6). Most probably, this effect has nothing to do with phenol and is a result of electrophoretic transport of the natural HCO_3^- and CO_3^{2-} ions [47] to the (positive) anode. A quick test of the pH showed indeed a neutral – basic milieu in the cathode beaker (7-8) and an increased acidity in the anode beaker (4-5).

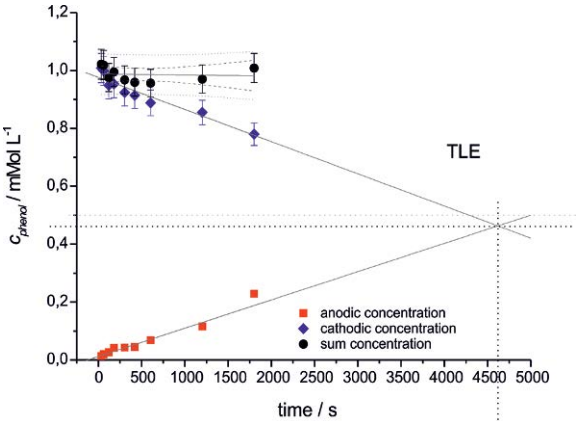

Figure 3. Exp. 1a: Transport of phenol from cathode to anodic beaker. The grey dashed line marks the theoretical mixture concentration (0.5 mmol L^{-1}); the black dashed lines show concentration and time at the theoretical linear equilibrium (TLE). The concentration sum is evaluated with a linear fit including 95% confidence (dashed) and 95% prediction (dotted) intervals.

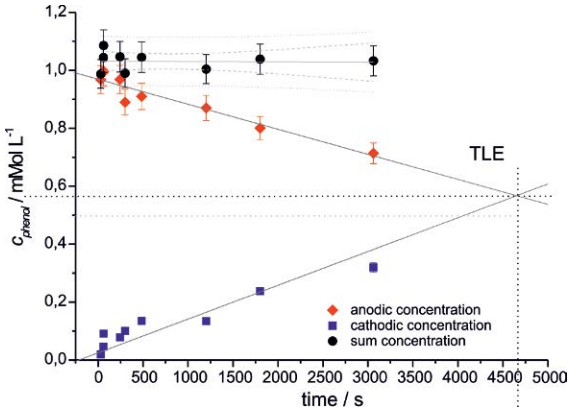

Figure 4. Exp. 1b: Transport of phenol from anodic to cathode beaker. The grey dashed line marks the theoretical mixture concentration (0.5 mmol L^{-1}); the black dashed lines show concentration and time at the theoretical linear equilibrium (TLE). The concentration sum is evaluated with a linear fit including 95% confidence (dashed) and 95% prediction (dotted) intervals.

The linear extrapolations in Figs. 3 and 4 were added in order to obtain the "theoretical linear equilibrium" (TLE), the time when the concentrations in both beakers would be the same provided that only water is transported from the water beaker, and the concentration in the phenol beaker remains the same. Strictly spoken, this is only true for the very first moment of bridging; and due to mixing in the beakers this behavior is in reality rather hyperbolic than linear. However, this extrapolation works well for the purpose of comparison. In case of the 1 mM solutions these times are 4667 s (anode to cathode) and 4623 s (cathode to anode), thus comparable within a 10% error. Furthermore, the theoretical end concentration is slightly above 0.5 mM (the concentration achieved after perfect mixing) in case of the anode to cathode transport, and below 0.5 mM in the cathode to anode experiment. This is due to the fact that in both cases the transport rate from anode to cathode is slightly higher than the flow from cathode to anode which is in general agreement with the mass transport observed in this work and in earlier experiments for pure water [3,6].

Previous experiments revealed mono-directional mass transfer rates between 40 and 280 mg s^{-1} [6]. In this work we provide additional proof that the mass transport is actually bidirectional, since whereas the phenol concentration is rising in the water beaker, it is declining in the beaker with the phenol solution. This is, for obvious reasons, only possible if a bidirectional flow occurs. The transport rates are of the same order of magnitude as the mono-directional ones observed with water [6], namely up to 182 mg s^{-1} when calculated from the actual weight, and up to 103 mg s^{-1} when calculated from the concentration differences.

When looking at the 10 mM series (exp. 2a and 2b) shown in Figs. 7 and 8, the chemical decomposition of phenol is no longer negligible. Here, a significant decline of the concentration sum is observed.

The phenol concentration decreases much faster in the cathode beaker than it increases in the anode beaker, resulting in a steeper decline of concentration sum in this case. The most plausible explanation for this is that a part of the phenol is immediately oxidized once it is transported to the anode. This happens faster when the phenol is transported to the anode (Fig. 8) than when it is already present there (Fig. 7). This seeming contradiction can be explained by the formation of a passivation layer on the anode [39] due to the high phenol concentration. Such a layer obstructs further chemical reactions (see chapter 4 for details on the phenol degradation process). However, if the phenol is transported to this electrode via the EHD flow, which leads from the bridge directly towards the electrode and along its surface downwards into the bulk (see [28] for a detailed description of the lemniscate flow shape), the formation of such a layer is probably hampered both due to the lower overall concentration and due to the flow itself which removes any oxidation products instantly from the electrode surface, and thus electrochemical oxidation processes can happen more easily.

The behavior of the conductivity does not appear to be very regular (Figs. 9 and 10), but as it was the case for the 1 mM concentration, it increases in the anode beaker whereas it decreases in the cathode beaker.

In experiments 2a and 2b the preferred substance transport direction was no longer from anode to cathode, but from water to phenol, as can be seen from

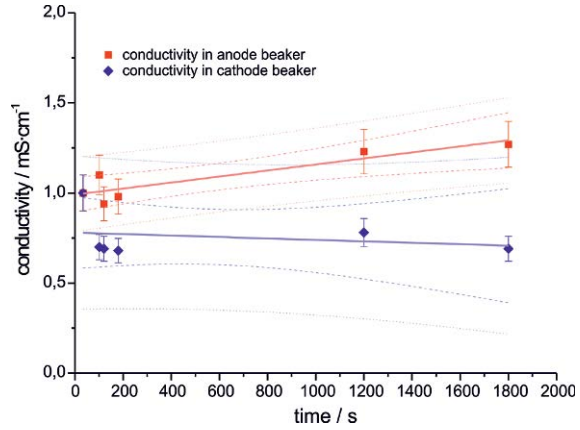

Figure 5. Exp. 1a: Transport of phenol from cathode to anodic beaker, conductivity measurement evaluated with a linear fit including 95% confidence (dashed) and 95% prediction (dotted) intervals.

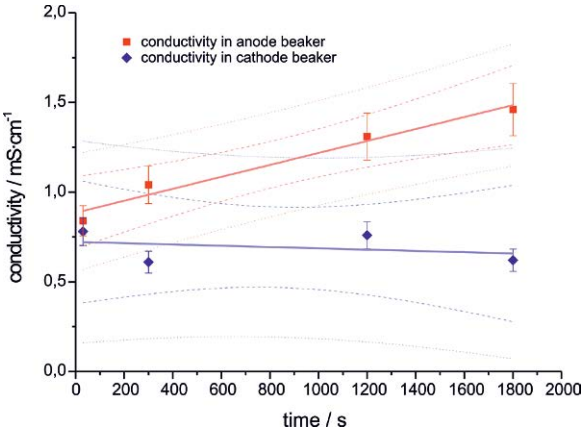

Figure 6. Exp. 1b: Transport of phenol from anodic to cathodic beaker, conductivity measurement evaluated with a linear fit including 95% confidence (dashed) and 95% prediction (dotted) intervals.

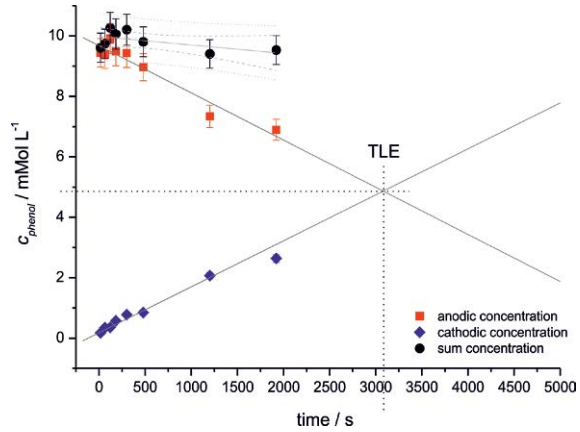

Figure 7. Exp. 2a: Transport of phenol from anode to cathode beaker. The grey dashed line marks the theoretical mixture concentration (5 mmol L^{-1}); the black dashed lines show concentration and time at the theoretical linear equilibrium (TLE). The concentration sum is evaluated with a linear fit including 95% confidence (dashed) and 95% prediction (dotted) intervals.

Figs. 7 and 8 where both TLE concentrations are below 5 mmol L^{-1}. However, this should not be confused with the actual mass transport behavior which remained the same and comparable to that of water [6] with the main flow from anode to cathode – with one exception: For reasons still to be discovered this direction was reversed in one measurement, resulting in more mass in the anode beaker than in the cathode beaker during bridge operation. This exception is compared to a normal mass transport behavior in Fig. 11. The exceptional bridge (orange and cyan lines) started with a mono-directional water flow with rates up to ~ 1000 mg s^{-1} for a few seconds. After ~5 g of water were transferred (~10 s) the behavior changed to that of a regular phenol bridge (blue and red lines).

The irregularities between 10 and 35 seconds (dotted grey markers) are caused by the beaker separation process on the balances and may not display actual mass changes.

This behavioral pattern could not be repeated since its cause is hitherto unclear; it may not be restricted to the phenol bridge only. A recent work about charge and mass transfer in the water bridge [28] showed that these issues still require some clarification, and future investigations will be aimed at a further understanding of the mass transfer and its directions.

The anode reactions of aqueous phenol solutions in low voltage electrolysis are very well understood and discussed in the literature [32,34,36,39]. Normally, an inhibited electrochemical process takes place on the anodic platinum surface; Gattrell and Kirk [32] showed that the oxidation of phenol to a phenoxy radical- and subsequent quinone- and ether structures at the outer Helmholtz layer is followed by an oxidation of these structures at the inner Helmholtz layer leading to a polymeric film on the anode, carboxylic acids in solution and finally CO_2. The formation of such a layer is common and for low-voltage electrolysis of phenolic solutions (see also [34], [36], [39]) and was also found in the current experiments. Gas formation at the anode could be observed as well, albeit only at very high (Exp. 5f, c = 50 g L^{-1}) concentrations (see Figs. 12 and 13). The chemical composition determined with EDX revealed a surface composition of 51% Pt, 46% C and 4% O which is consistent with partial covering of the electrode with the polymeric film mentioned above.

The formation of intermediate products can be observed indirectly by the schlieren formation close to the anode (see Figs. 13 b-d) and caused an increase in conductivity, which resulted in an increase of the current necessary to uphold the bridge over time (from 0.3 to 0.75 mA) and thus a relatively larger temperature increase of the solution (from 19°C to 27°C). Moreover,

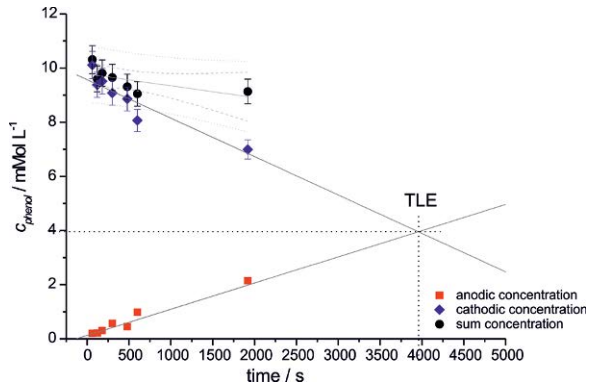

Figure 8. Exp. 2b: Transport of phenol from cathode to anode beaker. The grey dashed line marks the theoretical mixture concentration (5 mmol L^{-1}); the black dashed lines show concentration and time at the theoretical linear equilibrium (TLE). The concentration sum is evaluated with a linear fit including 95% confidence (dashed) and 95% prediction (dotted) intervals.

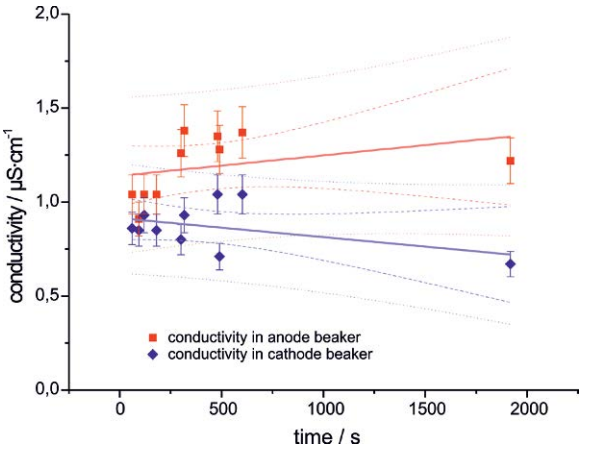

Figure 9. Exp. 2a: Transport of phenol from cathode to anodic beaker, conductivity measurement. The values are evaluated with a linear fit including 95% confidence (dashed) and 95% prediction (dotted) intervals.

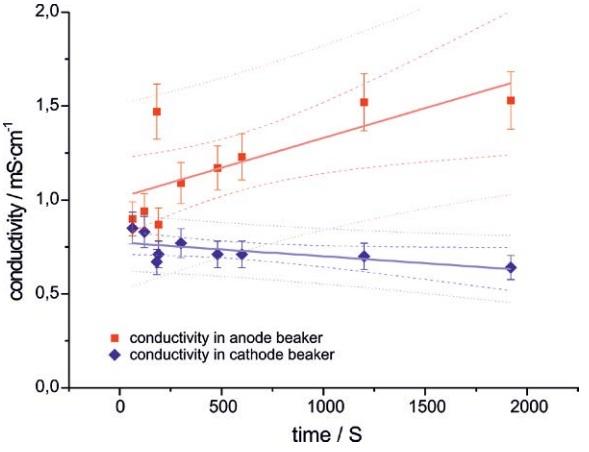

Figure 10. Exp. 2b: Transport of phenol from anodic to cathode beaker, conductivity measurement. The values are evaluated with a linear fit including 95% confidence (dashed) and 95% prediction (dotted) intervals.

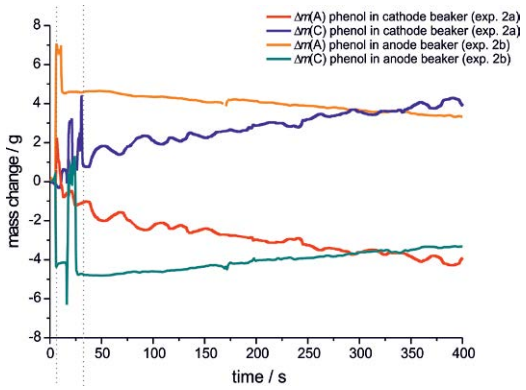

Figure 11. Comparison of the measured mass flow of one exemplary experiment of the series 2a with an extraordinary one of series 2b. The dotted grey lines mark the beaker separation time during which the read out of the balances is partly erroneous.

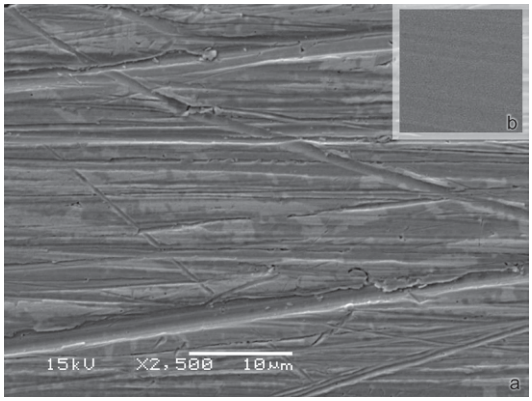

Figure 12. SEM picture of the anodic platinum electrodes after experiment 5f (a, 50 g L^{-1}, 9 kV, 0.75 mA). The insert (b) shows the surface of the clean cathode as comparison (same magnification).

a passivation of the electrode surface as suggested by. Xiao-yan Li *et al.* [39] could have contributed to the higher current requirement.

The equilibria experiments started with phenol solutions of the same concentrations in both beakers and showed that the concentrations remained constant throughout the experiment, thus no electrophoretic separation occurred (Exp. 3a-3e, see Fig. 14). Small deviations were caused by oxidation/precipitation on the anode as described above. Sometimes, especially at higher concentrations (0.531 mol L^{-1}) a few bubbles appeared after around 5 min on the anode (see also Fig. 13). Since there are no bubbles at the cathode and there is no bubble formation at all when lower concentrations were used, this work confirms the earlier findings [2-6] that electrolysis is not observable. Thus it is safe to assume that the gas formed at the anode is CO_2 due to the degradation of phenol.

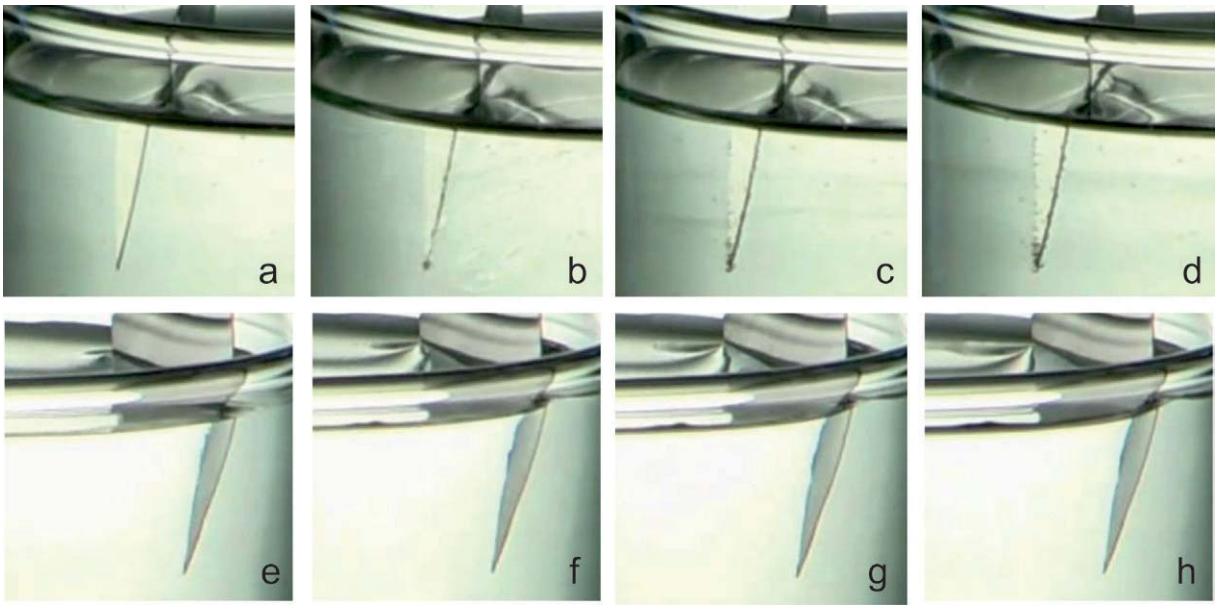

Figure 13. Gas formation over time at the anode (a-d) during experiment 5f (531 mM phenol in both beakers) in comparison to the cathode where no gas formation could be observed (e-h). The pictures were taken after 34 (a,e), 94 (b,f), 214 (c,g) and 274 s (d,h), respectively.

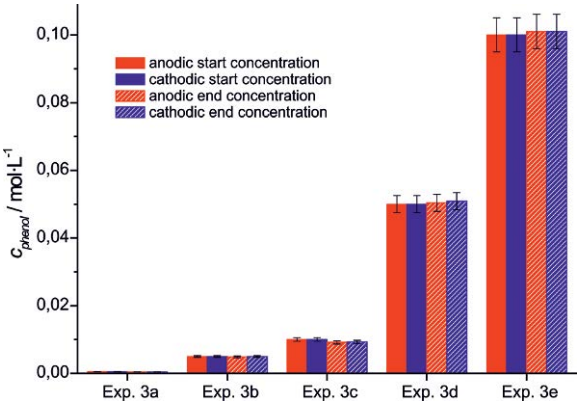

Figure 14. Concentration comparison after the equilibria experiments (3a-3e). The bridges were run for 600 s except Exp. 3c which was run for 580 s.

3.2. Ethylene glycol solutions

In contrast to phenol, ethylene glycol derivatives do not easily polymerize, thus neither the anode nor cathode showed any precipitates. The concentration and conductivity behavior was comparable to that of phenol of the same concentration (Exp. 2b, Figs. 7 and 8) and is shown in Figs. 15 and 16.

In Fig. 15 the concentration sum seems to increase over time. Naturally, this is impossible since the start concentration for all measurements was 10 mM. However, all sum values are within the measurement precision of 5%, thus the concentration sum can and will be considered as constant.

The behavior of the 10 mmol L^{-1} glycol solution is comparable to that of the phenol solution with the same concentration. The TLE times differ significantly, and the TLE concentrations are below the optimum mixture concentration (5 mmol L^{-1}) for both experiments (4a, 4b). As it is the case for phenol the concentration of glycol decreases more rapidly in the cathode beaker than it increases in the anode beaker (Fig. 16) resulting in a decline of the concentration sum, whereas this is not the case when glycol is transported from anode to cathode beaker (Fig. 15). The explanation for this behavior is also similar to that for phenol: Here, electrode poisoning may happen once a significant amount of formate [42] is formed on the anode surface – and again, this is much more likely to happen when the anode is all the time surrounded by glycol molecules – and much less likely to happen when the glycol is transported to the anode and any products like, *e.g.* formate or oxalate, are immediately removed by the EHD flow and diluted into the bulk. Details on the electrolytic glycol degradation are given in the next chapter.

The conductivity behavior is different from that of the phenol solution. In case of exp. 4a (Fig. 17) the conductivity of the anode beaker is slowly rising since it is being diluted by water, whereas the conductivity in the cathode beaker is decreasing, since the glycol content is increasing.

When looking at exp. 4b, the general trends are the same with the starting conductivities being reversed. This suggests that although glycol is transported towards the anode, the conductivity rises.

Actually, this is not true for short times, as can clearly be seen from Fig. 18. Only after ~120 seconds the

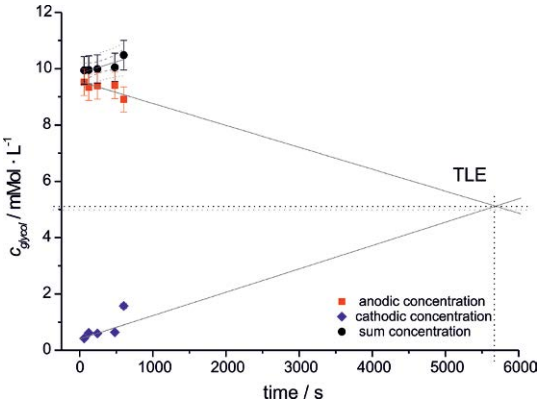

Figure 15. Exp. 4a: Transport of glycol from anode to cathode beaker. The grey dashed line marks the theoretical mixture concentration (5 mM); the black dashed lines show concentration and time at the theoretical linear equilibrium (TLE). The concentration sum is evaluated with a linear fit including 95% confidence (dashed) and 95% prediction (dotted) intervals.

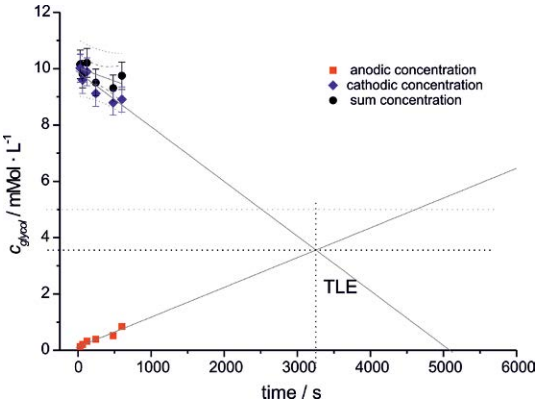

Figure 16. Exp. 4b: Transport of glycol from cathode to anode beaker. The grey dashed line marks the theoretical mixture concentration (5 mM); the black dashed lines show concentration and time at the theoretical linear equilibrium (TLE). The concentration sum is evaluated with a linear fit including 95% confidence (dashed) and 95% prediction (dotted) intervals.

chemical degradation of glycol is more important than the decrease due to the mixture of water with glycol, and the conductivity rises. As it was the case for all experiments, the conductivity in the cathode beaker slowly decreases, suggesting again that the transport of naturally dissolved carbonate and bicarbonate to the anode is the most important process responsible for that. As it was the case for the phenol solutions, a quick pH paper test confirmed this assumption (basic-neutral pH in the cathode, acidic pH in the anode beaker).

The equilibria experiments with glycol showed that the concentrations remained constant throughout the experiments, thus no electrophoretic separation occurred (Exp. 5a-5e, see Fig. 19) as it was also the case for phenol solutions. Small deviations occurred probably due to oxidation on the anode described above or are within the measurement error and thus not significant.

4. Electrochemistry aspects

4.1 General

Since no gas formation was observed during the experiments with lower solute concentration, it is assumed that the electrochemical pathway which leads to CO_2 formation is (partly) inhibited. In a first approximation it can be stated that without any electrolyte added an organic degradation is more difficult than with an electrolyte. The influence of the CO_2 concentration of the surrounding atmosphere on the bridge has been reported earlier [3] showing that a CO_2 increase lead to immediate destabilization and consequent destruction of the water bridge. This indicates that in an EHD bridge set-up the CO_2 solubility of the water is increased which could thus be a reason for the absence of bubble formation in the present experiment. It is also likely that dissolved CO_2 is concentrated in the anode beaker due to lower pH and a higher conductivity. A detailed analysis of the pH value and the behavior of pH dyes in an EHD bridge is discussed elsewhere [28] and corroborates this assumption, since even with pure water there is a slight pH difference after bridge operation with a slightly lower pH in the anode beaker (5) compared to the cathode beaker (6).

The solution on the anodic side was always a few degrees warmer than the cathode side after the experiment, partly due to the fact that more chemical reactions took place in that beaker. However, the temperature increases were the same for phenol and ethylene glycol solutions as well as for pure water where presumably no electrochemical reactions occur [4,28]. Thus, the more prominent effect here seems to be purely physical: After reaching a labile equilibrium [4], there is less water in the anodic beaker than in the cathode beaker, and a constant flow of hot water in both directions is established. Thus, a smaller volume (the anodic beaker) heats up more quickly than a larger volume (the cathode beaker) when sustained by the same heat source - the bridge.

4.2 Anodic phenol oxidation

There are three known pathways for phenol oxidation on an electrode discussed by Canizares *et al.* [40]:

a. A direct electrochemical “cold combustion”: $Pt(OH\bullet) + R \rightarrow mCO_2 + nH_2O + Pt$, which is catalyzed by physisorbed hydroxyl radicals on a metal surface yielding water and carbon dioxide (*complete oxidation*).

b. The “indirect” chemical oxidation in which

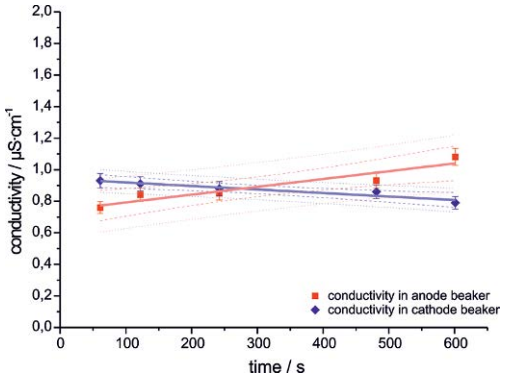

Figure 17. Exp. 4a: Transport of glycol from anode to cathode beaker, conductivity measurement evaluated with a linear fit including 95% confidence (dashed) and 95% prediction (dotted) intervals.

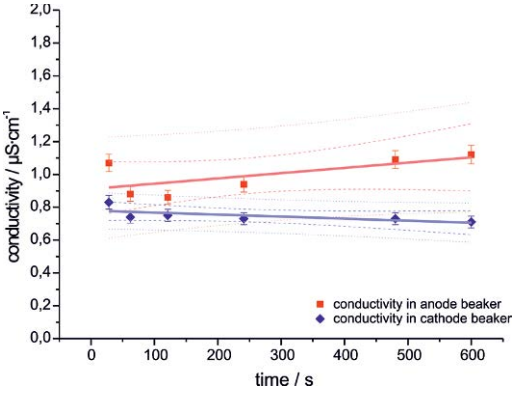

Figure 18. Exp. 4b: Transport of phenol from cathode to anode beaker, conductivity measurement. The values are evaluated with a linear fit including 95% confidence (dashed) and 95% prediction (dotted) intervals.

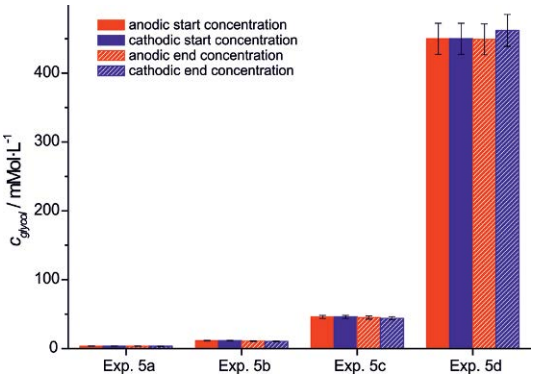

Figure 19. Concentration comparison after the equilibrium experiments (5a-5e). The bridges were run for 600 s except Exp. 5c which was run for 250 s.

chemisorbed hydroxyls selectively produce phenol intermediates via a heterogeneously catalyzed oxidation at the electro-oxidized active sites [40] (*partly oxidation*).

c. An electrophilic attack of hydroxyl on phenol, $C_6H_5(OH) + OH\bullet \rightarrow C_6H_5O\bullet + H_2O \rightarrow$ polymers, starting a *radical polymerization*. As the polymers formed have a lower oxidation potential than phenol, they are more easily oxidized to radicals which can interact with each other by forming polymers of higher molecular weights, leading to the development of a passivating film on the surface of the electrode.

The preferred pathway for a platinum/phenol/water system according to Gattrell and Kirk [32] is the indirect oxidation (b). The oxidation rate increases when more active PtOH• sites on the metal surface (inner Helmholtz layer, "IHL") are available since they are catalyzing this process. The number of hydroxyl ions desorbing from the Pt depends on the oxidized products in the outer Helmholtz layer ("OHL", approx. 2 nm from the metal surface [32]), *e.g.*: phenoxy radicals, benzoquinone, hydroquinone and aromatic radical polymer precursors, which are blocking the OHL reactions and let the IHL reactions predominate. The more reduced Pt sites are available on which OH can adsorb, the higher the oxidation rate of phenol. The polymerization (c) is always active, depending on pH, temperature and current density, thereby decreasing the active electrode surface as a function of time. If phenol directly is adsorbed on the Pt-surface, oxidation is suppressed whereas polymerization can still occur.

In our experiments, a polymeric film on the anode was always formed regardless of the phenol concentration. At the highest concentration used (0.531 mol L^{-1}), gas formation at the electrodes could be observed. These observations allow the following conclusions: Generally, polymerization (c) seems to be the predominant pathway for low concentration experiments, whereas partial and possibly full oxidation may play a role for the higher concentrations.

One has to keep in mind, however, that the quoted pathways and reactions are defined for experiments using voltages approximately 4-5 orders of magnitude lower than in the experiments presented. In low voltage experiments, the complete oxidation of phenol happens directly at the surface (IHL), whereas intermediates and successively polymers are formed a few nanometers away (OHL). When applying high voltage, it is plausible to assume that there might be more than two layers, and that the thickness of these layers is increased. Thus, an expanded OHL would provide more polymerization educts, which precipitate on the anode before direct cold combustion or the indirect chemical oxidation can become relevant.

Alternatively, one could imagine that the IHL layer is constantly depleted due to the dielectrophoretic, macroscopic mass transport to and from the electrode, thus all intermediate products are flushed away from the anode into the diffusion layer before they can decompose to CO_2. This would also explain why the CO_2 formation

starts anyway at a certain phenol concentration after some time, since in this case also the stream flowing toward the electrode might already contain intermediates formed shortly before, which can then be oxidized upon contact with the anode. The lemniscate flow shape reported in [28] allows such a hypothesis.

4.3 Anodic Ethylene Glycol oxidation

According to Christensen and Hamnett [44], the main products of low voltage ethylene electrolysis in acidic environments are glycolic acid and carbon dioxide. This reaction takes place at a relatively small number of active sites, which can be poisoned by carbon monoxide getting terminally bonded to the electrode. In alkali, the main products are glycolate, oxalate and carbonate [44]. De Lima *et al.* [41] describe also the formation of oxalic acid and formic acid as side products. The production of glycolate and carbonate appears to take place via the same intermediate, but oxalate is apparently produced by further oxidation of desorbed glycolate. Comparable results were found by Matsuoka *et al.* [42], which state that in alkaline solutions the oxidation of ethylene glycol on platinum occurs via glycol aldehyde – glyoxal- glycolate- glyoxylate- oxalate pathway yielding carbonate and carbon dioxide. According to them an electrode poisoning (formate formation) and a non-poisoning (oxalate formation) electrochemical pathway in electrooxidation of ethylene glycol exists. Kadirgan *et al.* [45] describe an adsorption process followed by an inherently concerted interfacial step, or series of steps in alkaline media. The necessary ability of platinum to dissociatively chemisorb organic reactants such as alcohols including ethylene glycol is well known in electrochemical as well as gas phase environments [46], the oxygen-transfer agent on platinum appears to be adsorbed water or hydroxyl species.

When using ethylene glycol solutions in the experiments presented the electrodes remained clean, and no gas formation could be observed. The observed increase in conductivity in the anodic beaker and the decrease in the cathode beaker is, if at all, only slightly higher than that observed in pure water and presumably only due to different pH values (different CO_2 concentrations from ambient CO_2) in these beakers (see also [28]). However, a partial chemical decomposition is certainly happening when the solution is transported to the anode (see Fig. 16). The interpretation of such an electrochemical behavior can be done in line with that of phenol, just that in this case no polymer precipitates on the electrodes, since the intermediate species are incapable of such a reaction. Any CO_2 formed could probably remain in solution and would thus not be observable via bubble formation. Alternatively, the degradation pathway towards CO_2 could be inhibited by the catalytically favored adsorption of hydroxyl ions on the surface of the electrode and subsequent formation of intermediates (glycolate and oxalate). This hypothesis is also supported by Kelaidopoulou *et al.* [43] who state that the oxidation of ethylene glycol on the electrode surface is shifted to a hydroxyl chemisorption at higher potentials. Moreover, as mentioned in the phenol section (4.2), the electrohydrodynamic mass flow could also disrupt and thus slow down chemical surface reactions significantly – or even prevent them completely.

5. Conclusions

In this work we report the transport and chemical reactions of phenol and ethylene glycol solutions in a special electrohydrodynamic environment, a “floating water bridge” set-up. Thereby, the substances are transported in both directions. The electrochemical activity is significantly higher when the solute is transported from the cathode beaker to the anode beaker, since passivation and electrode poisoning are in this case reduced due to the EHD flow. Phenol gets partially oxidized and polymerized at the anode, a complete decomposition resulting in CO_2 (bubble) formation is only observed at high concentrations. This can be due to an extension of the outer Helmholtz layer due to the extremely high potential, and/or to the depletion of the inner Helmholtz layer which is caused by the EHD water flow.

No precipitation, but indications for the formation of intermediate species of the full oxidation cycle could be detected when an ethylene glycol solution was used. The conductivity change in the beakers indicates that once phenol and ethylene glycol get oxidized at the anode, the generated species hardly pass the bridge to the other beaker. They seem to be ‘expelled’ from the lemniscate shaped flow [28] and are concentrating over time in regions of the anode beaker which do not take part in the EHD flow to the cathode. Naturally dissolved CO_2 or other ions which contribute to the conductivity of the solution also share this fate, since the conductivity in the cathode beaker decreased over time during all experiments conducted.

In summary, the experiments presented demonstrate that an EHD environment with a floating liquid bridge set-up provides interesting new possibilities for (electro-) chemical reactions. For future studies, the authors plan to examine these possibilities further by extending the research into the investigation of both other solvents and solutes.

Acknowledgments

This work was performed in the TTIW-cooperation framework of Wetsus, Centre of Excellence for Sustainable Water Technology (www.wetsus.nl). Wetsus is funded by the Dutch Ministry of Economic Affairs, the European Union Regional Development Fund, the Province of Fryslân, the City of Leeuwarden and the EZ/Kompas program of the "Samenwerkingsverband Noord-Nederland". The financial support of both the Applied Water Physics Theme of Wetsus and "Holding Graz" is thankfully acknowledged. The authors would like to thank the whole research team and staff of WETSUS, especially Luewton L.F. Agostinho, Cees Kamp and Adam D. Wexler; as well as Lukasz Piatkowski (AMOLF, Amsterdam). With great pleasure, the authors furthermore wish to thank Profs. Artem Aerov (Physics Department, Moscow State University), Huib Bakker (AMOLF, Amsterdam), Eshel Ben-Jacob (Tel Aviv University), Cees Buisman (Wetsus - Centre of Excellence for Sustainable Water Technology), Friedemann Freund (SETI Insitute, California), Karl Gatterer (Graz University of Technology), Emilio Del Giudice (Universitá di Milano), Ernst Lankmayr (Graz University of Technology), Jan C.M. Marijnissen (Delft University of Technology), Laurence Noirez (Laboratoire Léon Brillouin, CEA-CNRS/IRAMIS, CEA-Saclay), Gerald H. Pollack (University of Washington), Alan Soper (Rutherford Appleton Laboratories, ISIS, Oxford, UK), José Teixeira (Laboratoire Léon Brillouin, CEA-CNRS/IRAMIS, CEA/Saclay), Giuseppe Vitiello (Universitá degli studi di Salerno), John Watterson (Ashmore, Australia), and Jakob Woisetschläger (Graz University of Technology) for the ongoing discussion on the water bridge phenomenon (in alphabetic order).

References

[1] W.G. Armstrong, The Electrical Engineer 10, 154 (1893)
[2] E.C. Fuchs, J. Woisetschläger, K. Gatterer, E. Maier, R. Pecnik, G. Holler, H. Eisenkölbl, J. Phys. D: Appl. Phys. 40, 6112 (2007)
[3] E.C. Fuchs, K. Gatterer, G. Holler, J. Woisetschläger, J. Phys. D: Appl. Phys. 41, 185502 (2008)
[4] E.C. Fuchs, B. Bitschnau, J. Woisetschläger, E. Maier, B. Beuneu, J. Teixeira, J. Phys. D: Appl. Phys. 42, 065502 (2009)
[5] E.C. Fuchs, P. Baroni, B. Bitschnau, L. Noirez, J. Phys. D: Appl. Phys. 43, 105502 (2010)
[6] J. Woisetschläger, K. Gatterer, E.C. Fuchs, Exp. Fluids 48, 121 (2010)
[7] H. Nishiumi, F. Honda, Res. Let. Phys. Chem. (2009) art. ID 371650
[8] M. Tello, R. Garcia, J.A. Martín-Gago, N.F. Martínez, M.S. Martín-González, L. Aballe, A. Baranov, L. Gegoratti, Advanced Materials 17, 1480 (2005)
[9] T. Cramer, F. Zerbetto, R. Garcia, Langmuir 24, 6116 (2008)
[10] A. Widom, J. Swain, J. Silverberg, S. Sivasubramanian, Y.N. Srivastava, Phys. Rev. E 80, 016301 (2009)
[11] A. Castellanos, Electrohydrodynamics, International Centre for Mechanical Sciences, CISM Courses and Lectures No.380 (Springer, Wien, New York, 1998) ISBN 3-211-83137-1
[12] J. Mrázek, J. V. Burda, J. Chem. Phys. 125, 194518 (2006)
[13] W.L. Jorgensen, J. Tirado-Rives, PNAS Proc. Natl. Acad. Sci. 102, 6685 (2005)
[14] E. Del Giudice, Journal of Physics: Conf. Ser. 67, 012006 (2006)
[15] T. Head-Gordon, M.E. Johnson, PNAS Proc. Natl. Acad. Sci. 21, 7973 (2006)
[16] H.E. Stanley, S.V. Buldyrev, G. Franzese, N. Giovambattista, F.W. Starr, Phil. Trans. R. Soc. A 363, 509 (2005)
[17] C.A. Chatzidimitriou-Dreismann, T.A. Redah, R.M.F. Streffer, J. Mayers, Phys. Rev. Lett. 79, 2839 (1997)
[18] R. Arani, I. Bono, E. Del Giudice, G. Preparata, International Journal of Modern Physics B 9, 1813 (1995)
[19] E. Del Giudice, E.C. Fuchs, G. Vitiello, Water (Seattle) 2, 69 (2010) ISSN 2155-8434
[20] R.C. Ponterio, M. Pochylski, F. Aliotta, C. Vasi, M.E. Fontanella, F. Saija, J. Phys. D: Appl. Phys. 43, 175405 (2010)
[21] E.C. Fuchs, MDPI Water 2, 381 (2010)
[22] E.C. Fuchs, L.L.F. Agostinho, A.Wexler, R.M. Wagterveld, J. Tuinstra, J. Woisetschläger, J. Phys. D: Appl. Phys. 44 025501 (2011)
[23] G.H. Pollack, Cells, gels and the engine of life (Ebener & Sons, Seattle WA, 2001) ISBN 0-9626895-2-1
[24] K. Ovchinnikova, G.H. Pollack, Langmuir 25(1), 542 (2009)
[25] H. R. Corti, Langmuir 25(11), 6587 (2009)
[26] K. Ovchinnikova, G.H. Pollack, Langmuir 25(18), 11202 (2009)
[27] H.R. Corti, Langmuir 25(18), 11203 (2009)
[28] E.C. Fuchs, L.L.F. Agostinho, M. Eisenhut, J.

Woisetschläger, Proc. SPIE 7376, 73761E1 (2010) DOI:10.1117/12.868994
[29] F. Saija, F. Aliotta, M.E. Fontanella, M. Pochylski, G. Salvato, C. Vasi, R.C. Ponterio, J. Chem. Phys. 133, 081104 (2010)
[30] A.G. Marin, D. Lohse, Phys. Fluids 22, 122104 (2010)
[31] A.A. Aerov, Why the Water Bridge does not collapse, arXiv:1012.1592v1 (2010)
[32] M. Gattrell, D.W. Kirk, J. Electrochem. Soc. 140(6), 1534 (1993)
[33] B. Fleszar, J. Ploszynska, Electrochimia Acta 30(1), 31 (1985)
[34] D. Fino, C. Carlesi Jara, G. Saracco, V. Specchia, P. Spinelli, J, Appl, Electrochem. 35, 405 (2005)
[35] Ch. Comminellis, C. Pulgrain, J. Appl. Electrochem. 21, 703 (1991)
[36] S. Andreescu, D. Andreescu, O.A. Sadik, Electrochem. Comm. 5, 681 (2003)
[37] R.C. Kolle, D.C. Johnson, Anal. Chem, 51(6), 741 (1979)
[38] R. Menini, Y.M. Henuset, J. Fournier, J. Appl. Electrochem. 35, 625 (2005)
[39] X.-Y. Li, Y.-H. Cui, Y.-J. Feng, Z.-M. Xie, J.-D. Gu, Water Res. 39, 1972 (2005)
[40] P. Canizares, J.A. Domínguez, M.A. Rodrigo, J. Villaseñor, J. Rodríguez, Ind. Eng. Chem. Res. 38(10), 3779 (1999)
[41] R.B. de Lima, V. Paganin, T. Iwasita, W. Vielstich, Electrochimica Acta 49, 85 (2003)
[42] K. Matsuoka, Electrochimica Acta 51, 1085 (2005)
[43] A. Kelaidopoulou, E. Abelidou, A. Papoutsis, E.K. Polychroniadis, G. Kokkinidis, J. Appl. Electrochem. 28, 1101 (1998)
[44] P.A. Christensen, A. Hamnett, J. Electroanal. Chem. 260, 341 (1989)
[45] F. Hahn, B. Beden, F. Kadirgan, Electrochimica Acta. 23, 299 (1978)
[46] R. Parsons, T. VanderNoot, J. Electroanal. Chem. 257, 9 (1988)
[47] J. Kendall, J. Am. Chem. Soc. 38, 1480 (1916)

Journal of Physics: Conference Series **329** (2011) 012003 doi:10.1088/1742-6596/329/1/012003

Methanol, Ethanol and Propanol in EHD liquid bridging

Elmar C. Fuchs[1], Adam D. Wexler[1], Luewton L. F. Agostinho[1], Michael Ramek[2], Jakob Woisetschläger[3]

[1] Wetsus Centre of Excellence for Sustainable Water Technology, Agora 1, 8900CC Leeuwarden, The Netherlands

[2] Institute of Physical and Theoretical Chemistry, Stremayrgasse 9, 8010 Graz, Austria

[3] Experimental Turbomachinery Research and Optical Measurement Group, Institute for Thermal Turbomachinery and Machine Dynamics, Graz University of Technology, Inffeldgasse 25 A, 8010 Graz, Austria

e-mail of corresponding author: elmar.fuchs@wetsus.nl

Abstract. When a high-voltage direct-current is applied to two beakers filled with water or polar liquid dielectrica, a horizontal bridge forms between the two beakers. In this work such bridges made of methanol, ethanol, 1-propanol and 2-propanol are investigated with polarimetry and thermography. Whereas methanol, ethanol and 1-propanol bridges become warm like a water bridge, a 2-propanol bridge cools down relative to the surroundings. It is shown how the different stability of the primary and secondary alcoholate ions and the resulting small difference in conductivity between 1-propanol and 2-propanol is responsible for this novel effect.

1. Introduction

In 1893 Sir William George Armstrong first reported the formation of a horizontal bridge of water forming between two wine glasses filled with chemically pure water when a direct-current (DC) high-voltage was applied [1]. Recently, a number of publications made the broader scientific community aware of this experiment [2-7].

The experiment is stable, easy to reproduce, and grants free experimental access to water inside the bridge under variable high voltage and atmospheric conditions in air, thus giving insights into basic features of dipole-dipole interaction in water [8]. Therefore a number of experiments in the horizontal bridge of water was performed including neutron scattering [4,5], visualization and optical measurement techniques [6], Raman scattering [9], Brillouin scattering [10], reduced gravity experiments [11], and was discussed in relation to molecular vibration coupling [12] and the influence of some electrolytes [13] and non-ionic solvents [14] on the water bridge.

Several authors discussed the electrohydrodynamics of this phenomenon. Widom *et al*. [15] and Saija *et al.* [16] claim that the high dielectric permittivity of water is the reason for a stable bridge forming and used the Maxwell stress tensor to calculate tensions within the bridge. A similar approach was used by Marin and Lohse [17]. It has been shown that a horizontal bridge forms also in methanol [8] and glycerol [17]. Aerov [18] pointed out that a stable equilibrium for the bridge's surface is

reached when the axial electric field is strong enough to counteract distortions caused by surface tension.

All electrohydrodynamic discussions of these experiments use previous literature on a phenomenon also named 'liquid bridge', but resembling a vertical column of liquid, pinned at each end between planar electrodes, and surrounded by a non-conducting, dielectric gas. These experiments were performed with both AC and DC fields and led to a detailed analysis of this vertical liquid bridge and its stability [19-23]. It has been shown that the longitudinal field along a liquid jet axis has a stabilizing effect on the liquid – gas interface [24] which was later also discussed for vertical liquid bridges [25]. In this sense the liquid bridge formation can be explained as action of the electrohydrodynamic stress tensor replenishing the liquid within the bridge against any drainage mechanism. Recently, the formation of bridges with acetone, dichloromethane (DCM), dimethylformamide, dimethylsulfoxide, ethanol, glycerol, methanol, 1-propanol, 2-propanol, and tetrahydrofuran have been reported and investigated [26].

In this work the Armstrong experiment is repeated with methanol, ethanol, 1-propanol and 2-propanol. The polarimetric and thermographic properties are reported and discussed.

2. Experimental

For the DC experiments we use two 40 ml glass beakers with spouts, 15 x 5 x 0.25 mm platinum electrodes, a DC high-voltage 0-25 kV power supply Phywe 'Hochspannungs-Netzgerät 25kV' (No 13671.93, Göttingen, Phywe Systeme GmbH, Germany) with a maximum current of 0.5 mA and a 42nF capacitor in parallel to the bridge. For imaging a Canon 300D with a Sigma 105mm 1:2.8 macro lens, a Panasonic 3CCD NV-DX100 camcorder with Raynox DCR-150 or Raynox DCR-250 conversion lenses, a Photron FASTCAM SA1 high-speed camera with a Nikkor 60 mm 1:2.8 macro lens, or a CASIO Exilim High Speed EX-F1 - were used. All liquids are common solvents and were used in a chemically pure grade. Deionized water was provided by a Barnstead NANOpure type I ultrapure water system (Thermo Fisher Scientific Inc., Waltham, MA) with an initial conductivity of 0.056 μS cm-1 recorded with the integrated conductivity meter of the system. This conductivity rose quickly to 0.8 μS cm-1 with a pH value of 5 due to CO2 saturation under atmospheric conditions (Kendall 1916). All images were scaled. Infrared imaging (thermal imaging) was done with a FLIR 620 camera (FLIR systems, MA, USA). The images of the bridges chosen for analysis were taken at a point in time when either a temperature equilibrium was reached, or, if that was not possible, during a time before the bridge broke down when temperature changes were minimal. An emissivity of 0.92 was assumed for all liquids. The lengths of the bridges were the maximum lengths attainable for stable bridges in case of the alcohols. The length of the water bridge was intentionally kept shorter for reasons of better comparison.

For polarometric visualisations a ceramic glass diffuser (50 x 50 cm, 5 mm thick) was placed behind the beakers, illuminated by a halogen lamp from behind with a linear polarizer put on top of the diffuser. A second polarising filter was placed in front of the imaging device and used as the analyzer.

For high voltage conductivity measurements, the set-up consisted of two platinum electrodes dipped 10mm deep into the liquid in a glass cuvette (Groß-Küvette 700.000, Hellma GmbH & Co. KG, Müllheim Germany) with 50 mm inner width, 50 mm inner height and 10 mm inner depth, with 50mm electrode distance under atmospheric conditions. With this set-up, voltage versus current diagrams of the different liquids were recorded. .

3. Results

Fig. 1 shows the alcoholic bridges (b-e) in comparison to a water bridge (a) as well as polarimetric images of such bridges (f-j). Generally, the alcoholic bridges are thinner and shorter than the water bridge, more difficult to create and less stable [26]. The characteristic bright zones on the top and

bottom of the bridge initially discovered for aqueous bridges under polarized light [3,6] is present for all alcoholic bridges as well.

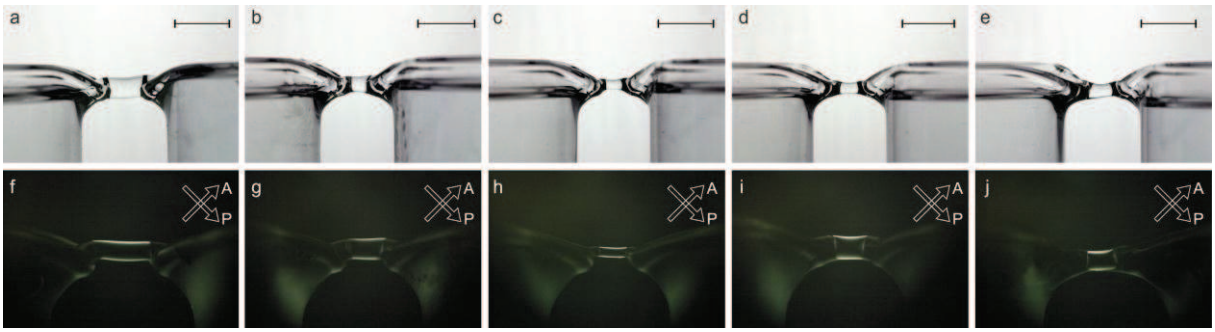

Fig. 1: (a)-(e): Horizontal bridges forming in different polar liquids under atmospheric conditions and DC voltage. The bars are 1 cm. (f)-(j): Liquid bridges between crossed linear polarisers. P indicates the direction of the polarizer, A the direction of the analyzer. (a,f) water 12 kV, (b,g) methanol 9.5 kV, (c,h) ethanol 9.5 kV, (d,i) 1-propanol 10 kV, (e,j) 2-propanol 8 kV

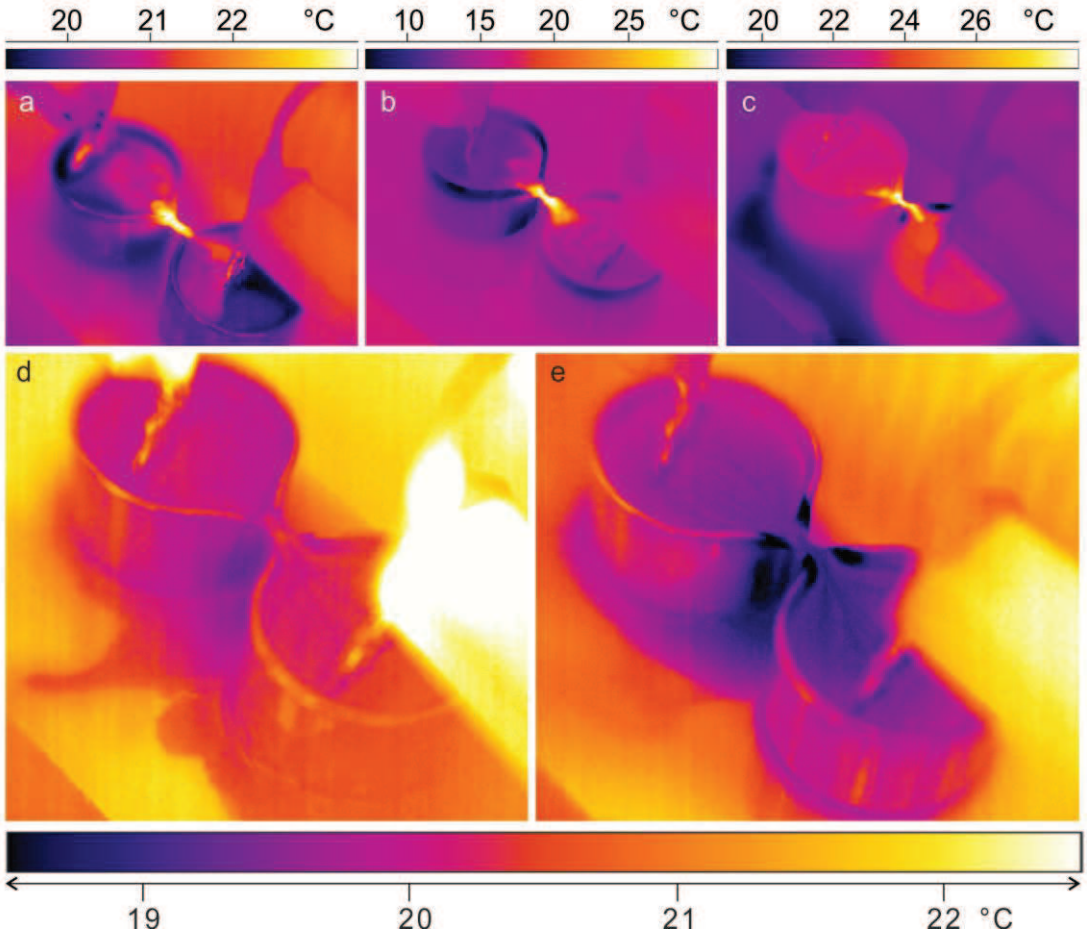

Fig. 2: Thermographic images of horizontal bridges forming in different polar liquids under atmospheric conditions and DC voltage. (a) water 12 kV, (b) methanol 9.5 kV, (c) ethanol 9.5 kV, (d) 1-propanol 10 kV, (e) 2-propanol 8 kV

Fig. 2 shows a thermographic analysis of the alcoholic bridges (b-e) in comparison to a water bridge (a). The scales of the images were adapted to match the observed temperature regions. For the sake of comparison, the same scale was chosen for 1- and 2-propanol, respectively.

The most prominent feature of this image is the fact that the water, methanol, ethanol and 1-propanol bridges are heating up whereas the 2-propanol is slightly cooling down. Next to that, the temperature of the methanol bridge was the highest, followed by ethanol, water, and 1-propanol. These trends are evaluated in Fig. 3.

In addition to the liquid bridge set-up, a single cuvette set-up was used to measure the high voltage conductivities of the liquids investigated under more stable conditions. The measurements showed that these properties are non-Ohmic under the conditions applied, and they are plotted in Fig. 4.

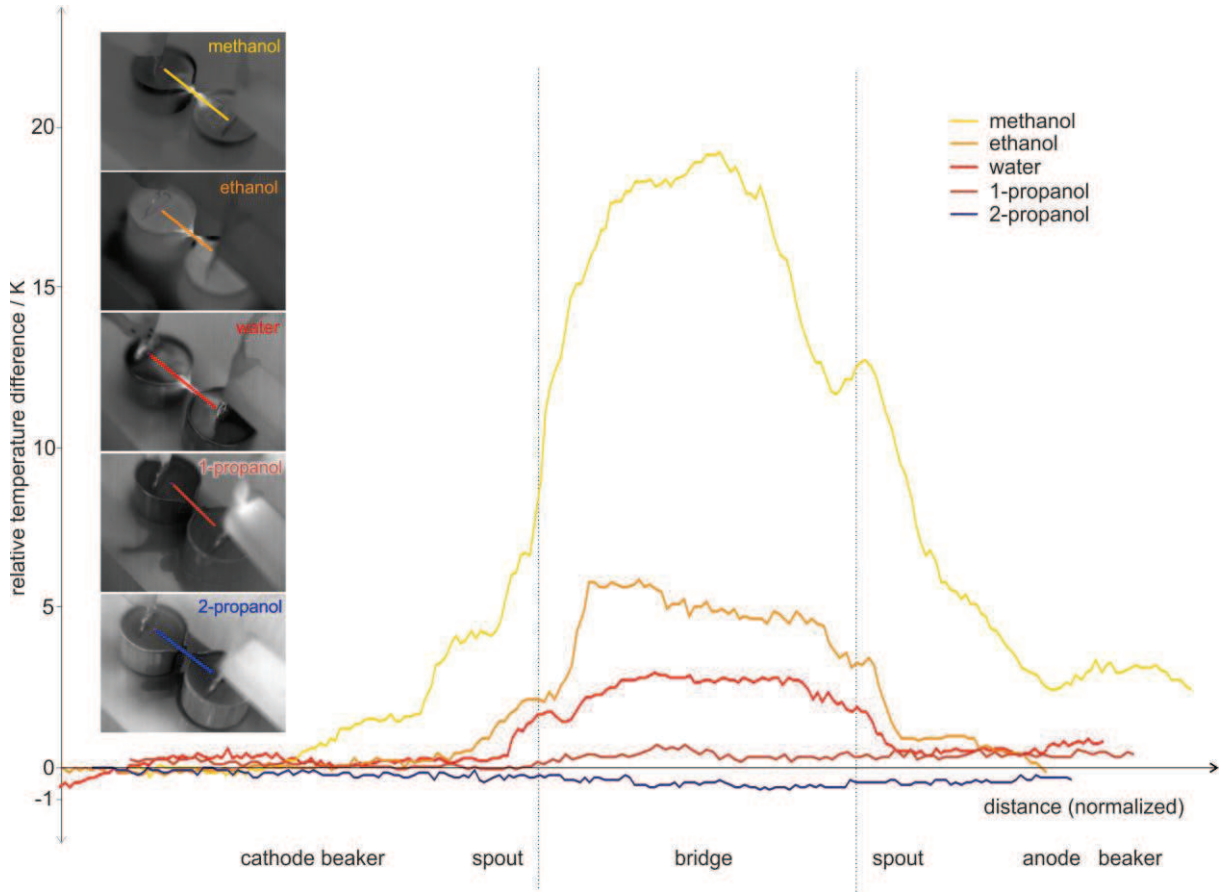

Fig. 3: Relative surface temperature changes across the liquid bridge set-ups. The evaluated paths are shown in the insets on the left. Lengths are normalized for reasons of comparison. The borders between bridge and spout are an approximation.

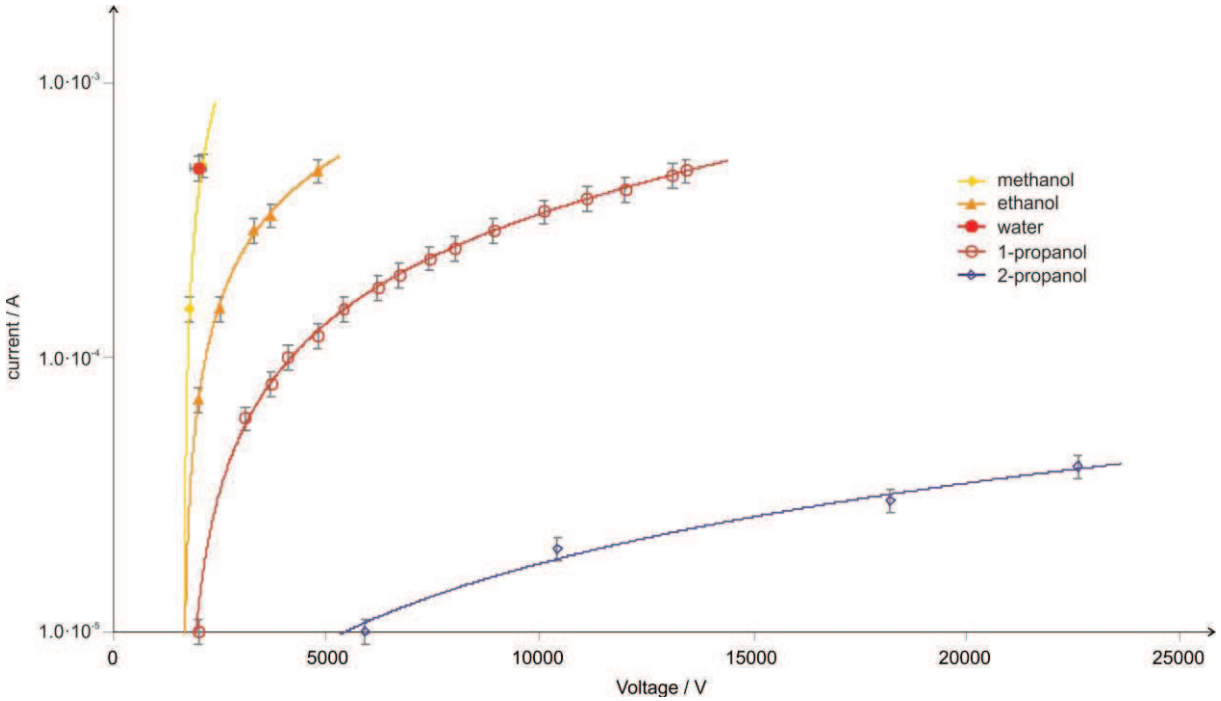

Fig. 4: Non-ohmic behaviour of the liquids used to form a horizontal bridge. The recordings were done up to 25 kV and up to 0.5 mA. The platinum electrodes dipped 10 mm deep into the liquid with 50 mm electrode distance under atmospheric conditions.

4. Discussion

There are two mechanisms at work in all liquids investigated responsible for the temperature changes: Ohmic resistivity causes heating, whereas evaporation causes cooling. In all liquids except for 2-propanol, the Ohmic heating outweighs the evaporation. The following subsections will discuss and explain these facts in detail.

4.1. Alcoholate ion stabilities

It is basic knowledge of organic chemistry that secondary alcoholate anions are less stable than primary ones because a primary carbon atom carries more positive partial charge than a secondary one, thus the negative charge of the oxygen can be distributed more easily in case of a primary alcoholate. This molecular feature becomes measurable as a macroscopic property when looking at the conductivity of the alcohols. Thus, there are far less alcoholate ions in 2-propanol than in 1-propanol, resulting in a lower current (see Fig. 4), and, consequently, in lower Ohmic heating of the liquid.

4.2. Dipole moment and conductivities

The field strength applied in the present experiments does not cause a significant influence on the dipole moment of the single alcohol molecules. Calculations using optimized RHF/6-311++G** structures, which were verified to be local minima via frequency analysis, showed that at the field strengths up to 20kV/cm results do not differ from calculations without external fields. First significant changes of charge distribution and geometry required 10^4 times higher field strengths. This result is in line with a similar calculation for water [27]. However, these calculations do not consider the dissociation of molecules into ion pairs. It is well known that the conductivity of dielectric liquids increases with permittivity due to an accompanying decrease of the electrostatic attraction between ion pairs [28]. Whenever a high-voltage DC field is applied to the fluid, an increasing number of ions

escape recombination, causing an increase in conductivity, as was discussed by Onsager and Brière [29,30]. While at low voltage Ohmic behavior is observed due to ions generated by dissociated molecules; at high voltage the dissociation rate is proportional to the electric field but the recombination rate is not and the current approaches saturation [31,32]. These effects are clearly visible for all alcohols in Fig. 4.

4.3. Evaporation

Of all alcohols, methanol has the lowest boiling point (65°C) followed by ethanol (78°C), 2-Propanol (82°C) and 1-Propanol (97°C). According to Hinds [33] a curved surface modifies the attractive forces between surface molecules facilitating diffusion from the liquid surface, and consequently favours evaporation. Thus, when compared to a flat air-liquid interface, an increase on the diffusion of molecules throughout this same interface is expected. Another important point is the presence of surface charge. According to Hartman *et al.* and Darabi *et al.* [34,35] the electrostatic stress created by the presence of these charges counter-acts the surface tension stress on the liquid surface. The net effect is the production of secondary motion that destabilizes the thermal boundary layer near the heat transfer surface, leading to higher effective heat transfer coefficients, and causing the production of vapour along the whole air-liquid interface of the set-up with most of the evaporation taking place where the electric field is highest – across the liquid bridge [26]. This is the reason why the 2-propanol bridge is cooler than the bulk liquid, as can be seen in Figs. 2 and 3.

4.4. Polarimetry

It has been suggested that either bubbles or density gradients [3,6] or birefringence [3,5] are possible sources of the bright zones visible when looking at a water bridge using a polarimetric set-up. Until now, this issue is still not resolved. We suggest that, since this effect is not intrinsic to water (see Fig. 1), what ever physics responsible may apply for the alcohols investigated as well, thereby ruling out water specific origins.

5. Conclusions

The infrared emission of alcoholic EHD bridges made of methanol, ethanol, 1-propanol and 2-propanol were compared to an aqueous EHD bridge. The temperature of the primary alcohol bridges is decreasing with their decreasing conductivity. Water is an exception because of its unusually high heat capacity (4.18 J / g·K) compared to methanol (2.59 J / g·K) and ethanol (2.44 J / g·K), thus aqueous bridges are cooler although the conductivity of water is higher than that of the alcohols. Furthermore, we found that a 2-propanol bridge cools down whereas all other bridges heat up. This effect can be explained by two mechanisms responsible for the temperature changes: Ohmic resistivity causing heating, and evaporation causing cooling. In all liquids except for 2-propanol, the ohmic heating outweighs the evaporation. Moreover, since evaporation is increased by electric fields [34,35] and surface curvatures [33], it is expected to be highest along the bridge, thus explaining why the 2-propanol bridge shows anomalous cooling.

In addition, the bright zones originally found in a polarimetric investigation of the water bridge [3] were reproduced for all liquids, thus showing that they are not a water-intrinsic effect.

6. Acknowledgements

This work was performed in the TTIW-cooperation framework of Wetsus, Centre of Excellence for Sustainable Water Technology (www.wetsus.nl). Wetsus is funded by the Dutch Ministry of Economic Affairs, the European Union Regional Development Fund, the Province of Fryslân, the City

of Leeuwarden and the EZ/Kompas program of the "Samenwerkingsverband Noord-Nederland". The authors would like to thank Profs. Eshel Ben-Jacob (Tel Aviv University), Harry Bruning (Wetsus), Cees Buisman (Wetsus), Gert-Jan Euverink (Wetsus), Friedemann Freund (NASA SETI Institute, California), Karl Gatterer (TU Graz), Xingua Guo (TU Graz), Emilio Del Giudice (Universitá di Milano), Gerald H. Pollack (University of Washington), José Teixeira (Laboratoire Léon Brillouin, CEA-CNRS/IRAMIS, CEA/Saclay), as well as Cees Kamp, Astrid H. Paulitsch-Fuchs, Martina Sammer (Wetsus) and especially Mathias Eisenhut (TU Graz), for the ongoing discussion on the water bridge phenomenon (in alphabetic order). The financial support of the participating companies of the Applied Water Physics Theme at Wetsus, Centre of Excellence for Sustainable Water Technology, is acknowledged.

7. References

[1] Armstrong, W.G. The Electrical Engineer **1893**, 10 February 1893, 154-145.
[2] Fuchs, E.C. J. Woisetschläger, K. Gatterer, E. Maier, R. Pecnik, G. Holler and H. Eisenkölbl, J. Phys. D: Appl. Phys. **2007**, 40, 6112-6114.
[3] Fuchs, E.C.; Gatterer, K.; Holler, G.; Woisetschläger, J. J. Phys. D: Appl. Phys. **2008**, 41, 185502-185507.
[4] Fuchs, E.C.; Bitschnau, B.; Woisetschläger, J.; Maier, E.; Beuneu B.; Teixeira, J. J. Phys. D : Appl. Phys. **2009**, 42, 065502:1-065502:4.
[5] Fuchs, E.C.; Baroni, P.; Bitschnau, B.; Noirez, L. J. Phys. D: Appl. Phys. **2010**, 43, 105502:1-105502:5.
[6] Woisetschläger, J.; Gatterer, K.; Fuchs, E.C. Exp. Fluids **2010**, 48-1, 121-131.
[7] Fuchs, E.C.; Agostinho, L.L.F.; Eisenhut, M.; Woisetschläger, J. Proc. SPIE **2010**, 7376, 73761E1-15.
[8] Fuchs, E.C. Water (MDPI) **2010**, 2, 381-410.
[9] Ponterio, R.C.; Pochylski, M.; Aliotta, F.; Vasi, C.; Fontanella, M. E.; Saija, F. J. Phys. D: Appl. Phys. **2010**, 43, 175405:1-175405:8.
[10] Fuchs, E.C.; Bitschnau, B.; Di Fonzo, S.; Gessini, A.; Woisetschläger, J. and Bencivenga, F. *under review*
[11] Fuchs, E.C.; Agostinho, L.L.F.; Wexler, A.; Wagterveld, R.M.; Tuinstra, J.; Woisetschläger, J., J. Phys. D: Appl. Phys. **2011,** 44**,** 025501:1-025501:8.
[12] Del Giudice, E.; Fuchs, E.C.; Vitiello, G. Water (Seattle) **2010**, 2, 69-82.
[13] Nishiumi, H.; Honda, F. Res. Let. Phys. Chem. **2009**, 2009, 371650:1-371650:3.
[14] Eisenhut, M.; Guo, X.; Paulitsch-Fuchs, A.H.; Fuchs, E.C.; Cent. Eur. J. Chem. **2011** Eisenhut, M.; Guo, X.; Paulitsch-Fuchs, A.H.; Fuchs, E.C.; Cent. Eur. J. Chem. **2011**, 9 , 391-403.
[15] Widom, A.; Swain, J.; Silverberg, J.; Sivasubramanian, S.; Srivastava, Y.N. Phys. Rev. E **2009**, 80, 016301:1-016301:7.
[16] Saija, F.; Aliotta, F.; Fontanella, M.E.; Pochylski, M.; Salvato, G.; Vasi, C.; Ponterio, R.C., J. Chem. Phys. **2010**, 133, 081104
[17] Marin, A. G.; Lohse, D.; Phys. Fluids **2010**, 22, 122104:1-122104:9.
[18] Aerov, A. A.; "Why the Water Bridge does not collapse", arXiv:1012.1592v1, **2010.**
[19] Raco, R.J., Science **1968**, 160, Issue 3825, 311-312.
[20] Gonzalez H.; McCluskey, F.M.J.; Castellanos, A.; Barrero, A., J. Fluid Mech. **1989**, 206, 545.
[21] Saville, D.A., Ann. Rev. Fluid Mech., **1997**, 29, 27-64
[22] Burcham, C.L.; Saville, D.A., J. Fluid Mech.**2000**, 405, 37-56.
[23] Burcham, C.L.; Saville, D.A., J. Fluid Mech. **2002**, 452, 163-187.
[24] Melcher, J.R. and Warren, E.P.; J. Fluid Mech. **1971**, 47, 127 – 143.
[25] Ramos, A.;Castellanos, A., Phys. Fluids **1993,** 6, 207 – 225.
[26] Woisetschläger, J.;Wexler, .A.D; Holler, G.; Eisenhut, M.; Gatterer, K.; Fuchs, E. C., *under*

review
[27] Rai, D.; Kulkami, A. D.; Pathak, R. K. J. Chem. Phys. **2006,** 128, 034310
[28] Watson, P.K.; Conduction, instabilities and breakdown in liquid dielectrics, in: Castellanos, A. (ed) (1998) Electrohydrodynamics, International Centre for Mechanical Sciences, CISM Courses and Lectures No. 380, Springer, Wien, ISBN 3-211-83137-1.
[29] Onsager, L., J. Chem. Phys. **1934,** 2, 599-615.
[30] Briere, G.B., Brit. J. Appl. Phys. **1964**, 15, 413-417.
[31] Jeong, S.I.; Seyed-Yagoobi, J., IEEE Trans. Ind. Appl. **2003,** 39, 355-361.
[32] Zhakin, A.J., Conduction phenomena in dielectric liquids, in: Castellanos, A. (ed) (1998) Electrohydrodynamics, International Centre for Mechanical Sciences, CISM Courses and Lectures No. 380, Springer, Wien, ISBN 3-211-83137-1.
[33] Hinds, W.C., Aerosol Technology. 2 ed. 1998: Wiley Interscience.
[34] Hartman, R.P.A.; Brunner, D.J.; Camelot, D.M.A.; Marijnissen, J.C.M.; Scarlett, B. J. Aerosol Sc. **2000**, 31, 65-95.
[35] Darabi, J.; Ohadi, M.M.; Desiatoun, S.V.; J. Heat Trans. **2000**, 122, 741.

Horizontal bridges in polar dielectric liquids

Jakob Woisetschläger, Adam D. Wexler, Gert Holler, Mathias Eisenhut, Karl Gatterer & Elmar C. Fuchs

Experiments in Fluids
Experimental Methods and their Applications to Fluid Flow

ISSN 0723-4864
Volume 52
Number 1

Exp Fluids (2012) 52:193-205
DOI 10.1007/s00348-011-1216-x

Springer

Exp Fluids (2012) 52:193–205
DOI 10.1007/s00348-011-1216-x

RESEARCH ARTICLE

Horizontal bridges in polar dielectric liquids

Jakob Woisetschläger · Adam D. Wexler · Gert Holler · Mathias Eisenhut · Karl Gatterer · Elmar C. Fuchs

Received: 5 April 2011 / Revised: 30 September 2011 / Accepted: 4 October 2011 / Published online: 16 October 2011

Abstract When a high-voltage direct-current is applied to two beakers filled with polar liquid dielectrica like water or methanol, a horizontal bridge forms between the two beakers. By repeating a version of Pellat's experiment, it is shown that a horizontal bridge is stable by the action of electrohydrodynamic pressure. Thus, the static and dynamic properties of the phenomenon called a 'floating water bridge' can be explained by the gradient of Maxwell pressure, replenishing the liquid within the bridge against any drainage mechanism. It is also shown that a number of liquids can form stable and long horizontal bridges. The stability of such a connection, and the asymmetry in mass flow through such bridges caused by the formation of ion clouds in the vicinity of the electrodes, is also discussed by two further experiments.

J. Woisetschläger (✉)
Experimental Turbomachinery Research and Optical Measurement Group, Institute for Thermal Turbomachinery and Machine Dynamics, Graz University of Technology, Inffeldgasse 25 A, 8010 Graz, Austria
e-mail: jakob.woisetschlaeger@tugraz.at

A. D. Wexler · E. C. Fuchs
Wetsus, Center of Excellence for Sustainable Water Technology, Agora 1, 8900 CC Leeuwarden, The Netherlands
e-mail: adam.wexler@wetsus.nl

E. C. Fuchs
e-mail: elmar.fuchs@wetsus.nl

G. Holler
Institute of Electrical Measurement and Measurement Signal Processing, Graz University of Technology, Kopernikusgasse 24/IV, 8010 Graz, Austria
e-mail: gert.holler@tugraz.at

M. Eisenhut
Institute of Analytical Chemistry and Food Chemistry, Graz University of Technology, Stremayrgasse 9, 8010 Graz, Austria

K. Gatterer
Institute of Physical and Theoretical Chemistry, Graz University of Technology, Stremayrgasse 9, 8010 Graz, Austria
e-mail: gatterer@tugraz.at

1 Introduction

In 1893, Sir William George Armstrong first reported on the formation of a horizontal bridge of water forming between two beakers filled with deionised water when a direct-current (DC) high voltage is applied (Armstrong 1893). Recently, a number of publications made the modern scientific community aware of this experiment (Fuchs et al. 2007, 2008).

When filling glass beakers with deionised water and applying a DC voltage between 10 and 20 kV, a watery connection forms between the beakers. Since the experiment is stable, easy to reproduce, and grants free experimental access to water inside the bridge under variable high voltage and atmospheric conditions in air, it promises insights into basic features of dipole–dipole interaction in water (Fuchs 2010). Therefore, a number of experiments in the horizontal bridge of water were performed, using neutron scattering (Fuchs et al. 2009, 2010b), visualization and optical measurement techniques (Woisetschläger et al. 2010), Raman scattering (Ponterio et al. 2010), Brillouin scattering (Fuchs et al. 2011b), zero gravity experiments (Fuchs et al. 2011a), and were discussed in relation to molecular vibration coupling (Del Giudice et al. 2010) and the influence of some electrolytes (Nishiumi and Honda 2009) and non-ionic solvents (Eisenhut et al. 2011) on the water bridge.

Due to its unique properties, several authors discussed the electrohydrodynamics of such a stable and horizontal bridge of water forming between two beakers under ambient conditions in air. Widom et al. (2009) and Saija et al. (2010) stated that the high dielectric permittivity of water is the reason for a stable bridge forming and used the electrohydrodynamic Maxwell stress tensor to calculate tensions in the water bridge. A similar approach was used by Marin and Lohse (2010) to explain the stability of the horizontal bridge. While Fuchs (2010) already demonstrated that a horizontal bridge also forms in Methanol, the works of Marin and Lohse (2010) or Saija et al. (2010) discovered other polar liquids do also form horizontal bridges, e.g., glycerol. Ponterio et al. (2010) used alternating-current (AC) experiment to form a stable water bridge, a technique used in electrohydrodynamics (EHD) whenever the screening effects of free charges want to be reduced or nullified. Finally, Aerov (2011) pointed out that a stable equilibrium for the bridge's surface is reached when the axial electric field is strong enough to counteract distortions caused by surface tension.

It must be mentioned that all EHD discussions of the horizontal liquid bridge experiments use previous literature on a phenomenon named 'liquid bridge', meaning a vertical column of liquid, pinned at each end between planar electrodes, and surrounded by a non-conducting, dielectric gas. These experiments were performed in AC and DC fields; the discussions led to a detailed analysis of this vertical liquid bridge and its stability (Raco 1968; Burcham and Saville 2000, 2002; Saville 1997; Gonzalez et al. 1989). These early experiments in vertical jets between charged electrodes also indicate that the longitudinal field along the jet axis has a stabilizing effect on the liquid–gas interface (Melcher and Warren 1971), which was later also discussed for vertical liquid bridges (Ramos and Castellanos 1993).

In order to discuss horizontal bridges forming in liquids, an experiment first performed by Pellat (1896) was repeated. For this experiment, two electrodes are immersed in an insulating, dielectric liquid. The experiment then demonstrates the rise of this fluid between the electrodes when a high voltage is applied and is often used to discuss the effects of non-uniform electric fields on liquids (Jones 2002; Melcher 1981). It will be shown that when lifting the electrodes out of the liquid while under voltage, a horizontal bridge forms between the electrodes revealing all the properties previously discussed for a horizontal water bridge.

2 Experimental set-up

For the DC experiments, we use two 40-mL glass beakers with spouts, 15 × 5 × 0.25 mm platinum electrodes, a DC high-voltage 0–25 kV power supply Phywe 'Hochspannungs-Netzgerät 25 kV' (No 13671.93, Göttingen, Phywe Systeme GmbH, Germany) with a maximum current of 0.5 mA and a 42nF capacitor in parallel to the bridge. For the AC experiments, we had a Voltcraft function generator FG 708S (Voltcraft, Germany), a Raveland amplifier XCA 1000 (Raveland, Germany) and a transformer coil with a maximum output of 15 kV at 11.5 kHz. The schematic set-up for flow visualisation is shown in Fig. 1. Alternatively, a glass cuvette (Groß-Küvette 700.000, Hellma GmbH & Co. KG, Müllheim Germany) with 50 mm inner width, 50 mm inner height and 10 mm inner depth was used, with or without Teflon spacer. This 15 × 10 × 45 mm Teflon spacer had one rounded side and was glued into a glass cuvette using acrylic glue (Loctite, liquid Cyanacrylat glue, Henkel Central Eastern Europe GmbH, Vienna, Austria).

For imaging a Canon 300D with a Sigma 105 mm 1:2.8 macro lens, a Panasonic 3CCD NV-DX100 camcorder with Raynox DCR-150 or Raynox DCR-250 conversion lenses, a Photron FASTCAM SA1 high-speed camera with a Nikkor 60 mm 1:2.8 macro lens, or a CASIO Exilim High Speed EX-F1 were used. All images were scaled. Infrared imaging (thermal imaging) was done with a FLIR 620 camera (FLIR systems, MA, USA).

While a fluid is electrically stressed, it might be slightly heated (and hence expanded) or compressed. These density changes affect the refractive index and can be recorded within an interferometer. The set-up used is presented in Fig. 2 and employed a 20 mW He–Ne laser (NEC cooperation, Japan), several mirrors, beam expanders, beam splitters, lenses and a $\lambda/2$ plate in order to test for polarization effects.

The experiments were performed with a number of polar liquids listed in Table 1. For the purpose of comparison, the non-polar liquid cyclohexane was also tested. All liquids are common solvents and were used in a chemically pure grade. Deionized water was provided by a Barnstead NANOpure type I ultrapure water system (Thermo Fisher Scientific Inc., Waltham, MA) with an initial conductivity of 0.056 μS cm^{-1} recorded with the integrated conductivity meter of the system. This conductivity rose quickly to 0.8 μS cm^{-1} with a pH value of 5 due to CO_2 saturation under atmospheric conditions (Kendall 1916).

3 Results and discussion

3.1 Horizontal bridges forming in polar liquids

Do horizontal bridges also form in other fluids than water? The answer is definitely yes. We built horizontal bridges in acetone, dichloromethane (DCM), dimethylformamide

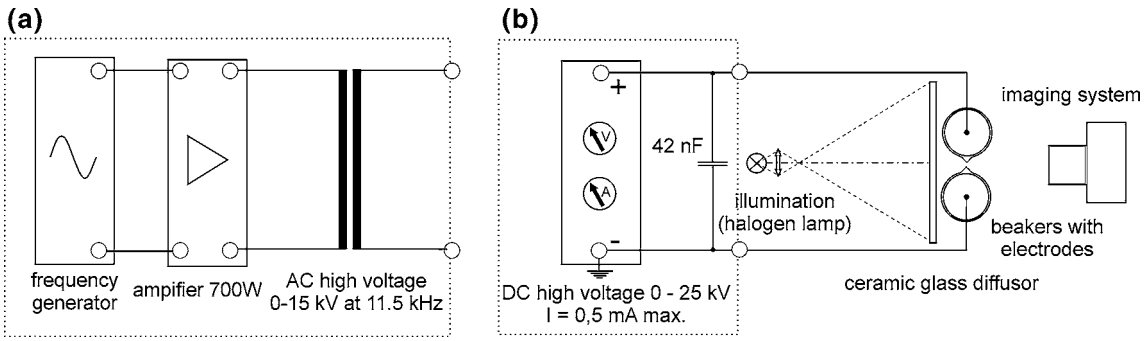

Fig. 1 Experimental set-up for the visualization of horizontal bridges between two beakers. **a** AC set-up including frequency generator, amplifier and transformer coil, **b** DC set-up including power supply, illumination, ceramic glass diffuser, beakers and imaging system

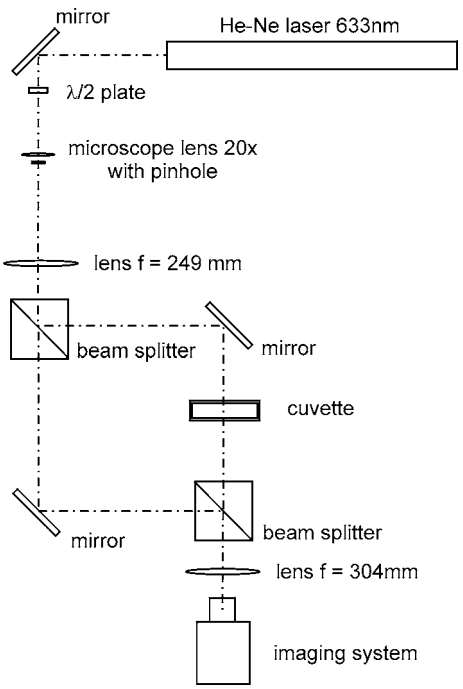

Fig. 2 Mach-Zehnder type interferometer used to record the changes in refractive index when a high voltage was applied to the liquid in the cuvette. The base length of the interferometer was 300 × 300 mm, the beam splitter cubes had 50 mm cubic side length

(DMF), dimethylsulfoxide (DMSO), ethanol, glycerol (propan-1,2,3-triol), methanol, 1-propanol, 2-propanol, tetrahydrofuran (THF), and water, all polar molecules. Under the experimental conditions presented above, we were not able to create a bridge in cyclohexane. As voltage is increased, above a threshold value bridge formation usually begins with the ejection of small liquid jets from one or the other beaker, in water accompanied by spark discharges (Fuchs et al. 2007; Woisetschläger et al. 2010). In methylformamide, no bridge is formed under atmospheric conditions, only discharges were observed. Fuchs et al. 2008 tested water bridges in air, nitrogen, oxygen, carbon dioxide and helium atmosphere, with the result that in a helium atmosphere, the bridge is replaced by a constant glow discharge between the glass beakers. While in cyclohexane neither fluid motion nor discharge was observed up to 25 kV with the beakers in close contact; with methylformamide discharges started at about 3 kV, which is the approximate breakdown voltage in air when the electrode gap is reduced to 3 mm. In all other liquids with a relative permittivity larger than 5 and a low-voltage conductivity lower than 0.8 μScm^{-1}, jet formation was observed. We would like to point out already in this section that in all polar liquids, the conductivity is a function of high voltage, while Table 1 gives the low-voltage conductivities.

Horizontal bridges forming in the different fluids are shown in Fig. 3. For THF, Fig. 3a shows the maximum length within the voltage range of the power supply. For DMF and water, the maximum current of 0.5 mA was reached in Fig. 3h and k. The liquids with a low surface tension had a tendency to leak at the spouts (DCM, propanol, acetone, ethanol and methanol).

3.2 What holds the bridge against gravity?

To answer this question, we varied an old experiment often used to discuss the effects of non-uniform electric fields on liquids—the Pellat experiment (e.g. Jones 2002). For the set-up, we used a glass cuvette with 50 × 50 × 10 mm inner dimensions, the two platinum electrodes, 16 mm apart, and a PVC spacer app. 10 mm thick and 50 mm broad to avoid air breakthrough between the electrodes. For all experiments, glycerol (99.9%) was used, with small tracer particles (polyamide spheres, 5 μm diameter) added. Although these tracers can carry charge causing mutual repulsion, they give a good impression of the fluid motion.

In 1896, Pellat demonstrated the ponderomotive force exerted on a dielectric, non-conductive liquid when two electrodes are dipped into the liquid (Pellat 1896). In Fig. 4, this experiment was repeated. When the voltage between the electrodes was increased, the glycerol level

Table 1 Liquids tested in a horizontal bridge (data at 298 K from Riddick and Bunger 1989; Wohlfarth 2008)

Name	Relative permittivity (static)	Conductivity (μS cm^{-1})	Dynamic viscosity (mPa s)	Surface tension (mN m^{-1})	Density (kg m^{-3})
Cyclohexane	2.02	0.05	0.883	24.4	773.9
Tetrahydrofuran	7.36	0.048	0.471	27.04	881.9
Dichloromethane	8.51	0.000043	0.413	27.2	1316.6
2-Propanol	19.45	0.058	2.039	21.1	780.7
Acetone	20.59	0.005	0.303	22.7	784.3
1-Propanol	20.73	0.00917	1.952	23.1	798.9
Ethanol	24.35	0.00135	1.067	22.3	784.9
Methanol	33.77	0.0015	0.542	22.1	768.3
Dimethylformamide	37.65	0.06	0.796	36.3	943.8
Glycerol	42.49	0.06	987.8	63.0	1258.1
Dimethylsulfoxide	47.13	0.002	1.98	42.8	1095.4
Water, deionised	79.5	0.05	0.89	72.01	997.1
Methylformamide	176.54	0.8	1.65	39.58	966.6

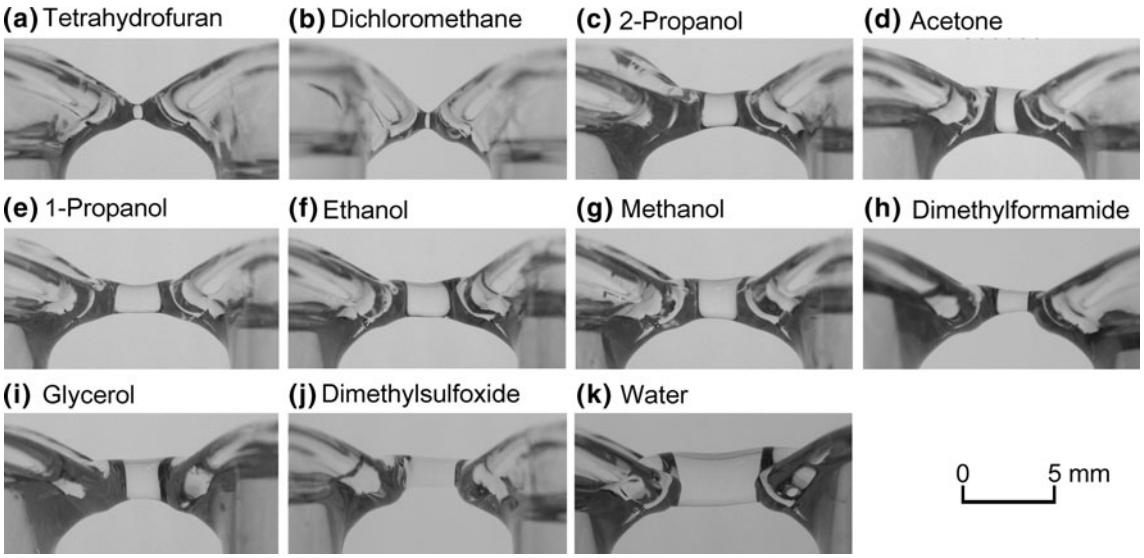

Fig. 3 *Horizontal bridges* forming in different polar liquids under atmospheric conditions and DC voltage. **a** Tetrahydrofuran 16 kV, **b** dichloromethane 19 kV, **c** 2-propanol 8 kV, **d** acetone 10 kV, **e** 1-propanol 10 kV, **f** ethanol 9.5 kV, **g** methanol 9.5 kV, **h** dimethylformamide 12.5 kV, **i** glycerol 11.5 kV, **j** dimethylsulfoxide 12 kV, **k** water 12 kV

rose accordingly (Fig. 4b). At 18 kV DC (approximately the breakdown voltage of air at the distance of the electrode tips), the cuvette was lowered mechanically, leaving a stable, horizontal bridge of glycerol between the electrodes (Fig. 4c and d). Inside the bridge (Fig. 4e and f), polyamide tracer particles indicated a slow motion between the electrodes, probably caused by cellular convection (Melcher and Taylor 1969). In the outer shell of the bridge, a strong rotation existed (Fig. 4f), with clockwise rotation direction when looking towards the cathode (in our experiments always at the left side and at ground potential).

The basic principles behind this experiment are well understood and discussed in several textbooks (e.g. Melcher 1981 for the Pellat experiment and Widom et al. 2009 for the horizontal water bridge). The best understanding is through the gradients of the Maxwell pressure, which is part of the Maxwell stress tensor

$$T_{ij} = \varepsilon_0 \varepsilon_r E_i E_j - \frac{1}{2} \delta_{ij} \varepsilon_0 \varepsilon_r E_k E_k \qquad (1)$$

with T_{ij} the stresses in the electric field, E_i the component of the electric field, δ_{ij} the Kronecker delta function, ε_0 the vacuum permittivity ($8.85 \cdot 10^{-12}$ A s V^{-1}m^{-1}) and ε_r the relative permittivity of the liquid as given in Table 1. With this approach, the pressure in the Bernoulli flow of an adiabatic, incompressible liquid is given by (Widom et al. 2009)

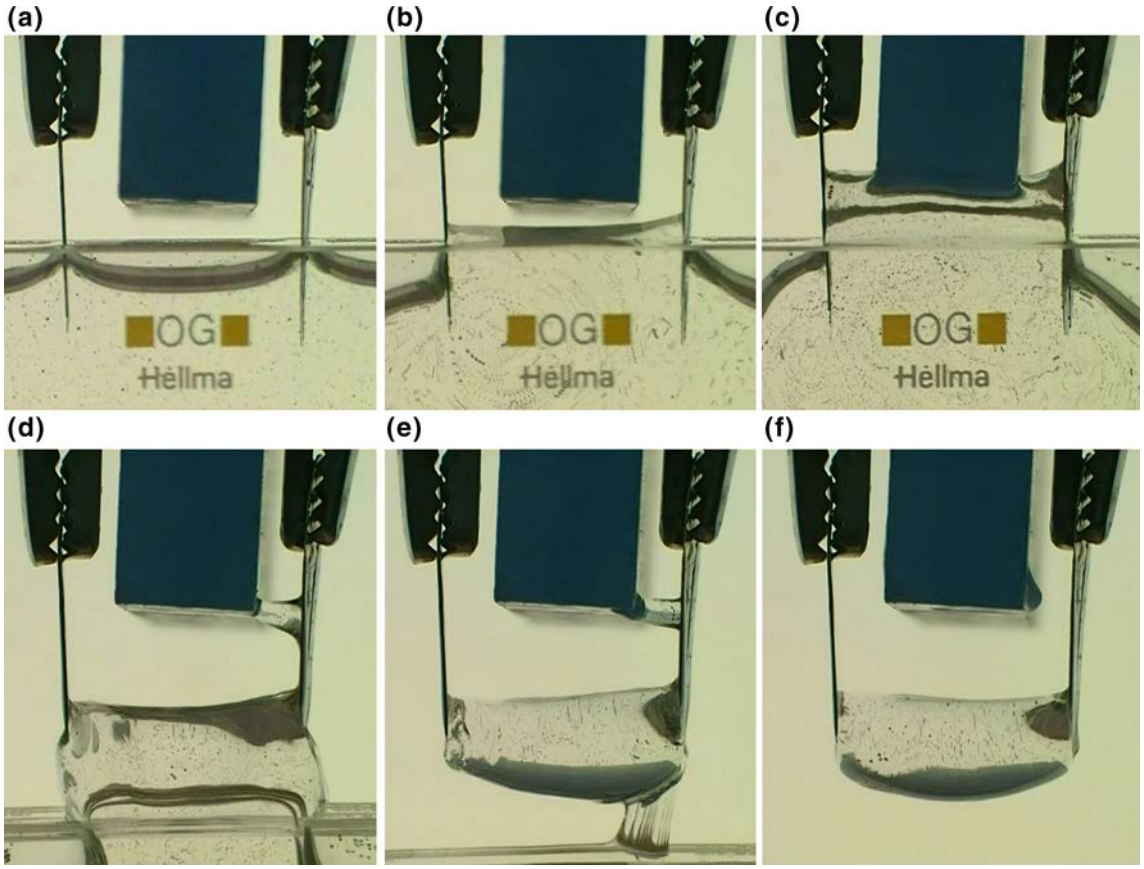

Fig. 4 Pellat experiment to form a horizontal bridge in glycerol pinned between two electrodes. **a** set-up 0 kV, **b** 13 kV DC, **c–f** 18 kV DC. The glass cuvette was lowered mechanically between **c** and **f**. **b–f** are averages of 6 images to better visualize the tracer particle motion

$$p + \frac{1}{2}\rho v^2 + \rho g h - \frac{1}{2}\varepsilon_0(\varepsilon_r - 1)E^2 = \text{const.} \quad (2)$$

with the pressure p, the fluid density ρ, the fluid velocity v, the height h of the level rise caused by the hydrostatic pressure $\rho g h$, and g the acceleration due to gravity ($g = 9.80665\ \text{ms}^{-2}$). In equilibrium, the hydrostatic pressure and the Maxwell pressure counteract, causing a rise of the liquid level as observed in Fig. 4b. Using the relation between force density and Maxwell pressure p_{Maxwell}, we obtain the Kelvin force density $\vec{f}_{\text{Kelvin}}$

$$\vec{f}_{\text{Kelvin}} = -\nabla p_{\text{Maxwell}} = \frac{1}{2}\varepsilon_0(\varepsilon_r - 1)\nabla(E^2). \quad (3)$$

Thus, the gradient of the Maxwell pressure gives the resulting force on a dielectric liquid in a varying electric field, directing upward into the region of higher field intensity. This relation is valid within a linear dielectric with constant permittivity. Therefore, glycerol is pushed into the electric field between the electrodes in Fig. 4b because of the force on individual dipoles in the fringing field between the tips of the electrodes.

When discussing the horizontal liquid bridges forming between two beakers as shown in Fig. 3 in terms of the Maxwell pressure, these bridges have a high electric field due to the small cross-section and hence a negative pressure that tends to replenish the liquid within the bridge against drainage.

Especially with long axial lengths, horizontal bridges slightly sag under their weight, leading to distortions of the electric field lines inside the bridge. This is schematically plotted in Fig. 5, with the electric displacement field $\vec{D} \equiv \varepsilon_0\varepsilon_r\vec{E}$ as number. Whenever a fluid element wants to drip from the bridge, the concomitant distortion in the electric field will counteract this motion and stabilize the bridge against gravity by the non-zero gradient of the Maxwell pressure (3) and the resulting force density.

Figure 5 is a numerical simulation of the electric field within the bridge using the electrostatic interface in the AC/DC module in Comsol 4.1 multiphysics software (Comsol Inc., Palo Alto, CA) based on Gauss' law, solving the elements grid with a quadratic interpolation. A 2-dimensional geometry was chosen, with two glass beakers 20 mm in width and 10 mm height (glass $\varepsilon_r = 4.2$), metal electrodes and a water bridge 10 mm long with 3 mm diameter at the beaker (water $\varepsilon_r = 80$), slightly sagging in the middle. Thus, for this simulation of the

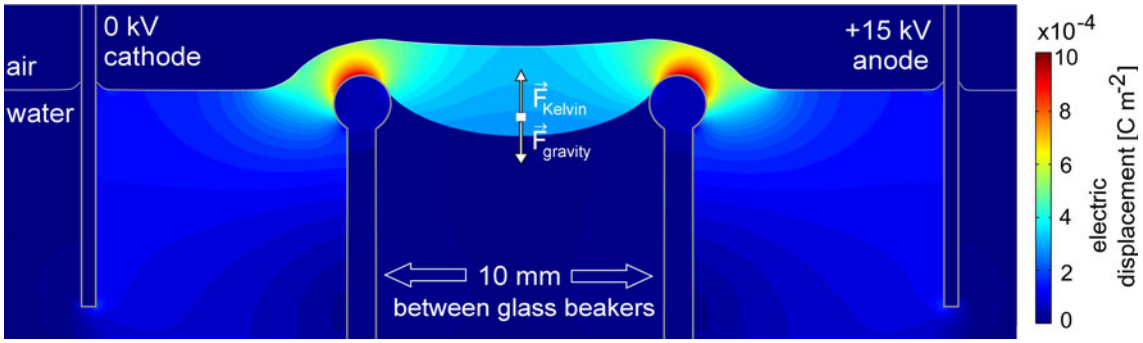

Fig. 5 Numerical simulation of the electric field within the water bridge using Comsol 4.1 software. Displayed are the absolute values of the electric displacement field. Ground potential is at infinity, cathode is at 0 kV (*left*), anode at 15 kV (*right*). The glass beakers have a slightly rounded brim. The Kelvin force density counteracts gravitational force

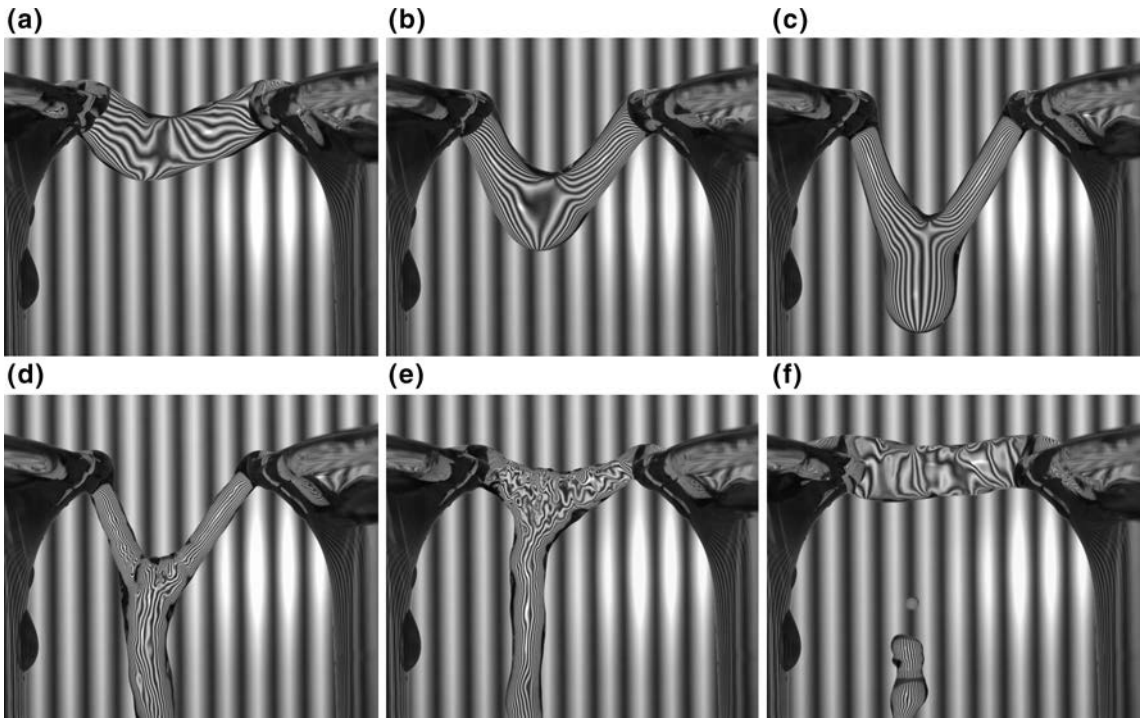

Fig. 6 Especially with long bridges instabilities can occur leading to a leaking of the bridge. These high-speed images were recorded at 0.25 s intervals with a periodic fringe pattern placed behind the bridge contouring its shape. Distortions of the otherwise *parallel fringe* pattern contour the shape of the bridge

electric field inside the bridge, the surface geometry was that for a stable bridge under equilibrium conditions. The infinite boundary for the mesh was set at a 50 mm radius away from the bridge centre.

With long bridges, instabilities can occur, leading to a leaking of the bridge. Such a process is shown for a water bridge at 15 kV DC and 9 mm spout to spout distance in Fig. 6 (two 60-mL beakers, anode beaker right, no capacitor in parallel). A periodic fringe pattern was placed behind the bridge on a glass–ceramic diffuser plate. This fringe pattern is imaged through the water bridge that acts as lens. Assuming a constant refractive index within the bridge, distortions of the otherwise parallel fringe pattern contour its shape.

Without a longitudinal electric field of sufficient strength, the leaking water flow decayed into drops by its surface tension (Fig. 6e and f). With a then reduced mass and smaller diameter, the leaking of the bridge stopped and

the bridge stabilized again. This motion between leakage and no leakage might periodically repeat at low frequency.

When comparing the horizontal bridge between two electrodes in Fig. 4f and the bridge forming between two beakers of glycerol in Fig. 7a, we see a similar flow pattern in both of them. Inside the bridges, there is a cellular convection, whereas the outer shell rotates. Fig. 7a is an average of 30 exposures, again with tracer particles added. Since polyamide particles can carry charge, it is likely that these tracers are pushed outwards by mutual electrostatic repulsion. Thus in water, tracer particles rotate only at the surface of the bridge (Woisetschläger et al. 2010) while in glycerol the viscosity is so high that some movement inside the bridge can still be identified.

For liquids with low conductivities, as listed in Table 1, Taylor and Melcher developed the leaky dielectric model, reviewed by Melcher and Taylor (1969) and Saville (1997). This model is based on the observation that whenever interfacial regions do exist in a fluid system, and electrical parameters suffer discontinuity, the electromechanics of these interfaces dominate the electrohydrodynamics of the system. If a liquid surface supports a surface charge, then tangential electric fields and interfacial electrical shear forces are induced leading to cellular convection in the liquid (Melcher and Taylor 1969); this can be seen in Fig. 7. It must be mentioned that the bridge itself gives the impression of a cylindrical structure with some rotational symmetry. The electric field outside the bridge certainly does not possess the same geometry because of the non-conducting glass beakers underneath the bridge and the more strongly insulating gas. This asymmetry in the outer field changes the tangential field components around the bridge and must lead to a cellular convection with circumferential components, much more complex than the more or less plane structures presented by Melcher and Taylor (1969).

Finally, with a high voltage of 15 kV AC at 11.5 kHz, a glycerol bridge was formed and is shown in Fig. 7a. In the AC field, the bridge was smaller, and no tracer movement was observed inside the bridge. The DC voltage showed driven flow phenomena associated with the tangential field associated with the surface charge and its relocation, while in the AC field, the bridge is closer to the pure dielectric condition, since the AC field tends to suppress effects due to interface charge.

This surface charge and its relocation have an important impact on the bridge morphology. For vertical bridges, Saville (1997) showed that within DC-driven bridges, leaky dielectrics require lower field strength for stability than perfect dielectrics. This effect will be discussed in the next section.

3.3 Stability of the horizontal bridge

By the pressure and viscous stresses, the Maxwell tensor balances the normal and tangential stresses on the bridge liquid/air interface. This tensor was used by Burcham and Saville (2002) to present a theory on the electrohydrodynamic stability on vertical liquid bridges in leaky dielectrics suspended in a dielectric gas. It was this approach that was also used by Widom et al. (2009), Saija et al. (2010) and Marin and Lohse (2010) to discuss horizontal bridges. Additionally, Aerov (2011) pointed at the importance of the surface tension included in the normal stresses at the bridge liquid/air interface.

In order to discuss stability of bridges, Burcham and Saville (2000) defined the following parameters. First the aspect ratio β,

$$\beta = \frac{l}{d}, \tag{4}$$

with l the length and d the diameter of the bridge. Then, the ratio of the electric energy contained in the liquid column related to the cylindrical surface energy (electrocapillary number C),

$$C = \frac{\varepsilon\varepsilon_0 E^2 d}{\gamma}, \tag{5}$$

with ε the relative permittivity of the liquid (see Table 1), ε_0 the vacuum permittivity, E the electric field strength and γ the surface tension of the liquid.

When building bridges in water, a relatively small influence of the accurate position of the electrodes in the beakers on the bridge dimensions was observed. This is due

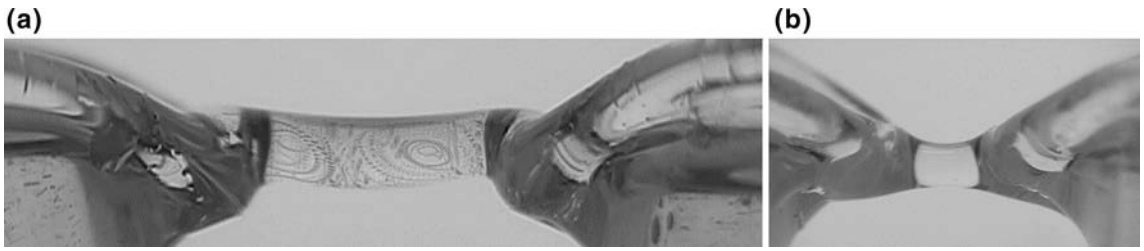

Fig. 7 **a** *Horizontal liquid bridge* in glycerol formed between two beakers, 16 kV DC. Polyamide tracers were added for *stream line* visualization, the picture is a 30 frames average. **b** *Horizontal bridge* formed at 15 kV AC, 11.5 kHz. No tracer movement can be observed

to the fact that the relative electric current I through the system with conductivity σ is constant, with the current density j as function of the cross-sectional area A,

$$I = jA = \sigma EA. \quad (6)$$

In a first approach, the conductivity of water was also assumed to be constant for the tested electric field strengths E inside the water region. From (6), it becomes evident that the electric field strength must be highest in the water bridge section and its closest vicinity (e.g. around the beakers edges). With the highest resistance and the highest voltage drop in this bridge area, the Ohmic losses must lead to heating, as can be seen in the thermographic image of the water bridge in Fig. 8. The temperature was calculated using an emissivity value of 0.96 for water by a thermal imager (FLIR 620).

A good approach to estimate the electric field strength in the water bridge is shown in Fig. 9. The total DC voltage between the electrodes in the beakers was recorded for constant current $I = 0.5$ mA and different beaker to beaker distances (length). The set-up used two 60-mL beakers with 56 mm inner diameter and platinum electrodes in the centres of the beakers. From that line, a constant voltage drop of about 5 kV in each beaker was estimated, resulting in a field strength of approximately 6 kV cm^{-1} in bridges between 4 and 16 mm length. The diameter of the bridge changed between 3.0 and 3.7 mm. With this field strength and the observed bridge diameters, the electrocapillary number C was between 10 and 13, indicating that the electric energy contained in this geometry was at the same order of magnitude as the energy from surface tension. (A factor of 8 would characterize equal energies, 10 slightly more energy in the electric field.) For better comparison to the data presented by Marin and Lohse (2010), we also used the diameter in (5), while the original papers by Burcham and Saville (2002) write the radius. For the water bridges presented in Fig. 9, the aspect ratios β were between 1 and 5.

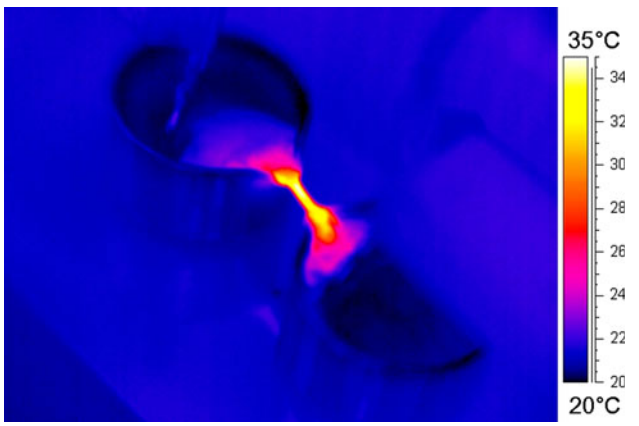

Fig. 8 Thermographic image of a water bridge (12 kV DC, 9 mm beaker to beaker distance)

Raco (1968) stabilized a vertical liquid bridge between electrodes in air by pulling an electrode out of a pool of liquid, and Gonzalez et al. (1989) discussed the stability of such a vertical bridge in a perfect dielectric by solving the electrohydrodynamic equations. Burcham and Saville (2002) did so for vertical bridges formed by leaky dielectrics. They observed that above a certain electric field strength, the vertical bridge was a perfect cylinder; when lowering the field strength, an amphora-shape, unstable configuration established, with a break-up into separate droplets. These instabilities can also be observed in horizontal bridges as demonstrated in Fig. 10. The recordings in Fig. 10 were done with an Exilim EX-F1 high-speed camera at 300 Hz frame rate. In order to get a horizontal bridge at low field strength, a small amount of soap (liquid hand soap) was added to the water used to form a horizontal bridge in two 40-mL beakers. Although the conductivity was increased by the soap, the surface tension decreased significantly, so that a high voltage below 20 kV stabilized bridges with aspect ratios $\beta \geq 20$.

Observed oscillations of such a horizontal water/soap bridge are shown in Fig. 10. Among them is an amphora-shape oscillation, a fundamental, a first harmonic string oscillation and the final break-up with subsequent decay

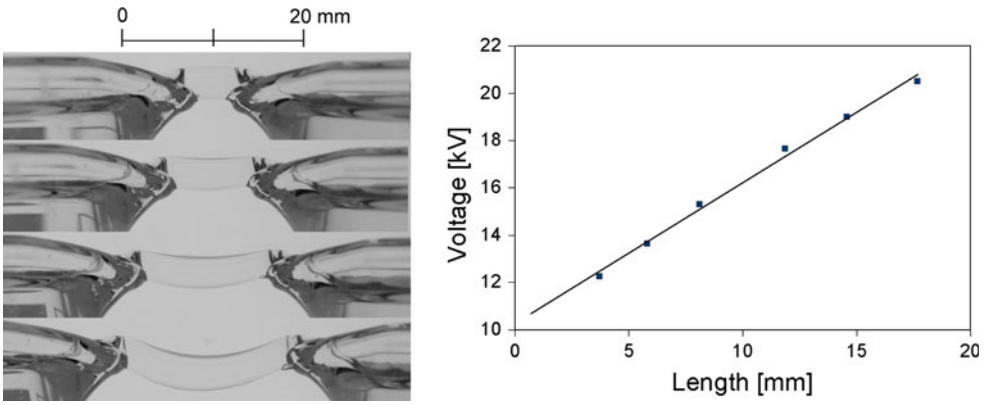

Fig. 9 DC voltage applied to the electrodes in the beaker vs. the spout to spout distance (length of the bridge) for a water bridge. Current was constant at 0.5 mA

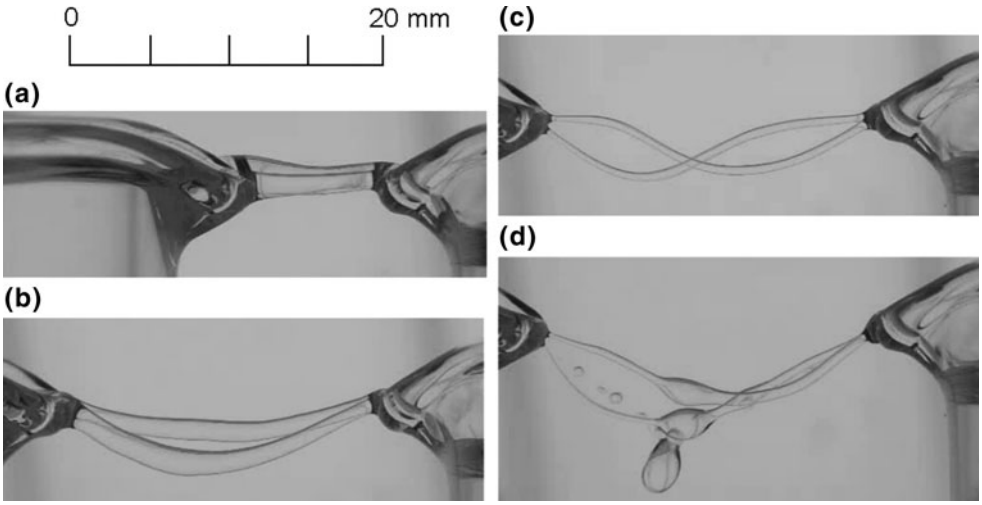

Fig. 10 Oscillations of a water bridge with a small amount of soap added. **a** 13 kV, **b–d** 17 kV applied to the electrodes. **a** shows a amphora type oscillation (1/10 s interval), **b** fundamental string oscillation (1/15 s interval), **c** first harmonic (1/30 s interval) and **d** bridge break-up (1/75 s interval). All images are multiple exposures

into (charged) droplets. One of the results from the Burcham and Saville (2002) study was that for the stability of a leaky dielectric bridge, the electric field parameters are much smaller, due to a larger number of free charges induced at the surface compared to bridges in pure dielectrics. While the normal stresses act to level perturbations, the tangential stresses force the charges on the interface away from bulges in the bridge, so that both effects reduce deformations in leaky dielectric bridges.

Burcham and Saville (2002) also mentioned the effects of the gas/liquid interface on vertical bridges, since conduction in the outer fluid allows charge to leak off the surface, influencing the electric field and the stability of the bridge surface. This effect was observed by us for horizontal bridges (Fig. 3) formed in all liquids listed in Table 1 by schlieren moving along the bridge surface, indicating distortions in the refractive index. A detailed discussion on these schlieren can be found in Woisetschläger et al. (2010). A possible explanation is the formation of electric double layers along the liquid bridge surface, as found in electrokinetics and electroosmosis, together with the ionic wind between the electrodes, influencing the surface charges and causing distortions in the electric surface layer. Burcham and Saville (2002) therefore introduced a surface conductivity to explain a different conductivity in the surface layer compared to the bulk. Since this charge transport is anisotropic, distortions in the electric field along the surface might occur, leading to refractive index gradients.

3.4 The bridge as electrohydrodynamic pump

During our first investigations of the charge and mass transfer through the bridge, we used pH dye to visualize the flow (Woisetschläger et al. 2010). We then showed that the addition of a pH dye does not directly visualize this charge, since it not only raises the conductivity, it also undergoes electrochemical reactions in the electric field (Fuchs et al. 2010a). Therefore, a pH dye can be used as tracer for qualitative visualization, but cannot be seen as non-involved indicator since the charges visualized are produced due to its presence. Thus, schlieren and interferometric techniques are better suited for mass and charge transfer measurements as they are less likely to influence the system under observation.

For that reason, the interferometer shown in Fig. 2 detected minute changes in the refractive index while changing the electric field between the electrodes placed in the 50-mm cuvette (compare Fig. 4a and b). The results for glycerol are presented in Fig. 11. Whenever light passes through a refractive index field in a liquid, this wavefront (object beam) suffers a phase lag compared to the wavefront passing through the second, reference beam without liquid. In order to observe a possible refractive index change by the electric force field, an interferogram was recorded without a voltage applied to the electrodes (Fig. 11a) and a second interferogram with 8 kV applied (Fig. 11b). For all recordings, one mirror in the interferometer was slightly tilted to superimpose a carrier fringe system which can be modulated by the phase lag caused by the refractive index changes. A fast-Fourier-transformation was then applied to extract the phase information from both interferograms at 0 and 8 kV. Finally, both phase maps were subtracted to obtain the phase change between both exposures without sign ambiguity. In order to calculate the refractive index change from the phase lag, a uniform refractive index distribution over the width of the cuvette (10 mm) was assumed. Finally, three refractive index maps were averaged to reduce the influence of flow instabilities; the resultant map is shown in Fig. 11c. Small-scale refractive index distortions along the surface and in the vicinity of the electrodes were also observed, likely caused

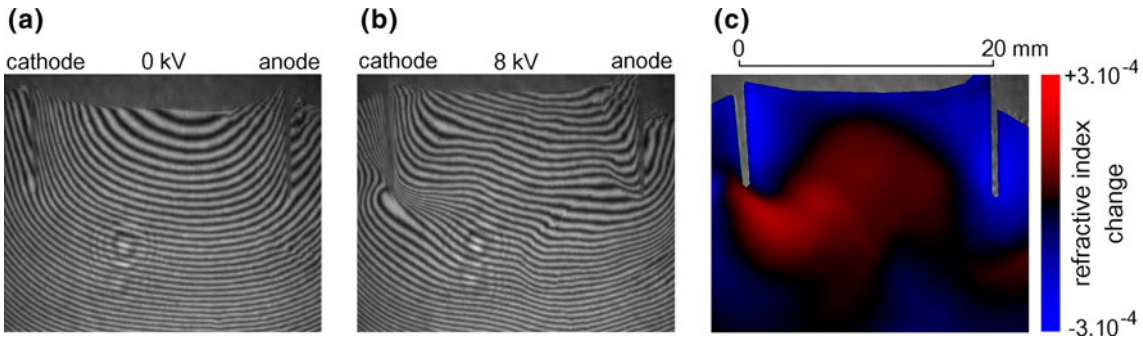

Fig. 11 Interferograms reveal changes in the refractive index due to the application of a high-voltage DC field in glycerol. **a** reference recording at 0 kV, **b** high-voltage interferogram, **c** change in refractive index calculated from the phase shifts recorded in **a** and **b**

by distortions of the diffuse electric surface layer. For data reduction software, IDEA was used (free download from Graz University of Technology http://www.optics.tugraz.at ; Hipp et al. 2004).

The interferograms were recorded in two sets with the polarization direction either vertical or horizontal. Due to the small Kerr constant of glycerol (Ho and Alfano 1979), no effect of the polarization direction was observed. Thus, the refractive index change recorded is due to a density change, either by pressure or by temperature. Discussing Fig. 11c, we can see the consequences of (1–3). Fluid material was pumped around the sharp edge of the cathode towards higher field strength (increasing refractive index in Fig. 11c). This upward fluid motion lifted the fluid level between the electrodes. But when looking at the anode side, this motion was not symmetrical since along the tip of the anode less fluid was pressed upwards. Such effects were first discussed by Pohl (1958) and Sumoto (1955) in terms of dielectrophoresis and electrohydrodynamic pumping. Both publications are of high relevance for the horizontal bridge, since Pohl (1958) presented a special electrode configuration which pumped liquid out of a beaker, and both authors observed a different height of liquid rise at anode and cathode for some fluids. Pickard (1962) suggested that 'the Sumoto effect appears to be the result of an abnormal fall of potential occasioned by the formation of an ion cloud near one of the electrodes' (Pickard 1962).

In dielectric liquids, it is well known that both permittivity and conductivity follow similar trends, they tend to increase or decrease together. This is due to the fact that with an increase in permittivity, the electrostatic attraction between ion pairs decreases (Watson 1998). Whenever a high-voltage DC field is applied to the fluid, an increasing number of ions escape recombination yielding a change in conductivity, as was discussed by Onsager (1934) and Briere (1964). While at low-voltage Ohmic behaviour is observed due to ions generated by dissociated molecules, at high voltage, the dissociation rate is proportional to the electric field, but the recombination rate is not and the current reaches saturation (Jeong and Seyed-Yagoobi 2003; Zhakin 1998). In regions where the dissociation–recombination rate is not in equilibrium complex heterocharge layers build up, inducing a fluid motion in the vicinity of the electrode (Jeong and Seyed-Yagoobi 2004). This fluid motion will lead to friction and cause the change in refractive index close to the electrodes as observed in Fig. 11c. At a certain electric field threshold charge injection from sharp edges might become no longer negligible, the current will increase again (Jeong and Seyed-Yagoobi 2003). All these effects depend also on the electrochemical processes taking place at the electrodes.

This behaviour was tested for the geometry used, i.e., the two platinum electrodes were submerged 10 mm deep into the liquid, with 50-mm electrode distance under atmospheric conditions, and electric current and voltage recorded. The result is shown in Fig. 12. The polar liquids used showed non-ohmic behaviour indicating that the fluid motion must be also influenced by secondary effects due to heterocharge layers building up close to the electrodes. This behaviour causes non-reflection-symmetric boundary conditions for the Maxwell pressure, resulting in a preferred flow direction.

The formation of non-discharged ions at one or both electrodes alters the electric field gradients in the vicinity of the electrodes causing an abnormal fall of potential and the asymmetry in fluid pressure mentioned previously. To test this effect, we used a glass cuvette with a rounded Teflon spacer glued into it (Fig. 13). When a high voltage was applied to the electrodes, the preferred flow direction was towards one electrode and was thus not symmetrical. This effect of asymmetry was also observed in the Pellat experiment and when doing mass flow measurements in the horizontal water bridge (Woisetschläger et al. 2010). When discussing the results in Fig. 13, it became evident that the alcohols used prefer redox reactions with an affinity towards the anode. In other polar fluids, the cathode electro-chemical reactions have a higher level than the anode

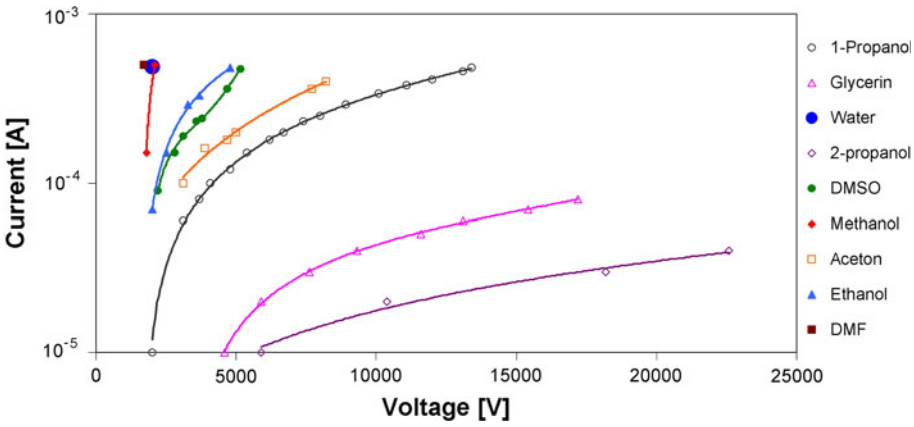

Fig. 12 Non-ohmic behaviour of the polar liquids used to form a *horizontal bridge*. The recordings were done up to 25 kV and up to 0.5 mA. The platinum electrodes dipped 10 mm deep into the liquid with 50 mm electrode distance under atmospheric conditions

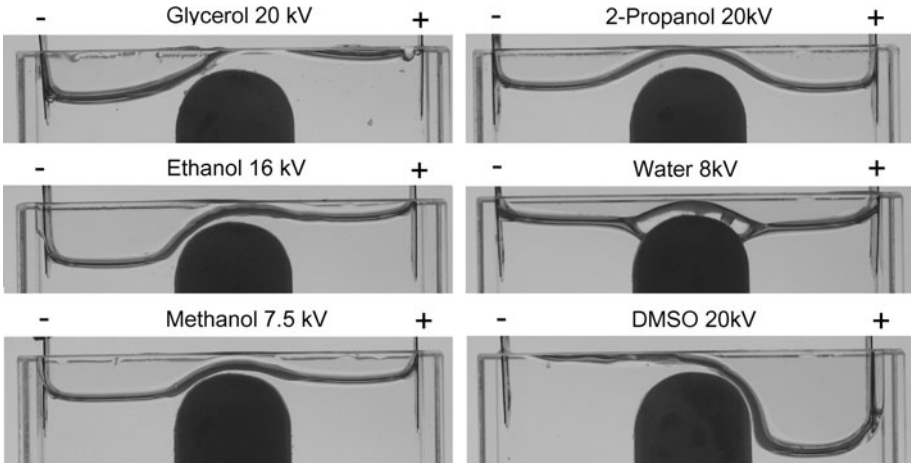

Fig. 13 Electrohydrodynamic pumping of polar liquids under the influence of a high-voltage DC field through a *horizontal bottle neck* (experimentally simulated 'bridge')

one (Zhakin 1998). Therefore, non-equilibrium heterocharge layers in some alcohols will build up faster at the anode than at the cathode, causing a difference in Maxwell pressure between the two electrodes (Fig. 13 left side), counteracted only by the hydrostatic pressure and the rim of the beaker. Electrochemical reactions of organic solvents in a horizontal bridge set-up have been described in detail for phenol and glycol solutions (Eisenhut et al. 2011).

In the vicinity of the electrodes, a strong fluid motion parallel to the surface was observed. This is essentially how electrowetting works—when the Maxwell pressure drives contact-line motion (Jones 2002).

Compared to other polar liquids, in water nearly no or only little preferred flow direction through the bridge was observed (Woisetschläger et al. 2010), enabling the bridge to stabilize for hours when platinum electrodes are used, preventing metal ions to dissolve. This stabilization is possible since long-term thermographic visualizations suggest a permanent directional change of flow direction through the bridge in the 5–20 Hz range. Similar effects were observed with other low-viscosity liquids, as methanol.

4 Conclusion

A 'floating water bridge' forms when glass beakers are filled with deionised water and a DC voltage between 10 kV and 20 kV is applied under atmospheric conditions. By repeating a version of Pellat's experiment, it was experimentally proven that such horizontal bridges can be explained by electrohydrodynamic relations only. They are stable by the action of electrohydrodynamic pressure, and furthermore, all static and dynamic properties of the phenomenon called a 'floating water bridge' can be discussed by the gradient of Maxwell pressure, replenishing the liquid within the bridge against any drainage mechanism. In a large number of other polar liquids tested, and having a relative permittivity larger than 5 and a not too high conductivity under the influence of an electric field (as in methylformamide), a horizontal bridge did form as well. On the one side, a persistent pumping of the liquid from one beaker into the other was observed due to the gradients in Maxwell pressure. On the other side, non-equilibrium heterocharge layers accumulate at the electrodes, presumably driven by electrochemical reactions, cause non-uniformities in the Maxwell pressure driven fluid motion

and therefore result in a preferred flow direction through the bridge. These non-uniformities in mass flow through the horizontal bridges were also discussed by a second experiment in a single beaker configuration.

Since polar liquids represent leaky dielectrics, the liquid surfaces conduct surface charges, interfacial electrical shear forces will be induced, leading to cellular convection in the bridge, together with reported instabilities of the system. Under the conditions discussed—electrocapillary number C between 10 and 13 and field strengths of 5–7 kV cm^{-1}—horizontal bridges of polar liquids can be operated under atmospheric conditions and provide a laboratory of their own.

5 Outlook

The experiments presented demonstrate that a horizontal liquid bridge provides interesting new possibilities to study basic interactions between electric fields and fluids and introduces a novel environment for (electro-)chemical reactions: Substances that remain mostly inert in the process could be brought in contact with other educts to chemically react within the bridge; substances that do react electrochemically might do this in a different manner, which could be used to specifically select one chemical pathway over others, or stop an oxidation process at an—otherwise possibly short-lived—intermediate (Eisenhut et al. 2011). By applying different potentials, the electrochemical environment can be changed without the addition of an acid or base; at the same time, educts could be oxidized to a more reactive form. This could be used, e.g., to start polymerization reactions of ultra-pure monomers in bridge building solvents like methanol. The affinity of certain liquids to one electrode can be used to separate them in the process. These possibilities should be considered exemplary for a large number of possible industrial applications of the techniques presented.

Finally, from a microbiological point of view, liquid bridge mechanisms could be important to further understand charge and substance transport through the cell membrane. Since the potential differences there are of comparable magnitude or even larger (e.g. Hülsheger et al. 1983), we suggest that microscopic bidirectional electrohydrodynamic flows may play a role within or next to the established mechanisms.

Acknowledgments This work was performed in the TTIW-cooperation framework of Wetsus, Centre of Excellence for Sustainable Water Technology (http://www.wetsus.nl) together with Graz University of Technology, Austria (http://www.tugraz.at). Wetsus is funded by the Dutch Ministry of Economic Affairs, the European Union Regional Development Fund, the Province of Fryslân, the City of Leeuwarden, the EZ/Kompas program of the 'Samenwerkingsverband Noord-Nederland' and the participating companies. The authors would like to thank the whole research team and staff of WETSUS, the Institute of Analytical Chemistry and Food Chemistry at the Graz University of Technology, especially Dr. Xinghua Guo for providing some of the solvents, and the Institute of Hydraulic Engineering and Water Resources at Graz University of Technology for sharing the Photron high-speed camera. With great pleasure, the authors furthermore wish to thank Profs. Marie-Claire Bellissent-Funel (Laboratoire Léon Brillouin, Saclay), Eshel Ben-Jacob (Tel Aviv University), Mariano Bizzarri (Università La Sapienza, Roma), Harry Bruning (Wetsus), Cees Buisman (Wetsus), Gert-Jan Euverink (Wetsus), Friedemann Freund (NASA SETI Institute, California), Emilio Del Giudice (Universitá di Milano), Ferenc Hajdu (Central Research Institute for Chemistry, Hungarian Academy of Sciences, Budapest), Franz Heitmeir (Graz University of Technology), Hideo Nishiumi (Chem. Eng. Lab., Hosei University, Japan), Laurence Noirez (Laboratoire Léon Brillouin, Saclay), Gerald H. Pollack (University of Washington), Alan Soper (Rutherford Appleton Laboratories, ISIS, Oxford), Piergiorgio Spaggiari (Istituti Ospitalieri Di Cremona, Milano, Italy), José Teixeira (Laboratoire Léon Brillouin, Saclay), Giuseppe Vitiello (Universitá degli studi di Salerno), Vladimir Voeikov (M.V. Lomonosov Moscow State University), John Watterson (Ashmore, Australia) as well as Luewton L.F. Agostinho, Cees Kamp, Astrid H. Paulitsch-Fuchs, Martina Sammer and Doekle Yntema (Wetsus) for the ongoing discussion on the water bridge phenomenon (in alphabetic order).

References

Aerov AA (2011) Why the Water Bridge does not collapse. Phys Rev E 84:036314

Armstrong LW (1893) Electrical phenomena. The Electrical Engineer, pp 154–155, 10 February 1893

Briere GB (1964) Electrical conduction in purified polar liquids. Br J Appl Phys 15(4):413–417

Burcham CL, Saville DA (2000) Electrohydrodynamic stability of a liquid bridge: Microgravity experiments on a liquid bridge suspended in a dielectric gas. J Fluid Mech 405:37–56

Burcham CL, Saville DA (2002) Electrohydrodynamic stability: Taylor-Melcher theory for a liquid bridge suspended in a dielectric gas. J Fluid Mech 452:163–187

Del Giudice E, Fuchs EC, Vitiello G (2010) Collective molecular dynamics of a floating water bridge. WATER (Seattle) 2:69–82

Eisenhut M, Guo X, Paulitsch-Fuchs AH, Fuchs EC (2011) Aqueous phenol and ethylene glycol solutions in electrohydrodynamic liquid bridging. Cent Eur J Chem 9(3):391–403

Fuchs EC (2010) Can a century old experiment reveal hidden properties of water? Water (MDPI) 2:381–410

Fuchs EC, Woisetschläger J, Gatterer K, Maier E, Pecnik R, Holler G, Eisenkölbl H (2007) The floating water bridge. J Phys-D-Appl Phys 40:6112–6114

Fuchs EC, Gatterer K, Holler G, Woisetschläger J (2008) Dynamics of the floating water bridge. J Phys-D-Appl Phys 41:185502–185507

Fuchs EC, Bitschnau B, Woisetschläger J, Maier E, Beuneu B, Teixeira J (2009) Neutron scattering of a floating heavy water bridge. J Phys-D-Appl Phys 42:065502:1–065502:4

Fuchs EC, Agostinho LLF, Eisenhut M, Woisetschläger J (2010a) Mass and charge transfer within a floating water bridge, Laser Applications in Life Sciences. Proc SPIE 7376:1E1–1E15

Fuchs EC, Baroni P, Bitschnau B, Noirez L (2010b) Two-dimensional neutron scattering in a floating heavy water bridge. J Phys-D-Appl Phys 43:105502:1–105502:5

Fuchs EC, Agostinho LLF, Wexler A, Wagterveld RM, Tuinstra J, Woisetschläger J (2011a) The behaviour of a floating water

bridge under reduced gravity conditions. J Phys-D-Appl Phys 44:025501
Fuchs EC, Bitschnau B, Di Fonzo S, Gessini A Woisetschläger J, and Bencivenga F (2011b) Inelastic UV scattering in a floating water bridge. J Phys Sc Appl 1(3) (in press)
Gonzalez H, McCluskey FMJ, Castellanos A, Barrero A (1989) Stabilization of dielectric liquid bridges by electric fields in the absence of gravity. J Fluid Mech 206:545
Hipp M, Woisetschläger J, Reiterer P, Neger T (2004) Digital evaluation of interferograms. Measurement 36:53–66
Ho PP, Alfano RR (1979) Optical Kerr effect in liquids. Phys Rev A 20:2170–2187
Hülsheger H, Potel J, Niemann EG (1983) Electric field effects on bacteria and yeast cells. Radiat Environ Biophys 22:149–162
Jeong SI, Seyed-Yagoobi J (2003) Theoretical/numerical study of electrohydrodynamic pumping through conduction phenomenon. IEEE Trans Ind Appl 39:355–361
Jeong SI, Seyed-Yagoobi J (2004) Fluid circulation in an enclosure generated by electrohydrodynamic conduction phenomenon. IEEE Trans Dielectrics Electrical Insul 11:899–910
Jones TB (2002) On the relationship of dielectrophoresis and electrowetting. Langmuir 18:4437–4443
Kendall J (1916) The specific conductivity of pure water in equilibrium with atmospheric carbon dioxide. J Am Chem Soc 38:1480–1497
Marin AG, Lohse D (2010) Building water bridges in air; electrohydrodynamics of the floating water bridge. Phys Fluids 22:122104
Melcher JR(1981) Continuum Electromechanics. Cambridge, MA: MIT Press, 1981. Copyright Massachusetts Institute of Technology. ISBN: 9780262131650. Also available online from MIT OpenCourseWare at http://ocw.mit.edu (accessed 01 19, 2011) under creative commons license attribution-noncommercial-share alike
Melcher JR, Taylor GI (1969) Electrohydrodynamics: A Review of the role of interfacial shear stresses. Annu Rev Fluid Mech 1:111–146
Melcher JR, Warren EP (1971) Electrohydrodynamics of a current carrying semi-insulating jet. J Fluid Mech 47:127–143 (2 plates)
Nishiumi H, Honda F (2009) Effects of electrolyte on floating water bridge. Res Let Phys Chem. doi:10.1155/2009/371650
Onsager L (1934) Deviations from Ohm's law in weak electrolytes. J Chem Phy 2(9):599–615
Pellat H (1896) Mesure de la force agissant sur les diélectriques liquides non électrisés placés dans un champ élitrique. C R Acad Sci Paris 123:691–696
Pickard WF (1962) An explanation of the de sumo to effect. J Appl Phys 33:941–942
Pohl HA (1958) Some effects of nonuniform fields on dielectrics. J Appl Phys 29(8):1182–1188
Ponterio RC, Pochylski M, Aliotta F, Vasi C, Fontanella ME, Saija F (2010) Raman scattering measurements on a floating water bridge. J Phys-D-Appl Phys 43:1754051–1754058
Raco RJ (1968) Electrically supported column of liquid. Science 160(3825):311–312
Ramos A, Castellanos A (1993) Bifurcation diagrams of axisymetric liquid bridges of arbitrary volume in electric and gravitational axial fields. Phys Fluids 6:207–225
Riddick JA, Bunger WB (1989) Organic solvents: Physical properties and methods of purification. Wiley, New York. ISBN 978-0471-08467-9
Saija F, Aliotta F, Fontanella ME, Pochylski M, Salvato G, Vasi C, Ponterio RC (2010) Communication: an extended model of liquid bridging. J Chem Phys 133:081104
Saville DA (1997) Electrohydrodynamics: The Taylor-Melcher Leaky dielectric model. Ann Rev Fluid Mech 29:27–64
Sumoto I (1955) An interesting phenomenon observed on some dielectrics. J Phys Soc Jpn 10(6):494
Watson PK (1998) Conduction, instabilities and breakdown in liquid dielectrics. In: Castellanos A (ed) Electrohydrodynamics, International Centre for Mechanical Sciences, CISM Courses and Lectures No. 380. Springer, Wien. ISBN 3-211-83137-1
Widom A, Swain J, Silverberg J, Sivasubramanian S, Srivastava YN (2009) Theory of the Maxwell pressure tensor and the tension in a water bridge. Phys Rev E 80:016301:1–016301:7
Wohlfarth CH (ed) (2008) SpringerMaterials—The Landolt-Börnstein Database (http://www.springermaterials.com). Springer, Berlin, Heidelberg, doi:10.1007/978-3-540-75508-1_31
Woisetschläger J, Gatterer K, Fuchs EC (2010) Experiments in a floating water bridge. Exp Fluids 48–1:121–131
Zhakin AJ (1998) Conduction phenomena in dielectric liquids. In: Castellanos A (ed) Electrohydrodynamics, International Centre for Mechanical Sciences, CISM Courses and Lectures No. 380. Springer, Wien. ISBN 3-211-83137-1

What we know

is a droplet,

what we don't know,

an ocean.

I.Newton

I'd like to thank my family, friends and teachers which encouraged me to deal with my curiosity about nature.

Abstract:

The initial incident of composing this work was the publication of a paper called: „The floating water bridge“, published on October 7th 2007 by Fuchs et. al. in Journal Physics D: Applied Physics. This paper deals with structural properties of water in a high-voltage electric field and the formation of a 'floating' bridge between two beakers filled with distilled water. Sparked by this publication, the cause for this work is the characterisation of water in all its physical, chemical and quantum mechanical properties for all its complex configurations and phase states. Therefore, herein a kind of water compendium is presented in which existing papers are integrated and structured with the aim of giving the reader an overview of the state-of-the-art experiments as well as the historic basics. It should become clear to the readers that water research is still an open field and every answered question throws up at least two new ones in this expanding field of research.

Table of contents

1. Introduction:

This work is a contribution to many scientists' work in finding correlations between water and its environment. It mainly consists of 2 main chapters, the first one dealing with the flow of water under an external electric field ("**jets"**). The second chapters discusses more generally many different theories concerning the structure of water and the interaction with foreign molecules and/or with itself. This can be due to specific quantum states of water or electrohydrodynamic effects leading to the term "**Q**uantum**E**lectro**H**ydro**D**ynamic" (**QEHD**) meaning Electrohydrodynamics (EHD) and Quantum Mechanics. This chapter is loose in its boundaries, but tries to focus on the connections between large working groups rather than specifying investigations on small topics by various authors throughout history.

The intention of this work is to act as an "information-categorizer", enabling the reader to analyse new theories by tracing them back to the primary publications. This work can also be used to provide a broad survey about modern developments and fields of research in nowadays science.

This work summarizes numerous papers published during the last 100 years, sorted chronologically by release date, authors and topics. The author of this report also provided a short summary to better understand the connections between different publications. These summaries are not exhaustive and represent the author's personal view. Generally, several publications summarized in this work are connected to each other. Those are marked with an identifier, e.g. "**historic**", meaning published before 1978. Other identifiers are "**Taylor**" for water in a electric field, electrohydrodynyamic atomization "**EHDA**", "**Kerr**" for Kerr,- Pockels-, Quantum Hall- and Faraday-Effects, "**Reactions**" summarizing water – molecule interactions in electric fields and/or in interface regions, "**structure**" refers to general experiments on the structure of water. A **date** is given for all publications related to the receipt of the manuscript by the journals or conference publications.

2. Summaries:

2.1 Jets:

Three sub-categories were identified for the topic '**jets**': ***historic articles***, which were the early basis for any recent findings and were published before 1978; **electrohydrodynyamic atomization *(EHDA)***, a research area founded by H.P. Smith in 1986, and the big category ***„Taylor's legacy*“** which concerns most investigations dealing with water in an external electric field (published since the 1960's).

In this section, the following phenomenons related to the collective term 'jets' are discussed: *streamer propagation*[21, 98, 40], *corona pulse discharge*[110], *space charge distribution*[63, 75, 87, 96], *bulk* and *surface characteristics* [142,143], *breakdown voltages* [60, 82, 83], *charge density/separation* [13] and *Electrohydrodynamic atomization (EHDA)* [23].

Dealing with theses publications a picture evolved, bringing out the high count of cross-linkages between the single phenomena. Based on the findings by G.I. Taylor[2]and his predecessors (e.g. Rayleigh, Zeleny[1]) this part reaches out to the investigations of the basics of *electrosprays* [31, 24, 44] by examination of *Taylor cones*[37] and the subsequent correlation to the basic physical values of voltage and current.

In general, different methods are used in the articles to determine special physical parameters of the investigated system, such as *surface tension* measurements[65], *molecular dynamics simulations* and nearly all kinds of spectrometric methods. Especially the interactions between water flows under external electric fields are studied in the following articles: Some very distinguished publications (often referenced) were written by J.Latham et al. [3] , R.P.A.Hartman et al. [12,17,20,22,23,25,26], A. Ajdari [13], D.P.H.Smith [11]and J.R. Melcher et al. [5,54]. The university of Delft, Netherlands, and the MIT, Cambridge, proved themselves to be leading in the development of the EHDA- technique. Together, they developed the basics of this procedure. After the paper from Dolly and Melcher [5] was released in 1969 it didn't cause any sensation, but in the 1990 their work was reassessed and numerous papers were published following the direction Melcher suggested. The Taylor-Melcher leaky model was first proposed by Saville [18], 1997. Therfore Taylor cones always were worth intense examinations and some fundamental properties are presented in works published by N. Ashgriz et al.[11],1993, J.F.de la Mora[44], 2007 and J.Eggers et al. [48], 2007.

1-historic 01.07.1917, J. Zeleny

Instability of electrified liquid surfaces

Summary:

In this article experiments with alcohol and glycerine in an strong electric field (up to 7 kV) and hydrostatic pressure were undertaken. The author used a glass tube with liquid in it and a grounded metal plate below it to generate a strong electric field with a static machine. He described instabilities of the liquids which he analysed with a microscope and came to the conclusion that the surface tension of the liquids interacts with the electric field and so disperses the liquid when the charge gets to a certain value. When these minute drops had taken enough charge away from the surface the drop stabilizes again. Furthermore, a Taylor cone like-shape is to be seen in one of his

photographs. He explains it with a combined action of the divergence in the electric field and the mutual repulsion of the drops. At the end he tries to connect the threads produced of molten sealing wax with his studies and suggests more studies in this field of "jet production" in the future.

2-historic **21.02.1964, G.Taylor**

Disintegration of water drops in an electric field

Summary:
After lots of researchers worked on a theory to explain water characteristics in an electric field, Taylor sums up his predecessors, beginning from the early 20th century, producing an interesting overview of research in this area. He worked with soap bubbles and described experiments with charged and uncharged water, water between charged metal plates as well as electrical properties of water drops on the top of capillaries.

3-historic **28.04.66, J. Latham**

Disintegration of pairs of water drops in an electric field

Summary:
After Taylors experiments with one water drop, this article is all about the interaction of two water drops in an external electric field. The authors try to make a linkage to clouds and the genesis of lightning bolts and present their study as a possible explanation for electrostatic interaction of water drops over their freezing point in clouds. They propose that the necessary electric field to disintegrate the 2 distinct drops decreases as the distance between them becomes smaller. Driving force of this process can be the decreasing minimum surface free energy of one big drop compared to two little drops, but only if the thin air film between them is punctured and a water bridge could build up. The question why the one drop knows where the other is relative to him stays unanswered.

4-historic **01.01.68**, **Y.G.Eliseev**

Stability of a liquid-dielectric jet in a electrostatic field

Summary:
The assumption in this article is that a liquid dielectric in the form of a cylinder travels in an external uniform electrostatic field surrounded by air. Calculations of the surface tension (based on Rayleigh) and the associated potential energy of the jet showed that a stabilizing effect is obtained if the disturbance wavelength is appropriate. As a result it is obtained that a longitudinal (axial) electrostatic field tends to stabilize a jet of liquid dielectric.

5-historic **01.11.68, R. J. Turnbull**

Electrohydrodynamic Rayleigh-Taylor Bulk Instability

Summary:
The article showed that bulk instabilities were essentially important for understanding conduction processes in highly insulating liquids and for electro-optical image reproduction effects of finite mobility or conductivity in cases involving space charge were likely to be important; nevertheless, the zero mobility (or zero conductivity) case developed here is significant as the limiting case for more complicated and hence more specialized configurations. A variational principle for determining the critical conditions for instability and the experiments, as they were successfully correlated with the theory, draws specific attention to the dielectrophoretic limit .

6-historic **04.02.69, D.C. Jolly**

Electroconvective instability in a fluid layer

Summary:
This case study gives quantitative insight to a class of instabilities characterized by incipience at a critical electric Hartmann number and ensuing steady convection at a rate proportional to an electric Reynolds number. There are three types of electrohydrodynamic interactions that appear related to the case described. The most obvious of these occurs in a diversity of situations in which liquid-liquid or liquid-gas interfaces are stressed by an electric field (Taylor 1966, Smith & Melcher 1967). The pumping motion resulting from shear stresses at the interface may be dominated by a form of instability analogous to that discussed here. A recent review has focused attention on this type of interaction (Melcher & Taylor 1969) to provide an overview of physical situations in which surface shear pumping and electro convective instability have been investigated. Included in this review is an alternative model (Jolly 1968) for the instability described here. Certain bulk instabilities found as a uniform ion current is passed through a highly insulating initially static layer of liquid also appear to have this electro-convective nature, with a critical electric Hartmann number for incipience (Schneider & Watson 1969). The convection resulting from this class of instabilities may be related to electro-optical liquid crystal effects currently being investigated for image processing purposes (Heilmeier , et a1 1968), and is certainly related to high-field conduction processes through insulating liquids (Watson & Schneider 1967)(Lewis& Secker 1967).
A third type of instability occurs in conjunction with an equilibrium flow; in pumps with ions flowing in the direction of equilibrium convection (Stuetzer 1959) or in channels with a transverse ion current (Jorgensen1968).Although the velocity profile and other particulars brought in by the equilibrium convection and characterized by the ordinary Reynolds number are certainly involved (Lin 1955), many electrohydrodynamic bulk flow instabilities appear to have an electro-convective nature also.

7-historic **05.05.69, A.H. Nayfeh**

Nonlinear stability of a liquid jet

Summary:
Rayleigh’s assumptions were proven partially wrong in this paper. His linear theory did not represent a proper solution in cases where the cutoff wavenumbers were exceeded. For measuring the cutoff wavenumbers a method called multiple time scales was used. Around this area there appeared to be one amplitude dependent and one amplitude independent frequency. It is stated that amplitude has an effect on cutoff wavenumbers contrary to Rayleigh’s equations and his equations are not practicable for the area where k-1=e^2 (k Wavenumber; e amplitude).

8-historic **11.11.1973, H.C.Lee**

Drop formation in a liquid jet

Summary:
Stream dynamics of a finite quasi stationary jet caused by a initial disturbance with a periodic distribution is the field of interest in this article. In linear form Rayleigh like equations are obtained respectively to calculations of the satellite drop size in nonlinear form. Satellite drops which are partially produced by parental drops through periodic electrostatic or magnetic disturbances have a optimum building ratio which depends on the wavelength of the periodic disturbance and the diameter of the jet.

9-historic **30.06.78, K.C. Chaudhary et al.**

The nonlinear capillary instability of a liquid jet

Summary:
This article deals with the satellite drop formation of water in a capillary. An initial velocity disturbance consisting of a fundamental and one harmonic component is used to derive equations for the build up and especially the prohibition of satellite drops build up. Therefore a nonlinear theory had to be developed and the solutions for the first, second and third order are given. Theoretical and practical work on the theory of oscillations in water.

10-Taylor **27.01.86, K. Varga et al.**

Observation of electrical effects with cavitating liquid flow

Summary:
Electrical fields and were proven to amplify mechanical effects of erosion due to cavitating flow formation. The building of H_2O_2, ultrasonic luminescence and the triggering of chemical processes are well known but no direct link to magnetic fields exists. On the base of a streaming potential cell, it was shown that a voltage increase is intercorrelated with a sound increase, which are both dependent on the streaming potential. The two suggested involved mechanisms here are the increased resistivity of the return path and the increased charge separation of the water molecules due to a higher flow rate. The measured sound and voltage changes are wavelike and periodic, which can be interpreted as a sudden increase of charge separation in moments of increasing/decreasing perturbations and therefore different dissociation constants of water.

11-EHDA **01.05.86, D.P.H. Smith**

The Electrohydrodynamic Atomization of Liquids

Summary:
The mechanism by which resistive liquids subjected to high electric potentials produce a filament and aerosol is under investigation in this article. An experimental study of the onset parameters of this electrohydrodynamic (EHD) atomization mode is presented. Data on the effect of onset potential, capillary radius, liquid conductivity, and viscosity, together with an observed hysteresis in the current-voltage characteristics, provide the basis for a qualitative model of the phenomena. The relationship between EHD mode onset voltage and the capillary-earth plane parameters is based on the assumption that identical field conditions are met. These conditions imply that the onset potential will increase with the square root of the surface tension, and this was observed with reasonable accuracy. However, the value of the field required for EHD onset on the liquid surface at the capillary is apparently greater than that required for ionization of the air. The large curvature on the surface and the presence of excess charge are known to affect the value of surface tension and the vapor pressure above the surface, but rough estimates of these effects suggest they are not large enough to account for the discrepancy. The value of liquid conductivity was found to have a marked effect upon the morphology of the liquid issued in the EHD mode. In general, as conductivity increases, the filament width, length, aerosol droplet size, and flow rate all decrease markedly. The main effect of increasing viscosity was an increase in the aerosol droplet size and possibly an increased flow rate. The model of the EHD mode outlined in Section III predicts that the flow rate decreases inversely with conductivity. Some previously observed features also give some support to the proposed mechanism. Before the EHD onset, i.e., while in the pulsating mode, it was found that charge is emitted before liquid extrusion occurs. The general features of the model seem to agree qualitatively with the experiments and give some justification to the approach. Some further features, such as the filament radius and the conditions under which individual droplets or a continuous jet may be formed at the apex, are considered as logical steps of this research field.

12-Taylor 15.11.93, N. Ashgriz et al.

Temporal analysis of capillary jet breakup

Summary:
The control the droplet size of capillary jets after their breakup is investigated in this article. The authors use different oscillating frequencies in linkage to Reynolds numbers and different amplitudes. They conclude that the formation and the size of a satellite drop depend on the "jet radius- wavenumber- amplitude" ratio. Furthermore, they discuss differently damped oscillations with stable wavenumbers, whose latter affects a smaller drop size due to a time-dependent decrease in amplitude size.

13-EHDA 14.08.1995, A. A.Naqwi et al.

Basic Studies of Electrohydrodynamic Atomization Process using Phase Doppler Measurement Technique

Summary:
This work illustrates how the phase Doppler technique can be used to obtain a better understanding of a complex two-phase flow. The realizability condition of the single jet mode of an electrospray is proposed, which is helpful in establishing whether a transition to multiple jet regime is taking place. Atomization would represent an abrupt vanishing of the current and hence could lead to a corona discharge, and/or highly charged droplets that would disintegrate as the surface charge will exceed the stability limit after some evaporation. In another scenario, a long internally stable jet may be generated that would break up only due to the flow structures in the surrounding gas. Furthermore, it is demonstrated that by combining the size information with the velocity measurement, the drag force on the individual drops can be estimated. If it is established that the drag force is primarily balanced by the electric force, then the power-law relationship between the charge on a drop and its diameter can be obtained. Using some preliminary data, it is shown that such an exercise can provide valuable insights into the atomization mechanisms.

14-Taylor 05.09.95, A. Ajdari

Generation of transverse fluid currents and forces by an electric field: Electro-osmosis on charge-modulated and undulated surfaces

Summary:
The consequence of charge nonuniformity on the generation of electro-osmotic flow and drag in a slab geometry is investigated in this paper. A modulation of the charge density on the wall induces convective patterns that can be taken advantage of to generate fluid currents and drag on the plates, provided one brakes the +/- symmetry, e.g., by modulating the shape of the plates. This could be of use in microfabricated geometry to design pumps or motors. It is shown that the electro-osmotic flow generated parallel and perpendicular to the undulation are of different amplitudes, so that transverse components can also be generated. However, this effect is only of second order in the amplitude of the undulation, whereas the component parallel to the applied field is of zero order which implicitly indicates that in situations where large amplitude undulations are possible, uniformly charged walls can be efficient generators of transverse effects. In finite size-systems it is legitimate to consider additional geometries, e.g., undulation and charge modulations along different axes, whereas these are ruled out on symmetry grounds for infinite systems. Finally, the present analysis seemingly does not take into account the polarization charges that will appear on the wall surfaces. In conclusion, the combination of charge and shape effects seems a promising way to generate a wide variety of electromechanical effects, where three-dimensional flows arise with the symmetries and characteristics imposed by surface-drawn patterns.

15-Taylor 28.09.95, J.M.Sun et al.

Shear flow of one-component polarizable fluid in a strong electric field

Summary:
Investigations of a polarizable fluid with electro-rheological (ER) methods have been carried out in this paper fluids have a critical shear-stress value when an electric field is applied. Below this value fluid's flow (in the x direction) is governed by a flowing-chain structure (FC), consisting of tilted or broken chains along the field (in the z direction). Above this critical value FC structure gives way to a flowing- hexagonal-layered (FHL) structure, consisting of several two-dimensional layers which are parallel to the x-z plane. Within one layer, particles form strings in the flow direction. Strings are constantly sliding over particles in strings right beneath. The effective viscosity drops dramatically at the structural change. Surprisingly, as the shear stress is decreased, the FHL structure persists if the thermal fluctuation is very weak, thereby introducing a large hysteresis effect.

16-Taylor 08.12.95, A. M. Ganan-Calvo

On the theory of electrohydrodynamically driven capillary jets

Summary:
In this work electrohydrodynamically driven jets in the parametrical window corresponding to steady Taylor's jets, namely jets issuing from needles of small diameter, or from equilibrium Taylor's cones (forming the so-called cone jet mode) is analysed .A quasi-one-dimensional EHD model retaining the temporal terms, for characteristic times larger than the electrical relaxation times $t_e \sim \varepsilon_o/K$, is presented. It is shown that the large axial length-to-diameter ratio of these jets did not allow the convective terms in the charge conservation equation to be neglected. Applying classical techniques, the axial propagation speed of disturbances along the jet's surface is obtained, showing (i) the supercritical nature of EHD-driven jets issuing from a Taylor's cone, (ii) the existence of a critical point at which the flow changed from a subcritical to a supercritical regime when the electrical self-induction of the jet is not precluded, and (iii) that the upstream wave speed, measured respect to the moving liquid (as usual) is slower than the downstream wave speed. The conspicuous longevity and stability of these jets is explained in terms of the existence of a supercritical and stable region of the jet that shields the fragile equilibrium meniscus giving rise to the jet from the strong perturbations produced at the jet's breakup point. An experimental study is also carried out, based on the analysis of a real electrohydrodynamically driven Taylor's jet shape, allowing the quantification of the EHD variables of the problem, the identification of the supercritical region of the jet, and the point of convective instability. The main EHD hypotheses of the present model are also checked and confirmed in this experiment, within the limits of the one-dimensional assumption.

17-Taylor 30.08.96, K. Zakaria

Nonlinear instability of a liquid jet in the presence of an uniform electric field

Summary:
The nonlinear instability of an irrotational jet stressed by an axial uniform electric field is analysed. The study takes into account the influence of the capillary force and the viscous stress on the free surface. The method of multiple scales leads to two partial differential equations which can be combined to receive two alternate nonlinear modified Schrödinger's equations. The stability conditions of the steady-state solution of one of the modified Schrödinger's equations are obtained using the modulation. The new transition curves between the stable and unstable regions are investigated. One of the transition curves is independent of the viscosity coefficient. The viscous stress can produce a break in the perturbed disturbance of the steady state. The break means that the

viscous stress reflects the progressive waves high energy if the stability equations is fulfilled. Furthermore it becomes obvious that the viscous stress gets more dominant the more away the critical states are.

18-EHDA 01.09.1996, R.P.A Hartman

Developement of electrohydrodynamic sprays related to space charge effects

Summary:
This paper concerns the effects that occur during jet break-up and the effects that occur in the first few centimetres of a spray produced by electrohydrodynamic atomization in the cone-jet mode. In detail it deals with the balance between electrical force and drag force, the size segregation mechanism, the acceleration of the surrounding gas, the effect of electrical interaction between charged droplets on the axial droplet velocity and the relation between droplet size and droplet charge. As a measuring system a light scattering- (droplet size) was linked to a Laser Doppler system (axial velocity), which enabled the authors to cut the lower detection limit to 3 μm when determining above mentioned physical properties of ethanol, acetone and etyhlene gylcol. It is stated that mutual electric interaction of charged droplets and differences in inertia are found to be the main reason for the size segregation effect. Moreover, an equation is found to describe the ratio of droplet size and droplet charge for ethylene gylcol. It is assumed that during the jet break-up mechanism when the time constant of the moving charge on the jet is considerably smaller than the time constant of jet break-up, smaller droplets have a slightly higher charge density than larger ones.

19-Taylor 01.01.97, D.A. Saville

ELECTROHYDRODYNAMICS: The Taylor-Melcher Leaky Dielectric Model

Summary:
This review deals with the foundations of the leaky dielectric model and experimental tests designed to probe its usefulness. It is chronologically structured and gives a good inside view of some milestones in the field of EHD: In the mid 1960s GI Taylor introduced the leaky dielectric model to explain the behaviour of droplets deformed by a steady field, and JR Melcher used it extensively to develop electrohydrodynamics. Although the early experimental studies supported the qualitative features of the model, quantitative agreement was poor. Even though the model was originally intended to deal with sharp interfaces, contemporary studies with suspensions also agree with the theory. The development of the leaky dielectric model formed an important step in the construction of a unified treatment of electrohydrodynamics. The model encompasses a wide range of phenomena in polar as well as apolar liquids. The leaky dielectric and electrokinetic models of electrohydrodynamics represent behaviour in two rather separate circumstances: the former when free charge is induced by the field, the latter when it is an intrinsic property of an interface. In either case, it is the interaction of charge with the applied field that produces dynamical effects. Both sorts of behaviour are encompassed by the same fundamental theory, with simplifications appropriate to the circumstances at hand. Insofar as the behaviour of poor conductors is concerned, Taylor's recognition of the pivotal role of charge transport and Melcher's incisive use of the model were truly significant steps. Their contributions to the development of the model justify referring to it as the Taylor-Melcher model. Although the Taylor-Melcher model involves approximations at several levels, it finds support in most of the experimental studies to date. Certainly its qualitative predictions are in full accord with the experimental data. However, there is much to be gained from further efforts to test the theory, to uncover new phenomena and establish boundaries on its applicability.

20-Taylor 01.01.97, J.S.Turner

G. I. Taylor in his later years

Summary:
This paper mainly is a tribute to G.I. Taylor who was rather unskilled socially, but a remarkable scientist. The last of the major new themes G. I. took up in the years after his retirement began with a more detailed study of the stability of a soap bubble in an electric field, a problem on which he had worked briefly in the 1920s. This led him to the general problem of jets of conducting liquid moving under the influence of an electric field in various geometries. He examined the jets drawn from the free surface of a conducting liquid at the open end of a vertical tube when a potential difference was applied between the liquid and a horizontal plate above the liquid, and showed that the free surface becomes conical as the potential difference is increased, and ultimately discharges a jet, with a steady surface shape and inflow into the jet. With Angus McEwan, G. I. Examined the stability of a plane interface between a conducting and a non-conducting fluid in the presence of a normal (vertical) electric field (Taylor & McEwan 1965). They showed theoretically that when the field strength exceeds a critical value, which is a function of the surface tension and the density difference, the interface is unstable to small disturbances. The theory predicts the length scale of this instability. Experiments using several pairs of fluids confirmed these predictions. For an air/water interface, fine jets of water are ejected toward the upper electrode (at field strengths smaller than those required to produce sparking due to electrical breakdown of an air layer of the same thickness between solid electrodes). His scientific spirit is maybe contained in G. I.'s last published "dialogue" with George Batchelor (1975). G. I. wrote, in part, ": : : I do not see how one can plan a 'strategy of research in fluid mechanics' otherwise than by thinking of particular problems."

21-EHDA 01.09.97, R.P.A. Hartman et al.

Electro Hydrodynamic Atomization in the cone-jet mode. A physical model of the liquid cone and jet.

Summary:
To encircle the electrohydrodynamic atomization in cone-jet mode with a complete physical model without any fitting parameters is the aim of this paper. Consisting of the jet radius as a function the liquid flow rate as well as of the conductivity, the model of the cone-shape seemed to show a different result compared to the scaling laws. One reason was that the model calculated the jet radius where the scaling law is fitted to the droplet size. The other reason is that this fitting is done, using a dimensionless number ($e_0Q/Kr3$). This dimensionless number seemed to be invalid. The cone-shape model gives the electric field strengths, the charge density and the cone and jet shape. This allows further investigations of electrical discharges of the surrounding air, of the jet breaking up into droplets, of the movement of droplets in the electric field after production and of the influence of electrode configurations.

22-Taylor 01.03.98, A. Beroual

Propagation and Structure of Streamers in liquid Dielectrics

Summary:
The streamer structure and its characteristics were examined in this article. There are several parameters known causing the structure of a streamer: the chemical composition of the liquid (pure or containing selective additives); the applied voltage (shape, magnitude, and polarity); the electrode arrangement (gap length and electrode radius of curvature); and the hydrostatic pressure. Between the electrode gap there are even more parameters, like the local electric field on the streamer tip, the average electric field in the gap, and the physico-chemical properties of the liquid. Streamer propagation phenomena in dielectric liquids are governed by both electronic and gaseous

mechanisms. The former dominates when the energy injected in the medium is very important and/or in presence of halogens or aromatic molecules in the liquid. This is supported by the following facts: (i) the strong influence of small concentrations of electronic scavenger or low ionization potential additives on the shape and velocity of streamers, the corresponding current and emitted light, and the spectroscopic analysis of the emitted light by streamers, which indicate the presence of electronic processes; (ii) the strong effect of the hydrostatic pressure on the initiation and propagation of streamers, and the corresponding currents and emitted light, which indicate that the physical nature of the streamers is gaseous, confirmed by chromatographic analysis of the dissolved gases due to discharges.

23-EHDA 30.04.98, D. J. Brunner

Electrohydrodynamic atomization in the cone jet mode: Physical modelling of the liquid cone and jet

Summary:
Electrohydrodynamic atomization in the cone}jet model can be modelled by means of a physical model without any fitting parameters. Such a model should consist of at least three parts. The presented model is the first part, and is able to calculate the shape of the liquid cone and jet, the electric fields in and outside the cone, and the surface charge density on the cone and jet. The model also estimates the liquid velocity at the liquid surface. From these results the current through the liquid cone can be calculated. The model allows further investigation of electrical discharges of the air surrounding the cone, it gives more insight in the phenomena itself, which makes it possible to come to better current scaling laws, and the influence of electrode configurations can be investigated much more easily. The second part of the physical model describing the cone}jet mode should describe the jet breaking up into droplets. The results of the presented first part of the model make it possible to do this, because the shape of the jet, the velocity of the jet and the surface charge on the jet can be calculated. The third part of the physical model describing the cone}jet mode should describe the movement of droplets in the electric field after production. The presented part of the model allows the calculation of the background electric field in which the highly charged droplets are moving.

24-EHDA 30.04.1998, R.P.A. Hartman et al.

Jet break-up in electrohydrodynamic atomization in the cone jet mode

Summary:
The jet break-up mechanism in the cone-jet mode was investigated, as function of the liquid flow rate. In this paper two models are presented for the simulation of the jet break-up in the cone-jet mode. The analytical model is the first physical model for the cone-jet mode, which calculates the droplet size for a droplet which has the volume of one main droplet plus the volume of the accompanying secondary and satellite droplets, calculates the total charge on these droplets, calculates the droplet velocity at jet break-up, and calculates the wavelength at break-up. A disadvantage of the analytical model is that it cannot distinguish between main and secondary droplets. This disadvantage is overcome by the second model. This numerical model still needs some improvement in order to use it for an accelerating jet. For all seven liquids, the same trend was observed. The jet break-up mechanism went through two jet breakup modes with increasing flow rate. In the varicose jet break-up mode three regimes can be distinguished. The first regime is the regime without secondary droplets and satellites produced. The small filament between two main droplets breaks at the first main droplet produced. The surface tension in the tip of the broken filament creates an area of high pressure. Due to this high pressure, possibly due to the influence of the surrounding air at high jet velocities, and possibly due to the acceleration caused by the electric field, the liquid in the filament starts to flow back into the other main droplet. The second regime

occurs when the filament also breaks near the second main droplet before the liquid can flow back into this droplet. Between every pair of main droplets one smaller secondary droplet is formed. The third regime occurs when the filament between two main droplets forms a secondary droplet. The liquid filament between the secondary droplet and one of the main droplets forms an even smaller satellite droplet.

25-EHDA 06.06.1998, A.M. Ganan-Calvo

The surface charge in electrosprying: Its nature and its universal scaling laws

Summary:
In this work, we present an experimental-numerical approach to the EHD atomization of liquids in steady cone-jet mode which allows the calculation of all electrohydrodynamic variables involved in the problem along the emitted charged jet. From the experimental results obtained, a universal scaling of all the variables and, in particular, of the surface charge is finally proposed. The collapse of the different dimensional values from a series of experimental measurements into well defined, universal functions validate the scaling proposed, for low and moderate electrolytes and liquid permittivity up to 31.2 times e_0. It is shown that the EHD atomization of liquids is actually an electrochemical quasi-equilibrium process in the sense that the liquid bulk is quasi-neutral and the free charges form a quasi-equilibrium charge layer at the liquid surface. The inner electric field in the liquid necessary to drive the bulk Ohmic current is some orders of magnitude smaller than the external one. Therefore, the EHD atomization of liquids is independent of the liquid permittivity within the parametric window explored in this work. It is shown that the ratio of the inner to the outer electric displacements, as well as the ratio of the tangential to the normal electric fields on the surface increase as the liquid flow rate decreases. The total emitted current *I* and the resulting average main droplet diameter *d* seem both to be independent on the liquid permittivity. The surface charge on the jet and on the emitted droplets is shown to have a universal value independent of the jet size and the liquid flow rate. It is only slightly dependent on the axial coordinate along the jet, and its maximum is located close to the cone's apex, with an approximate universal value given by a equation in the text. This value can be used to assess the possibility of gas discharge (local ionization) effects when electrospraying a given liquid, which will first appear close to the cone's apex. As a general result, it may be shown that this value is always above the one corresponding to the “charge evaporation" surface electric field threshold for very strong electrolytes and liquid metals.

26-EHDA 01.09.1998, D.M.A Camelot

Mechanisms of jet break-up for EHDA in the conejet mode

Summary:
It is of key interest in this paper to define among which circumstances which type of break-up mechanism takes place. For the purpose of clarity, an electrospray in the cone jet mode produces a bimodal size distribution composed of primary droplets (sometimes referred to as main droplets) and secondary droplets (sometimes referred to as satellites).Observation of the jet break-up reveals two regimes: the varicose break-up due to radial instabilities and the kink break-up due to both radial and azimuthal instabilities. The jet breakup passes from the first to the second regime due to an increase in flow rate (Q). Similarly, at a given flow rate an increase in conductivity (K) also provokes a change in the break-up regime from radial towards azimuthal instabilities. The liquid cone, the jet and the spray were observed using a high speed spray imaging system (Oxford Laser), which was connected to a long distance microscopic lens enabling pictures of 1 mm detail to be taken 5 cm away from the object. Ethanol, butanol, 2-butanone, isobutanol and ethylene glycol were electrosprayed with the conduct ivies, the flow rates and the voltages as variables. The measurements comprise the diameter of the jets, the diameter of the droplets, the wavelength of the

instabilities, the velocity of the droplets. Besides, the current of the sprays was also measured.

27-EHDA 12.11.1998, R.P.A. Hartman et al.

The evolution of electrohydrodynamic sprays produced in the cone-jet mode, a physical model
Summary:
The model presented in this paper predicts well the droplet size as function of the radial position, the concentration profile in the spray, and the dispersion of the main droplets. The measurements were performed close to the maximum flow rate for the varicose jet break up. However, it underestimated the radial dispersion of the secondary droplets and satellites in the spray. Neglecting the dispersion due to flow of the surrounding air is thought to be the main reason for this underestimation. The model confirmed that the mutual electric interaction of charged droplets, and differences in inertia are found to be the main reason for the size segregation effect. The droplet mass determines the change in droplet velocity due to this electric force, and the radial component of this force. The dark-zone, the low droplet concentration at the boundary between main droplets and secondary droplets, only occurs when a bimodal size distribution is produced.

28-Taylor 24.08.1999, V. G. Suvorov et al.

Dynamic Taylor cone formation on liquid metal surface: numerical modelling
Summary:
Maxwell stress, viscosity stress and the surface tension are made responsible for the formation of Taylor cones if the Maxwell stress exceeds mainly the surface tension and the viscosity of a liquid. As an initial application, the authors investigated the time evolution of molten mercury near the onset of instability based on assumptions by Belozerkowskii(1994), but changed in a way to catch the time behaviour of the physical values involved. Limiting factors for the dynamic Taylor cone are the initial liquid disturbance, the value of the applied voltage and the presence of space-charge (if charged particle emission occurs). A computer simulation showed that as the tip height increases, the radius of the apex curvature decreases due to normal EHD forces and can achieve very small values. The process of apex formation is accompanied with the intensive growth of the Maxwell stress term, which overtakes, greatly, the surface-tension term. Hence, as the surface evolves towards a more cone-like shape the resulting pressure on the surface tends to be very large and negative.

29-Taylor 09.05.2000, T. Sugimoto et al.

Negative corona discharge at a tip of water cone deformed under dc field
Summary:
The negative corona discharge phenomena occurring at a tip of water cone was investigated focusing on the motion and the shape of the water surface using a high-speed video camera. Main results are as follows: (1) The negative corona discharge from the water surface was observed during the period when the cone jet returned to an initial hemi-ellipsoidal shape. (2) The time variation of the magnitude and the interval of the Trichel-like pulse are caused by the corona from water surface with an increase in the radius curvature. (3) The increase in the magnitude of the Trichel-like pulses with the conductivity of water drop is due to the increase in the height of a water cone. The relationship between the conductivity of water and the shape of the water cone should be investigated.

30-Taylor 08.12.2000, Y. Higashiyama et al.

DC corona discharge from water droplets on a hydrophobic surface
Summary:

The corona discharge occurring in the water droplets placed on a hydrophobic insulating sheet under the DC field was investigated using SR (silicone rubber) and PTFE sheets. The droplets placed on the borders of SR sheets and the foil electrodes were elongated by the electric field and formed water filaments. During extension, corona discharge occurs at the sharp tip of a deformed water droplet at a distinct angle. Some amount of charge is emitted by electrical discharge or the disruption of a water droplet into small fractions. In general negative droplets tend to form a water channel, whereas positive droplets retain the round shape, permitting the extension of the negatively charged droplets due to the upkeep of the full capacity of the electric field(a positive droplet would decrease the electric field). The emission of fine water drops also affects the formation of water channel extended from the water droplets, thereby altering the direction of the electric field. Furthermore, the flashover voltage between two droplets on the SR sheet is also quite different; that is, the positive and negative flashover voltages are 10 and 12 kV, respectively. In contrast, the flashover voltage on the PTFE sheet is 16 kV, regardless of polarity. This might be due to the higher surface resistance of PTFE than SR.

32-Taylor 24.04.2002, J. Wei et al.

Naturally and externally pulsed electrospray

Summary:

In this paper electrospray ionization, and pulsed electrospray ionization (ESI) under an external electrical control are reviewed. The pulsations are natural phenomena in the ESI process. Numerous equations from other scientists are cited and hence an own picture of the electrospray-process is developed. A number of investigations have shown that two types of pulsation processes exist: low-frequency fluctuation and high-frequency droplet formation. Low-frequency pulsation results from an imbalance between the flow-rate of the input sample to the Taylor cone and the output-solution feed-rate to the liquid filament, whereas a high-frequency pulsation corresponds to the initial droplet-disturbance process, modulated by the low-frequency pulsation. The high- and low-frequency pulsation can both be produced electronically under an external control. However, readers may notice that the pulsed ESI has not yet been synchronized purposely with the natural pulsation process in ESI at the present time. This synchronization may be very important to achieve an ideal ESI performance. For example, a low-frequency pulsation greater than 10 Hz can be controlled in the pulsed ESI mode to record a peak profile eluted from a HPLC or a CE column; and a high-frequency pulsation of app. 1 kHz might be utilized in a synchronized mode to control a TOFMS detection for a signal average.

99-Taylor 07.07.2002, T. Aka-Ngnui et al.

A Predicting Model for Branching Streamers Propagating in Liquid Dielectrics using a Computation Electrical Network

Summary:

Main topic of this article is to find out how an electrical discharge (streamer) could be characterized within an insulating liquid under an divergent electric field using computation electrical network. This model enables to predict the different characteristics of the streamer (30kV) such as its pattern and its propagation velocity, the associated electrical charge and the local electric field. It is stated that the smaller the electrode gap and/or the higher the voltage, the higher the electrical charge, the instantaneous velocity and the electrical
field are. The pattern of a streamer is shown after the first few micro-seconds and the velocity of propagation is calculated.

33-EHDA 20.02.2004, M. Seipenbusch et al.

Catalytic soot oxidation in microscale experiments

Summary:
Different strategies of the formation of catalyst and carbon particles are presented in this article. For Pt/SiO2-catalysed oxidation of soot in air and air/NO, a strong dependency of the reactions rates on the Pt surface area is observed. For air/NO, the reaction rate is linearly proportional to the Pt-surface area. For carbon oxidation in air, two effects of the Pt seem to exist. However, the method of particle production, laser ablation with subsequent sintering or EHDA, did not seem to have an effect on the activity of the catalyst. This method has potential for optimizing catalyst dispersion and also catalyst particle properties with respect to the catalytic activity.

34-Taylor 19.08.2004, H.Kawamoto et al.

Electrohydrodynamic deformation of water surface in a metal pin to water plate corona discharge system

Summary:
To study the kinetics of a pin-to-plate discharge system that consists of a rigid pin electrode made of metal and an ion-conductive liquid electrode is the main objective in this article. The authors suggest that throughout an electrohydrodynamic experiment based on an expectation that the liquid level may be deformed by the Coulomb force and the ionic wind that kinetics between pressure and deformation could be revealed. A simple experiment device was built to gather following conclusions: (1)At voltages lower than the corona onset water lifted up in the order of several tens of micrometres at the centre. (2)Over a threshold voltage corona discharge took place and a relatively large repulsive force, in the order of 100μN, was induced due to ionic wind. It depressed the water surface and a large depression of water, in the order of several hundreds of micrometres at the centre. (3) Ionic wind flows almost parallel to the pin electrode even when the pin electrode leans to the plate electrode.(4) If the tip of the pin electrode is not round, ionic wind was injected from the edge.

35-EHDA 2.11.2004, J. van Erven et al.

Platinum Nanoparticle Production by EHDA

Summary:
It has been shown in this paper that platinum nanoparticles can be produced by EHDA using two methods. The first method uses the capillary-plate set up to deposit precursor particles on a plate and subsequent decomposition will form platinum particles. The second method uses the aerosol reactor set up which keeps the produced precursor particle aerosolized after discharging the droplets. These particles are ducted through a furnace where they are recomposed forming platinum particles. In both cases nanoplatinum particles are formed of about 10 nanometer. As a final remark we would like to state that EHDA offers a unique possibility to produce mono-sized nanoparticles on a small scale.

36-Taylor 23.02.2005, M. Gunji et al.

Self-propulsion of a water droplet in an electric field

Summary:
The phenomenon of electrostatic droplet transportation, in which a water droplet runs along a simple parallel-strip electrode when energized by DC or low frequency AC voltage, has been discovered and studied for the first time. The self-propelling mechanism is caused by the imbalance in Maxwell stress between its advancing and trailing side, which is due to the shielding effect by the conductance of the moisture layer left behind in the particle. The existence of such a moisture layer

is experimentally verified by a real-time measurement of the surface conductance.

37-Taylor 18.03.2005, S.Castro et al.

Water-based compound Taylor cone held in vacuum: Feasibility and application to colloidal Propulsion

Summary:

Based on the electrospray effect the authors develop a picture of water as a feasible propellant in applications related to propulsion and state that this technique could be used to provide a thrust in the range of hundreds of nano Newtons. They suggest a use in vacuum (e.g. :space missions) in which water immediately freezes but adding a oil coating a highly reproducible, stable jet (current) develops. Difficulties of this technique are represented mostly by the low volatility of water.

38-Taylor 01.04.2005, Z. Guan et al.

Electric Field Analysis of Water Drop Corona

Summary:

In this paper,based on a model with two parallel electrodes water drop corona is studied. The relationship between initial corona voltage and different sets of water drops is obtained from experiments. Then several factors, which may affect the electric field analysis of water drop corona, are studied by numerical calculation on computer. As their results the authors state that: Electric field (EF) will be enhanced by water drops. The EF could be 3 times of E_0 for a single water drop with contact angle of 90° . When the contact angle is small (20°), the EF could be 4 times of E_0 .E_{max}/E_0 increases as the length of the water along the EF increases. EF enhances the most when several water drops are in the direction of the EF. Also EF increases when the number of the water drops increases or the distance between the water drops decreases.

39-Taylor 9.8.2005, L. Sirghi et al.

Volume of a Nanoscale Water Bridge

Summary:

Water bridges formed through capillary condensation is the main topic of this article. When nanoscopic contacts are ruptured, the capillary water bridges formed at the contacts stretch until a certain contact separation distance (water bridge breakup distance), when they breakup. Experimental force-distance curves obtained by AFM pull-off experiments with sharp and blunt hydrophilic tips on hydrophilic samples showed that the water bridge breakup distance is generally much larger than twice of the Kelvin radius. This indicates that, during the contact rupture, the water bridges stretch with an important decrease of meniscus curvature. Because of the decrease in curvature, the stretched water meniscus is not in thermodynamic equilibrium with the water vapour phase, which may cause water evaporation.. Based on these experimental observations, a theoretical model that predicts the shape and force of the elongated meniscus of the stretched water bridge is proposed. The model considered a constant water volume, a receding movement of the water meniscus contact lines at the tip and sample surfaces, constant receding water contact angle values for the two solid bodies, and an increase of the water meniscus curvature radius.. During stretching, the water meniscus force decreases monotonically to zero, because of a decrease in the meniscus Laplace pressure as well as in the area of the meniscus interface with the solid bodies. The theoretically predicted force-distance curves matched very well the experimental force distance curves obtained by AFM pull-off force measurements. The results of the proposed theoretical model showed that the volume of the water menisci is roughly equal to the cubic power of the meniscus breakup distance, and this relationship does not depend much on the tip curvature radius. However, small water bridges are likely to form at sharp tip-sample contacts, whereas big water bridges are

likely to form at blunt tip-sample contacts.

40-Taylor 18.08.2005, N. Dubash

Behaviour of a conducting drop in a highly viscous fluid subject to an electric field

Summary:
The slow deformation of a relatively inviscid conducting drop surrounded by a viscous insulating fluid subject to a uniform electric field is examined in this paper. The electric field stretches the drop in the direction of the field. As the drop elongates, surface tension becomes less important except at the drop ends, with the primary balance between viscous and electric stresses. Some numerical results based on a boundary integral formulation are presented. For weak electric fields the known equilibrium drop shapes are recovered, while for the electric field strength(β) exceeding some critical value, the time evolution of the drops is obtained. For electric fields above the critical strength, two charged lobes formed and break off from the ends of the drop. The droplets formed are highly charged and are themselves unstable. As the electric field strength increased, the volume of the lobes decreased and eventually the lobe formation disappeared – the drop breakup then consisted of a highly charged jet-like structure being ejected from the end of the drop. Moreover, an equation is derived, which models the deformation of a slender drop. The model has a similarity solution (albeit unstable) where the shape of the drop is always spheroidal, and where the drop length scales according to equation 4.35 (see in the text). As well, the general solution for the slender-body equations are obtained. Unfortunately, the slender-body model did not appear to capture properly the dynamics of breakup. Naturally, the slender-body analysis applied best to drops which extend indefinitely. The deformation of the drop was a slow process, i.e. that the Reynolds number of the flow is small. The velocities were highest during the later stages of the deformation, near breakup. If, for example, one take the pedestal insulator problem, where we have a drop of rainwater in bitumen, then Reynolds number (Re)~10^{-5} near break up, (density ρ ~10^3 kgm−3, velocity U ~10−4 ms−1, length ~10−1 m, viscosity ~103 Pa s, and β ~O). However, if we have a water drop in oil (viscosity~1Pa s, velocity ~10−1 ms−1), then *Re~10* near break up.

41-Taylor 27.10.05, G. S. Sarkisov et al.

Observation of electric field enhancement in a water streamer using Kerr effect

Summary:
It is reported in this article of the Kerr effect (using a 2-channel polarimeter, maximum voltage 600kV/cm^{-1}) in a streamer head in experiments with electrical breakdown of water. After the voltage collapse and start of the current in the gap the Kerr effect disappears because there is no more significant induced linear anisotropy in the water. The magnetic field from the current channel induces a circular anisotropy in the water which results in a rotation of the polarization plane of the probing beam. Estimations show that at a moment when the streamer head has closed 75% of the gap space, the electric field is 1.7–2.2 MV/cm, which is approximately six times higher than the maximum inter-electrode electric field. 2D electrostatic simulations support this enhancement factor. For well defined electrode geometries, it is possible to reconstruct the spatial distribution of the electric field by using the Kerr effect.

42-EHDA 13.05.2006, M. E. Kuil et al.

Nano-dispensing by electrospray for biotechnology

Summary:
Liquid transport of minute amounts of biomaterials is of paramount importance in many biotechnological applications. One of the challenges is the transport of viscous liquids without heating. Electrohydrodynamic atomization or electrospray is a viable method for the controlled

transport of nanoliter volume of viscous liquids presented in this paper. Using a sufficiently fast high switching voltage, much smaller liquid depositions could be produced at a higher production rate, which will enable EHDA to be used for other applications as a sub-nanoliter dispensing method.

43-Taylor 01.10.2006, J. Qian et al.

Model Analysis of Self- and Laser-Triggered Electrical Breakdown of Liquid Water for Pulsed-Power Applications

Summary:

In this article an analysis of the pre-breakdown physics in liquid water in response to a short 200-ns electrical pulse is presented. A two-dimensional time-dependent model based on the generalized flux-FCT method was used for the numerical calculations as well as a laser-induced breakdown was studied. These include the experimental observations of pre-breakdown, current fluctuations, streamer propagation, disparities between the anode and the cathode polarities in hold-off voltage and breakdown initiation times, and stronger dendritic structures for cathode-directed streamers. It is assumed that their model predictions hold for every liquid always following the empirical theory of J.C.Martin. Interestingly, the simulations showed that electric fields necessary for generating a breakdown streamer were lower for an anode-side-triggering event. Moreover, laser induced breakdown showed the development of string of point plasmas which eventually expand and form a continuous steamer due to localized turn on at microbubble sites.

44-Taylor 01.01.2007, J. F. de la Mora

The Fluid Dynamics of Taylor Cones

Summary:

In this review, first the idealization of static pointed liquid tips is considered, which does not hold rigorously, but whose simplicity has enabled considerable progress in the field. The formation of cone-jets in charged liquids with electrical conductivities larger than 10^{-4} S/m is reviewed for steady supported menisci and transient Coulomb fissions in charged drops. Taylor's hydrostatic model forms the basis for subsequent developments. The jet structure is critically dependent on the model used for charge transport, which has been based mostly on a constant conductivity assumption. Saville's (1997) more general model predicts the formation of rarefaction fronts with wide space charge–dominated regions near the liquid surface, which apparently do arise in polar liquids near the minimum flow rate. The effect of the finite conductivity of the liquid is considered, the main factor fixing the width of the jet. It has been modelled mostly via a constant conductivity (ohmic model), although a more general model (Saville 1997) is also discussed. Taylor cone-jets at high electrical conductivity, either supported on stationary menisci or drops are examined. Finally, the extreme limit when the electrical conductivity reaches values of 1 S/m is considered, at which the resulting jet diameters of about 10 nm give rise to electric fields in the range of 1 V/nm and evaporation of ions.

45-Taylor 01.05.2007, N. Kasayapanand

Numerical modeling of natural convection in partially open square cavities under electric field

Summary:

Numerical modelling of the electric field effect on natural convection in the partially open square cavities is investigated in this article. The interactions between electric, flow, and temperature fields are analysed by using a computational fluid dynamics technique. Flow pattern of a fluid is affected by the supplied voltage at the wire electrodes. The thermal boundary layer along the surface is perturbed by the electric field and decreased at the high supplied voltage. The EHD enhancements of flow and heat transfer increase in relation with the supplied voltage but decrease with the

Rayleigh number. The volume flow rate and heat transfer coefficient inside the partially open square cavity are significantly improved by EHD, especially at the low aperture size and high aperture position due to the disadvantage from non-EHD phenomenon. Moreover, the volume flow rate enhancement reaches to a maximum at an intermediate number of electrodes and reduces furthermore when the number of electrodes is rather high due to the pressure drop effect. Surprisingly, a minimum heat transfer enhancement occurs at an intermediate number of electrodes. For the high inclined angle, which generally performs the lowest volume flow rate and heat transfer coefficient in non-EHD are substantially renovated by EHD.

46-Taylor 15.05.2007, P. Bruggeman et al.

Water surface deformation in strong electrical fields and its influence on electrical breakdown in a metal

Summary:
Electrical breakdown in a metal–water electrode system with DC applied voltages is studied for small inter-electrode spacing distances (2–12 mm). Calculations of the water deformation before electrical breakdown are undertaken are in good accordance to the experiments. Empirically it was discovered that the character of the discharge changes when the electrode-electrode distance exceeded 7mm. For distances smaller than 7mm the calculated stability limit of the water surface corresponds with the experimentally obtained breakdown voltage. High speed images (CCD)of the breakdown and calculations of the electrical field in the air gap before breakdown show that the water surface instability is necessary to trigger the electrical breakdown for small inter-electrode spacings forming a Taylor cone like-shape. In the case of 8mm the conductive channel is formed at breakdown between the pin electrode and the water surface at its static position prior to breakdown. The CCD images for the latter case, especially when the metal pin electrode is the cathode show different breakdown structures compared with the case where the breakdown is triggered by the water surface instability. In the case of negative polarity of the pin electrode a glow to spark transition is observed.

47-Taylor 09.07.2007, X. P. Lu

One-dimensional bubble model of pulsed discharge in water

Summary:
In this paper, a one-dimensional bubble model of pulsed discharge in water is presented. With a total input energy of 0.63 J, the simulation results show that when the bubble collapses at the centre of the bubble, the plasma pressure oscillates strongly. It oscillates between 800 and 1150 atm with an oscillation frequency of about 6.9 MHz, while at r=R/2 (R: bubble radius), the gas velocity oscillates intensely at the same frequency. It oscillates between −235 and 229 m/s when the bubble radius reaches its minimum. But it does not oscillate at r=R because of the inertia of the surrounding water. Since the plasma gas oscillates with the frequency of the megahertz range due to the mass difference between positive ions and electrons, charge separation probably happens inside the bubble. Therefore, it may also emit UV or even x ray as observed in sonoluminescence bubble. So, it may be able to measure the UV or x-ray emission at the time when the bubble radius reaches its minimum.

48-Taylor 09.08.2007, J. Eggers et al.

Physics of liquid jets

Summary:
Jets, i.e. collimated streams of matter, occur from the microscale up to the large-scale structure of the universe. The focus in this paper will be mostly on surface tension effects, which result from the cohesive properties of liquids. Paradoxically, cohesive forces promote the breakup of jets, widely

encountered in nature, technology and basic science, for example in nuclear fission, DNA sampling, medical diagnostics, sprays, agricultural irrigation and jet engine technology. Liquid jets thus serve as a paradigm for free-surface motion, hydrodynamic instability and singularity formation leading to drop breakup. In addition to their practical usefulness, jets are an ideal probe for liquid properties, such as surface tension, viscosity or non-Newtonian rheology. They also arise from the last but one topology change of liquid masses bursting into sprays. Jet dynamics are sensitive to the turbulent or thermal excitation of the fluid, as well as to the surrounding gas or fluid medium. The aim of this review is to provide a detailed unified description of the fundamental and the technological aspects of these subjects.

2.1.2 EHD:

The aspects in this section are numerous and the full understanding often depends on intense studying of the single articles and its references. At first, the *historic articles* are dealt with. which gives the reader a starting point of how and why a research field has developed.

Three general categories developed from these historic articles, all depending on the quantum-electrohydrodynamic properties of water. One topic, well explored, is the *Kerr-effect* in water [42, 56, 57, 58, 59, 62, 67, 68, 76, 83]. Additional research was done on the *quantum Hall effect* in water [71, 90] , the *Faraday effect* in water[113] and the P*ockels effect* in water [131], together with the development of different experimental techniques to measure and visualize these effects.

The next category of publications is connected to *chemical reactions* [33, 64.66, 77, 80, 84, 107, 131, 134] of water with foreign atoms or molecules, mainly related to the investigation of electric fields. Examples are *electrolytes*[95, 138], low-molecular gases, *bacteria* [105, 121, 140]or polymers[96,101] embedded in the amorphous structure of water at the interface or in bulk regions and the inherent predominant product formation.

The last category deals with general *stuctural analysis* of water *[72, 91,92,107, 116,135]*, experimentally (spectrometric, interferometric[83], atomic force microscopy[118]) as well as with *molecular dynamic simulations[70, 74, 109, 127]*. Also included are all kinds of *theoretical quantum analysis[132]*, theses and predicted as well as verified models associated with *autodissociation*[136, 142, 143], *quantum entanglements*[81,103,105] and *nano applications*[35,39] of water.

49-historic 01.02.1914, J. Zeleny

The electrical discharge from liquid points, and a hydrostatic method of measuring the electric intensity at their surfaces

Summary:

In this article the main topic concerns water in an electric field and the effects it has on the surface tension, discharge , temperature. In a very empirical way the author suggests to undertake experiments concerning hydrostatic pressure, increase of surface tension, discharge characteristics and even the effects of beta and gamma rays on the starting potential of high voltage aqueous applications. This work represents a important corner stone in the field of water structure research, gaining “first contact points” to a difficult research field in a simple approach.

50-historic 01.02.1914, J. Kendall

In conclusion it may be said that adiabatic calorimeters eliminate cooling corrections, thereby excluding errors from precision work and saving time in commerical work. They permit a slow and careful reading of a thermometer while the temperature is constant, and the taking of temperature before and after a determination becomes unnecessary. Errors from evaporation are negligible in the Richards type of calorimeter or in the modification described in this article, as there is no colder matter in contact with the vapor; and heat can not be lost or gained from the room by conduction. For high temperatures, for slow reactions, or for large temperature differences, these calorimeters are absolutelynecessary. The description of an adiabatic calorimeter of new design is given and it has proved to be accurate and simple of operation. The automatic control of this calorimeter by

means of a selenium cell has been successful, and this very sensitive relay may find application in other work.The calorimeter herein described is being used in this laboratory inthe accurate determination of the specific heats of salt solutions and of organic liquids.

51-historic 08.02.1932, H. D. Carter et al.

ELECTRIC DISCHARGES IN LIQUIDS. PART I THE ARC DISCHARGE IN WATER.

Summary:
In this article the chemical nature of the gaseous, liquid, and solid products is examined. With regard to gaseous products, the results of previous workers are qualitatively but not quantitatively confirmed, and considerable attention is given to a gaseous inactive residue. The solid products are shown to be hydroxidic in character ; the solid product from carbon arcs is shown to be a body of the nature of graphitic acid ; in the latter case, traces of a sparingly soluble, high-melting acid are simultaneously produced. The mean temperatures of the under-water arcs are investigated by means of an optical pyrometer, and their variation with temperature of the surrounding water. The variation of total gaseous yield with temperature and pressure is investigated. The mechanism of the process is discussed in the light of the results communicated, and the following probabilities are arrived at : (I) The process is not a mere thermal reaction ; (2) A certain proportion of the reaction is no doubt due to the fairly considerable dissociation of water vapour at the high temperatures in question, but (3) it is shown that very probably an electrical dissociation of water vapour into H and OH ions is responsible for at least the solid products; (4) Short wave radiation effects are not excluded.

52-historic 1.4.67, A. von Hippel

The dielectric relaxation spectra of water,ice and aqueous solutions and their interpretation

Summary:
This article deals with the interpretation of static and infrared permittivity and the linked water structure. The authors present a lot of theories from different scientists and try to define the terms relaxation time, dipole orientation and electric field on a molecular level. It’s interesting, but no remarkable progress is made.

53-historic 01.04.1967

The dielectric relaxation spectra of water,ice and aqueous solutions and their interpretation, 2

Summary:
In this article an electric field is used to determine polarization spike signals in the time domain as an indicator of thermal phonon excitation and the subsequent reorganisation of dipoles. The infrared spectrum and the relaxation spectrum of water indicates that at higher temperature dipole jumps are in favour due to a decrease in average bond angle and a breakdown of the tetrahedral molecule structure. Measurements showed that infrared excitation and microwave relaxation in the frequency domain are coupled inversely. The assumptions for that changes are numerous: the classical dragging around of dipoles, quantum processes from dipole jumps in the infrared or the ion and electron transfer at even higher frequencies are reasonable.

54-historic 01.04.1967

The dielectric relaxation spectra of water,ice and aqueous solutions and their interpretation, 3

Summary:
We encounter here a theory of proton migration in ice-I which is based on a intermolecular and intramolecular shift in and between water molecules. In contradiction to the double-well model for polarization and conduction in ice (Gränicher) a new model is developed by using infrared and dielectric relaxation spectra of water. A reasonable mechanism is suggested and backed up with

calculations of activation energies for ion pair formation, , dipole strengths and hydrogen-bond cleavage. Moreover, the author points out that the general Debye rule to determine the dipole moment of molecules is only valid for a few phase states of water.

56-historic 01.06.1974, E. C. Cassidy et al.

Kerr-Effect Studies of an Insulating Liquid Under Varied High-Voltage Conditions

Summary:
In this article refined Kerr electro-optical fringe-pattern methods were used to study time and space variations in the electric field between the electrodes of parallel-plate capacitors filled with liquid nitrobenzene. Photographs of fringe-pattern data recorded during application of high direct (both positive and negative) and sinusoidal voltages, ranging in frequency from 40 to 200 Hz, were compiled to enable computation of space-charge distortions of the field in bulk of the liquid during the stress of high-field (up to 85-kV/cm) operation. They used two probing cells and came to following conclusions: In a cell with electro-polished stainless-steel electrodes, the interelectrode-field distribution was approximately linear and the net space-charge density was positive during operation under high dc and low-frequency voltages. Observations with a cell having glass-blasted nickel electrodes showed different results. The interelectrode field distribution was linear under direct voltage, but parabolic under alternating voltages. Their DC fields were both linear functions of position between the electrodes, and both showed space-charge enhancement of the field behind the negative electrode. Finally, these observations still offer no conclusive results for reliable prediction of steady-state field and charge behaviour (like the onset of breakdown).

57-historic 30.06.1975, M.J. Aroney et al.

The Kerr Constant of Water and other Pure Liquids at 633 nm

Summary:
In this article the the accurate determination of the Kerr constant of pure water for d = 633 nm is carried out. Kerr effect measurements were made also on the solvents benzene, p-xylene, toluene, carbon disulphide, chloroform and chlorobenzene at the same wavelength and temperature (20°C). Parallel, but independent determinations of the Kerr constants were carried out using static as well as pulsed techniques for all the liquids studied except water which, because of conduction, could not be examined by this method.

58-historic 17.05.1977, R. K. Khanna et al.

An apparatus for Kerr effect measurements in water and conduction liquids

Summary:
In this article the experimental procedure, the needed analytical tools and some illustrative results are presented for carrying out Kerr-effect constant measurements. The suggested apparatus is applicable for water and other highly conducting media and works with 2 μs pulses of high voltage (8MV/m).

59-historic 03.07.1978, M. S. Beevers et al.

Measurement of Kerr Constants of Conducting Liquids

Summary:
An apparatus is described in this article to measure the Kerr constant of conducting as well as non conducting liquids and solutions. High-voltage pulses of short duration (1.5 ps) were applied across the Kerr cell and the resultant birefringence was measured by a signal-nulling technique. Expressions for the null conditions were derived for an optically active birefringent medium. Results were presented at 633 nm and 293 K for water, methanol, ethanol, propan-1-ol and propan-

2-ol. It has thus been shown that the pulsed method with signal-nulling offers a simple and rapid means of measuring the Kerr constants of conducting aqueous solutions. Problems associated with conductivity were overcome. By using a signal-nulling technique, the problems associated with light fluctuation, slight misalignment of the Kerr cell and long-term drifts in the gain of the detection system were overcome. The Kerr constant of optically active molecules could also be measured by this method.

60-historic 01.08.1978, A. H. Sharbaugh et al.

Progress in the field of electric breakdown in dielectric liquids

Summary:
In this paper, some of the difficulties which are encountered in the measurement and interpretation of breakdown phenomena in the liquid state shall first be examined. The research specifically concerned with "purified" organic liquids is considered. Comparisons and generalizations with breakdown in gases and solids are made, wherever possible. The concept of the "intrinsic strength" of a liquid is discussed, as well as the development of the very important experimental techniques which have been used in conduction and breakdown studies. Broadly speaking, workers in the field have been divided into two principal schools of thought. There are those who favour an electron multiplication theory of breakdown, analogous to the Townsend theory of breakdown in gases. According to this theory, breakdown will occur when an electron, on the average, makes a suitable number of ionizing collisions in its transit across the breakdown gap. On the other hand, there are those who doubt the existence of collision ionization in liquids and favour the so-called "bubble mechanism" of breakdown. In one example of this theory it is proposed that a bubble of gas is formed by vaporization of liquid by local heating in the strong-field region at the tips of asperities on the cathode. A bubble, so formed, will grow and breakdown will take place in the low strength vapour within the bubble. This rapidly leads to rupture of the bulk liquid. At the end of the article arguments for and against both theories of breakdown are summed up.

61-kerr 22.06.1982, M. Zahn et al.

Charge injection and transport in high voltage water/glycol capacitors

Summary:
A model is developed by the authors which explains the circuit voltage decay curves in water/glycol capacitors. Moreover, it is stated that water gets electrically birefringent when stressed by high voltage and this birefringency is proportional to the square of the electric field magnitude. As the voltage polarity is reversed, the fringe pattern of kerr-electro-optic measurements also reverses so that the moving fringe propagates from the now positive lower electrode towards the upper negative electrode. A secondary complication at later times was the loss of sensitivity because the voltage is dropping fast. Presumably, the charge injection parameter Â depends on the state of the electrode surface, hence the decay should be sensitive to changes in surface preparation of the electrodes and gave the possibility to prove the anode as the primary injecting surface.

62-kerr 11.10.1982, M.Zahn et al.

Kerr- electro optic field mapping measurements in water using parallel cylindrical electrodes

Summary:
Main topics of this article are space-charge effects of the electric field and the Kerr-effect refringe patterns which were examined in distilled water. Pulsed high voltages across parallel cylindrical electrodes with a 1 cm gap were applied on millisecond time scales to reveal that at early times (<500µs) the measured results agree with the space-charge-free electric field distribution, while for times greater than 500µs there is significant space-charge distortion due to positive charge injection.

63-kerr 10.01.1983, M. Zahn et al.

High voltage electric field and space-charge distributions in highly purified water

Summary:
A research is carried out in this article which contributes to the features known of hydronium ions and the migration of charge between electrodes. The measurements included calculation of the Kerr- effect constants, the background charge densities, the space charge effects and hydrodynamic effects. A unipolar drift dominated conduction model is proposed and qualitatively agrees with the Kerr-effect measurements. The problem of too much space charge measured in a distinct charge migration time in comparison to the dielectric relaxation time at low voltage rises, but at high voltages a good agreement is reached if the low resistivity is increased by a factor of five. Further research on the subject of electrohydrodynamic mobility could solve these anomalies.

64-kerr 01.04.85, M. Zahn et al.

Electro-optic charge injection and transport measurements in highly purified water and water/ethylene glycol mixtures

Summary:
Extensive Kerr electro-optic field mapping and voltage/current measurements have been taken out in this article with highly purified water over the temperature range of T=0° to 300C° using parallel plane electrodes with average field strengths up to 160 kV/cm. The Kerr constant of water B was measured to be at about B , 3.4 to 3.6^{-14} m/V^2 for free-space light wavelength 590 nm and varies only slightly with temperature over the measurement range. Photomultiplier tube measurements at 633 nm at 100C° found water to have a Kerr constant B of 2.7 to $2.9*l0^{-14}$ m/V^2 while ethylene glycol had a negative Kerr constant B of $(0.8 \text{ to } 0.9)^{-14}$ m/V^2. Water/ethylene glycol mixtures had an essentially linear variation of Kerr constant between these limits as a function of weight fractions, having a zero Kerr constant at about 79% glycol/21% water by weight. It appeared best to the authors to inhibit unipolar charge injection that increases the electric field at the opposite electrode/ dielectric interface leading to electrical breakdown and to encourage bipolar homocharge injection at the electrodes where injected charge shields the electrodes, causing a lower field at the dielectric/ electrode interfaces. Even though this causes the electric field to be larger in the dielectric volume, the intrinsic strength of the dielectric is larger than at interfaces. The net effect is to allow higher voltage and higher energy operation without breakdown.

65-structure 03.11.1986, G. Colacicco

Electrical potential of the water surface

Summary:
Measurements of a clean water surface to determine its electrical potential were arranged with a radioactive air electrode and a calomel electrode in solution. Thermodynamically important operating figures were calculated from the results of these measurements, which brought out an interesting thesis: ionic dipoles of the water align themselves in the surface area at extremely high densities, OH^- is concentrated on the interface liquid-gas, whereas H_3O^+ is beneath the negatively charged molecules but also in the very thin(10-100 Angstroms) double layer of the surface. It is suggested that hydration energy of H^+ is so big that the lattice stabilizes the dissociation. The other possible mentioned reason being that magnetic fields, which are produced by the proton circuits during resonance, stabilize the enormous charge separation on the surface area.

66-reaction 01.03.1987, J. S. Clements et al.

Preliminary Investigation of Prebreakdown Phenomena and Chemical Reactions Using a Pulsed High-Voltage Discharge in Water

Summary:
Prebreakdown phenomena (O_3 formation, streamer lengths, interpretation of emission spectra, colorimetric/spectrometrically analysis of chemical reactions in the aqueous solution) in water with and without gas bubbling were investigated in this article for point-plane geometries using high-voltage pulses. In deionized water an intense white-spot discharge and numerous isolated microdischarges were observed, but only a small number of streamers were produced. In more conductive water, the white spot was weaker and very few microdischarges were observed. The microbubble production rate was much larger for the positive polarity voltage than for the negative polarity. Streamer length increased with increasing voltage or pulse width, and was much longer for positive polarity than for negative polarity. The streamer spectrum contained the hydrogen Balmer lines, which indicates that gaseous atomic hydrogen was present in the streamers. The spectrum of the whitespot discharge contained atomic iron lines and molecular emission bands, which suggests that excited (chemically active) species were present. The O_3 concentration of the water was very dependent on the voltage, treatment time, and O_2 flow rate. When N_2 or N_2-O_2 mixtures were bubbled through the discharge, a chemical was produced which caused a slow decolourization of the indigo dye used in the colorimetric O_3 test. Operating the discharge with O_2 bubbling in anthraquinone dye resulted in a decolourization of the dye, but with N_2 bubbling the discharge produced no decolourization.

67-kerr 10.01.1994, S. Palese et al.

Femtosecond Optical Kerr Effect Studies of Water

Summary:
In the current study an optical Kerr effect measuring was undertaken to analyse the dynamic properties of water which have been probed with two different laser sources, providing pulse widths in the range 38-45 fs. These studies (optical heterodyne detection) attained sufficient signal to noise ratios (S/N) and time resolution to observe the librational modes near 700 cm^{-1} down to the diffusive translational and rotational motions around 5 cm^{-1} The present experiments have determined the upper intensity threshold for following the nuclear contributions before higher order nonlinear electronic effects dominate the matter-field interaction.. From the out-of- phase heterodyne-detected signal, there are two prominent features centred at 40 and 165 cm^{-1}, which are currently assigned as the overdamped shear and underdamped longitudinal translational modes, respectively. Correlating the OKE components to the dynamic Stokes shift measurements, the different types of motions and their relative importance in the relaxation process can be identified to give a microscopic picture of solvent relaxation. At present, water relaxation appears to be determined largely by the nondiffusive, hindered translational and orientational motions and diffusive relaxations. The degree of relaxation energy attributable to the librational or inertial components to the water response is an important parameter that still needs to be quantified. The various librational and hindered translational modes are all strongly coupled. For example, the displacement of a translation mode for a particular solvent configuration affects the centre frequency of the librational modes of the same configuration and also the lifetimes of these modes. It is the anharmonic coupling between these motions which leads to the irreversible change in solvent configuration and, hence, repolarization. This information is contained in the effective homogeneous lifetime of the broad distribution of different modes within the water structure. Water has the smallest moment of inertia for small molecule polar fluids and as such demonstrates the fastest solvent relaxation dynamics known.

68-kerr 01.04.94, M. Zahn

Transform Relationship between Kerr-effect Optical Phase Shift and Nonuniform Electric Field Distributions

Summary:
The main topic of this article is the measurement of electric field distributions influenced by the Kerr effect. This effect is responsible for a phase shift between light components polarized parallel and perpendicular to the electric field which in turn is used to determine the electric field distribution. The integral methods developed here using Abel transformations are restricted to cases when the electric field magnitude is axisymmetric and direction is constant along the path length and for Radon transformations with non-axisymmetric electric fields, the electric field must be perpendicular to the plane of light propagation. Often, these restrictions require the light path to be directed along an equipotential planar surface, or along suitable line of symmetry. Its hoped by the author that future extensions of the work can relax these very restrictive conditions, so that the magnitude and direction of the electric field can be determined everywhere in arbitrary geometries.

69-reaction 01.04.94, A.A.Joshi et al.

Formation of Hydroxyl radicals, hydrogen peroxide and aqueous electrons by pulsed streamer corona discharge in aqueous solution

Summary:
A unique method of streamer corona discharge was employed to characterize the grade of organic compound degradation in distilled water in an external electric field. Kinetic considerations and a sophisticated model of a laboratory–use reactor were the bases of the work. They also gave rise to a initial rate determining method utilizing carbonate ions as a radical scavenger for the emerging hydroxyl radicals. As a major difference the authors pointed out that the hydrogen peroxide: hydroxyl radical ratio in their experiments were much higher than any other author had described in their work. They assumed that the employed technique led to this result. Surprisingly, the hydroxyl radical formation seems to follow non-linear kinetics, whereas hydrogen peroxide increases linearly with voltage and time. The experiments regarding phenol compound oxidation showed that at a reasonably high concentration ($>5{,}4*10^{-5}$M) the expected degradation occurred. At lower concentrations there have to be made further investigations.

70-structure 12.12.94, J. H. Jensen et al.

Ab Initio Localized Charge Distributions: Theory and a Detailed Analysis of the Water Dimer-Hydrogen Bond

Summary:
The method of localized charge distributions, originally implemented for semi-empirical molecular orbital (MO) theory, is reintroduced and implemented for ab initio self-consistent field MO theory. This theory is then used in conjunction with localized second-order Möller-Plesset (MP2) pair energies to analyse the hydrogen bond in the water dimer. Following questions are asked and tried to be responded to in this article:Why does the electron-neutron attraction term dominate the potential energy of interaction? What is the source of the sharp increase in energy for R < Req? It is found that the hydrogen bond can be explained as the competition between the intrawater electronic kinetic energy pressure and the interwater potential energy suction. The lack of correlation leads SCF (self consistent field) theory to underestimate both the magnitude of the interaction energy and the increase in the internal energies of the monomers. The former is larger in magnitude, so the MP2 energy correction lowers the relative energy of the water dimer at all R.

71-structure 20.03.95, S. Curilef et al.

Dynamics of interacting particles in a magnetic field in two dimensions

Summary:
In this article trajectories of two identical particles or two particles with an opposite charge under the influence of a external magnetic field are discussed. The authors present the simplest and more complex trajectories of particles always under the negation of radiation and relativistic effects. They hope to provide some inside for the interacting pair from a classical point of view so the quantum counterpart could be more easily understood in future.

72-structure 13.10.95, N. Agmon

The Grotthuss mechanism

Summary:
Many theories of proton moving mechanisms are confuted developing the Grotthus mechanism as rate determining for proton mobility. A transition from the H9O4+ cation to the H5O2+ cation and the linked hydrogenbond-cleavage could explain the genesis of moving protons. It is stated that the theories of Hückel, Eigen and Conway are fragmentary and a mechanism in dependence on Zundel and Markov is mentioned. Computational simulations provide consistent information with experimental data as far as hydrogen bond length and structural questions are concerned. X-ray diffraction, Raman NMR, Rayleigh lightscattering and inelastic neutron scattering are used to confirm the thesis. At the end a rather interesting question is asked: Could Proton migration be speeded up by a hydrogen bond-cleaving IR wave?

73-structure 23.10.95, A. El Magd A. Mohamed et al.

Electroviscoelastic Rayleigh-Taylor instability of Kelvin fluids. Effect of a constant tangential electric field

Summary:
In this paper by using the method of multiple scales, an investigation of the Rayleigh-Taylor problem of interfacial stability in a two-layer system of electroviscoelastic Kelvin fluids is performed. Examination of the effects on the stability of the interface by applying a constant tangential electric field is carried out. Through the linear perturbation analysis a fourth-order partial differential equation which governs the motion of rheological fluids is obtained. The scheme reported here depends on the idea that the flow of a slightly non-Newtonian fluid is about the same as that for a Newtonian fluid. The contribution of elasticity is included in the first-order problem. A solvability condition is obtained in this analysis. A first-order differential equation which controls the surface deflection is obtained and solved. Also, stability conditions are introduced theoretically. Some graphs are drawn to indicate the stability regions. The case of large viscosity is considered for numerical calculations. It is found that the elasticity parameter plays a destabilizing role under the effect of a tangential electric field, while the viscosity having a damping nature in Newtonian fluids plays a dual role in non-Newtonian fluids. It is shown that the electric field plays a dual role in stability criteria.

74-structure 08.12.95, S. M. Pimblott et al.

Monte Carlo Simulation of Range and Energy Deposition by Electrons in Gaseous and Liquid Water

Summary:
A stochastic simulation method employing suitable experimentally based cross sections has been developed for probing the spatial distribution of energy loss and the trajectory of 100 eV to 1 MeV electrons in gaseous and liquid water. Elastic collisions and large-energy-loss inelastic collisions strongly influence the passage of electrons such that the separation between the initial and final

position is considerably smaller than the path length. The path length of an electron of energy greater than 1 keV is adequately described by the CSDA (continuous slowing down approximation) range; however, for lower energy electrons the CSDA range underestimates the path length. The axial penetration of an energetic electron is influenced by the occurrence of elastic collisions while the radial penetration is primarily determined by trajectory deviations due to inelastic events. The question how low-energy (<25eV) electrons affect the radiation properties of water is unanswered.

75-structure 01.07.96, D.G. Frood et al.

Space-charge dielectric properties of water and aqueous electrolytes

Summary:
In aqueous media it is well known that at low frequencies space-charge double layers form at the electrodes of a capacitor. The dielectric constants and losses caused by these double layers are so large that they completely mask the inherent contributions to the measured permittivity arising from the polarizability and rotation of the water molecules. In practice the inherent properties are not observable until the frequency is increased to at least several kHz or more. The dielectric properties of water having various degrees of purity are measured at room temperature between 20Hz and 1MHz using a parallel plate condenser having brass electrodes in this article. Dielectric properties of de-ionized water containing different concentrations of copper sulphate are also presented. The results are in fair agreement with Coelho's theory of the space charge response of a medium containing mobile ions only when an additional contribution to the permittivity arising from DC conduction in the electrolyte is taken into account. This conduction is consistent with the assumption that the carriers are free electrons of high mobility and low number density. Using non-dispersive blocking electrodes, electron transfer from the external circuit to the electrolyte may be eliminated and the resultant Maxwell-Wagner effect for the whole shows a Debye response.

76-Kerr 15.07.96, A. Üstündag et al.

Kerr Electro-Optic Measurement Technique For Determination of nonuniform Electric Fields

Summary:
In this article an improvement of a measurement technique is being reported of. To increase the sensitivity of Kerr-electro-optic measurements some technical concepts were altered in the past few years, but here it is suggested to allow the electric field direction to vary along the light path. It is shown that it is possible to measure three "characteristic parameters", analogous to non-uniform photo-elastic stress analysis, that allow determination of the electric field magnitude and direction. These three parameters are related to the electric field through the matrix of the differential equations that govern the Kerr-media and reduce to the electric field direction and light phase retardation proportional to the electric magnitude squared for the case where the electric field direction is constant. These parameters can be used to recover the electric field distribution in radial and angular discretization of space.

77-reaction 14.11.96, B. Sun et al.

Optical study of active species produced by a pulsed streamer corona discharge in water

Summary:
In the present investigation, analysis of optical emission spectra was used for the detection of O, H and OH radicals, and the effects of the physicochemical parameters and discharge conditions on radical formation were studied. It is concluded that: (1) Atomic oxygen radicals were produced by the pulsed streamer corona discharge in water, in addition to hydroxyl radicals and atomic hydrogen. (2) The OH radical density increased with increasing pulse voltage, and the rate of increase of the intensity was faster for positive polarity than for negative polarity. The positive polarity streamer onset voltage was lower than that for negative polarity. The OH radical emission

intensity increased as the electrode radius of curvature was made smaller, and the intensity increased faster for positive polarity than for negative polarity. (3) When oxygen gas was injected into the reactor, the OH and O radical densities increased with increasing oxygen gas flow rate for both pulse polarities, and saturated at about 50 ml/min. In addition, for both voltage polarities, the H radical intensity changed when the oxygen flow rate was raised. When an inert gas (argon) was used instead of oxygen, the OH, H, and O radical densities increased when the inert gas flow rate was raised. However, the increase of the H radical density was much greater for argon than for oxygen. (4) The radical emission intensity reached a maximum at conductivities between 10 and 80 gS/cm, and was stronger in the KOH solution than in the KC1 solution.

78-reaction 29.03.97, B. Sun et al.

Non-uniform pulse discharge-induced radical production in distilled water

Summary:
In this article the OH- formation due to the active species (radicals) or radiation are examined. The experimental method was based on a spark discharge and a streamer corona discharge linked to an oscillator which also made it possible to measure initiation spark time and breakdown time of the current. As a result it was obtained that the higher the voltage or the electromagnetic field was, the shorter became the equivalent breakdown time, respectively the initiation spark time. A recorded spectrum of the spark discharge showed a broad intensity maximum of 400-500nm (2*10^4 as strong as sunlight at sea level) and the genesis of radicals. Hydrogen peroxide was produced with both methods but at a distinctly higher rate with the spark discharge method (at equal energy levels).The OH- cations were mainly produced in the discharge channel but also could be caused to a lower extent in the area around it due to the produced UV radiation of the discharge itself.

79-structure 29.07.97, G. Sutmann

Structure formation and dynamics of water in strong external electric fields

Summary:
In this paper the mean value of the polarization due to the action of an external electric field is studied and calculations of the susceptibility constant x are carried out. In particular the author studied the crossover between the linear and nonlinear regimes of the dielectric response, i.e. where dielectric saturation effects start to be important. The dielectric response is found to be linear up to fields E_0:0.01 V/Angstroms from where dielectric saturation effects become important. At fields of E_0:3 V/Angstroms a phase transition into an ordered, ice-like structure is observed, which is stabilized through hydrogen-bonds. With an increasing external electric field, the frequency spectrum of the water dynamics showed a remarkable red shift of the intramolecular modes and a blue shift of the librational motions, where the frequency varies quadratically with the field strength.

80-reaction 01.10.97, M. Kurahashi et al.

Radical formation due to discharge inside bubble in liquid

Summary :
The experiment which was undertaken in this article deals with the possibility to electrolytically produce an O_2 bubble in water and then let in this bubble a discharge take place which was examined with an oscilloscope, light emission spectroscopy (200-950nm), UV absorption spectroscopy and after experiment accessible to titration with sodium thisulfate (hydrogen peroxide , ozone proof). Moreover, the sterilization effect was tested with yeast cells which were exposed to the electrolysis and discharge process over a period of time. All experiments were accomplished under minor pressure ranging from 110 Torr to 300 Torr. As a result the authors

stated that with their “needle to plate-method” it is possible to gain a discharge in a bubble which is mainly filled with vaporized water molecules emitting light at 2 distinct wavelength due to the OH and H-alpha formation. They also produced hydrogen peroxide independent of the width of the gap between the 2 electrodes up to 50 ppm and proved a moderate killing effect of yeast cells exposed to the electric field and their consequences.

81-structure 13.10.97, C.A. Chatzidimitriou-Dreismann et al.

Anomalous deep inelastic neutron scattering from liquid H2O-D2O

Summary:
The main topics in this article are the dynamics of proton transfer and H-bonds in condensed matter, in particular quantum aspects of scattering processes. TOF spectra and Raman light scattering were used as methods to measure H2O-D2O mixtures. The inelastic neutrons scatter is different for protons or deuterons nucleii. At the detector the ratio of H/D (Q) can be measured. Surprisingly, the ratios (Q) detected were proven to be independent on the scattering angle, though the peaks were shifted by different scattering angles. Furthermore, the widths of the determined H and D peaks are independent from the molar composition. Most intriguingly, Q isn’t constant, which led to the thesis that quantum entanglement mechanisms take place in the mixture with electronic charges mediating quantum variations of the nuclei.

82-structure 01.01.98, M. Kristiansen et al.

High voltage water breakdown studies

Summary:
Two electrodes immersed in water were examined when exposed to different chemicals, coatings of the electrodes and external magnetic field strengths. With a voltage of up to 400 kV /cm the breakdown time, the breakdown voltage and the fall time of the voltage across the electrodes were measured (by Magne Kristiansen et al.). The author suggests that the interface between the solid-liquid system is responsible for the initiation of the arc and also the breakdown of the electric field. “Electrically smoothing” the electrodes surfaces could change the diffusive character of the electrodes, which means that water is used to be a conductive layer in a higher grade before the intrinsic maximum voltage of the gap between the electrodes is reached. With that procedure, the magnetic field strength of water is enhanced to gain higher voltages.

83-kerr 01.01.98, S.N.Komin et al.

Electro-optic study of prebreakdown processeses in deionized water

Summary:
Mach-Zehnder interferometer and a electronic optical photochronograph were used to detect optical changes of the refractive index of deionized water. Additionally, the chronograms showed a spatial and a time resolution. Voltages of up to 750kV/cm were used in a stainless steel environment, which gave rise to a nonuniform electric field. It was found out that two waves spread from the electrodes with sonic velocity and in the area of the electrodes, water got opaque due to the incidental perturbations. The refractive index highly varied when voltage was applied at various moments. It is stated that the breakdown process begins in close cathode areas and moves towards the anode, which forms a discharge channel when electrons are getting close. Vapour gas cavities are responsible for the opaque character of the water during this process

84-reaction 28.04.98, H.C. Allen et al.

Molecular structure and absorption of Dimethyl Sulfoxide at the surface of aqueous solutions

Summary:
The surface vibrational sum frequency spectroscopy (VSFG) of DMSO is examined in this paper. A red-shift of the methyl symmetric stretch is determined at the surface of the pure DMSO solution, whereas its' blue shift increase when DMSO solution becomes diluted. It is assumed that free energies of adsorption of -19,8 (+/- 0,4) kcal/mol represent the surface partitioning of DMSO. It is stated that at low concentrations a monomer regime is predominant at the interface areas and the higher the concentration becomes the more dominance is ruled out from dimers and clusters, thereby influencing solvation and biological membrane transport effects. Moreover, the methyl transition dipole moment of neat DMSO is oriented a maximum of 55° from the surface normal, more detailed investigations over the full DMSO concentration range at the air/liquid interface planned in the future.

85-structure 10.09.1998, D. H. Jung et al.

The effect of an external electric field on the structure of liquid water using molecular dynamics simulations

Summary:
The authors used molecular dynamics simulations with 1000 equilibrated TIP4P (30000steps; 10000 ad hoc scaling, trajectories of 20000 steps of NVT) water molecules to investigate the temperature dependency of the liquid water structure and the change of the liquid water structure induced by an external electric field. Experimental densities were applied at all temperatures except sub-zero temperatures; at all sub-zero temperatures, 1.0 g/cm^3 was used. They state that different transitions ,eg. from liquid to ice-I, depend on the nature of the electric field and try to connect configurational changes on the macroscopic level with a temperature dependency of ring structures, especially the correlation between 3,4,5 and 6-membered rings under the influence of different temperatures and electric fields. They observe a structural change of water at field strengths over 0,15 V/Angstroms,namely a large increase of 6-membered rings. If they take into account the induced electric dipole moment by the external electric field, the threshold field strength will be a lower value than 0.2 V/Angstroms . They also state that water can contain an analogous structure to ice structure, keeping its liquid property from the calculated data of the diffusion coefficient of water under an electric field.

86-structure 30.09.1998, C. E. Dykstra

External electric field effects on the water trimer

Summary:
One starting point for a detailed picture of the interplay of external fields and intermolecular forces is to examine the orienting effects of fields in small molecular clusters. The proposed model potential consists of three terms. One term has the functional form of atom–atom dispersion, an attractive R^{-6} dependence where R is the distance between a pair of atoms on different waters. There is a similar R^{-12} term that is repulsive. The third term is the classically evaluated electrical interaction energy. It is stated in this article that the equilibrium structure of the water trimer is cyclic and going around the ring there is one O–H bond of each water directed essentially toward the oxygen of the next water. The other three O–H bonds are directed out of the plane of the ring, with two ‘up’ and one ‘down’.The effect of an external field is not a sharp distortion of the structure of the cluster but rather a shift in the conformational energetics. The ‘up–up–down’ zero field equilibrium structure of the trimer holds as a field is applied, but two other conformers, first ‘up–up–up’ and then linear, become the energetically preferred forms as field strength increases. Most of

the shifts in conformer energetics can be associated with dipolar interactions with the field, but mutual polarization energetics amplify the effects.

87-structure 01.10.1998, Y. Ohki et al.

Space Charge Formation in Water-treed insulation

Summary:
In this article the degradation of insulation due to water-tree formation (e.g.:cross-linked polyethylene cables) is examined. In detail the authors determined the space-charge formation of so-called vented and bow-tie trees in water. They used different ionic species to spike the aqueous solution and applied high voltage between 4 to 23 kV for their studies. New analysing methods enabled them to measure space charge around water trees quantitatively with a high spatial resolution. This, in turn, is making it possible to discuss the origin of space charge in the water tree region and to clarify the electrical properties of water trees. It has become clear that carriers with two different origins, one due to interfacial polarization caused by high conductivity, and the other due to carrier injection, must exist around the tip of water trees in the cable insulation.

88-structure 28.11.1998, D.V. Tikhomolov et al.

Estimating the orientation component of stationary water dipoles in constant electric fields

Summary:
The thickening of a water film in a hydrophillic capillary filled with a nonpolar (gas or organic liquid) and a polar component (water) under a external magnetic field is the main topic in this article. Based on Frenkel and Gubanov (1940) as well as on Debye (1935) Onsager and Kirkwood a new semi-empirical entropy changing orientation factor is brought upon dipole molecules, which corresponds well to voltages of about 10^3 to 10^4 V/m and therefore results in a different thickness in the capillary. It is stated that due to the inhomogenous electric field a pressure gradient in the liquid occurs which is related to the dipole orientation of the liquid. Kirkwoods' theory seems to be the most applicable one according to the authors results.

89-structure 01.01.1999, S.T Bramwell

Ferroelectric ice

Summary:
A review on the research issues concerning ice structure is given ranging from the 1920s' to the end of the 20th century. Structural modifications in water and the possibility to analyse them trough new analytical methods are compared to each other. Some recent techniques (Su et al, Iedema et al., Jackson et al.,…) are enumerated as well as the clear statement that no scientist ever did persuade his colleagues with the statement that he has the capability of generating structurally hydrogen-ordered ice (ferroelectric ice).(Even though a procedure was developed by Iedema et al. which proved to be capable of generating 0,2 % aligned water molecules.)

90-structure 22.01.1999, M.Taut

Two particles with opposite charge in a homogenous magnetic field: particular analytical solutions of the two dimensional Schrödinger equation

Summary:
The author explains in his article that for a two-dimensional system of two particles (with opposite charge) in an external magnetic field there are countable solutions of the Schrödinger equation. These discrete magnetic field strengths exist only for certain set of values, whereas the polynomials of those in between are described by an infinite eigenfunction. The singular solution seems to be correlating with the system of n electrons in a magnetic field, which in turn describe the fractional

Quantum Hall effect. No suggestions are made for the physical properties which would arise from this singular solution.

91-structure 01.02.1999, D. Marx et al.

The nature of the hydrated excess proton in water

Summary:
In this article it is stated that the Eigen and the Zundel are positively charged cation which are only ideal forms of water molecules. The variety of molecules with a positively charge distribution ranges approximately over more than the half of the charged molecules which do not belong to the ideal forms but having more exotic structural forms. The authors point out that many of the difficulties in interpretation might arise from the attempt to interpret complex behaviour within the limits of a favoured structure. Furthermore, they link some acquired experimental data to quantum effects, activation energies and the disapproval of tunneling effects by protons. Also claimed in this article is that the rate of proton diffusion is determined by thermally-induced hydrogen-bond cleavage in the second solvation shell.

92-structure 18.02.99, J.T. Hynes

The protean proton in water

Summary:
The author investigates old concepts and develops a state of the art hypothesis of the H_3O+ cation structure. He works with the Eigen and the Zundel cation which are concluded in the Grotthuss mechanism. Surprisingly, ab-initio calculations showed that the proton transfer isn't only a matter of proton motion but of the (surrounding) water rearrangement capability.

93-structure 25.10.1999, T.T. Truong et al.

Exact low-lying states of two interacting equally charged particles in a magnetic field

Summary:
The main topic of this article is the interaction of two electrons and their mutual coulomb repulsion which give rise to a new quantum condition based on the biconfluent Heun equation (BCH), a generalization of the confluent hypergeometric equation or Kummer's equation. It is stated that some more exotic states could be found with this method. Discussing the work of Taut the authors believe that if the usual quantization of angular momentum is applied to electrons whether a discrete magnetic field or discrete values of the frequency of the oscillator potential would develop. With this work an alternative access to the stationary states of two planar equally charged particles in a uniform external magnetic field is granted.

94-structure 7.1.2000, C. A. Angell et al.

Water and its anomalies in perspective : tetrahedral liquids with and without liquid-liquid phase transitions

Summary:
In this paper it is shown how water with its small proton bridge between tetrahedrally coordinated oxygen centres, forms a provocative series with the archetypal glassformer and strong liquid, SiO the analogue ionic compound, BeF in which the Be ions are bridged by Fluoride ions, and elemental Si with no bridge at all. As the size 2 of the bridging unit decreases from the polarizable oxide of silica through the unpolarizable Fluoride of BeF_2, the tiny proton of water, and finally vanishes at silicon, the constraints on the network tighten. As the constraints become more severe, the departures from simple activated diffusion behaviour of SiO_2 during heating of the amorphous phase at ambient pressure, become more pronounced. In the case of Si, the extreme of a first-order

transition from strong to extremely fragile liquid state is manifested in the supercooled regime. With water the behaviour is intermediate. In both cases the anomalous regime is located in the supercooled state which greatly complicates its investigation and leads to much controversy. It is suggested that such glasses, which will include many Si analogs such as Ge, InSb, etc, might constitute a distinct class of amorphous material with the attributes (low residual entropy, etc.) of the hypothetical perfect glass state.

95-structure 14.06.2000, A.A. Rashin et al.

Charge distributions in water and ion-water clusters

Summary:
Multipole fitting of molecular electrostatic potentials and the charge integration based on the Gauss electric field flux theorem was used in this article to study the quantum mechanical charge distributions in ionic and uncharged molecules, in their complexes and in clusters. It is shown with computational methods that changes in the charge distribution upon formation of ionic bonds are similar to hydrogen bonds. Moreover, it is stated that partial charges on atoms are preserved upon formation of ion-ion or water clusters and the concomitant charge redistribution can be fully accounted for by the polarization represented by induced atomic dipoles and sometimes quadrupoles, thus eliminating the need to invoke a "charge transfer". The radii of ion-water clusters spherical volumes are suggested to have the classical ionic radii if full ionic charge of ±e is contained. And last but not least water clusters try to compensate missing electron density from an individual water cavity through penetrating diffuse electron density of the surrounding molecules.

96-structure 01.02.2001, T. Toyoda et al.

Estimation of conductivity and permittivity of water trees in PE from space charge distribution measurements

Summary:
Crosslinked Polyethylene (XLPE) cables in an strong electric field are under investigation in this article. Especially their behaviour as a conductor when space-charge formation occurs and the changed permittivity of the solution is examined by applying an 5kHz AC voltage of 5kV for long periods. With high resolution PEA (pulsed- electro acoustic) methods the space charge distribution (spatially) can be analysed, as well as the temporal resolution can be measured with a pulse generator which is capable of generating repetitive pulses with a duration of 5ns and 40kHz , to a greater extent than ever before. It is concluded that the conductivity of the treed region becomes by the factor 10^{10} bigger compared to the untreed regions.

97-structure 09.06.2001, S. V. Shevkunov et al.

Electric field induced transitions in water clusters

Summary:
The influence of a external uniform electrostatic field on the internal energy and polarization of a medium-sized water cluster, consisting of 40 molecules is studied at four temperatures (150,170,200,240 K), by means of the Monte Carlo method. The external electric field is slowly varied in the 0,5*10^7 – 7*10^7 V/cm range. The system shows an abrupt change of its properties at a treshold value of the field ($E_{tr,}$ transition field) , where a transition from a normal (solid-like or liquid –like) to a superpolarized cluster state is observed. This process has the character of a first-order phase transition and is accompanied bay the absorption of heat. The authors explain this effect with the angle correlations between dipoles which in general lose their oscillatory character during melting and show a monotonic character in the liquid state. Also E_{tr} has been found to decrease with increasing temperature, in contrast to the behaviour dictated by the Clausius-Clayperon equation for field–induced transitions between equilibrium states.

98-structure 04.01.2002, M. E. Tuckermann et al.

The nature and transport mechanism of hydrated hydroxide ions in aqueous solution

Summary:
This article tries to show the implicit difference between the mobility of H_3O^+ and OH^- ions through configuration assumptions, symmetry arguments and ab-initio calculations of the activation energy for complexes which resemble those measured with Raman-NMR and Neutron scattering based on the Car- Pirinello algorithm. The author points out that with his pronounced mechanism it would get obvious why a H/D isotope effect is by far more effective in basic than in acidic solutions. Moreover, basic quantum calculations suggest a activation energy of the proposed mechanism of 3 kcal mol-1 which is all about the same in the experimental data from hydroxide mobility data. The proposed mechanism consists of four steps: (1) transformation of $OH^-(H_2O)_4$ to oh-$(H_2O)_3$ by first solvation- shell H-bond breaking;(2)activation of $OH^-(H_2O)_3$ by formation of the H'---O H-bond; (3)formation of the transient $H_3O_2^-$ complex by partial proton transfer resulting in a new O* and $OH^-(H_2O)_3$ complex; (4) acceptance of a fourth H-bond by the new O* resulting in a change from $OH^-(H_2o)_3$ to $OH^-(H_2O)_4$ and consequent inactivation of the complex.

31-reaction 02.02.2002, A. T. Sugiarto et al.

Oxidative decolouration of dyes by pulsed discharge plasma in water

Summary:
The Degradation of organic dyes by a pulsed discharge plasma between needle-to-plane electrodes in contaminated water was investigated with a spectrophotometer in three discharge modes: streamer, spark and spark–streamer mixed mode. Moreover, an amount of low-concentrated hydrogen peroxide was added and changes in energy efficiency, radiation intensity and decolouration efficiency was measured. It became obvious that the decoloration rate increases from streamer- to sparc- to spark with streamer-mode due to a direct photodissociation of the dyes and that this is process is subject to the adjusted pH. The added H2O2 increased the energy efficiency and altered the AOPs (advanced oxidation processes) leading to a higher hydroxyl radical formation due to advanced light stimulated photolysis.

++-reaction 02.10.2002, B.F. Bolund et al.

Dielectric study of water/methanol mixtures for use in a pulsed-power water capacitors

Summary:
In this article experiments concerning breakdown strength and energy density were carried out. A solid capacative primary storage and a water capacitor for secondary storage is normally used for a large pulsed-power system. The authors suggest a mix of water and methanol (1:1 or 2:1)to increase the maximal storage time and thereby enable the use of a inductive primary storage. Measurements were taken out with different temperatures combined with low- and high voltage pulses. In slowly charged systems charge injection tends to become a problem in pure water or water/ethylene gylcol mixtures. This effect is decreased in water/methanol mixtures at the expense of lowering breakdown strenghts.

100-structure 01.12.2002, M. Zahn et al.

Optical Measurement of non-uniform Electric Field Vector Distribution in a Dielectric Liquid Using Triplet Measurement System

Summary:
In this article a review of the work of H. Ihori, M. Fujii, and K. Ani,("Optical Measurement of Non-uniform Electric Field Vector Distribution in a Dielectric Liquid Using Triplet Measurement System") , is discussed between Markus Zahn and Afsin Ustiindag from the Massachusetts Institute

of Technology and the authors mentioned earlier. It is of great interest for the scientist if their model is applicable to arbitrary non-uniform electric field distributions and if the reduction of measurement directions is of any importance.

101-structure 01.06.2003, Z.-M. Dang et al.

Space Charge Distribution in Polyethylene due to the Water Diffusion

Summary:
Space charge distribution and water absorption in polyethylene (PE) are studied in this paper. PE is a very important material to produce XLPE cable.Therefore, it has a key signification to study the water absorption characteristics and the other dielectrics after water absorption that is what we report in this paper.PE of hydrophobicity has a content hydrophility by modification using Ethylene-acrylic acid (EAA) and sorbital. Space charge distributions were measured by pulsed electro-acoustic (PEA) methods.Conclusionally, PE modified by EAA and sorbital can improve water immigration and inhibit the formation of the space charge. This is because the feature of PE changes from unpolar to polar when polar EAA and sorbital are added into pure PE. The water treeing can be also inhibited if water into the samples distributes uniformly.

102-structure 17.07.2003, L. Rey

Thermoluminescence of deuterated amorphous and crystalline ices

Summary:
Low-temperature thermoluminescence was used in this paper to assess the structure of solids. When applied to frozen liquids it can also provide interesting information on the initial product in the liquid state. It's shown, in previous publications (C.R. Phys. 1 (2000) 107, Physica A 323 (2003a) 67) that two major light emission peak areas were displayed in the case of deuterated ice, one of them linked to the crystal network and, most probably to the pre-existing hydrogen bonding in the original water. In the present research the thermoluminescence glow of several types of deuterated ices obtained by compression at 77K including amorphous solids was investigated. It is observed, in this latter case, an almost complete disappearance of the peak area that is attributed to crystal lattice and hydrogen bond systems. This confirmed that high pressures, when applied to hexagonal ice at 77 K, can induce ‘‘melting’’ in the solid state and give rise to an unstructured ‘‘liquid’’.

103-structure 1.08.2003, C.A. Chatzidimitriou-Dreismann et al.

Comparison of neutron and electron Compton scattering from entangled protons

Summary:
Experiments to prove a quantum entanglement in solids were conducted with NCS (neutron Compton scattering) and ECS(electron-nucleus scattering). The determined proton peaks appeared to be up to 50% smaller than expected due to short-lived quantum entanglement. The two methods showed similar results and it was shown that average lifetimes of such entangled states never lasted longer than a few hundred attoseconds. Moreover, ECS has presented itself as a useful complementary tool for the experimental investigation of anomalous shortfall of scattering intensity of protons in condensed matter.

104-reaction 02.04.2004, A. M. Anpilov et al.

The effectiveness of a multi-spark electric discharge system in the destruction of microorganisms in domestic and industrial wastewaters

Summary:
With two electric chambers each equipped with 4-5 discharge units, supplied with a waste water

flow rates (different specific energy!) between 2-5 litre min^{-1} ,a frequency between 0-100 Hz, an applied voltage of 20 kV over 4-5 µs the decrease of total CFU were determined. An empirical formula is found for CFU decrease and the mechanism of disinfection over high-temperature plasma channels and the subsequent UV radiation formation is explained , while proposing a two-stage process for the development of UV radiation. Furthermore, lots of empirical data for killing different bacteria species is given and a comparison between UV-lamp irradiation and the SSD (slipping surface discharge) method is made.

105-structure 01.07.2004, C.A. Chatzidimitriou-Dreismann

Wo ist der Wasserstoff?

Summary:
This German article deals with the question if and why protons seem to disappear when NCS (neutron Compton scattering) measurements are carried out. The hypothesis was a predicted quantum entanglement of protons especially in water and benzole. It was found out that neutrons can't "see" entangled protons because of the decoherence of their quantum state. This is the reason why, after measuring Benzole or water, the structural formula would exhibit the following: $C_6H_{4,5}$ respectively $H_{1,5}O$.

106-kerr 07.07.2004, M. S. Skaf et al.

Optical Kerr Effect in Supercooled Water

Summary:
A molecular dynamics simulations of the optical Kerr effect in liquid and supercooled water is presented in this article and compared with recent time-resolved Kerr spectroscopy measurements by R. Torre et al., [Nature (London) 428, 296 (2004)]. Molecular dynamics (MD) simulations and experimental works have been reported to successfully interpret the dynamics of weakly supercooled water (T * 250 K) within the framework of the mode coupling theory (MCT) of ordinary glass forming liquids. It is reported of MD simulations for the OKE (optical Kerr effect) response of liquid and weakly supercooled water and compared the results directly to the most recent experimental Kerr study [21]. We find that the short time features of the Kerr response have a limited temperature dependence, whereas the behaviour of the long-time relaxation is well described, with a nearly constant stretch parameter and in very good agreement with experiments.

107-reaction 12.09.2004, B.C.Garett et al.

Role of water in electron-initiated processes and radical chemistry

Summary:
Multiple methods to show the electronic and ionic properties of water and supercritical water and their subsequent reactions are presented. Special attention is paid to the energetic levels and scattering processes of water molecules in a bulk, respectively in an interface area. Lots of up to date techniques are described, which confirm data of earlier measurement series that hadn't been intensified since the middle of the 20^{th} century. Especially x-ray light sources and computational resources seem to be a rational approach to energetical, solvational and dynamical phenomenons such as radical and ionic development, hydration of electrons or pathways of scattering of high energy electrons. Structural and conformational theories of water are briefly mentioned in this article, which draws the bow from excitement states to dissociation pathways, including the significant question whether water is the reactant or the media for reactants like organic molecules and how water clusters can change the physical properties of these.

108-structure 09.10.2004, Y. Meng et al.

Control of local friction of metal/ceramic contacts in aqueous solutions with an electrochemical method

Summary:
Ball-on-plate sliding friction experiments were designed and performed to show the possibility of local friction control by electrochemical methods. Local friction of metal/ceramic contacts in aqueous solutions is determined by the distribution of boundary lubricating films on the metal surfaces. By introducing electrochemical charging methods, a boundary lubricating film on a local region of the metal surface can be generated or removed, depending on when and where electrical energy is introduced, and thus friction can be manipulated to some extent at desired locations and at a desired time. It is shown that two techniques, one being the partition of the metal part and the other the arrangement of the auxiliary anode are effective for this purpose.

109-structure 29.10.2004, M. Sharma et al.

Intermolecular Dynamical Charge Fluctuations in Water: A Signature of the H-Bond Network

Summary:
In this article it is reported of a simulation of deuterated water using a Car-Parrinello approach based on maximally localized Wannier functions. This provides local information on the dynamics of the hydrogen-bond network and on the origin of the low-frequency infrared activity. The oscillator strength of the translational modes, peaked around 200 cm^{-1}, is anisotropic and originates from intermolecular-not intramolecular-charge fluctuations. These fluctuations are a signature of a tetrahedral hydrogen-bonding environment.

110-kerr 10.11.2004, M. T. Sonoda et al.

A simulation study of the optical Kerr effect in liquid water

Summary:
In this work an molecular dynamics simulation study of the polarizability anisotropy relaxation of SPC/E water is presented, focusing on the Kerr nuclear responses in the time- and frequency domains. The simulations require a model for the collective polarizability which has been described by a sum of individual molecular polarizabilities obtained from ab initio electronic structure calculations with a dynamical modulation given by a dipolar coupling. Some degree of nonlinear electronic response is incorporated through fixed (intrinsic) values of molecular hyperpolarizability tensors. the relaxation of the polarizability anisotropy in terms of the dynamics of intrinsic and induced polarizabilities is analysed and the OKE response and its spectrum in the light of the different contributions is interpreted. The spectrum of the total nuclear response presents peaks at different frequencies corresponding to the intricate motions of water. The slow rotational-diffusion dynamics is mainly characterized by a central band near 3 cm^{-1} and a shoulder between 20 and 30 cm^{-1}. The rotational-diffusion relaxation obtained from SPC/E-based simulations is slower than that reported for the TAB/10D model, which has a maximum in the reorientational band near 8 cm^{-1}. For higher frequencies, two main peaks are identified in the total spectrum at ca. 230 and 500 cm^{-1}, which are due to induced and molecular polarizability auto-correlations, respectively. The simulated spectrum is qualitatively compared with the experimental analyses from different groups, which ascribe the measured broad band in the range 400–800 cm^{-1} to hindered reorientational motions (librations) about the different molecular axes, and the peaks at app 60 and 170 cm^{-1} to collision-induced effects from hindered translational motions associated with the stretching and bending of hydrogen bonds. The experimentally observed feature near 60 cm^{-1} is not resolved in the present simulations because the intrinsic polarizability contribution picks up intensity as ω falls below app.. 60 cm^{-1}. This suggests that the intrinsic polarizability tensor used in the simulations may

overestimate the anisotropy of water.

111-reaction 09.12.2004, M.J Kirkpatrick et al.

Hydrogen, Oxygen and hydrogen peroxide formation in aqueous phase pulsed Corona electrical discharge

Summary:
In this article the formation and the ratios of Hydrogen:Hydrogen peroxide:Oxygen in an aqueous solution with an electrical discharge device are analysed. Dependent on the actual current, frequency and voltage different equilibria are favourable in the system. As a rough rule of thumb it can be stated that the ratios in the measured area were 4:2:1 (hydrogen:Hydrogen peroxide: oxygen). The experimental conditions based on a 1 litre reactor in which a nearly 1mm thick Nichrome (Ni-Cr) electrode was submerged; pulses between 0.62-1.2 J/pulse (37-72 W) and 60 Hz were supplied by an AC transformer.

112-structure 22.12.2004, E.Stanley et al.

Static and dynamic heterogenities in water

Summary:
Phase Transitions of liquid supercooled forms of water are discussed in this article. Stanley gives a hypothetical proof of at least two possible static configurations of water heterogeneities (low density amorphous and high density amorphous). The potential-energy surface and the number of mountain passes separating valleys within seem to be the controlling factors. HDA could be seen as a metastable form of VHDA (very high density amorphous). As far as static and dynamic heterogeneities are concerned, the Adam-Gibbs relation seems to be an indirect indicator of dynamic heterogeneities. The diffusion coefficient and the configurational entropy increase with pressure, whereas dynamic heterogeneities decrease with pressure. Thus, these characteristics suggest that static and dynamic heterogeneities may correlate on the microscopic level as well.

113-faraday 10.03.2005, G. S. Sarkisov et al.

Measurement of the current in water discharge using magneto-optical Faraday effect

Summary:
The observation of magneto-optical Faraday effect with a CCD camera in a water discharge is presented in this article. This effect derives from the interaction of the probing electromagnetic wave with bounded electrons. The magnetic field from a water discharge induces circular anisotropy of the refraction coefficient in a direction perpendicular to the current. The propagation of the linear polarized electromagnetic wave through the medium with circular anisotropy results in the rotation of the polarization plane. To reconstruct the magnetic field and current it is enough to measure the rotation of the polarization plane using a two-channel polarimeter and apply the Verdet constant for water. The pulsed green yttrium-aluminum-garnet laser (90 mJ, 7 ns pulse width and 532 nm wavelength) caused intermittent currents and voltages in the breakdown channel of up to 4 kA and 140 kV.

114-structure 29.03.2005, R. Szoszkiewicz et al.

Nucleation Time of Nanoscale Water Bridges

Summary:
The kinetics of capillary condensation at the nanoscale is studied here using friction force microscopy. It is stated that capillary condensation of water is a thermally activated phenomenon. The capillary nucleation times are found to grow exponentially with 1/T obeying an Arrhenius law. The times increase from 0.7 up to 4.2 ms for T decreasing from 332 to 299 K. We find a nucleation

energy barrier of 7,8 *10^-20 J in excellent agreement with classical thermodynamic models. The attempt frequency ranges between 4–250 GHz. It is suggested that this frequency is related to the surface vibrations of nanoscopic water droplets adsorbed on the contacting surfaces.

115-structure 20.04.2005, V. M. Kozhevnikov et al.

Self-Organization in a Layer of Magnetic Fluid in Strong Electric Fields

Summary:
The effect of a polarizing voltage on the electrical properties of a magnetic fluid confined between the plates of a plane capacitor connected to a series resonance circuit has been studied in this paper. The magnetic fluid layer features the formation, development, and self-organization of aggregates with dimensions on the order of several millimeters. These processes influence the physical properties of the magnetic fluid layer. The electrical properties of this layer under such conditions are determined by the near-electrode regions, which are characterized by low conductivity. The application of a polarizing voltage to the cell with the magnetic fluid gives rise to correlated motions of the charge carriers, which is manifested by the observed macroscopic structures. The behaviour of the resonance current in the circuit as a function of the polarizing voltage changes when the magnetic fluid layer thickness is decreased below a certain level, which is explained by a decrease in the number of magnetite particles in the interelectrode space, which are involved in the formation of dissipative structures.

116-structure 25.04.2005, S. S. Iyengar et al.

The properties of ion-water clusters. I. The protonated 21-water cluster

Summary:
The ab initio atom-centered density-matrix propagation approach and the multistate empirical valence bond method have been employed to study the structure, dynamics, and rovibrational spectrum of a hydrated proton in the “magic” 21 water cluster. Based on these simulations it was concluded that the protonated species in this cluster resides on the surface. In one approach the harmonic frequencies were analysed for the “inherent” structures in the dynamics whereas in the other approach the vibrational properties were obtained from autocorrelation functions of ab-initio dynamics data. The results thus obtained were found to be very different from each other in the important 2000–3000-cm^{-1} frequency region. The dynamical autocorrelation results seem to match previous experiments while the frequencies of the inherent structures do not match experiment and deviate in a fashion similar to the 0-Kelvin theoretical results. Thus as a conclusion dynamical and finite-temperature effects seem to play a critical role in defining the spectral properties of this system.

117-structure 05.07.05, Z.G.Chiragwandi et al.

Vortex rings in pure water under static external electric field

Summary:
The authors experimented with a kind of on-chip electrochemical cell, which was used to characterize water subject to some voltage. Surprisingly, effects only occur at the anode and aren’t subject to any kind of dielectric response. The phenomenon is understood as an ion current caused by the Faraday process of hydrolysis. A vortex build up is subsequent to the proton defects interacting with a increased OH- concentration in the anode area. Proton current is expected to display an effective angle to the applied field, which may drive the vortex rotation.

118-structure 8.7.2005, A. Moukengué Imano et al.

Deformation of water droplets on solid surface in electric field

Summary:
The purpose of this paper is to analyze the deformation of water droplets on a solid surface under electric stress. A mathematical model making it possible to simulate the axisymmetric as well as non-axisymmetric deformations of droplets is developed. According to this model, the droplet deformation depends on several parameters such as the volume and the number of droplets, the conductivity and the permittivity of droplets, their proximity to one another, the surface of the solid material, and the location of each droplet on the dielectric surface. The results of the simulation show the disturbance of the background field through the presence of a single or multiple droplets. An experimental study is also achieved by considering one to three droplets aligned simultaneously on a dielectric smooth surface between two electrodes subjected to AC voltages. The influence of the background field and the droplet location regarding the electrodes on the deformation of water droplets are evidenced.

119-structure 13.09.2005, J.D. Eaves et al.

Hydrogen bonds in liquid water are broken only fleetingly

Summary:
In this paper a combination of femtosecond 2D-IR spectroscopy and molecular dynamics simulations is examined to investigate the stability of NHB species in an isotopically dilute mixture of HOD in D2O. The mechanism by which water molecules switch hydrogen-bonded partners is specifically under investigation. In this mechanism, the role of nonhydrogen bonded configurations (NHBs) between adjacent molecules is of particular importance. A molecule may switch hydrogen-bonding partners either through thermally activated breaking of a hydrogen bond that creates a dangling hydrogen bond before finding a new partner or by infrequent but rapid switching events in which the NHB is a transition state. Measured 2D IR spectra reveal that hydrogen-bonded configurations and NHBs undergo qualitatively different relaxation dynamics, with NHBs returning to hydrogen-bonded frequencies on the time scale of water's fastest intermolecular motions. Simulations of an atomistic model for the OH vibrational spectroscopy of water yield qualitatively similar 2D IR spectra to those measured experimentally. Analysis of NHBs in simulations by quenching demonstrates that the vast majority of NHBs are in fact part of a hydrogen-bonded well of attraction and that virtually all molecules return to a hydrogen-bonding partner within 200 fs. The results from experiment and simulation demonstrate that NHBs are intrinsically unstable and that dangling hydrogen bonds are an insignificant species in liquid water.

120-structure 04.10.2005, T. Head-Gordon et al.

Unified description of temperature-dependent hydrogen-bond rearrangements in liquid water

Summary:
Using temperature-dependent spontaneous Raman spectroscopy in conjunction with Monte Carlo simulations, it is shown in this paper that the distribution of hydrogen bonded geometries and energies in liquid water are continuous. A microscopic interpretation is presented for many of the experimentally observed features in the Raman spectrum long considered to be strong evidence for a multi state system, including the isosbestic point, asymmetric band profile, and van't Hoff behaviour. Furthermore, an effective HB energy is calculated indicating a single basin of attraction, consistent with recent findings from ultra fast dynamics measurements

**-structure 20.10.2005, C.J. Burnham et al.

The properties of ion-water clusters. II. Solvation structures of Na^+, Cl^-, and H^+ clusters as a function of temperature

Summary:
The present work investigates the temperature-dependent solvation of Na^+, Cl^-, and H^+ ions in various water clusters [Four different clusters were studied: $Na^+(H2O)_{20}$, $Cl^-(H2O)_{17}$, $Na^+(H2O)_{100}$ and $H^+(H2O)_{100}$] with respect to their equilibrium properties, especially across the solid-liquid phase transition. Methods of choice were the multi state empirical valence bond potential and a polarizable model, whereas the water-ion-clusters were examined within the temperature region 100–450K using a hybrid parallel basin-hopping and tempering algorithm. Surprisingly, NA+ and Cl- was excluded from the cluster surface above the freezing point tending towards the inside of the clsuter whereas H+ stayed always on the surface of the cluster.

121-structure 21.10.2005, S.J.Suresh et al.

Influence of electric field on the hydrogen bond network of water

Summary:
We encounter a very interesting study of water in this article based on simple physical assumptions. Three topics are discussed within: First it is shown what impact temperature has on the dielectric constant of bulk water. This is carried out with low- and high-field applications and with an solid aggregate state (ice-I) in comparison to liquid water. The dielectric constant clearly decreases with increasing temperature and field strength. Second, it is tried to understand the interaction of H-bonds with various interfaces like ions, charged electrodes or within a biological nanopore. They find out that electric fields can only enhance the H-bond structure never disrupt it at any of the attainable field strengths. Water reacts as a media with ions, or electrodes mediating any transitions but not causing them. Third, within a certain window of field strength, H-bonds can stabilize molecules with their dipoles lying perpendicular to that of the field. The fraction of such molecules is relatively small (one tenth of a percent) and the genesis or the intrinsic use of this defects are unclear.

122-reaction 25.10.2005, J. Xie et al.

Microparticles developed by electrohydrodynamic atomization for the local delivery of anticancer drug to treat C6 glioma in vitro

Summary:
In this paper, polymeric particles with controllable morphology and uniform size were successfully developed for drug delivery applications by a modified EHDA (electrohydrodynamic atomization) setup under different operating conditions.Controllable morphologies such as spheres, donut shapes and corrugated shapes with sizes from several tens of microns to hundred nanometers of particles were observed by scanning electron microscopy (SEM) and field emission electron microscope (FSEM). The differential scanning calorimetry (DSC) study indicated that this anticancer drug could be either in an amorphous or disordered-crystalline phase of a molecular dispersion or a solid solution state in the polymer matrix after fabrication. The X-ray photoelectron spectroscopy (XPS) result suggested that some amount of paclitaxel could exist on the surface layer of the microparticles.Cell cycling results suggested that the anticancer drug after encapsulation by EHDA could keep its biological function, thus being promising for the local drug delivery to treat malignant glioma in vivo.

123-structure 03.11.2005, S.F. Lyuksyutova et al.

Atomic force microscope tip spontaneous retraction from dielectric surfaces under applied electrostatic potential

Summary:
A time-resolved method for tip' retraction at ms-scale away from dielectric surfaces has been developed. The analysis of the forces in the system indicates that the equilibrium distance is comparable to the tip's radius. It suggests that the spontaneous tip lift-up is associated with the tip' electrostatic repulsion from the surface in the double layered (water and polymer) configuration. A spontaneous lift-up of the tip has been monitored experimentally and found to be proportional to the height of nanostructures raised in films. The method allows to investigate a real tip–surface dynamical response separately from the response associated mainly with electrostatic attraction between AFM lever and arbitrary surfaces. Moreover, it is suggested that in the future the AFMEN (atomic force microscopy-assisted (AFM) electrostatic nanolithography) technique could become useful in the field of data storage. It generates features by mass transport of polymer without chemical cross-linking, polymer degradation, or ablation.

124-structure 14.11.2005, Y.C.Choi et al.

Electric field effects on water clusters (n=3-5): Systematic ab initio study of structures, energetics and transition states

Summary:
The main topic in this article deals with water clusters, more precisely with the trimer to pentamer forms of water, under the influence of an electric field. To calculate the structure of the molecules the hybrid density functional theory of Becke's three parameters were employed with the Lee-Yang-Parr correlation and the second–order Möller-Plesset perturbatio nhteory to obtain the single-point energy of the optimized structures. Different field strengths were applied (from zero to 0,016 a.u.; i.e 0,3-0,4V/Angström) and the most favourable structure under this condition was determined. The authors believe that at a certain threshold level, the ring structure of water breaks up due to te realignment in the electric field. They state that this is the effect of an enhanced dipole moment of the linear molecules which interacts with the external electric field very strongly and is therefore the more stable configuration.

125-structure 09.12.2005 , T. Head-Gordon et al.

Tetrahedral structure or chains for liquid water

Summary:
This paper demonstrates excellent agreement of simulated structure factors with experimental x-ray structure factors (XAS) for both a static asymmetric hydrogen electron density model of water and a polarizable model of water. However, the TIP4P-pol2 polarizable model's excellent agreement with x-ray scattering structure factors over all Q indicates that no specific asymmetry persists and thus is consistent with tetrahedral structure signatures in intensities and analysis of ring statistics. It is stated that the charge asymmetry in water's electron density arises from symmetry- breaking environments that fluctuate rapidly on the femtosecondtimescale. The deduction from the XAS experiments and interpretation that asymmetry is a time-invariant feature of the hydrogen electron density means that liquid water should organize into strongly hydrogen-bonded water chains or large rings embedded in a weakly hydrogen-bonded disordered network. Although these instantaneous asymmetries may be seen in an XAS experiment , the long time scale (or ensemble) averages inherent in bulk structural experiments such as x-ray scattering tell us that they do not persist, as shown in this article. It is thus important to reconcile the XAS data with a symmetric charge density approximation to the fluctuating charge environments that still remains most compatible with the authors view of water as a tetrahedral hydrogen-bonded liquid.

126-structure 01.01.2006, D. Marx

Proton transfer processes in hydrogen-bonded networks

Summary:

The author gives an overview of actual research strategies in the field of hydrogen-bonding and water structure. He covers the early beginnings and their representatives in science, quantum mechanical thoughts and an possibility to solve existing problems with ab-initio methods. Particularly, the effect of biological molecules in water and ice in it's various configurations are mentioned in this work. All in all a good sum-up of state -of -the -art techniques accompanied by interesting schemes as well as free-energy profiles of hydrogen bonds depending on their temperature, pressure and distance to each other.

127-structure 20.01.2006, S.A. Hassan et al.

Effects of electric fields on proton transport through water chains

Summary:

Investigation of the transport of a single proton along a water chain through a carbon nanotube (CNT) with and without a perturbing electrical field (normal to the axis of the CNT) were systematically studied through QM/MM molecular dynamics simulations. The authors try to find out at which field strengths the imidazole ring at the one end of the CNT doesn't get protonated from the water cations on the other side of the CNT and what happens instead. They suggest that at 0,5V/Å protonation is inhibited due to a hydronium cation blocking the CNT "tunnel". In the low electric field regime(<0.5 V/Å) this competition leads to a relatively complex dynamics of the water molecules and excess charge. A back-and-forth motion of the charge is observed in all cases, spanning the entire chain but concentrated mainly in the middle of the nanotube. Theoretically one can say that at a distinct field strength the dipoles align themselves in the electric field rather than to keep water bridge bonds stable, thereby prohibiting any charge transport.

128-reaction 20.03.2006, B. Sun et al.

Characteristics of ultraviolet light and radicals formed by pulsed discharge in water

Summary:

In this investigation, the ultraviolet light characteristics and OH radical properties produced by a pulsed discharge in water were studied. Conclusion of the report is as follows: The ultraviolet light changed with the peak voltage and electrode distance. In addition, the properties of hydrogen peroxide and ozone were also studied under arc discharge conditions. Ultraviolet light and OH radicals were produced by the pulsed discharge in water. For the plate–rod reactor, the energy of the ultraviolet light is 3.2% of the total energy injected into the reactor. Many OH radicals, H2O2 and O3 were produced during the arc discharge in water. The intensity of the OH radicals was the highest for the 40mm electrode distance reactor. The state of the OH radicals was the ground state and the excited state when the pulsed arc discharge was generated. Hydrogen peroxide (H2O2) was effectively formed by both the streamer corona and spark discharge. The concentration of hydrogen peroxide increased with the input energy. Ozone was produced by the arc discharge even if oxygen gas is not bubbled into the reactor. The ozone concentration exists at a maximum value with the treatment time.

129-reaction 29.04.2006, F. de Baerdemaeker et al.

Hydrogen peroxide production in capillary underwater discharges

Summary:

The author experimented with AC voltage of 15 kV in an environment of a capillary underwater discharge in which plasma is generated due to submerged electrodes separated by a dielectric plate.

As analytical determining instrument a colorimetric method based on a specific reaction between Titanium and hydrogen peroxide was used. Results showed that the peroxide production is slightly higher at the high voltage side of the capillary and the initial formation of peroxide is correlated to the applied power. Effects of conductivity of the aqueous solution didn't play any role regarding k_{H2O2}, probably due to the increased H-bond cleavage and thereby decreased interaction between the dipoles (lower dielectric constant) of the water.

130-structure 30.06.2006, P. Toncoso et al.

Bound and trapped classical states of an electric dipole in a magnetic field

Summary:
The Article deals with the classical calculation of dipoles in an external magnetic field, not regarding any quantum effects. As a result a simple equation for the frequency of motion in the approximation of small oscillations is received. What is more an equation for trapped motion is found where are no turning points present and thereby permitting access to a range of values for the constant of motion.

131-pockels 01.08.2006, E. Tokunaga et al.

Pockels effect of water in the electric double layer at the interface between water and transparent electrode

Summary:
In this article it is stated to have found a proof for the Pockels (first-order electrooptic) effect in aqueous solutions, namely in the EDL (electronic double layer) interface region between water and a ITO (indium –tin-oxide, transparent, In2O3 doped with SnO2) electrode. A strong electrolyte solution, 0.1 M NaCl aqueous solution, was prepared from distilled water. Two ITO-electrodes were immersed in the solution filled in the glass cell. One electrode was grounded and AC voltage of 2 V (peak amplitude) was applied to the other at the frequency of f = 20–500 Hz. Measurements of the refractive index indicated a negative index change in the interface region. The result of theoretical and experimental analysis shows that most of the signal is caused by water in the EDL. The large anisotropy of the Pockels effect of water is deduced from the incidence angle dependence of the p-polarization signal. At the same time, the ITO shows a blue shift of the band gap in the UV due to the band population effect in the space charge layer. The plasma frequency in the near IR is also expected to increase due to the band population effect, since the ITO has a high doped carrier population close to metal. A negative refractive index change in the ITO space charge layer is induced from both effects, but its effect on the signal is estimated to be much smaller than that of the negative refractive index change of water in the EDL.

132-structure 17.09.2006, J. Mrázek et al.

Can the pH value of water solutions be estimated by quantum chemical calculations of small water clusters?

Summary:
In the study,various water clusters were explored from the point of view of the proton transfer between H-bonded neighbors. A relatively modest approach—the MP2/6-31+ +G(d, p) level—was chosen as acceptable considering the fact that also larger systems have to be included. The tight ion-pair model (with usually three fixed O–O distances) was adopted for the autodissociation process. The first thing that can be noticed is a fast pH decrease when cluster size increases from 2 to 6. For large clusters in gas phase, the topology of H bonds plays an important role, varying pH from 7 to 13 in hexamers or from 5 to 15 in octamer clusters. The important relationship between energy/distance was quantified (in the form of a linear equation) for the given method and basis set, which enables a fast estimation of pH values within the considered set of clusters. For larger

clusters, there is a great amount of the diverse ion-pair formation energies G_b. Since the 1/RT equals 1.6 kcal at 298 K, the weights of energetically distant local minima quickly become negligible. However, local minima may become significant for larger clusters. Moreover, considering the autodissociation process to be infinitely fast for some higher-lying cluster, the ratio of cluster distribution is changed and one can get out of equilibrium and thus outside the Boltzmann distribution. Enhancing this model with the COSMO approach brought significant improvement in the description of the autodissociation reaction with a stable hybrid-ionic structure, due to the price that the polarizable continuum model also smoothed the differences between various topologies and cluster families. Averaging the explored clusters in vacuum, the series of pH 25-18-14-13-10 was obtained in the range of dimer to octamer clusters. Using the COSMO approach, the same series is 15-14-12-10-9. That means that still two units from the experimentally known pH and probably larger clusters (by about 20 water molecules) are needed to reach the size-independent (bulk) value. However, the situation is far from hopeless since the 4_w type molecules are not involved in the autodissociation process which was demonstrated in this article.

133-structure 18.10.2006, T.D. Li

Structured and viscous water in subnanometer gaps

Summary:
Direct and simultaneous measurements of the normal and lateral forces encountered by a nanosize spherical silicon tip approaching a solid surface in purified water are reported. With experiments and grand canonical molecular-dynamics simulations the conclusion is gained that on hydophillic surfaces layering of the confined water density and the development of hexagonal order in layers proximal to a quartz surface is enhanced. For subnanometer hydrophilic confinement, the lateral force measurements show orders of magnitude increase of the viscosity with respect to bulk water, agreeing with a simulated sharp decrease in the diffusion constant. No viscosity increase is observed for hydrophobic surfaces.

134-structure 7.11.2006, C. Costentin et al.

Concerted Proton-Electron Transfer Reactions in Water. Are the Driving Force and Rate Constant Depending on pH when Water Acts as Proton Donor or Acceptor?

Summary:
The competition between stepwise and concerted (CPET) pathways in proton-coupled electrontransfer reactions in water is discussed on thermodynamic and kinetic bases.
(1)It is stated that concerted proton-electron oxidations involving water as proton acceptor may well compete favourably with electron first, proton second (ETPT) stepwise pathways. A necessary but not sufficient condition for this to happen is that the pK of the reduced form of the substrate is smaller than 0. This excess driving force has to be large enough for overcoming pre-exponential and reorganization factors that are somewhat unfavourable to the CPET pathways in the competition. The overall backward reaction rate includes the proton as a reactant and thereby leaves the rate constat for this process constant. (2)In the basic pH range, concerted proton-electron oxidations involving OH- as proton acceptor may similarly compete with proton first, electron second (PTET) stepwise pathways. The driving force of the reaction is likewise independent of pH. The overall oxidation rate constant is an increasing function of pH, not because the driving force varies with pH, but because OH- is one reactant of the forward process. Conversely, the rate constant of the backward reaction is independent of pH. The competition between such CPET-OH- reactions and the stepwise PTET process depends on the pK of the substrate being below or above 14. In the first case, the PTET pathway predominates. In the second, the CPET pathways may be the most favourable. (3)When the reactions are carried out in a buffered medium, basic components of the buffer may serve as proton acceptor in a CPET mechanism. The excess driving force thus provided

may make the CPET pathway predominant over the stepwise pathways. (4) The above conclusions are based on first principles. It follows that interpretations of previous experimental data based on the incorrect notion that the driving force of CPET-H2O reactions depends on pH 5 should be revised.

135-structure 05.01.07, J.M.J. Swanson et al.

Proton Solvation and Transport in Aqueous and Biomolecular Systems: Insights from Computer Simulations

Summary:

The authors developed a usable methodology to investigate characteristics of proton solvation and transport mechanisms in different aqueous solutions and in interface areas. They examined lots of biomolecular systems and from these try to deduce a general pattern of proton transport. MS-EVB (multi state - empirical valence bond) enables a variety of structural calculations to finally understand the charge defect associated with excess protons, but the assembling picture seems to be incomplete yet.

136-structure 26.03.07, R. Vacha et al.

Autoionization at the surface of neat water: is the top layer pH neutral,basic, or acidic?

Summary:

Numerous experiments show a different character of surface water areas in macroscopic and microscopic respect. macroscopic experiments, such as zeta potential and titration measurement show a hydroxide enriched surface area, whereas recent molecular simulations and spectroscopic experiments show a hydronium enriched surface area. With simulations the authors tried to identify low energy structures of water, they undertook isolated D2O exchanges on surface areas of ice and nanocrystalls and they took out measurements of charged air bubbles and oil droplets in water and their subsequent effects on the water surface area. Methods of choice were spectrometric ones (VSFG, SHG, IR, ion scattering) in diluted solutions as well as zeta-potential measurements in emulsions.

137-structure 27.04.07, T. Yamamoto et al.

The interacting electrostatic charge model on the shape formation of monolayer domains at the air–water interface comprised of tilted dipoles with orientational deformation

Summary:

The contribution of orientational deformation to the electrostatic energy due to the dipole–dipole interaction has been analysed for the study of monolayer domain shapes. The orientational order parameters $Sn \equiv [P_n(\cos\theta)]$ have been introduced to represent the orientational structure of monolayers, where $Pn(\cos\theta)$ is the Legendre polynomials of n-th rank. A monolayer domain is viewed as a system of interacting induced charges, and electrostatic energy is rewritten in terms of the interaction between induced charges. The electrostatic energy is further expanded by the curvature of boundary curve, and is expressed as the Frank splay elastic energy with spontaneous splay and curvature elastic energy with spontaneous curvature, where they are analogous to the free energy of phenomenological theory by Rudnick and Bruinsma .This theoretical approach is useful to investigate the orientational deformation and domain shapes from the viewpoint of the electrostatic energy, based on x-ray diffraction measurements of earlier researchers.

138-reaction 18.05.07, L. Holysz et al.

Effects of a static magnetic field on water and electrolyte solutions

Summary:
Experiments concerning the conductivity as well as the partial pressure of water under standard conditions were undertaken in this article using several mixtures of inorganic salts and a permanent magnet (15mT). They compared physical values of after a period of time . Mainly the authors tried to prove the connection between the exposure time of water to a MF (magnetic field) or EMF (electromagnetic field) with changes of the solubility of the ions within. They used PE (polyethylen) vessels in which they poured their test water and the reference water. In the cylinder (6cm diameter, 50 cm height) they put a magnet with a PE coating and tested the physical properties (Hydration energy, Gibbs- Free enthalpy, heat capacity) against a cylinder in which no magnetic device was put. They suggest that due to a magnetic input to the solvation shell of the ions the hydrating water structure is changed, but no systematic approach or mechanism is given.

139-reaction 11.06.07, S Mededovic et al.

Primary chemical reactions in pulsed electrical discharge channels in water

Summary:
A mathematical model for the primary chemical processes occurring in 1 J/pulse electrical discharges in water was developed in this article. The concentration and temperature profiles inside the discharge channel as well as a general scheme for the water dissociation and molecular species formation are also reported. The model assumes that the discharge channel is composed of two sequentially coupled zones: the core and the recombination region. It simulates the experimentally measured values of molecular hydrogen, oxygen, hydrogen peroxide and hydroxyl radicals very closely. Based on the set of reactions considered, the model predicts that of all the molecular hydrogen found at the end of the pulse, 79% is formed in the core at high temperature, 21% is formed in the recombination region and that the main reaction for hydrogen formation is the recombination of hydrogen atoms. Hydrogen peroxide is formed in the recombination region via recombination of hydroxyl radicals. In the core 47% of the oxygen is formed by reactions between oxygen radicals and hydroxyl radicals. the recombination of oxygen radicals is not the major pathway for molecular oxygen formation as in the case of hydrogen. Approximately 53% of the total oxygen found at the end of the pulse is formed in the core whereas the other 50% is formed in the recombination region. In the latter region 20% of the molecular oxygen is formed by the same mechanism as in the core (reaction between hydroxyl and oxygen radicals) and 33% is formed via reaction of hydroperoxy radicals and hydroxyl radicals.

140-structure 12.06.2007, A. Klimov et al.

Visualization of charge-carrier Propagation in water

Summary:
The article' s main topic is the separation of OH^- and H^+ clouds as they occur in aqueous, salty and intercellular solutions. Method of choice was an indicator dye in a solution in which two vertically or horizontally platin electrodes were submerged and supplied with low current (up to 4,3 V and 25 μA). As a result they found out that up to 3 hours areas of 3 different pH- values grew around the electrodes without any mixing effects taking place. One very low around the positive electrode, one very high around the negative electrode and one thin layer between them with the average value of low and high. Even after current was stopped and a resistive load was placed in the electric circuit instead, the areas did not mix much, but current was driven through the resistive load. Interestingly, in salty solutions the process was generally faster and differed at the cathode area to that in distilled water: A finger- like protuberance stretched towards the anode area and increased in volume after

time. This phenomenon is believed to take place in all physiological solutions. Other characteristics were similar to that in distilled water. The question arose if those zones of distinct pH values are stable due to a matrix in which semiconductor properties are featured, or if there are some kind of counter-ions which are “invisible” to the applied current.

141-structure 13.08.2007, J.L. England et al.

Theory for an order-driven disruption of the liquid state in water

Summary:

Main topic of this article is any configurational change of the density of water by applying strong electric fields (up to 6V/nm). The study is based on a theoretical thesis which is supported by a Hamiltonian operator in which only simple physics participate. The emerged nonpolarizable, non-ionizable model of water made the authors understand why at certain values of an electric field (Graphite plates were used) water expands whereas at similar values it contracts. It is stated that different chemical potentials and a different state of the coupled water molecules could be the reason for the different outcome of both experiments. (“Vaitheeswaran et al.” vs. “Bratko and Luzar”). The simple physical argument for this character is : every field-driven reduction of the conformational entropy of molecules reduces their interaction with their neighbours, resulting in an destabilizing effect on the liquid state due to the ambition of the molecules to increase their own enthalpy e.g. with the transition to another aggregate state.

142-structure 06.09.2007, J.K. Beattie

Comment on Autoionization at the surface of neat water: is the top layer pH neutral, basic, or acidic?

Summary:

The author of this article argues that the article published by Robert Va´ cha, Victoria Buch, Anne Milet, J. Paul Devlin and Pavel Jungwirth is invalid due to the fact that their measurements were taken out in highly acidic solutions in which it is known that the isolelectric point of water itself in interface areas (published by Exerowa) is higher. He comes to the conclusion that there cant be an acidic layer on the surface of water films and that the article he comments on assumes ionic concentrations which on the one hand cant be extrapolated to near neutral water and on the other hand doesn’t imply a controversial point of view to the actual state of the art of scientific knowledge.

143-structure 24.09.2007, R. Vacha et al.

Response to Comment on Autoionization at the surface of neat water:is the top layer pH neutral, basic, or acidic?

Summary:

As a reply on a given comment this article states that there is no proof for an increased autoionization of water at surface or interface areas. The possible systematic errors made in the foregoing work could depend on the electrolyte concentration, respectively could be a result of a false ab-initio calculation of an infinite-diluted solution. Numerous errors may even occur in interpretation of the data, but as far as the author believes water has a stronger autoionizaion at interface areas so Hydronium ions concentrate on the top level surface of liquids whereas hydroxide ions are in the layer below the cations.

144-structure 02.11.07, G. Xie et al.

Micro-Bubble Phenomenon in nanoscale water-based lubricating film induced by external electric field

Summary:

The effect of an high voltage external electric field (EEF) on water-based thin films has been investigated in this article. It is shown that with the increase of molecular weight of PEG solution, the threshold EEF intensity for micro-bubble emerging increases, but there is
a reverse trend when the molecular weight reaches 10,000 Da, and micro-bubbles in the film of PEG solutions with higher concentration are more difficult to generate due to the reduction of the polarity. The overheating effect plays a significant role in micro-bubble emerging. Microbubble can be easier to be induced when the steel ball was applied with negative potential, and electronic process is used to account for it. The EEF intensity has great influence on the micro-bubbles' amount and intensity in water film, and as time progresses, the micro-bubbles gradually disappear.

145-reaction 15.11.2007, Y.-M. Jung et al.

Electrical charging of a conducting water droplet in a dielectric fluid on the electrode surface

Summary:
In this study, electrical charging of a water droplet at the electrode has been studied. To estimate the amount of charge, the moving velocity of a droplet in the middle region of the electrode cell is measured. Under the assumption that the droplet has a spherical shape and follows the Stokes law, the measured velocity is used to estimate the charge amount by using the force balance. The experimental results show that the electric field strength and the droplet size are the important key factors to the electrical charging process. On the other hand, the viscosity of the medium fluid does not have a significant effect in the parameter range of the present study. The experimental results are summarized in the form of a scaling law. In the scaling law, the amount of electrical charging of a water droplet is proportional to the power 1.59 of the droplet radius and the power 1.33 of the electric field strength. In the case of a perfect conductor sphere, the charge is proportional to the square of radius (the power 2) and proportional to the electric field (the power 1). In order to understand these fundamental differences, numerical computations have been performed for the (idealized) perfect conductor droplets with predefined shapes (experimentally obtained shapes, prolate shapes, and spherical shapes). The numerical results reveal an important fact. Perfectly conducting droplets (even with the deformed shapes) follow the scaling law in which the charge amount is proportional to the square of the radius and proportional to the electric field just like the well-known theoretical result for a perfect conductor sphere. So, the fundamental differences are due to other reasons such as the ionization reaction at the electrode and the relatively low electrical conductivity of the water droplet.

146-structure 08.01.2008, B.M. Weon et al.

Stable freestanding thin films of pure water

Summary:
This article discusses the possibility to produce ultra pure water films in capillaries due to x-ray bombardment. The authors put a micron litre of 18 M-Ω ultrapure water into a capillary and fired with a PLS synchrotron source x-ray photons with an energy between 10-60 keV on the capillary. In this way a stable film is produced in which the capillary pressure equals the sum of the van de Waals force and the repulsive double- layer electrostatic force. The second factor is mainly believed to be accountable for the stability because the electrostatic force "works" against the surface tension. (see equations in the text).Surprisingly, the produced water film was stable for about 60 min before it ruptured. X-ray radiation is believed to be a surrogate for electrolytes in the film stabilization.

3. References:

Jets:

1:J. Zeleny, 'Instability of electrified liquid surfaces', sec. Series, Vol.X., No.1, 1917
2:G.Taylor, 'Disintegration of water drops in an electric field', Proc. Roy. Soc. A.. Vol. 280. plate 24, pp. 383-397,1964
3:J. Latham, I.W. Roxburgh, 'Disintegration of Pairs of Water Drops in an Electric Field', Proceeding of the Royal Society of London. Ser. A., Mathematical and Physical Sciences, Vol. 295, No. 1440, pp. 84-97, 1966
4:Y.G.Eliseev, G.S.Pogosov, 'Stability of a liquid-dielectric jet in a longitudinal electrostatic field', Izvestia VUZ. Fizika, Vol. 11, No.7, pp. 134-137,1968
5:R. J. Turnbull, J. R. Melcher, 'Electrohydrodynamic Rayleigh-Taylor Bulk Instability', NASA CR 97784, Continuum Electromechanics Group, 1968
6: D.C. Jolly, J.R. Melcher, 'Electroconvective instability in a fluid layer', CSR-TR-69-2, NASA CR 100455, Center for Space research, MIT, 1969
7: A.H. Nayfeh, 'Nonlinear stability of a liquid jet', The physics of fluids, Vol. 13, No. 4, 1969
8: H.C.Lee, 'Drop formation in a liquid jet', IBM J. Res. Develop., 1973
9: K.C. Chaudhary et al., L.G. Redekopp, 'The nonlinear capillary instability of a liquid jet', J . Fluid Mech. (1980), vol. 96, part. 2, pp. 267-274, 1978
10: K. Varga et al., R.S. Seymour, 'Observation of electrical effects with cavitating liquid flow', J. Phys. D: Appl. Phys. 19, 2293-2300, 1986
11: D.P.H. Smith, 'The Electrohydrodynamic Atomization of Liquids', IEEE Transactions on industry applications, Vol. IA-22, No. 3, 1986
12:N. Ashgriz et al., F. Mashayek, 'Temporal analysis of capillary jet breakup', J . Fluid Mech. (1995), 001. 291, pp. 163-190, 1993
13: A. A.Naqwi et al., R.P. A. Hartman, J.C.M. Marijnissen, 'Basic Studies of Electrohydrodynamic Atomization Process Using Phase Doppler Measurement Technique',Part. Part. Syst. Charact. 13 (1996) 143-149, 1995
14: A. Ajdari, 'Generation of transverse fluid currents and forces by an electric field: Electro-osmosis on charge-modulated and undulated surfaces', Physical review E, Vol. 53, No. 5, 1995
15:J.M.Sun et al., R. Tao, 'Shear flow of one-component polarizabel fluid in a strong electric field', Physical Review E, Vol. 53, No.4, 1995
16:A. M. Ganan-Calvo, 'On the theory of electrohydrodynamically driven capillary jets', J. Fluid Mech. (1997), vol. 335, pp. 165-188, 1995
17:K. Zakaria, 'Nonlinear instability of a liquid jet in the presence of an uniform electric field', Fluid Dynamics Research 26 (2000), pp.405-420, 1996
18: R.P.A Hartman J-P. Borra, J.C.M. Marijnissen, B. Scarlett, 'Developement of electrohydrodynamic sprays related to space charge effects', J.Aerosol Sci., Vol.27, Suppl. 1, pp. 177-178, 1996
19:D.A. Saville, 'ELECTROHYDRODYNAMICS: The Taylor-Melcher Leaky Dielectric Model', Annu. Rev. Fluid Mech. 29:27–64, 1997
20:J.S.Turner, 'G. I. Taylor in his later years', Annu. Rev. Fluid Mech., 29:1-25, 1997
21:R.P.A. Hartman et al., J.C.M. Marijnissen, B. Scarlett, 'Electro Hydrodynamic Atomization in the cone-jet mode. A physical model of the liquid cone and jet', J. Aersol Sci. Vol.28, Suppl.1, pp.227-228, 1997
22:A. Beroual,.M. Zahn, A. Badenti et al., 'Propagation and Structure of Streamers in liquid Dielectrics', Electrical Insulation Mag., IEEE, Vol. 14, No. 2, 1998
23:D. J. Brunner, R. P. A. Hartmand D. M. A. Camelot, J. C. M. Marijnissen, B. Scarlett, 'Electrohydrodynamic atomization in the cone-jet mode: Physical modeling of the liquid cone and jet', J. Aerosol Sci. Vol. 30, No. 7, pp. 823-849, 1998
24:R.P.A. Hartman et al., D. J. Brunner, D. M. A. Camelot, J. C. M. Marijnissen, B. Scarlett, 'Jet break-up in electrohydrodynamic atomization in the cone-jet mode', J. Aerosol Sci. Vol. 31, No. 1, pp. 65-95 , 1998
25:A.M. Ganan-Calvo, 'The Surface Charge In Electrospraying: Its Nature and Its Universal Scaling Laws', J. Aerosol Sci. Vol. 30, No. 7, pp. 863-872, 1998
26:D.M.A Camelot, D. Brunner, R.P.A Hartman, J.C.M Marijnissen, B. Scarlett, 'Mechanisms of jet break-up for EHDA in the conejet mode', J. Aerosol Sci. Vol. 29. Suppl. I, pp. 841-842, 1998
27:R.P.A. Hartman et al., J.-P. Borra, D.J. Brunner, J.C.M. Marijnissen, B. Scarlett, 'The evolution of electrohydrodynamic sprays produced in the cone-jet mode, a physical model', Journal of Electrostatics 47 (1999), pp.143-170, 1998
28:V. G. Suvorov et al., E.A. Litvinov, 'Dynamic Taylor cone formation on liquid metal surface: numerical modelling', J. Phys. D: Appl. Phys. 33 (2000), pp.1245–1251, 1999
29:T. Sugimoto et al., K. Asano, Y. Higashiyama, 'Negative corona discharge at a tip of water cone deformed under dc field', Journal of Electrostatics 53 (2001), pp.25–38, 2000
30: Y. Higashiyama et al., S. Yanase, T. Sugimoto, 'DC corona discharge from water droplets on a hydrophobic surface', Journal of Electrostatics 55 (2002), pp.351–360, 2000

32:J. Wei et al., W. Shui, F. Zhou, Y. Lu, K. Chen, G. Xu, P. Yang, 'Naturally and externally pulsed Electrospray', Mass Spectrometry Reviews Vol. 21, Issue3 , pp.148-162, 2002
99:T. Aka-Ngnui et al., A. Beroual, P. Auriol, 'A Predicting Model for Branching Streamers Propagating in Liquid Dielectrics using a Computation Electrical Network', ICDL 2002, Graz, July 7-12, 2002
33:M. Seipenbusch et al., J.van Erven, T. Schalow, A. P. Weber, A.D.van Langeveldd, J.C.M. Marijnissen, S.K. Friedlander, 'Catalytic soot oxidation in microscale experiments', Applied Catalysis B: Environmental 55 (2005), pp.31–37, 2004
34:H.Kawamoto et al., S. Umezu, 'Electrohydrodynamic deformation of water surface in a metal pin to water plate corona discharge system', J. Phys. D: Appl. Phys. 38 (2005) 887–894, 2004
35:J. van Erven et al., R. Moerman, J. C. M. Marijnissen, 'Platinum Nanoparticle Production by EHDA', Aerosol Sci. a. Tech.,39:10, pp. 941- 946,2004
36:M. Gunji et al., M. Washizu, 'Self-propulsion of a water droplet in an electric field', J. Phys. D: Appl. Phys. 38 (2005) 2417–2423, 2005
37:S.Castro et al., R.Bocanegra, 'Water-based compund Taylor coned held in vacuum: Feasabillity and application to colloidal Propulsion', Appl. Phys. Letters. 88, 123105 (2006), 2005
38:Z. Guan et al., L. Wang, B. Yang, X. Liang, Z. Li, 'Electric Field Analysis of Water Drop Corona', IEEE Transactions on power delivery, Vol. 20, No. 2, 2005
39:L. Sirghi et al., R. Szoszkiewicz, E. Riedo,'Volume of a Nanoscale Water Bridge', Langmuir, 22, pp.1093-1098, 2005
40:N. Dubash ,A. J. Mestel, 'Behaviour of a conducting drop in a highly viscous fluid subject to an electric field', J. Fluid Mech. (2007), Vol. 581, pp. 469–493, 2005
41:G. S. Sarkisov et al., N. D. Zameroski and J. R. Woodworth, 'Observation of electric field enhancement in a water streamer using Kerr effect', J.of Appl. Phys. 99 (2006), 083304, 2005
42:M. E. Kuil et al., J. P. Abrahams , J. C. M. Marijnissen, 'Nano-dispensing by electrospray for biotechnology' , Biotechnol. J. 2006, 1, 969-975, 2006
43: J. Qian et al., R.P. Joshi, , K.H. Schoenbach, J. R. Woodworth, G. S. Sarkisov, 'Model Analysis of Self- and Laser-Triggered Electrical Breakdown of Liquid Water for Pulsed-Power Applications', IEEE transactions on plasma science, (2006), Vol. 34, No. 5, 2005
44:J. F. de la Mora, 'The Fluid Dynamics of Taylor Cones', Annu. Rev. Fluid Mech. .39:217-243, 2007
45:N. Kasayapanand, 'Numerical modeling of natural convection in partially open square cavities under electric field', International Communications in Heat and Mass Transfer 34 (2007) 630–643, 2007
46:P. Bruggeman et al., L. Graham, J. Degroote, J. Vierendeels, C. Leys, 'Water surface deformation in strong electrical fields and its influence on electrical breakdown in a metal', J. Phys. D, Appl. Phys. 40 (2007), pp.4779–4786, 2007
47:X. P. Lu, 'One-dimensional bubble model of pulsed discharge in water', J. Appl. Phys. 102, 063302, 2007
48: J. Eggers et al., E. Villermaux, 'Physics of liquid jets', Rep. Prog. Phys. 71 (2008) 036601 (79pp), 2007

QEHD

49:J. Zeleny, 'The electrical discharge from liquid points, and a hydrostatic method of measuring the electric intensity at their surfaces', Physical Review, Sec. Series, Vol. III, No.2, 1914
50:J. Kendall, 'The specific conductivity of pure water in equilibrium with carbon dioxide', Journ. Am. chem. Soc. 38, 1916
51:H. D. Carter et al., A. N. Campbell, 'Electric discharges in liquids. Part I The arc discharge in water.',Trans. Faraday Soc., Vol. 28, pp.634 – 644, 1932
52:A. von Hippel, 'The Dielectric Relaxation Spectra of Water, Ice, and Aqueous Solutions,and their Interpretation, 1. Critical Survey of the Status-quo for Water', Tech. Rep. 1, L.I.R., M.I.T, 1967
53:A. von Hippel, 'The Dielectric Relaxation Spectra of Water, Ice, and Aqueous Solutions,and their Interpretation, 2. Tentative Interpretation of the Relaxation Spectrum of Water in the Time and Frequency Domain', Tech. Rep. 2, L.I.R., M.I.T, 1967
54:A. von Hippel, 'The Dielectric Relaxation Spectra of Water, Ice, and Aqueous Solutions,and their Interpretation, 3. Proton Organization and Proton Transfer in Ice', Tech. Rep. 3, L.I.R., M.I.T, 1968
56:E. C. Cassidy et al., R. E. Hebner, M. Zahn, R. J. Sojka, 'Kerr-Effect Studies of an Insulating Liquid Under Varied High-Voltage Conditions', IEEE Transactions on electrical insulation, Vol. EI-9, No. 2, 1974
57:M.J. Aroney et al., M. R . Battaglia, R. Ferfoglia, D. Millar, R. .K. Pierens, 'The Kerr Constant of Water and other Pure Liquids at 633 nm', J. Chem. Soc., Faraday Trans. 2, 1976, 72, 724-726, 1975
58:R. K. Khanna et al., E. Dempsey, G. P. Jones, 'An apparatus for Kerr effect measurements in water and conduction liquids', J. Phys. E: Sci. Instrum., Vol. 11, 1977
59: M. S. Beevers et al., G. Khanarian, 'Measurement of Kerr Constants of Conducting Liquids', Aust. J. Chem., 1979, 32, 263-9, 1978
60:A. H. Sharbaugh et al., J. C. Devins and S. J. Rzad, 'Progress in the field of electric breakdown in dielectric liquids', IEEE Trans. Electr. Insul. Vol EI-13 No 4, 1978
61:M. Zahn et al., S. Voldman , T. Takada, D.B. Fenneman, 'Charge injection and transport in high voltage water/glycol capacitors', J. Appl. Phys., Vol. 54, No.1, 1982

62:M.Zahn et al., T. Takada, S. Voldman, 'Kerr electro-optic field mapping measurements in water using parallel cylindrical electrodes', J.appl. Phys., Vol. 54, No. 9, 1982
63:M. Zahn et al., T. Takada, 'High voltage electric field and space-charge distributions in highly purified water', J. Appl. Phys., Vol. 54, No.9, 1982
64:M. Zahn et al., Y. Ohki, K. Rhoads, M. LaGasse, H. Matsuzawa, 'Electro-optic charge injection and transport measurements in highly purified water and water/ethylene glycol mixtures', IEEE Transactions on Electrical Insulation Vol. EI-20 No.2,1985
65:G. Colacicco, 'Electrical potential of the water surface', Chemica Scripta, 28, pp. 141-144, 1986
66:J. S. Clements et al., M.Sato, R. H. Davis, 'Preliminary Investigation of Prebreakdown Phenomena and Chemical Reactions Using a Pulsed High-Voltage Discharge in Water', IEEE Transactions on industry applications, Vol. IA-23, No. 2, 1987
67:S. Palese et al., L. Schilliig, R. J. D. Miller,P . R. Staver , W. T. Lotshaw, 'Femtosecond Optical Kerr Effect Studies of Water', J. Phys. Chem. , 98**,** 63086316**,** 1994
68:M. Zahn, 'Transform Relationship between Kerr-effect Optical Phase Shift and Nonuniform Electric Field Distributions', IEEE Transactions on Dielectrics and Electrical Insulation Vol. 1 No. 2, 1994
69:A.A.Joshi et al., B.R.Locke, P. Arce, W.C.Finnev, 'Formation of Hydroxyl radicals, hydrogen peroxide and aqueous electrons by pulsed streamer corona discharge in aqueous solution', J. of Hazardous Materials 41 (1995) 3-30, 1994
70:J. H. Jensen et al., M. S. Gordon, 'Ab Initio Localized Charge Distributions: Theory and a Detailed Analysis of the Water Dimer-Hydrogen Bond', J. Phys. Chem. 1995, *99,* 8091-8107, 1994
71:S. Curilef et al., F. Claro, 'Dynamics of interacting particles in a magnetic field in two dimensions', Am. J. Phys. 65, No.3, 1995
72:N. Agmon, 'The Grotthuss mechanism', Chem. Phys. Lett. 244, pp.456-462, 1995
73**:**A. El Magd A. Mohamed et al., E. F.A. Elshehawey, Y. O. El-Dib, 'Electroviscoelastic Rayleigh-Taylor instability of Kelvin fluids. Effect of a constant tangential electric field', Fluid Dyn. Res. 19, pp.327-341,1995
74:S. M. Pimblott et al., J. A. LaVerne, A. Mozumder, 'Monte Carlo Simulation of Range and Energy Deposition by Electrons in Gaseous and Liquid Water', J. Phys. Chem. (1996)**,** 100*,* 8595-8606, 1995
75:D.G. Frood et al., T.J.Callagher, 'Space-charge dielectric properties of water and aqueous electrolytes'**,** Journal of Molecular Liquids 69 183-200, 1996
76:A. Üstündag et al., T. J. Gung, M. Zahn, 'Kerr Electro-Optic Measurement Technique For Determination of Nonuniform Electric Fields', ICDL '96 12th Intemational Conference on Conduction and Breakdown in Dielectric Liquid, 1996
77:B. Sun et al., M. Sato , J. S. Clements, 'Optical study of active species produced by a pulsed streamer corona discharge in water', Journal of electrostatics 39 (1997), pp. 189-202, 1996
78:B. Sun et al., M. Sato, A. Harano, J.S. Clements, 'Non-uniform pulse discharge-induced radical production in distilled water', Journal of Electrostatics 43 (1998) 115Ð126, 1997
79:G. Sutmann,'Structure formation and dynamics of water in strong external electric fields', Journal of Electroanalytical Chemistry 450 (1998) 289–302, 1997
80: M. Kurahashi et al., S. Katsura, A. Mizuno, 'Radical formation due to discharge inside bubble in liquid', Journal of electrostatics 42, pp. 93-105, 1997
81:C.A. Chatzidimitriou-Dreismann et al., T. Abdul-Redah,R.M.F.Streffer, J.Mayers, 'Anomalous deep inelastic neutron scattering from liquid H2O-D2O', Physical Review letters, Vol. 79, No. 15, 1997
82:M. Kristiansen et al., L.L. Hatfield, 'High voltage water breakdown studies', Defense Special Weapons Agency, VA 22310-3398, Department of Electrical Engineering, DSWA-TR-97-30, 1998
83:S.N.Komin et al., E.A. Morozov, 'Electro-optic study of prebreakdown processes in deionized water', 3rd international conference on properties and Applications of dielectric materials, 1998
84:H.C. Allen et al., D.E. Gragson, G.L. Richmond, 'Molecular structure and absorption of Dimethyl sulfoxide at the surface of aqueous solutions', J.Phys.chem. B,103,pp. 660-666,1998
85:D. H. Jung et al., J. H.Yang , M. S. Jhon, 'The effect of an external electric field on the structure of liquid water using molecular dynamics simulations', Chemical Physics 244 1999. 331–337, 1998
86: C. E. Dykstra, 'External electric field effects on the water trimer', Chemical Physics Letters 299 (1999). 132–136, 1998
87:Y. Ohki et al., Y. Ebinuma, S. Katakai, 'Space Charge Formation in Water-treed insulation', IEEE Transactions on dielectrics and Electrical Insulation Vol. 5 No. 5,1998
88:D.V. Tikhomolov et al., O.N. Slyadneva, 'Estimating the orientation component of stationary water dipoles in constant electric fields', International Journal of Multiphase Flow 26 (2000) 1891-1903, 1998
89:S.T Bramwell, 'Ferroelectric ice', Nature, Vol. 397, pp.211-212, 1999
90:M.Taut, 'Two particles with opposite charge in a homogenous magnetic field: particular analytical solutions of the two dimensional Schrödinger equation', J. Phys. A: Math. Gen. 32 (1999) 5509–5515, 1999
91:D. Marx et al., M.E.Tuckermann, J.Hütter, M. Parrinello, 'The nature of the hydrated excess proton in water', Nature, Vol. 397, pp. 601-604, 1999

92:J.T. Hynes, 'The protean proton in water', Nature, Vol. 397, pp.565-566, 1999
93:T.T. Truong et al., D. Bazzali, 'Exact low-lying states of two interacting equally charged particles in a magnetic field', Physics Letters A 269 (2000). 186–193, 1999
94:C. A. Angell et al., R. D. Bressel, M. Hemmati, E. J. Sarec and J. C. Tucker, 'Water and its anomalies in perspective : tetrahedral liquids with and without liquid-liquid phase transitions', Phys. Chem. Chem. Phys., 2, pp.1559-1566, 2000
95:A.A. Rashin et al., I.A. Topol, G.J. Tawa, S.K. Burt, 'Charge distributions in water and ion-water clusters', Chem. Phys. Letters 335 (2001), pp.327-333,2000
96:T. Toyoda et al., S. Mukai, Y. Ohki, Y.Li, T. Maeno, 'Estimation of conductivity and permittivity of water trees in PE from space charge distribution measurements', IEEE Transactions on dielectrics and electrical insulation, Vol. 8, No.1, 2001
97:S. V. Shevkunov et al., Al. Vegiri, 'Electric field induced transitions in water clusters', J. Of molecular Structure (Theochem) 593 (2002), pp.19-32, 2001
++:B.F. Bolund et al., M. Berglund, H. Bernhoff, 'Dielectric study of water/methanol mixtures for use in pulsed-power water capacitors', Appl. Phys. , Vol. 93, No. 6, 2002
31:A. T. Sugiarto et al., S. Ito, T. Ohshima,M. Sato, J. D. Skalny, 'Oxidative decoloration of dyes by pulsed discharge plasma in water', Journal of Electrostatics 58 (2003), pp.135–145, 2002
98:M. E. Tuckermann et al., D. Marx, M. Parinello, 'The nature and transport mechanism of hydrated hydroxide ions in aqueous solution', NATURE | Vol. 417, pp. 925-929, 2002
100: M. Zahn et al., A. Ustiindag; replied by H. Ihori, M. Fujii and K. Arii, 'Optical Measurement of Non-uniform Electric Field Vector Distribution in a Dielectric Liquid Using Triplet Measurement System', IEEE Transactions on Dielectrics and Electrical Insulation Vol. 9, No. 6, 2002
101:Z.-M. Dang et al. , D.-M. Tu , C.-W. Nan, 'Space Charge Distribution in Polyethylene due to the Water Diffusion', Proceedings of the 7th Intemational Conference on Prop. and Appl. of Dielectric Materials, pp. 654-657, 2002
102: L. Rey, 'Thermoluminescence of deuterated amorphous and crystalline ices', Radiation Physics and Chemistry 72 (2005) 587–594, 2003
103:C.A. Chatzidimitriou-Dreismann et al., M.Vos, C. Kleiner,. T.Abdul-Redah, 'Comparison of neutron and electron compton scattering from entangled protons', PRL , Vol. 91, No. 5, 2003
104:A. M. Anpilov et al., E. M. Barkhudarov, I. A. Kossyi, M. I. Taktakishvili, N. Christofi, Yu. V. Zadiraka, 'The effectiveness of a multi-spark electric discharge system in the destruction of microorganisms in domestic and industrial wastewaters', J. Of Water and Health, 02.4, pp.267-277, 2004
105:C.A. Chatzidimitriou-Dreismann , 'Wo ist der Wasserstoff?', Nachrichten aus d. Chemie, 52, pp.773-776, 2004
106: M. S. Skaf et al. , M. T. Sonoda, 'Optical Kerr Effect in Supercooled Water', PRL 94, 137802 (2005), 2004
107:B.C.Garett et al., Curt Wittig et al. , 'Role of water in electron-initiated processes and radical chemistry', Chem. Rev. 2005, 105, pp. 355-389, 2004
108:Y. Meng et al., B. Hu, Q. Chang, 'Control of local friction of metal/ceramic contacts in aqueous solutions with an electrochemical method', Wear 260 (2006) ,pp.305–309, 2004
109:M. Sharma et al.,R. Resta, R. Car, 'Intermolecular Dynamical Charge Fluctuations in Water: A Signature of the H-Bond Network', PRL 95,(2005), 187401, 2004
110:M. T. Sonoda et al., S. M. Vechi , M. S. Skaf, 'A simulation study of the optical Kerr effect in liquid water', Phys.Chem.Chem. Phys ., 2005 , 7 , pp. 1176-1180, 2004
111:M.J Kirkpatrick et al., B.R. Locke, 'Hydrogen, Oxygen and hydrogen peroxide formation in aqueous phase pulsed Corona electrical discharge', Ind. Eng. Chem. Res. 2005, 44, 4243-4248, 2004
112:E.Stanley et al., S.Buldyrev, G.Franzese, N. Giovambattista, W. Starr, 'Static and dynamic heterogenities in water', Phil. Trans. R. Soc. A (2005) 363, 509–523, 2004
113:G. S. Sarkisov et al., J. R. Woodworth, 'Measurement of the current in water discharge using magneto-optical Faraday effect', J. Appl. Phys. 99,(2006), 093307, 2005
114:R. Szoszkiewicz et al., E. Riedo, 'Nucleation Time of NanoscaleWater Bridges', PRL 95, 135502, 2005
115:V. M. Kozhevnikov et al., I. Yu. Chuenkova, M. I. Danilov, S. S. Yastrebov, 'Self-Organization in a Layer of Magnetic Fluid in Strong Electric Fields', Technical Physics Letters, Vol. 31, No. 11, pp. 932–933, 2005
116:S. S. Iyengar et al., M. K. Petersen, T. J. F. Day, C. J. Burnham, V. E. Teige, G. A. Voth, 'The properties of ion-water clusters. I. The protonated 21-water cluster', J. Chem. Phys. 123, 084309, 2005
117:Z.G.Chiragwandi et al., O.Nur, M.Willander, I.Panas, 'Vortex rings in pure water under static external electric field', Appl. Phys. Letters 87, 153109, 2005
118:A. Moukengué Imano et al. , A. Beroual, 'Deformation of water droplets on solid surface in electric field', Ultramicroscopy 106 (2006) 909–913, 2005
119:J.D. Eaves et al., J. J. Loparo, C. J. Fecko, S. T. Roberts, A. Tokmakoff, P. L. Geissler, 'Hydrogen bonds in liquid water are broken only fleetingly', PNAS Vol. 102, No. 37, pp. 13019-13022, 2005
120: T. Head-Gordon et al., M. E. Johnson, 'Unified description of temperature-dependent hydrogen-bond rearrangements in liquid water', PNAS , Vol. 102 , No. 40 , pp. 14171–14174 , 2005
**:C.J. Burnham et al., M.K. Petersen, T. J. F. Day, S. S. Iyengar, G. A. Votha, 'The properties of ion-water clusters. II.

Solvation structures of Na^+, Cl^-, and H^+ clusters as a function of temperature', J.Chem. Phys. 124, (2006), 024327, 2005
121:S.J.Suresh et al., A.V. Satish, A. Choudhary, 'Influence of electric field on the hydrogen bond network of water', J. Chem.Phys. 124, (2006), 074506, 2005
122:J. Xie et al., J.C.M. Marijnissen, C.-H. Wang, 'Microparticles developed by electrohydrodynamic atomization for the local delivery of anticancer drug to treat C6 glioma in vitro', Biomaterials 27 (2006), pp. 3321–3332, 2005
123:S.F. Lyuksyutova et al., P.B. Paramonova, O.V. Mayevskaa, M.A. Reagana, E. Sancaktara, R.A. Vaiab, S. Juhl, 'Atomic force microscope tip spontaneous retraction from dielectric surfaces under applied electrostatic potential', Ultramicroscopy 106 (2006), pp. 909–913, 2005
124:Y.C.Choi et al., C.Pak, K.S.Kim, 'Electric field effects on water clusters (n=3-5): Systematic ab initio study of structures, energetics and transition states', J. Chem. Phys. 124, 094308 2006, 2005
125:T. Head-Gordon et al, M. E. Johnson, 'Tetrahedral structure or chains for liquid water', PNAS , Vol. 103, No. 21, pp. 7973–7977, 2005
126:D. Marx , 'Proton transfer processes in hydrogen-bonded networks', ChemPhysChem, Vol. 7, 1848 – 1870, 2006
127:S.A. Hassan et al.,G. Hummer, Yong-Sok Lee, 'Effects of electric fields on proton transport through water chains', J. Chem. Phys. 124, 204510, 2006
128:B. Sun et al., S. Kunitomo and C. Igarashi, 'Characteristics of ultraviolet light and radicals formed by pulsed discharge in water', J. Phys. D: Appl. Phys. 39, pp. 3814–3820, 2006
129:F. de Baerdemaeker et al., M.Simek, M. Clupek, P. Lukes, C. Leys, 'Hydrogen peroxide production in capillary underwater discharges', Czechoslovak Journal of Physics, Vol. 56 , Suppl. B, pp.1132-1139, 2006
130:P. Toncoso et al., S. Curilef, 'Bound and trapped classical states of an electric dipole in a magnetic field', Eur. J. Phys. 27, pp. 1315-1322, 2006
131:E. Tokunaga et al., Y. Nosaka, M. Hirabayashi, T. Kobayashi, 'Pockels effect of water in the electric double layer at the interface between water and transparent electrode', Surface Science 601, (2007), pp.735–741, 2006
132:J. Mrázek et al., J.V. Burda, 'Can the pH value of water solutions be estimated by quantum chemical calculations of small water clusters?', J. Chem. Phys. 125, 194518, 2006
133:T.D. Li, J. Gao, R. Szoszkiewicz, U. Landman, E. Riedo, 'Structured and viscous water in subnanometer gaps', Physical review B 75, 115415, 2007
134:C. Costentin et al., M. Robert, J.-M. Saveant, 'Concerted Proton-Electron Transfer Reactions in Water.Are the Driving Force and Rate Constant Depending on pH when Water Acts as Proton Donor or Acceptor?', J. Am. Chem. Soc., Vol. 129, pp. 5870-5879, 2007
135:J.M.J. Swanson et al., C.M. Maupin, H. Chen, M.K. Petersen, J. Xu, Y. Wu, G.A. Voth, 'Proton Solvation and Transport in Aqueous and Biomolecular Systems: Insights from Computer Simulations', J. Phys. Chem. B ,(2007), 111, pp. 4300-4314, 2006
136:R. Vacha et al., V. Buch, A. Milet, J. P. Devlin, P. Jungwirth, 'Autoionization at the surface of neat water: is the top layer pH neutral, basic, or acidic?', Phys. Chem. Chem. Phys., Vol. 9, pp.4736–4747, 2007
137:T. Yamamoto et al. , T. Manaka , M. Iwamoto, 'The interacting electrostatic charge model on the shape formation of monolayer domains at the air–water interface comprised of tilted dipoles with orientational deformation', Thin Solid Films 516 (2008), pp. 2660–2665, 2007
138:L. Holysz et al., A. Szczes, E. Chibowski, 'Effects of a static magnetic field on water and electrolyte solutions', Journal of Colloid and Interface Science, 316, pp. 996-1002, 2007
139:S Mededovic et al., B R Locke, 'Primary chemical reactions in pulsed electrical discharge channels in water', J. Phys. D: Appl. Phys. 40, pp. 7734-7746, 2007
140:A. Klimov et al., G.H. Pollack, 'Visualization of charge-carrier Propagation in water', Langmuir, 23, pp. 11890-11895, 2007
141:J.L. England et al., S. Park, V.S.Pande, 'Theory for an order-driven disruption of the liquid state in water', J. Chem. Phys. 128, 044503, 2007
142:J.K. Beattie, 'Comment on Autoionization at the surface of neat water: is the top layer pH neutral, basic, or acidic?', Phys. Chem. Chem. Phys., (2008), 10, pp. 330–331, 2007
143:R. Vacha et al.,V. Buch, A. Milet, J. P.Devlin, P. Jungwirt, 'Response to Comment on Autoionization at the surface of neat water:is the top layer pH neutral, basic, or acidic?', Phys. Chem. Chem. Phys., (2008), 10, pp. 332–333, 2007
144:G. Xie et al., J. Luo, S. Liu, C. Zhang, X. Lu, 'Micro-Bubble Phenomenon in Nanoscale Water-based Lubricating Film Induced by External Electric Field', Tribol Lett (2008) 29:169–176, 2007
145:Y.-M. Jung et al., H.-C. Oh, I. S. Kang, 'Electrical charging of a conducting water droplet in a dielectric fluid on the electrode surface', Journal of Colloid and Interface Science 322 (2008), pp. 617–623, 2007
146:B.M. Weon et al., J.H.Je, Y.Wu, G. Margaritondo, 'Stable freestanding thin films of pure water', Applied Physics Letters 92, 104101, 2008
147:Elmar C Fuchs, Jakob Woisetschläger, Karl Gatterer,Eugen Maier, Rene Pecnik, Gert Holler, Helmut Eisenkölbl, 'The floating water bridge', J. Phys. D: Appl. Phys. 40, pp. 6112–6114, 2007
148:Elmar C Fuchs, Karl Gatterer, Gert Holler and Jakob Woisetschläger ,'Dynamics of the floating water bridge', J. Phys. D: Appl. Phys. 41 185502 (5pp), 2008